**University of Naples**
**Federico II**

*Department of Civil, Architectural and Environmental Engineering*

Ph.D. Programme in Civil Systems Engineering
XXIX Cycle

Naples, Italy

# Experimental and Numerical Investigation of Pumps As Turbines in Water Distribution Networks

Francesco Pugliese

| **Supervisors** | **Ph.D. Programme Coordinators** |
|---|---|
| Prof. Maurizio Giugni | Prof. Andrea Papola |
| Prof. Francesco De Paola | Prof. Elvira Petroncelli |

**2017**

This work was supported by the EU PON/FESR “Ricerca e Competitività” 2007-2013 under project PON04a2_F “BE&SAVE – AQUASYSTEM – SIGLOD”.

*to Silvana, Umberto*
*and Agata*

# ABSTRACT

The present Ph.D. thesis is devoted to the experimental and numerical analysis of the Pumps As Turbines (PATs) application in hydraulic systems and, specifically, in Water Distribution Networks (WDNs) to generate Energy Recovery (ER) in both urban and rural areas.

The use of PATs in WDNs represents a relevant topic in the field of the innovative Best Management Practices (BMPs) of WDNs because addressed to both the pressure regulation and the hydropower generation. Thus, it could represent an alternative approach to the use of Pressure Reducing Valves (PRVs), benefitting of the exceed pressure to produce sustainable energy, otherwise dispersed.

The PATs application consists in the use of pump models commercially available running in reverse mode, by inverting the flow direction and making use of the motor as an electrical generator. Their employment can be intended as an effective alternative to the traditional micro-turbines in WDNs, having lower investment and maintenance costs and allowing the model selection among a wide set of pump models available in the market. Conversely, PATs usually assure lower operative ranges, however expandable by arranging proper hydraulic and/or electrical regulations.

In addition to the evaluation of the effective opportunities for pressure reduction in water systems, one of the main issue, concerning the PATs use for hydropower generation, regards the limited knowledge about their performance curves, rarely made available by manufactures. In the literature, several experimental, theoretical and numerical models have been proposed, aiming at both predicting the PAT performances and reproducing the internal fluid dynamics. In this regard, Computational Fluid

Dynamics (CFD) models are widely applied, because able to both simulate the fluid dynamics of actual configurations and analyse the performance improvement obtainable by modifying the geometric properties of the considered turbo-machine.

However, the current knowledge about PAT performances, available in the literature, does not allow to characterize the wide set of pump models, which are on the market, useful for running as turbines.

With the aim of making this limitation smaller, in the present study an experimental and numerical investigation of centrifugal PAT models was performed, presenting an operative procedure for the optimal selection of centrifugal PATs in WDNs.

A laboratory set-up was specfically installed at the Department of Civil, Architectural and Environmental Engineering (DICEA) of the University of Naples (IT) Federico II where several centrifugal PATs, having different geometric configurations and motor equipment, were tested. The experiments were performed in wide flow rate ranges, typical of WDNs supplying small-medium sized urban and rural centers, by varying the PAT rotational speed from 300 to 3000 rpm. A total of about 7400 operative configurations were investigated, in compliance with the laboratory set-up potentialities, achieving generated head drops up to about 70 m and produced electrical powers up to 16.3 kW.

From the experimental analysis, with the aim of characterizing the investigated PATs, comparison with models from the literature was performed and, in order to provide effective tools for predicting the performances of centrifugal PATs, analytic relationships were derived, as a function of the geometric configuration, the number of stages and the motor efficiency class equipment.

The attention was specifically drawn to the experimental characterization of: a) a classical Horizontal Axis Single-Stage PAT running at wider operative ranges than those discussed in the literature; b) PAT models, not adequately taken into account in the literature, such as centrifugal Single-Stage and Multi-Stage Vertical Axis PATs.

Taking advantage of the experimental results, an operative procedure was developed for the optimal selection of PATs in WDNs, able to maximize the potential ER in

WDNs. It could be intended as a basic tool for implementing a Decision Support System (DSS) for hydropower generation in WDNs.

Finally, the development of a numerical CFD model, by applying the ANSYS® Fluent™ code, allowed to test the reliability of numerical simulations to both predict the PAT performances and investigate the fluid behaviour across centrifugal PATs.

**Keywords**: Centrifugal Pumps As Turbines (PATs), Water Distribution Networks (WDNs), Energy Recovery (ER), Performance Curves, Experimental Analysis, Computational Fluid Dynamics (CFD).

# ACKNOWLEDGMENTS

During these three years of my Ph.D. course I have had the pleasure and honour to both meet and collaborate with several people who have truly been decisive for my professional and personal growth.

First of all, I want to express my sincere gratitude to my Tutor, Prof. Maurizio Giugni, for the opportunity he gave me to make part of his research team, representing a real example of expertise, dedication and kindness. An acknowledgement is also due to my Co-Tutor Prof. Francesco De Paola, who has believed in my abilities since I was a junior student, encouraging my improvements.

Special and sincere thanks go to the members of the research team at the Department of Energy of the University of Oviedo (ES). My sincere acknowledgments specifically go to Prof. Joaquín Fernández Francos, who supported me in implementing the CFD model, with great expertise and kindness, and facilitated each side of my Spanish experience, continuing even now, with his review of this Ph.D. thesis, his suggestions and support.

I direct special thanks to Prof. Eduardo Blanco Marigorta, Prof. Jorge Parrondo and Prof. Eduardo Álvarez Álvarez, for their support in performing my research activities in Spain.

I would also like to express my deep gratitude to Prof. Stefano Malavasi, Ivan Stoianov and Tullio Tucciarelli for reviewing this Ph.D. thesis, providing useful suggestions, which improved this work.

I express sincere gratitude to Prof. Nicola Fontana, for his exemplary dedication and interest to the developed topic. I would also like to thank Dr. Gustavo Marini for his

support since I was a junior student, and Furio Buonopane, Paolo Esposito, Alessandro Reale, Antonio Fusco and Domenico Palmiero for their capabilities, availability and helpfulness during the performed experimental activities.

I would also like to thank Prof. Andrea Papola and Prof. Elvira Petroncelli for their support and patience as Ph.D. Programme Coordinators.

Furthermore, I wish to acknowledge Prof. Adolfo Senatore and his research team for providing the graphical support to the CFD modelling.

I affectionately thank my colleagues at DICEA, who have played a supporting role for achieving this aspired goal. In particular, my thoughts go to the old friends Giuseppe Ascione, Ilaria Del Vita, Daniela Salerno, Giuseppe Speranza and Vittorio Pasquino, to which, after these three years, I feel even more connected.

Special mention is addressed to Andrea D'Aniello, Gerardo Caroppi, Maria Chiara Conte, Vincenzo Abate and Ilaria Henke, who have been met during the Ph.D. activities. I have had the pleasure to forge a sincere friendship, as well as a professional relationship, which, I candidly hope, will continue in the future.

Special greetings are devoted to Enzo Galdiero, to which I fell a sincere friendship and immense esteem. Despite his absence from DICEA, he still continues to be an irreplaceable point of reference during my working days.

Affectionate greetings are also directed to colleagues Doddy, Irene and Ana who helped me during my stay in Gijón.

I would also like to deeply thank my whole family for supporting me during these years, pandering my choices and being, in any case, available to meet me. To Silvana, Umberto, Gina, Sara, Stefano, Virginia, Camillo, who have to bear me every day.

Last but not the least, my lovely thanks go to my sweetheart Agata, for her immeasurable affection, care, support and patience in each aspect of my life. She makes everything easier.

# TABLE OF CONTENTS

# LIST OF FIGURES

# LIST OF TABLES

# LIST OF SYMBOLS

- $a^*$ [-] Yang et al. (2012a) Correlation Parameter
- $b^*$ [-] Yang et al. (2012a) Correlation Parameter
- $bhp$ [bhp] Brake Horsepower
- $c$ [$ms^{-1}$] Meridional Velocity
- $c^*$ [-] Yang et al. (2012a) Correlation Parameter
- $f$ [Hz] Grid Frequency
- $f^*$ [-] Error Propagation Function
- $g$ [$ms^{-2}$] Acceleration of Gravity
- $h$ [-] Head Ratio
- $k$ [$m^2s^{-2}$] Turbulence Kinetic Viscosity
- $p^*$ [-] Number of Pole Pairs
- $\overline{p}_r$ [$Nm^{-2}$] Mean Pressure
- $p_r'$ [$Nm^{-2}$] Fluctuating Pressure
- $q$ [-] Flow Rate Ratio
- $r$ [m] Runner Radius
- $s^*$ [-] Standard Deviation
- $t^*$ [-] Torque Ratio
- $t_{95}$ [-] *t*-Student Distribution Variable at 95% Confidence Interval
- $x$ [m] Cartesian Component
- $x_i$ [-] Measured parameter
- $x^*$ [-] True value of the entity measurement
- $\bar{x}$ [-] Sample Mean
- $u$ [$ms^{-1}$] Peripheral Velocity
- $v$ [$ms^{-1}$] Velocity
- $\bar{v}$ [$ms^{-1}$] Mean velocity
- $v'$ [$ms^{-1}$] Fluctuating velocity
- $z$ [-] Index of iterative procedure for PAT selection
- $z_t$ [m] Suction Static Head
- $B$ [-] Fixed or Bias Error
- $C_,$ [-] Experimental Values of *k*-$\varepsilon$ Turbulence Model
- $C'$ [-] Williams (1994) corrective factor
- $D$ [m] Impeller Diameter
- $D_p$ [mm] Pipe Diameter
- $D_s$ [m, $m^3s^{-1}$] Specific Diameter
- $E$ [-] Elasticity
- $F$ [m] Stator Height
- $G$ [-] Turbulent Kinetic Energy Increasing
- $H$ [m] Head or Head Drop
- $H_\Delta$ [m] Net Positive Suction Head
- $I$ [A] Current Intensity
- $L$ [m] Length
- $M$ [-] Number of Measured Experimental Parameters
- $N$ [rpm] Rotational Speed
- $N^*$ [-] Number of Experimental Measurements
- $N_s$ [rpm, m] Specific Speed

- $P$ [W] Power
- $P_r$ [m] Pressure
- $NP$ [kW] Nominal Power
- $Q$ [$m^3s^{-1}$] Flow Rate
- $R$ [-] Random Error
- $Re$ [-] Reynolds Number
- $S$ [$ms^{-2}$] Strain Tensor
- $S^*$ [-] Number of Iterations of PAT Selection Procedure
- $T$ [Nm] Torque
- $U$ [-] Uncertainty
- $W$ [$m^3$] Water Volume
- $WH$ [-] Suter (1966) Head Parameter
- $WT$ [-] Suter (1966) Torque Parameter
- $Y_M$ [-] Fluctuating dilation
- $\alpha$ [$m^{3/\beta}s^{-1}$] Discharge Coefficient
- $\overline{\alpha}$ [rpm, m] Derakhshan and Nourbakhsh (2008a) Specific Speed at BEP
- $\alpha^*$ [-] Fecarotta et al. (2016) Experimental Coefficient
- $\alpha^{**}$ [-] Damping Coefficient
- $\beta$ [-] Leakage Exponent
- $\overline{\beta}$ [rpm, m] Derakhshan and Nourbakhsh (2008a) Specific Speed at BEP
- $\beta^*$ [-] Fecarotta et al. (2016) Experimental Coefficient
- $\gamma$ [$Nm^{-3}$] Specific Weight
- $\bar{\gamma}$ [-] Derakhshan and Nourbakhsh (2008a) Correlation Coefficient
- $\gamma^*$ [-] Fecarotta et al. (2016) Experimental Coefficient
- $\delta^*$ [-] Fecarotta et al. (2016) Experimental Coefficient
- $\varepsilon$ [$m^2s^{-3}$] Dissipation Rate
- $\eta$ [-] Efficiency
- $\bar{\eta}$ [-] Minimum allowable efficiency in PAT selection procedure
- $\theta$ [-] $\omega^*$ and $q$ Ratio
- $\lambda$ [-] Mechanical Failure Rate
- $\pi$ [-] Power Number
- $\rho$ [$kgm^{-3}$] Fluid Density
- $\sigma$ [$m^2$] Runner Section
- $\sigma^*$ [-] Variance of Normal Distribution
- $\sigma_k$ [-] Prandtl Number for Kinetic Energy
- $\sigma_\varepsilon$ [-] Prandtl Number for Dissipation Rate
- $\sigma_t$ [-] Cavitation Parameter
- $\tau$ [$kgm^{-1}s^{-2}$] Reynolds stress tensor
- $\nu_T$ [$m^2s^{-1}$] Kinetic Eddy Viscosity
- $\varphi$ [m] Stator Diameter
- $\phi$ [-] Flow Rate Number
- $\chi$ [-] Nautiyal et al. (2011) Correlation Parameter
- $\psi$ [-] Head Number
- $\omega$ [$s^{-1}$] Angular Velocity
- $\omega^*$ [-] Rotational Speed Ratio
- $\omega^I$ [$s^{-1}$] Specific Dissipation Rate
- $\mu$ [$Nsm^{-2}$] Fluid Dynamic Viscosity

- $\bar{\mu}$ [-] Mean Value
- $\Delta H$ [m] Specific Head

# LIST OF SUBSCRIPTS

- $a^*$ [-] Turbo-machine type
- *av* [-] Available
- *b* [-] Best Efficiency Point
- $b^*$ [-] Turbo-machine type
- $g^*$ [-] Generator
- $h^*$ [-] Hydraulic
- *i* [-] Counter index
- *in* [-] Input
- *j* [-] Counter index
- $i^*$ [-] Internal
- $m^*$ [-] Motor
- *min* [-] Minimum value
- *max* [-] Maximum value
- *o* [-] Outlet
- *out* [-] Output
- *p* [-] Pump Mode
- *req* [-] Required
- *s* [-] Suction eye
- *t* [-] Turbine Mode
- *tot* [-] Total
- *v* [-] Vapour
- $v^*$ [-] Volumetric
- *w* [-] Water
- *z* [-] Counter index
- *P** [-] Plant
- $\Delta$ [-] Net Positive Suction Head

# LIST OF ABBREVIATIONS

- AC Alternative Current
- AL Affinity Laws
- ATO Optimal Territory Ambit
- BABE Burst and Background Estimation
- BEP Best Efficiency Point
- BMP Best Management Practice
- CARL Current Annual Real Losses
- CFD Computational Fluid Dynamics
- CSHN Combined Suction Head Number
- DC Direct Current
- DICEA Department of Civil, Architectural and Environmental Engineering
- DMA District Metering Area
- DSS Decision Support System
- ER Energy Recovery
- ERT Energy Recovery Turbine
- ESHA European Small Hydropower Association
- FAO Food and Agriculture Organization of the United Nations
- FAVAD Fixed And VAriable Discharge
- FEM Finite Element Method
- GIS Geographic Information System
- HA Horizontal Axis
- IEC International Electrotechnical Commission
- IGBT Insulated-Gate Bipolar Transistor
- IIS Integrated Information System
- ILI Infrastructure Leakage Index
- ISTAT Italian National Institute of Statistics
- IWA International Water Association
- MAL Modified Affinity Laws
- MNF Minimum Night Flow
- MRF Multiple Reference Frame Technique
- MS Multi-Stage
- NPSH Net Positive Suction Head
- OD Opening Degree
- PAT Pump As Turbine
- PID Proportional Integrative Derivative controller
- PLC Programmable Logic Controller
- PON National Operative Programme
- PRGA Italian Master Plan of Water Systems
- PRV Pressure Reducing Valve
- RANS Reynolds-Averaged Navier-Stokes
- RTC Real Time Control
- SCADA Supervisory Control and Data Acquisition
- SHP Small scale HydroPower
- SII Integrated Water Service
- SIMPLE Semi-Implicit Method for Pressure-Linked Equations
- SIMPLEC Semi-Implicit Method for Pressure-Linked Equations Consistent

- SM Sliding Mesh
- SS Single-Stage
- UARL Unavoidable Annual Real Losses
- UNESCO United Nations Educational, Scientific and Cultural Organization
- UNIDO United Nations Industrial Development Organization
- VA Vertical Axis
- VOS Variable Operating Strategy
- VSI Voltage Source Inverter
- VSR Voltage Sensitive Relay
- WDN Water Distribution Network
- WSS Water Supply System
- 5BTP Five Blade Tubular Propeller

# Chapter 1

# Introduction

As a consequence of the indiscriminate use of water, often unregulated and not sustainable, the undertaken direction is heading towards scenarios which make evidence of the structural lacks of the sustainable management of water resources, which usability represents an *essential necessity and an unalienable right* (UNESCO, 2015).

Analysing the worldwide status of water uses, significant inequalities, among different countries, are observable, as a consequence of both the higher or lower availability of resources and the discrepancies in development, treatment and rehabilitation works and costs, necessary to attain exploitable natural resources (FAO, 2003). In the poorest and arid regions, water availability is strongly scarce, resulting in further deterioration because of both the ongoing climate changes and the inadequate infrastructures for water transportation, storage and treatment.

Conversely, in areas with sufficient economic and natural resources, the increasing water demands, generated by the industrialization, and the actual status of the infrastructure systems are determining irreconcilable disparities between the water requests and the effective satisfaction of users' requirements.

More specifically, the obsolescence status in which the hydraulic systems operate and the ongoing strategic approaches devoted to their management and improvement, still not totally effective, are causing high levels of water losses with undeniable environmental, social and economic disadvantages.

By analysing the status of the worldwide countries, it was found that high water losses in the hydraulic systems resulted to be not restricted by geography or level of economic development, pointing out how industrialized countries, such as Canada, China, France and Italy, are characterized by water leakages in hydraulic systems comparable with those referred to developing countries, such as Kenya, Nepal and Mexico (Frost & Sullivan, 2015).

In greater detail, concerning the Italian country, in spite of the high availability of water resources for civil uses, estimated in about 9 billion of cubic meters per year (ISTAT, 2014), the water demand, particularly in the southern part of the country, is not completely fulfilled. A preeminent cause of this unbalance is ascribable to the high water wastefulness in the hydraulic systems and, specifically, to the significant water losses in the Water Distribution Networks (WDNs), which represent a non-negligible, although sometimes predominant, ratio of the total inflow water volumes.

Large amounts of water losses generate negative impacts, not only for the environmental detriment, but also for economic sectors, such as agriculture, tourism, industry, energy and transport, in turn affecting the national competitiveness and the internal financial market (EU Commission, 2015).

In this field, latest studies on the hydraulic infrastructures in Italy (ISTAT, 2014) pointed out that, in reference to the Italian WDNs, the water losses represent a significant ratio, estimated in the range between the 20% and 60% of the applied resources, with remarkable socio-economical effects and environmental detriments. The recovery of part of the dispersed resources could allow, on one hand, to restrain the ongoing research of new supply sources and, on the other hand, to reduce the managing costs related to the existent infrastructures.

## 1.1 Problem Statement

One of the most critical issues of water losses in hydraulic systems and, expressly, in WDNs, is represented by the significant exceed pressure levels, which cause huge stresses on pipes and on the other devices of a water network.

Indeed, several studies pointed out the correlation between pressures and physical water losses, individuating in the application of regulation valves, such as PRVs, an effective approach to modulate the pressure levels, in compliance with the dynamic operative conditions in the network. In this context, the Energy Recovery (ER) in WDNs, by using micro-turbines or Pumps As Turbines (PATs), allows, on one hand, to regulate the exceed pressures and, on the other hand, to generate sustainable energy, otherwise dispersed.

In this regard, the use of PATs could be intended as an effective and cheap approach for energy production in both urban and rural areas, because devoted to the application of pumps commercially available in reverse mode, with low investments, maintenance costs and ease of installation. Conversely, the actual knowledge, about the performances of the wide set of available pump models running as turbines, still results to be not adequately strengthened. Moreover, the PAT application to complex hydraulic systems, such as WDNs, characterized by dynamic operative conditions, necessitates of effective tools for the optimal model selection, aiming at guaranteeing the required effectiveness and reliability.

## 1.2 Research Objectives

The general objective of this thesis is to investigate the physical behaviour of centrifugal PATs, used for both hydropower generation and pressure regulation in hydraulic systems and, specifically, in WDNs. The developed methodology is based upon both an experimental and a numerical approach, aiming at analysing the main parameters and peculiarities correlated to the PAT application. Instruments for estimating the PAT effectiveness, as a function of the dynamic operative conditions in WDNs, are provided.

In greater detail, the main goals aim at:

- characterizing the performances of several models of centrifugal PATs, having different geometric configurations and equipment;
- providing analytic formulations to predict the performances of several centrifugal PAT models;

- developing an operative procedure, intended as a basic tool for a Decision Support System (DSS) addressed to the optimal PAT selection in WDNs;
- both investigating the physical behaviour of PAT models, not adequately taken into account in the literature (such as Vertical Axis centrifugal PATs), and evaluating the dependence of motor equipment for the estimation of the overall PAT performances;
- developing a CFD model to characterize the performances and the fluid dynamics of centrifugal PATs.

The applied methodology provides, as first step, the analysis of the models available in the literature, devoted to the specification of the characteristics related to the PAT applications, in order to verify which improvements are feasible to extend the actual knowledge about their application in WDNs. Furthermore, an experimental analysis on different centrifugal PAT models operating at wide operative conditions is performed, aimed at both veryfing the reliability of models from the literature and providing novel formulations to predict the PAT performances. Starting from the achieved results, an operative procedure is developed for the optimal selection of PATs in WDNs, then analyzing the reliability of CFD models to both predict the PAT characteristic curves and reproduce the internal fluid dynamics.

## 1.3 Outline of the Thesis

The thesis presents the following structure:

- **Chapter 1**, which contains a brief introduction of the treated topic, and of the fields in which it operates;
- **Chapter 2**, where an overview concerning the management criteria of Water Supply Systems (WSS) and, expressly, of WDNs, is introduced, drawing specifically attention to the methodologies and practices, used to both detect and limit the water losses in WDNs;
- **Chapter 3**, in which a wide review of the engineering literature related to the ER in WDNs is presented, drawing particularly the attention to the mechanical and managing properties concerning the use of PATs;

- **Chapter 4**, in which the applied procedure and results of an intensive experimental analysis on several centrifugal PAT models are reported and discussed. The laboratory experiences are illustrated and the developed predicting criteria are introduced. The PAT performance characterization is expressly considered, in reference to both wider operative ranges than those available in the literature and models not adequately considered in previous researches, such as centrifugal Vertical Axis models with different motor equipment. An operative procedure to optimize the PAT selection in WDNs is also proposed, aiming at furnishing a basic tool for a DSS devoted to the PAT selection in WDNs;
- **Chapter 5**, where the Computational Fluid Dynamics (CFD) modelling of a centrifugal PAT is introduced, making evidence of the model ability to reproduce the internal behaviour of PATs to both estimate the PAT performances and evaluate the internal fluid dynamics fields;
- **Chapter 6**, in which a brief synthesis of the content and achieved results is included, stating their contribution to the engineering research. The potential improvements, connected to the considered research, are also specified.

# References


- European Union Commission (2015). EU reference document Good Practices on Leakage Management WFD CIS WG PoM. Main Report. Office for Official Publications of the European Communities. http://dx.doi.org/10.2779/102151
- Food and Agricultural Organization of the United Nations (2003). Review of world water resources by country. Water report, Rome 2003, Italy.
- Frost & Sullivan Company (2015). Smart technologies will plug water leaks. http://www.slideshare.net/FrostandSullivan/2015-to-thepoint-trend-10-water-infrastructure
- Italian National Institute of Statistics (2014). Censimento delle acque per uso civile. Anno 2012. Statistiche Report (in Italian). ISTAT website: http://www.istat.it/it/files/2014/06/2014_06_26_Report_censimento_acqua.pdf?title=Censimento+delle+ac-
- United Nations Educational, Scientific and Cultural Organization (2015). World Water Council, Final report 7th World Water Forum 2015. 13th April 2015, Daegu & Gyeongbuk, Republic of Korea.

# Chapter 2

# Water Supply Systems: Configurations and Management

A Water Supply System (WSS) represents the engineering system characterized by variable complexity, used for interception, treatment, adduction, storage and distribution of water resources, in favour of urban, industrial, irrigation and rural centres. It can be schematized as composed of the following components (Fig. 2.1):

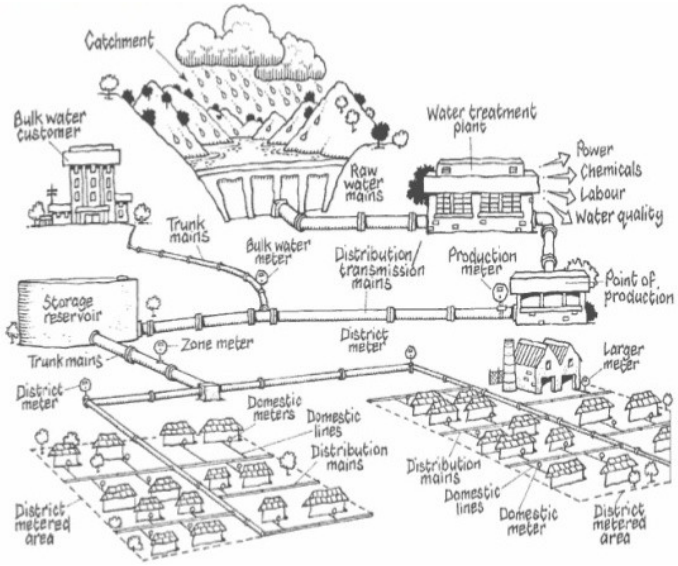


**Fig. 2.1 Water Supply System scheme (www.pacificwater.org)**

- **Intake systems**, which collect the water resources derived from the natural cycle;
- **Treatment plants**, which assure the required physical, chemical and biological properties of water resources, in compliance with their use (drinkable use, industrial use, agricultural use, etc.);

- **Adduction systems**, which behave the water movement from the sources to the urban or industrial centres. They can be *free surface systems*, usually considered for large size systems, or *pressure systems*, more flexible and applicable than the previous subcategory, because able to both overcome the geodetic gradients and provide better environmental protection from external contaminations;
- **Storage Systems (Tanks)**, having the multiple functions of fixing the hydrostatic pressure on the water network, containing the compensation and reserve volumes and guaranteeing the fire-fighting volumes. An additional ratio is usually included, in order to compensate the water losses in the supplied WDNs;
- **Water Distribution Networks (WDNs)**, composed of the sets of pipes and devices which supply the private and public users. As a function of their topological configuration, they are classified into: a) *open networks*, with low interconnection levels causing, in presence of failures, limited capability of assuring the users' requirement; b) *interconnection or closed networks*, with greater flexibility than the previous subcategory being able to assure the users' supplying when the flow through a pipe is interrupted, through the identification of alternative paths to reach the delivery points. They also allow to convey significant water entities in singular points, for example, for fire-fighting purpose; c) *mixed networks,* presenting both the abovementioned configurations.

In the field of management activities of WSSs and, specifically of WDNs, significant issues regard the detection and reduction of water leakages, which result not negligible, sometimes even prevalent, with respect to the water volumes essentially supplied to the users.

Concerning the Italian infrastructures, the Italian National Institute of Statistics ISTAT (2014) pointed out that the obsolescence status, in which the hydraulic systems operate, is causing significant water loss rates in WDNs, estimated in the range from 22.2% for the Aosta Valley region to 54.8% for the Sardinia region, of the total inputted volume resources (Fig. 2.2). An average national percentage of 37.4% was expressly estimated.

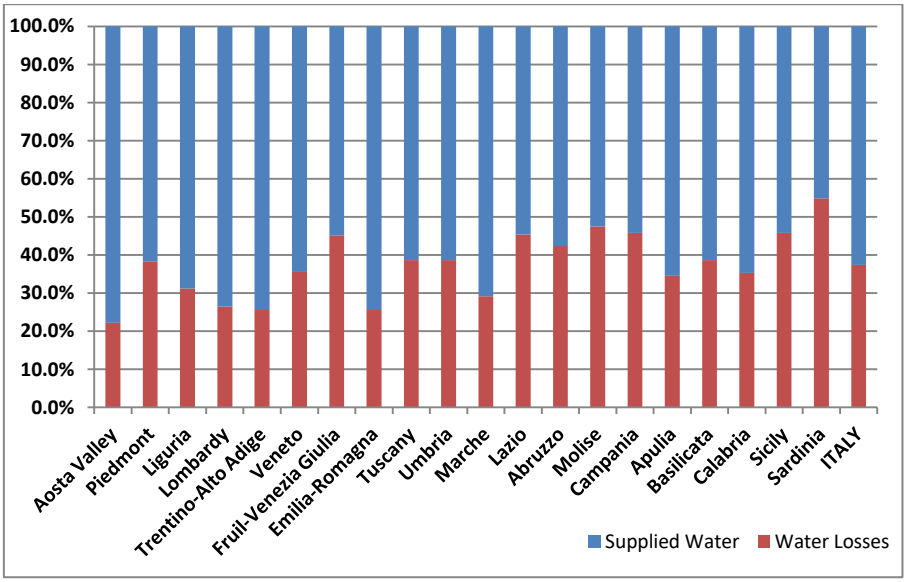


**Fig. 2.2 Percentage of water losses and supplied water in Italian regions (ISTAT, 2014)**

The analysis of water losses in WDNs during the last years makes evidence that partial improvements have been reached by applying the ongoing management approaches, even defining an average national leakage rate of about 4% higher than that estimated during the time span of the previous four years (ISTAT, 2014).

Significant socioeconomic and environmental detriments are correlated to high water losses in hydraulic systems, simulataneusly determining the inability to accomplish the users' demand, the necessity of introducing higher volumes to satisfy the users' requirements and the uneconomic aspect of water volumes uselessly treated and/or pumped.

Starting from the abovementioned considerations, the necessity of developing proper approaches to improve the effectiveness of WDNs management results a preeminent topic in the field of the Best Management Practices (BMPs) of hydraulic systems.

## 2.1 Management of Water Supply Systems

A proper management of WSSs is based upon the fulfilment of satisfied standards, to be reached by applying managing criteria, foundend on three operative factors: *Effectiveness*, *Efficiency* and *Cheapness* (Italian Legislative Decree L.D. 152/2006). In

order to accomplish the above criteria, the system management should be performed by applying different but complementary approaches:

- *Physical Management*, based upon the in-deep knowledge of both the monitored hydraulic system and its parts, obtainable through the use of Geographic Information Systems (GIS) and by managing the dynamic operative conditions with Supervisory Control and Data Acquisition (SCADA) systems;
- *Socio-Economic Management,* based upon the consideration of water resource as a social asset but, at the same, providing its management from the financial and profitable point of view;
- *Legal Management,* focused on the principle of ensuring a level of service to the users, in compliance with the quali-quantitative standards settled by the in-force laws;
- *Technical Management,* based upon the "engineering" control of the system, in each operative phase, reachable through a programming scale, with increasing time horizons: a) *daily management,* to manage the standard operations; b) *multi-year management*, to take into account, through proper planning and management criteria, the future operative scenarios; c) o*utstanding management*, aimed at facing unpredicted and extraordinary events (i.e. seismic actions, consecutive drought periods).

## 2.2 Italian Legislation on Water Resources

Starting from the second middle of XIX century, in reference to the Italian region, several rules were promulgated about the planning, tutelage and management of both water resources and hydraulic infrastructures. However, only starting from the second middle of XX century, as a consequence of the increasing environmental conscience, the rules on water resources management begun to rotate around the principle of a rational use of natural resources.

The fundamental normative steps for the Italian Legislation are summarized as follows:

- *Law No. 2248/1865*, first normative legislation on water sector;

- *Normative Reforms 1916-19,* focused on the use of water resources for hydropower use;
- *Consolidated Law No. 1775/1933*, in which a basin-scale program planning was introduced;
- *Italian Master Plan of Water Systems PRGA Law No. 129/63* (*approved on March 1967*), based upon the studies realized up to year 1961 about the per-capita water consumption and the population statistics for each Italian municipality. A hydraulic scheme was designated for each municipality and a *necessary water need* ($ls^{-1}$) was evaluated with forecast horizon to year 2015. A *water per-capita endowment* ($lin^{-1}d^{-1}$), which included the domestic and tertiary uses, was also considered;
- *Italian Law No. 319/1976* (*Merli's Act*), in which the guidelines of the environmental protection were introduced;
- *Italian Law No. 183/1989,* with which the hydrographic basin was identified as the basic territorial entity for estimating both the availability of water resources and their uses. The first territorial authority for water resources planning and management, named *Basin Authority*, was also promoted;
- *Italian Law No. 36/1994* (*Galli's Act*), which represented an essential step to overcome the fragmentation of Italian water utility systems. It introduced the concept of *Integrated Water Service* (*SII*), according to which a unique management for the whole technological cycle of urban water was identified. Specific local authorities, named *Optimal Territory Ambits* (*ATOs*), circumscribed as a function of geographical and environmental criteria, were instituted to guarantee the rational use of water resources; the *Water Balance* was identified as the essential instrument for the evaluation of the quali-quantitative discrepancies between the available water resources and their effective fruition. Industrial criteria to manage the *SII*, through the separation between the holders and the management companies able to determine an economical and financial equilibrium, were also introduced and a basic water tariff was applied to cover the service costs, its management and investments. Furthermore, technical criteria to quantify the *minimum service requirements* were established, such as the minimum per-capita endowment of 150 $lin^{-1}d^{-1}$, the

minimum discharge of 0.1 $ls^{-1}$ per each household, the minimum pressure of 5 m at each delivery point, to be evaluated with respect to the top floor of the buildings. The maximum pressure of 70 m was also set for each delivery point.

- *Italian Legislative Decree No. 152/2006 (Italian Environmental Unique Law)*, which abrogated the Galli's Act and established the discipline of water resources planning and management, based upon the ATOs. It introduced the principles of *Effectiveness*, *Efficiency* and *Cheapness*, conferring the opportunity of redefining the ATOs to the Regional Authorities, in compliance with the principle of *unified tendency*;
- *Italian Law No. 42/2010*, through the which the Regional Authorities assumed the ATOs functions.

Concerning the specific ambit of water leakages in WSSs, following Italian legislative references can be cited:

- *Italian Prime Ministerial Decree 04/03/1996*, in which the necessity of developing proper managing activities, devoted to the reduction of water leakages, the recovery of the unbilled volumes and the containment of the wastes of water were explicitly introduced. Moreover, specific actions were required for hydraulic systems, having leakage percentage higher than 20% of the total inputted volume;
- *Italian Ministerial Decree No. 97/1999*, which introduced the mandatory intervention of the water utility companies to annually monitor and manage the water losses in WDNs. The *Water Balance* was identified as the basic instrument to both quantify and monitor the water leakages; the necessity of identifying proper performance indicators was pointed out, as well.

## 2.3 Performance Indicators for Water Distribution Networks

A synthetic evaluation of the *Effectiveness*, *Efficiency* and *Cheapness* principles can be established by applying proper *Performance Indicators*. In this regard, the *IWA Manual of Best Practice* (Alegre et al., 2000) introduced 133 indicators, belonging to 6 different ambits: water and environmental resources, personnel, physical characterization of the system, system practicality, service quality and economy and finance.

As regards the water losses, three levels of indicators were established; the first one (*Level 1 indicators, L1*) included the basilar indices, usually adopted by water utilities to analyse the overall status of the hydraulic systems. In greater detail, they numerically explicated the principles of *Effectiveness*, *Efficiency*, *Cheapness* and *Elasticity*, as summarized in the following Tab. 2.1.

| **Effectiveness Indicator** | **Efficiency Indicators** | | **Cheapness Indicator: Mechanical Failure Rate** | **Elasticity Indicator** |
|---|---|---|---|---|
| $W_{req}/W_{out}$ | $W_{out}/W_{in}$ | $W_{met}/W_{in}$ | $\lambda = N_F/(L \cdot T)$ | $E = \sum_{i=1}^{n} E_i \cdot \frac{Q_i}{Q_{tot}}$ |

**Tab. 2.1 *L1* main Performance Indicators**

In Tab. 2.1 $W_{req}$ is the required water volume, $W_{out}$ the supplied water volume, $W_{in}$ the inputted water volume and $W_{met}$ the metered water volume, whereas, to calculate the *mechanical failure rate* $\lambda$, $N_F$ is the total number of pipe failures, $L$ the overall length of the network pipe (km) and $T$ the considered time period (year).

The mechanical failure rate $\lambda$ analytically quantifies the network vulnerability, inasmuch it evaluates the failure density, as a function of the considered observation time period $T$. High $\lambda$ values indicate hydraulic systems with high vulnerability to failures, thus representing low cheapness and vice versa. This parameter can vary over a wide range, depending on several factors, such as the pipe diameter (Su et al., 1987; Goulter et al., 1993), the pipe age (Shamir and Howard, 1979) and the climatic conditions (Harada, 1988; Ahn et al., 2005).

To estimate the netowrk *elasticity*, the indicator $E_i$ represents the elasticity of the *i-th* pipe, $Q_i$ the flow rate across the *i-th* pipe, $Q_{tot}$ the overall flow rate through the network. The elasticity $E_i$ of the *i-th* pipe is evaluated as a function of the ratio between the flowing flow rate through the *i-th* pipe and the maximum allowable flow rate $Q_{\max i}$. For $E_i$ tending towards 0, the *i-th* pipe is characterized by low elasticity because of a flowing rate almost equal to the maximum allowable value. Conversely, for $E_i$ tending towards 1, the pipe is capable to conduct flow rates higher than the actual one, by ensuring greater elasticity. On the other hand, it implicates greater vulnerability, as a consequence of the higher pressure level.

Further index concerns the estimation of the *water losses per unit length of pipes*, mainly applied in case of users' connections up to 20 (i.e. in urban areas) to estimate the water losses.

For more detailed analyses, complex indicators (*Level 3 Indicators*, *L3*) are adopted. Among them, the following main indexes are cited:

- *Unavoidable Annual Real Losses* (*UARL*), which represents the minimum limit of physiological water losses, estimated, according to Lambert et al. (1999), as a function of the overall length of the network pipes, the average pipe length of private users and the mean operating pressure;
- *Current Annual Real Losses* (*CARL*), which estimates the physical losses generated during the considered yearly time span;
- *Infrastructure Leakage Index* (*ILI*), which measures the effectiveness of the maintenance activities, performed in the network, in presence of the existing pressure regime. It could be estimated as a ratio between *CARL* and *UARL* indexes. Thus, *ILI* values higher than 1 estimate how many times the physical losses are higher than the unavoidable losses, in presence of the operating pressure or, similarly, it quantifies how many real losses should be detected and removed. On the other hand, *ILI* values tending towards 1 are representative of good performances, assured by the applied management approaches.

## 2.4 Water Losses in Water Distribution Networks

The water volumes lost in a WDN are intended as the difference between the total water quantities supplied to the network and the overall volumes recorded by the users' flowmeters. Hence, the losses rates, caused by the incorrect use of water resources by users (such as the useless opening of taps or showers) and the losses into the household systems are not contemplated as "water losses", but, rather, they are intended as "wastes of water".

The effective water losses are categorized into two groups, as widely specified in the Par. 2.5.1:

- **Apparent Losses,** constituted by the consumed, but not recorded, water volumes (Fig. 2.3) and mainly composed of a) *service volumes*, depleted for the regular functioning of the network (i.e. pipe or tank cleanings); b) *losses volumes due to the incorrect operation of the system*; c) *losses volumes due to measurement errors* and d) *unauthorized volumes*, caused by illegal connections or flowmeter tampering.


**Fig. 2.3 Apparent losses**

The apparent losses represent a not negligible ratio of the total losses but, however, lower than the real loss category. They are usually evaluated as the 30% of the overall losses, therefore detailed detection campaigns and reduction approaches are strictly connected to expensive investment costs.

- **Real losses** or *Physical Losses* represent the lost volumes, caused by the integrity lacking of the network components such as junctions, pipes and tank walls. In case of delayed detection, long time periods, during the which the water losses operate, will occur. The Burst And Background Estimation (BABE) method (Lambert, 1994) classified the real losses into the following categories: a) *Background Losses*, caused by the junction failures or by less detectable leakages. They generally result undetectable during ordinary campaigns for leakage detection, unless their location is close to the inspection wells; b) *Reported Bursts*, characterized by the water emersion on the ground level (Fig. 2.4) or by the interruption of users' services, thus resulting easily detectable and suppressible by performing dedicated maintenance operations; c) *Unreported Bursts*, strongly lower than the *Reported Bursts*, not presenting macroscopic visual effects on the ground level. They can be exclusively detected through proper and distinctive instrumental campaigns.

**Fig. 2.4 Reported bursts**

The determination of real water losses is ascribable to several causes; among them, following factors result the most widespread: the high operating pressures, the mechanical properties and the configuration of the laying soils, the defects in realization and selection of pipe materials, the presence of many devices, the number of users' derivations, the pipe length and age, the junction type and quality, the mechanical stresses on pipes caused by external stress, the lack of proper ordinary and extraordinary maintenances.

The real losses are generally estimated as equal to the 70% of the total losses and, on them, the common detection campaigns are usually addressed.

Even if the water losses interest the overall producing and transporting water cycle, they mainly involve the WDNs, in compliance with the categorization summarized in the following Tab. 2.2, referred to an overall water system having water loss rate equal to 41%.

| **Water system components** | **Water losses [%]** |
|---|---|
| Water intakes | 2 |
| Treatment plants and transmission mains | 15 |
| Storage Facilities | 4 |
| Distribution networks and customer connections | 20 |

**Tab. 2.2 Loss ratios in the water system components (Portolano, 2008)**

From an economic standpoint, if the water demand is satisfied and the water losses result to be not greater than 5÷10% of the total intake volumes, proceeding with

detection and mitigation campaigns of water leakages results economically unsustainable, because the savings connected to the leakage reduction are less than the required investments. As an example, in the following Fig. 2.5 the leakage and the cost functions are plotted, detecting the leakage value which minimizes the total generalized costs for leakage detection campaigns.

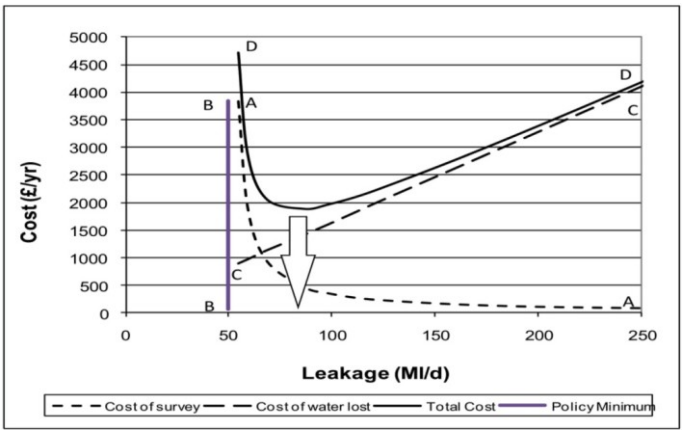


**Fig. 2.5 Leakage and cost functions (EU Commission, 2015)**

## 2.5 Estimation of Water Losses in Water Distribution Networks

Concerning the management and maintenance methods to evaluate the water losses in WDNs, two approaches are mainly adopted: the *Top-Down* approach, based upon the application of the WDN *Water Balance*, and the *Bottom-Up* approach, based upon the measurement and calculation of the *Minimum Night Flow* (*MNF*), instead.

The application of the aforementioned *Performance Indicators* (Par. 2.3) is also suggested to detect the network area having higher vulnerability and then interesenting to actuate proper management approaches.

### 2.5.1 The Top-Down Approach: the Water Balance

An effective application of the *Water Balance* is strictly connected to a preliminary in-deep knowledge about the considered water system and its subparts. Proper information about the hydraulic patterns are unavoidable to determine the input and output entities of the several devices which constitute a hydraulic system. Moreover, the knowledge of

the supply fonts and the technical and operative properties of the system can permit a truthful estimation of water losses.

A widely adopted method to compile the *Water Balance* was proposed by the International Water Association (IWA) (Hirner and Lambert, 2000), based upon the repartition of the volumes per year (or per quarter, as a function of the considered time scale) into the subcategories summarized in the following Tab. 2.3.

<table>
<tr><td rowspan="8">System Input Volume</td><td rowspan="4">Authorized Consumption</td><td rowspan="2">Billed Authorized Consumption</td><td>Billed Metered Consumption</td><td>Revenue Water</td></tr>
<tr><td>Billed Unmetered Consumption</td></tr>
<tr><td rowspan="2">Unbilled Authorized Consumption</td><td>Unbilled Metered Consumption</td><td rowspan="6">Non-Revenue Water</td></tr>
<tr><td>Unbilled Unmetered Consumption</td></tr>
<tr><td rowspan="4">Water Losses</td><td rowspan="2">Apparent Losses</td><td>Unauthorized Consumption</td></tr>
<tr><td>Metering Inaccuracy</td></tr>
<tr><td rowspan="3">Real Losses</td><td>Leakage on Transmission and/or Distribution Mains</td></tr>
<tr><td>Leakage and Overflows at Utility's Storage Tanks</td></tr>
<tr><td>Leakage on Service Connections up to point of Customer Metering</td></tr>
</table>

**Tab. 2.3 IWA Water Balance scheme (Hirner and Lambert, 2000)**

In Tab. 2.3, each category defines the water volume rate as follows:

- *System Input Volume*: volume inputted into the WDN or into a sub-part of its, composed of:
- *Authorized Consumption*: rate of inputted volume, depleted as authorized consumption, dividable into a) *Billed Authorized Consumption* and b) *Unbilled Authorized Consumption;*
- *Water Losses:* lost rate of water volumes, equal to the difference between the System Input Volume and the Authorized Consumption. They are divided into:
  - *Real Losses:* volumes corresponding to the physical losses of the WDN, depending on the entity, the frequency and the duration of each loss. As analysed in Par. 2.4, this category is composed of the *Background Losses*, the *Reported* and the *Unreported Bursts*. Further ranking is also applied, as a function of the hydraulic system in which the leakages are generated (i.e. main systems, storage tanks, service connections, etc.);

- *Apparent Losses:* complementary ratio to the Real Losses, as indicated in Par. 2.4, they are divided into *Unauthorized Consumption*, referred to lost volumes caused by illegal takings and *Metering Inaccuracies*, composed by unmeasured volumes during the metering acquisition, as both input volumes and users' consumption.

From an economic standpoint, the System Input Volume can be classified into:

- *Revenue Water*: sum of water volumes which provide revenues for the water utility agency;
- *Non-Revenue Water:* sum of volumes which do not produce revenues, corresponding to the sum of Water Losses and of the Unbilled Authorized Consumption.

### 2.5.2 The Bottom-Up Approach: the Minimum Night Flow

The Bottom-Up approach is generally applied to water sub-networks or District Metered Areas (DMAs) (Par. 2.5.5) and it provides the leakage estimation, obtainable through the in-continuous measurement of the *Minimum Night Flow* (*MNF*). It is applicable during the time slots presenting lowest users' demand, namely from 1:00 to 4:00 a.m. (Ratanayaka et al., 2009), in reference to a time period with sufficient duration to collect statistically significant data.

This approach consists in the flow measurement and recording during the night time slot, through provisionally or permanently installed flowmeters. Gate valves are applied to both delimit and isolate the investigated areas. It is applicable as both a water balance method for the estimation of water losses, and a monitoring instrument, by comparing the measured *MNF* with reference parameters from the literature (evaluated as a function of the network length, the users' category, the applied time slot and the annual period in which the measurements are recorded). Specifically, the evidence of higher measured *MNF* than the reference one recommends the development of proper monitoring and location campaigns for leakage detection.

The approach is based upon the consideration that, at night, due to the higher pressures on the network correlated to the low users' demands, the discrepancy between

the inflow measured volumes and the outflow ones can be mainly attributed to the water losses (Fig. 2.6).

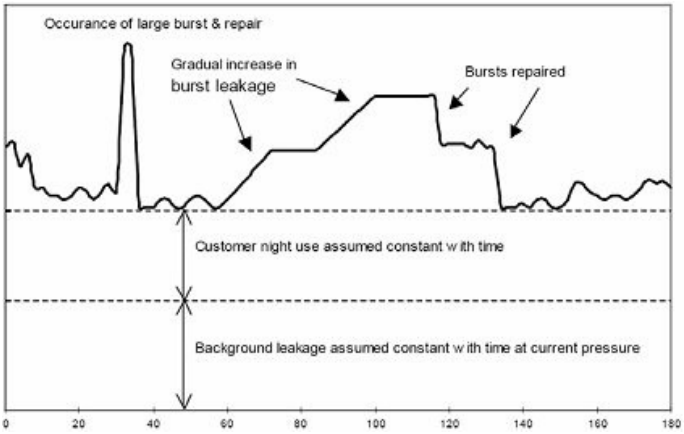


**Fig. 2.6 Minimum Night Flow in a considered area (Morrison, 2004)**

### 2.5.3 Control and Management Practices of Water Losses

Control and management of water losses in WDNs can be assessed according to different approaches:

- *Passive control*, based upon ex-post maintenance interventions, applied when the leakage is already appeared on the ground level, or as a consequence of further dysfunctions referable to it. It provides the restoration of the generated bursts. This approach, on one hand, requires low maintenance costs but, on the other hand, determines the high system susceptibility to the leakage formation, thus exposing the hydraulic system to significant risks of relevant inefficiency;
- *Systematic control,* obtainable through both the application of periodic and systematic detecting campaigns and the inspection of the accessible hydraulic components;
- *Proactive control,* based upon the monitoring, control and intervention of the physical parts which cause significant stresses on the system. It consists in the in-continuous monitoring of inlet flow rates and demands, with the aim of developing dynamic water balances and performing effective leakage control and reduction. The pressure management in WDNs (Par. 2.5.4) can be performed by arranging the

network repartition into District Metering Areas (DMAs) (Par. 2.5.5) and/or the pressure regulation through Pressure Reducing Valves (PRVs) (Par. 2.5.6).

### 2.5.4 Pressure Management in Water Distribution Networks

The operative approach, devoted to the pressure management in WDNs, consists in the smart and dynamic pressure regulation. Against reduced investment and management costs, an effective limitation of water losses and, expressly, of background losses (the most difficult leakage ratio to be detected and suppressed) can be accomplished.

This method is based upon the principle that the WDNs are designed to guarantee the minimum level of service (minimum pressure required to accomplish the users' water demand) during the dynamic operative conditions of the system. Being the maximum water demand achieved only in few daily hours, during the further daily time periods, the pressure results higher than that strictly required to fulfil the users' demand, thus generating significant removable stresses on the hydraulic components. In this regard, a typical daily demand pattern for civil users, is depicted in the following Fig. 2.7 where it can be observed how, during the time steps with users' demand lower than the peak demand, high pressures generate significant solicitations on the system, at the expense of its stability and integrity.

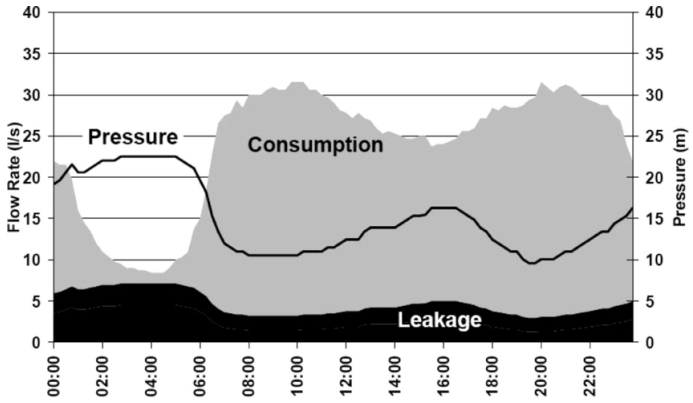


**Fig. 2.7 Demand, pressure and leakage daily patterns (Puust et al., 2010)**

The application of Pressure Management strategies corresponds to an effective leakage management approach (Thornton, 2003), being able to both limit the current amount of water losses and reduce the probability of generating further failures.

In the literature, the analytic correlation between pressures and water leakages expresses the direct relationship between the exceed pressures and the suppressible water losses. It is represented by the well-known *Leakage Law*, defined, according to the classical monomial form, proposed by Lambert (2001), as:

$$Q = \alpha P_r^{\beta} \tag{2.1}$$

where $Q$ is the water leakage, $P_r$ the water pressure, whereas $\alpha$ and $\beta$ are the *Discharge Coefficient* and the *Leakage Exponent*, respectively.

Several studies were carried out to calibrate the $\alpha$ and $\beta$ parameters; among them, Greyvenstein and Van Zyl (2006) considered both the linear correlation between $\alpha$ and the orifice area and the dependance of $\beta$ by both the pipe material and the orifice geometry.

Furthermore, May (1994) developed the Fixed And Variable Discharge (*FAVAD*) model to correlate the acting pressures with the orifice size. On the other hand, De Paola and Giugni (2012) carried out experiments on metallic pipes presenting an orifice with circular and rectangular forms. They calibrated the Leakage Exponent $\beta$ between 0.47 and 0.50, pointing out its numerical variation to be not dependent from the orifice size.

### 2.5.5 District Metering Areas Sectorization

The District Meter Areas (DMAs) approach is based upon the WDNs sectorization into hydraulically separated areas (Cheong, 1993). This scheme is counterpoised to the classical approach of water networks highly interconnected because oriented to the delimitation of separated hydraulic areas, supplied by few inlet points. On them, flowmeters are installed for the district water balance and areas are isolated through gate and shut-off valves (Fig. 2.8). Thus, the DMA approach provides lower elasticity of the hydraulic system, due to the few interconnection, presenting limited capability of assuring the required level of service in presence of failures. On the other hand, benefits from the DMAs sectorization consist in the better control and ability to both detect and isolate the critical areas, at the same time guaranteeing greater capabilities of monitoring the inlet flow rates. In this field, an in-continuous control and monitoring

can be applied to detect the leakage levels for each DMA, developing proper detecting approaches.

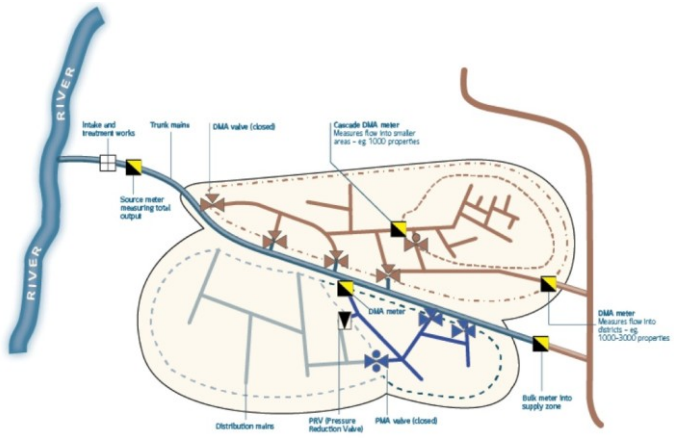


**Fig. 2.8 District Metered Areas sectorization (EU Commission, 2015)**

The DMA sectorization is also able to generate benefits on the water quality, both allowing simpler sample collections for chemical-physical analyses and isolating the warning areas, exposed to accidental or malicious contaminations (Herrera Fernandez, 2011).

The IWA summarized the basic factors for an effective design of the DMAs (Morrison et al., 2007); among them, following aspects result unavoidable: the geometric size and the number of user connections, the required pressure level, the number of valves and flowmeters, the infrastructure characteristics and the existing water loss entities. The repartition of DMAs is applied so to gather hydraulically similar conditions in each district, thus assessing optimal pressure levels. With regard to real networks, the DMA approach should be forerun by preliminary tests to evaluate the hydraulic and secondary effects, determined by the district repartition (Galdiero et al., 2016).

In terms of pressure management, the DMAs sectorization implicates the limitation of water loops into the network, by generating pressure drops able to limit the exceed pressures and, consequently, the background losses. Moreover, by coupling the DMAs repartition with PRVs, a further pressure control is achievable, for both pressure regulation and water loss management.

In the field of the DMA sectorization, the reliability of ER by using micro-turbines or PATs (Par. 2.5.7) can be considered by installing devices for hydropower generation at inlet pipes or reservoirs of the district, as a function of the operating exceed pressure. The flow variability has also to be taken into account, in order to evaluate the device regulation as a function of the dynamic operative conditions of the network.

### 2.5.6 Pressure Regulation through Pressure Reducing Valves

Alternative and/or complementary approach to the DMAs sectorization concerns the application of Pressure Reducing Valves (PRVs), or, rather, further hydraulic devices able to regulate the pressure in WDNs, by generating punctual head losses, in compliance with the required backpressure.

Several operating criteria can be taken into account, depending on the requirement of static or dynamic set points. In the first case, static PRV settings are accounted for assuring, during the dynamic operative conditions in the network, constant pressure, in compliance with the level of service, able to satisfy the users' demand.

Conversely, a time-regulation approach implicates the set point variation, as a function of the dynamic hydraulic regime on the network. This last clearly represents a more accurate criterion, because based upon the PRV modulation, at varying the operative conditions in the system. As an example, the set point diversification could be applied in compliance with the hydraulic variability during the daily time steps, in order to modulate the pressure, in agreement with the dynamic users' demand.

Further standards are based upon the regulation of valve settings, in compliance with the real-time hydraulic behaviour of the network, so to realize a flow modulation through Supervisory Control And Data Acquisition (SCADA) systems (Fanner et al., 2007; Fontana et al., 2016) for Real Time Control (RTC), data collection and elaboration.

In the field of SCADA application for water system management, Ramirez-Llanos and Quijano (2009) introduced an adaptive controller in WDNs with the aim of dynamically regulating the system operations against the e-coli bacterial circulation. An algorithm for PRV applications was implemented, comparing the proposed approach

with results from a PID regulation. Li and Li (2010) carried out a technical analysis of the installation of SCADA systems in WDNs in China, developing a leakage detection model, based upon both the cluster-analysis and the fuzzy pattern recognition theorem. Stoian et al. (2010) proposed an original architecture, named "SCADA federation", for data acquisition, measurement and control, devoted to both hydropower generation and water management, implementing a hierarchic structure based upon two basic models: the observability and the controllability. Wu et al. (2011) integrated a SCADA system with a hydraulic simulation model to develop a RTC in WDNs, whereas Campisano et al. (2012) implemented a method to calibrate a RTC model for pressure valves, aimed at decreasing the water losses in WDNs.

Moreover, Kang (2014) applied a SCADA system to find out the optimal solution of the pump scheduling issue in WDNs, by combining the hydraulic solver EPANET 2.0 (Rossmann, 2000) with an optimization Genetic Algorithm (De Jong, 1975; Goldberg, 1989). Cheng et al. (2014) generated a field data interface between a SCADA system and a computer simulation model, by testing the proposed approach to the Guangzhou (CH) WDN. The model was composed of three modules: a SCADA system, able to handle the data acquired from sensors, the real-time solver server, for data storing and optimization, and the client terminal, operating as a real-time DSS.

In reference to real WDNs, as a consequence of their topological complexity and significant variability and uncertainty of users' demand, based on dynamic hourly and seasonal patterns, the application of optimization procedures results strongly widespread, for both DMAs sectorization and PRVs location and setting. In this field, the use of optimization criteria, supported by the evoluation of the computational potentialities, allowed, during the last decades, to develop several optimization models, able to combine admissible solutions with acceptable computational time-consuming. For complex systems, exhaustive models result barely applicable, therefore simplified models have been proposed (Alperovits and Shamir, 1977; Kessler and Shamir, 1989; Pecci et al., 2015; Menke et al., 2016).

Moreover, the application of meta-heuristic evolutionary algorithms results widely considered, because able to the define feasible solutions, with respect to the imposed

physical and technical constraints, in tolerable computational times (De Paola et al., 2016a). Among them, natural inspired algorithms, such as Genetic Algorithm, Simulated Annealing (Kirkpatrick et al., 1983; Cunha and Sousa, 2001), Tabu Search (Glover, 1989, 1990), Ant Colony Optimization (Dorigo et al., 1996) and Harmony Search (Geem, 2002; De Paola et al. 2016a,b) procedures, were widely applied in WDNs to optimize a) the pressure regulation (Savic and Walters, 1997), b) the DMA sectorization (Galdiero, 2015), c) the PRVs location and setting (Creaco et al., 2010; Giugni et al., 2014), d) the Pump Scheduling (De Paola et al., 2016b) and e) the Energy Recovery (Giugni et al., 2009; Corcoran et al., 2016).

### 2.5.7 Energy Recovery in Water Distribution Networks

In the field of the innovative management criteria of WDNs, the potentiality, related to small-scale hydropower generation in WDNs, was analysed to benefit of the exceed pressure, otherwise dissipated through regulation valves, to generate electrical power (Ramos and Borga, 1999; Arriaga, 2010, Sammartano et al. 2016a). This approach allows to combine the modulation of the exceed pressure in the networks (with the aforementioned hydraulic and operative advantages) with the generation of sustainable and environmental energy.

During the last years, the technical and economical feasibility of substituting regulation valves with devices for hydropower generation in WDNs, such as micro-turbines and Pumps As Turbines (PATs) is finding effective interest. Specifically, several operative and theoretical applications were developed (Giugni et al., 2009; Motwani et al., 2013), aiming at analysing both the technical effectiveness and the economical sustainibilty connected to the generation of small-hydropower in urban and rural areas.

In this field, the evaluation of the hydropower generation in WDNs is in-deep introduced and discussed in the following Chapter 3. In it, the attention is specifically drawn to both the main peculiarities connected to the ER in WDNs and the evaluation of PAT characteristics and performances, aiming at contributing to the knowledge of their applications, which represents the main focus of this Ph.D. work.

# References


- Ahn J.C., Lee S.W., Lee G.S., Koo J.Y. (2005). Predicting water pipe breaks using neural network. *Water Science and Technology: Water Supply*, 5(3-4), 159-172.
- Alegre H., Hirne W., Baptista J.M., Parena R. (2000). Performance indicators for water supply services. Manual of Best Practice Series, 1st ed., IWA Publishing, London.
- Alperovits E., Shamir U. (1977). Design of optimal water distribution systems. *Water Resources Research*, 13(6), 885-900. http://dx.doi.org/10.1029/WR013i006p00885
- Arriaga M. (2010). Pump As Turbine – A pico-hydro alternative in Lao People's Democratic Republic. *Renewable Energy*, 35, 1109-1115. http://dx.doi.org/10.1016/j.renene.2009.08.022
- Campisano A., Modica C., Vetrano L. (2012). Calibration of proportional controllers for the RTC of pressures to reduce leakage in water distribution networks. *Journal of Water Resources Planning and Management*, 138(4), 377–384. http://dx.doi.org/10.1061/(ASCE)WR.1943-5452.0000197
- Cheng W.P., Yu T.C., Xu G. (2014). Real-time model of a large-scale water distribution system. Procedia Engineering, 89, 457-466. http://dx.doi.org/10.1016/j.proeng.2014.11.212
- Cheong L.C. (1993). International report on unaccounted for water and economics of leak detection. *Proceedings of the IWA World Conference*, Budapest, Hungary.
- Consolidated Law No.1775/1933. Testo Unico sulle Disposizioni di Legge sulle Acque e Impianti Elettrici (in Italian).
- Corcoran, L., McNabola, A., Coughlan, P. (2016). Optimization of water distribution networks for combined hydropower energy recovery and leakage reduction. *Journal of Water Resources Planning and Management*, 142(2), 04015045. http://dx.doi.org/10.1061/(ASCE)WR.1943-5452.0000566
- Creaco E., Franchini M., Alvisi S. (2010). Optimal placement of isolation valves in Water Distribution systems based on valve cost and weighted average demand shortfall. *Water Resources Management*, 24(15), 4317-4338. http://dx.doi.org/10.1007/s11269-010-9661-5.
- Cunha M.D.C., Sousa J. (2001). Hydraulic infrastructures design using simulated annealing. *Journal of Infrastructure Systems*, 7(1), 32-39. http://dx.doi.org/10.1061/(ASCE)1076-0342(2001)7:1(32)
- De Jong K.A. (1975). An analysis of the behaviour of a class of genetic adaptive systems. *Ph.D. Thesis*, University of Michigan Ann Arbor, USA.
- De Paola F., Giugni M., Galdiero E. (2012). Una ricerca sperimentale sulla relazione tra pressioni e perdite idriche per differenti tipologie di condotte. *Proceedings of the H2O Conference*, 23rd-25th June 2012, Ferrara, Italy (in Italian).
- De Paola F., Galdiero E., Giugni M. (2016a). A jazz based approach for optimal setting of pressure reducing valves in water distribution networks. *Engineering Optimization*, 48(5), 727-739. http://dx.doi.org/10.1080/0305215X.2015.1042476
- De Paola F., Fontana N., Giugni M., Marini G., Pugliese F. (2016b). An application of the Harmony-Search Multi-Objective (HSMO) optimization algorithm for the solution of pump scheduling problem. *Procedia Engineering*, 162, 494-502. http://dx.doi.org/10.1016/j.proeng.2016.11.093

- Dorigo M., Maniezzo V., Colorni A. (1996). Ant system: optimization by a colony of cooperating agents. *IEE Transactions on Systems, Man and Cybernetics, Part B: Cybernetics*, 26(1), 29-41. http://dx.doi.org/10.1109/3477.484436
- European Union Commission (2015). EU reference document Good Practices on Leakage Management WFD CIS WG PoM. Main Report. Office for Official Publications of the European Communities. http://dx.doi.org/10.2779/102151
- Fanner P., Sturm R., Thornton J., Liemberger R. (2007). Leakage Management Technologies. *AWWA Research Foundation*, Denver, Colorado, USA.
- Fontana N., Giugni M., Glielmo L., Marini G. (2016). Real time control of a prototype for pressure regulation and energy production in water distribution networks. *Journal of Water Resources Planning and Management*, 142(7), 04016015, 19. http://dx.doi.org/10.1061/(ASCE)WR.1943-5452.0000651
- Galdiero E. (2015). Multi-Objective Design of District Metered Areas in Water Distribution Networks. *Ph.D. Thesis*, University of Naples Federico II, Naples, Italy.
- Galdiero E., De Paola F., Fontana N., Giugni M., Savic D. (2016). Decision support system for the optimal design of district metered areas. *Journal of Hydroinformatics*, 18(1), 49-61. http://dx.doi.org/10.2166/hydro.2015.023
- Geem Z.W., Kim J.H., Loganathan G.V. (2002). Harmony search optimization: application to pipe network design. *International Journal of Modelling and Simulation*, 22(2), 125-133.
- Giugni M., Fontana N., Portolano D. (2009). Energy saving policy in water distribution networks. *Proceedings of the International Conference on Renewable Energies and Power Quality ICREPQ' 09*, 15th-17th April 2009, Valencia, Spain.
- Giugni M., Fontana N., Ranucci A. (2014). Optimal location of PRVs and turbines in water distribution networks. *Journal of Water Resources Planning and Management*,140(9), 06014004. http://dx.doi.org/10.1061/(ASCE)WR.1943-5452.0000418
- Glover F. (1989). Tabu Search - Part 1. *Journal on Computing*, 1(3), 190–206.
- Glover F. (1990). Tabu Search - Part 2. *Journal on Computing*, 2(1), 4–32.
- Goldberg, D.E. (1989). Genetic Algorithms in Search, Optimization and Machine Learning, *Addison-Wesley Longman Publishing Co*., Inc. Boston, Massachusetts, USA.
- Goulter I.C., Davidson J., Jacobs P. (1993). Predicting water-main breakage rates. *Journal of Water Resources Planning and Management*, 119(4), 419-436. http://dx.doi.org/ 10.1061/(ASCE)0733-9496(1993)119:4(419)
- Greyvenstein B., Van Zyl J.E. (2006). An experimental investigation into the pressure – leakage relationship of some failed water pipes. *Journal of Water Supply: Research and Technology – AQUA*, 56(2), 117-124. http://dx.doi.org/10.2166/aqua.2007.065
- Harada H. (1988). Statistics of the cold wave in the temperate region and prediction of the number of damaged service pipes. *Journal of American Water Works Associations*, 57(8), 12-15.
- Herrera Fernandez A.M. (2011). Improving water network management by efficient division into supply clusters. *Ph.D. Thesis*, Universitat Politecnica de Valencia, Spain.

- Hirner W., Lambert A.O. (2000). Losses from Water Supply Systems: Standard Terminology and Recommended Performance Measures. IWA website: http://www.iwahq.org.uk/bluepages.
- Italian Law No. 319/1976 (Merly's Act). Norme di tutela delle acque dall'inquinamento (in Italian).
- Italian Law No. 183/1989. Norme per il riassetto organizzativo e funzionale della difesa del suolo (in Italian).
- Italian Law No. 36/1994 (Galli's Act). Disposizioni in material delle risorse idriche (in Italian).
- Italian Law No. 42/2010. Conversione in legge, con modificazioni, del decreto-legge 25 gennaio 2010, n. 2, recante interventi urgenti concernenti enti locali e regioni (in Italian).
- Italian Legislative Decree No. 152/2006 (Italian Environmental Unique Law). Testo Unico Ambientale. Norme in Materia Ambientale.
- Italian Master Plan of Water Systems P.R.G.A. Law No. 129/1963. Piano Regolatore Generale degli Acquedotti e delega al governo ad emanare le relative norme di attuazione (in Italian).
- Italian Ministerial Decree No. 97/1999. Regolamento sui criteri e sul metodo in base ai quali valutare le perdite degli acquedotti e delle fognature (in Italian).
- Italian National Institute of Statistics (2014). Censimento delle acque per uso cvile. Anno 2012. Statistiche Report (in Italian). ISTAT website: http://www.istat.it/it/files/2014/06/2014_06_26_Report_censimento_acqua.pdf?title=Censimento+delle+ac-
- Italian Prime Ministerial Decree 04/03/1996 (implementation of Law No. 36/1994). Disposizioni in materia di risorse idriche (in Italian).
- Kang D. (2014). Real-time optimal control of water distribution systems. *Procedia Engineering*, 70, 917-923. http://dx.doi.org/10.1016/j.proeng.2014.02.102
- Kessler A., Shamir U. (1989). Analysis of the linear programming gradient method for optimal design of water supply networks. *Water Resources Research*, 25(7), 1469-1480. http://dx.doi.org/10.1029/WR025i007p01469
- Kirkpatrick S., Gelatt C.D., Vecchi M.P. (1983). Optimization by Simulated Annealing. *Science,* 220, 671–680. http://dx.doi.org/10.1126/science.220.4598.671
- Lambert A.O. (1994). Accounting for losses: the bursts and background concept. *Water and Environment Journal*, 8(2), 205-214. http://dx.doi.org/10.1111/j.1747-6593.1994.tb00913.x
- Lambert A.O., Brown T.G., Takizawa M., Weimer D. (1999). A review of performance indicators for real losses from water supply systems. *Journal of Water Supply: Research and Technology – AQUA*, 48, 227-237.
- Lambert A.O. (2001). What do we know about pressure: leakage relationships in distribution systems?. *IWA Conference on System Approach to Leakage Control and Water Distribution Systems Management*, May 2000, Brno, Czech Republic.
- Law No. 2248/1865. Legge sulle Opere Pubbliche. Attachment F (in Italian).

- Li X., Li G-J. (2010). Leak detection of municipal water supply network based on the cluster-analysis and fuzzy pattern recognition. *Proceedings of the E-Product E-Service and E-Entertainment International Conference ICEEE 2010*, 7th-9th November 2010. http://dx.doi.org/ 10.1109/ICEEE.2010.5660550
- May J. (1994). Pressure dependent leakage. *World Water and Environmental Engineering*, October.
- Menke R., Abraham E., Parpas P., Stoianov I. (2016). Exploring optimal pump scheduling in water distribution networks with branch and bound methods. *Water Resources Management*, 30, 5333-5349. http://dx.doi.org/10.1007/s11269-016-1490-8
- Morrison J. (2004). Managing leakage by district metered areas: a practical approach. *Water21*, 6.1, 44-46.
- Morrison J., Tooms S., Rogers D. (2007). DMA Management guidance notes. *IWA Publication*.
- Normative Reforms 1916-19. Disposizioni sulla derivazione ed utilizzazione di acque pubbliche, norme di giurisdizione, e di procedura (in Italian).
- Motwani K.H., Jain S.V., Patel R.N. (2013). Cost analysis of Pump As Turbine for pico hydropower plants – a case study. *Procedia Engineering*, 51, 721-726. http://dx.doi.org/10.1016/j.proeng.2013.01.103
- Pecci F., Abraham E., Stoianov I. (2015). Mathematical programming methods for pressure management in water distribution networks. *Procedia Engineering*, 115, 937-946. http://dx.doi.org/10.1016/j.proeng.2015.08.974
- Portolano D. (2008). Il controllo delle perdite nei sistemi acquedottistici: criteri innovativi di gestione. *Ph.D. Thesis* in Analisi dei Sistemi Ambientali, University of Naples Federico II, Naples, Italy (in Italian).
- Puust R., Kapelan Z., Savic D., Koppel T. (2010). A review of methods for leakage management in pipe networks. *Urban Water Journal*, 7(1), 25-45. http://dx.doi.org/10.1080/15730621003610878
- Ramirez-Llanos E., Quijano N. (2009). E. Coli bacterial foraging algorithm applied to pressure reducing valves control. *Proceedings of American Control Conference ACC 2009*, Curran Associates, Red Hook, NY, 10–12. http://dx.doi.org/10.1109/ACC.2009.5160549
- Ramos H.M., Borga A. (1999). Pumps As Turbines: an unconventional solution to energy production. *Urban Water*, 1, 261-263. http://dx.doi.org/10.1016/S1462-0758(00)00016-9
- Ratnayaka D.D., Brandt M.J., Johnson M. (2009). Twort's water supply. (6th ed.). Oxford: Butterworth-Heinemann.
- Rossmann L. (2000). EPANET 2 users manual. U.S. Environmental Protection Agency, Cincinnati, OH, 2000.
- Sammartano V., Sinagra M., Spada E., Tucciarelli T. (2016a). Regolazione delle pressioni mediante produzione di energia idroelettrica nelle reti di distribuzione. *Proceedings of the 35th Convegno Nazionale di Idraulica e Costruzioni Idrauliche*, 14th-16th September 2016, Bologna, Italy. http://dx.doi.org/10.6092/unibo/amsacta/5400

- Savic D.A., Walters G.A. (1997). Genetic Algorithms for Least-Cost Design of Water Distribution Networks. *Journal of Water Resources Planning and Management*, 123(2), 67-77. http://dx.doi.org/10.1061/(ASCE)0733-9496(1997)123:2(67)
- Shamir U., Howard C.D.D. (1979). An analytical approach to scheduling pipe replacement. *Journal of American Water Works Associations*, 71, 248–258.
- Stoian I., Stancel E., Ingat S., Balogh S. (2010). Federative SCADA – Solution for evolving critical systems. *Control Engineering and Applied Informatics*, 12(3), 52-58.
- Su Y.C., Mays L.W., Duan N., Lansey K.E. (1987). Reliability based optimization model for water distribution systems. *Journal of Hydraulic Engineering*, 114(12), 1539-1556. http://dx.doi.org/10.1061/(ASCE)0733-9429(1987)113:12(1539)
- Thornton J. (2003). Managing leakage by managing pressure: a practical approach. *Water21*, 5.5, 43-44.
- Wu W., Gao J., Yixing Y., Hongbin Z., Kui C. (2011). Water Distribution Network Real-Time Simulation Based on SCADA System using OPC Communication. *Proceedings of the 2011 International Conference on Networking, Sensing and Control*, 11th-13th April 2011, Delft, The Netherlands.

# Chapter 3

# Energy Recovery in Water Distribution Networks

The Energy Recovery (ER) in Water Distribution Networks (WDNs) represents a relevant topic in the field of the Best Management Practices (BMPs) of hydraulic systems, and specifically of WDNs, because devoted to both the reduction of the exceed pressure (*Pressure Management*) and the hydropower generation. It is based on benefitting of pressure energy, otherwise dissipated by regulation valves. In this field, the ER is actually recognized as a basic contributor factor of the energy life cycle of WDNs (Filion et al., 2004), being included in the operative approach defined as *Proactive control* of WDNs (Par. 2.5.3).

In this regard, the application of micro-turbines or Pumps As Turbines (PATs) is considered to realize Small-scale HydroPower (SHP) systems in WDNs. According to the European Small Hydropower Association (ESHA, 2005), the categories in Tab. 3.1 are defined to classify the hydropower plants.

| **Hydropower Category** | **Power *P*** |
|---|---|
| Pico – Hydro | < 5kW |
| Micro – Hydro | 5 – 100 kW |
| Mini - Hydro | 100 kW – 1 MW |
| Small - Hydro | 1 – 10 MW |
| Medium - Hydro | 10 – 100 MW |
| Large - Hydro | > 100 MW |

**Tab. 3.1 Categories of hydropower plants (ESHA, 2005)**

According to the above categories, the Energy Recovery in WDNs, by using micro-turbines or PATs, in compliance with the dispersible pressure, allows to realize pico,

micro or mini-hydro plants, representing an effective point of convergence between the pressure control for leak reduction and the energy recovery in urban areas (Giugni et al., 2009).

## 3.1 Micro-Turbines for Hydropower Generation in Water Distribution Networks

Installation of micro-turbines for hydropower generation in WDNs, namely Energy Recovery Turbines (ERTs), implies the use of devices which convert a portion of water energy pressure into mechanical power to be utilized to drive an electricity generator (Paish, 2002). The mechanical power produced by turbines can be evaluated as a function of the head drop $H_t$ and the flow rate $Q_t$, according to the following Eq. (3.1).

$$P_t = \eta_t \gamma_w Q_t H_t \tag{3.1}$$

where $P_t$ is the generated power (W), $\eta_t$ is the overall efficiency of turbine (-), $\gamma_w$ the specific weight of water ($Nm^{-3}$), $Q_t$ the flow rate ($m^3s^{-1}$) and $H_t$ the effective head drop across the turbine (m).

The micro-turbine selection for hydropower generation in WDNs necessitates of proper technical-economic analyses to assure the compatibility of the generated head drops $H_t$ with the set backpressure to guarantee at each delivery point, at varying the operative conditions in the network.

Among the turbine models commercially available, in WDNs reaction turbines are more reliable because working with the runner always within a totally water-filled casing, allowing to guarantee the required set pressure at the delivery points. These models are composed of a draft tube, which operates as a diffuser to discharge the water by reducing the static pressure and generating the increase of the effective head. Francis (Fig. 3.1), Propeller and Kaplan (Fig. 3.2) micro-turbines are mainly applicable in WDNs, even though impulse micro-Pelton turbines could be considered for small-scale hydropower generation (Jain and Patel, 2014).

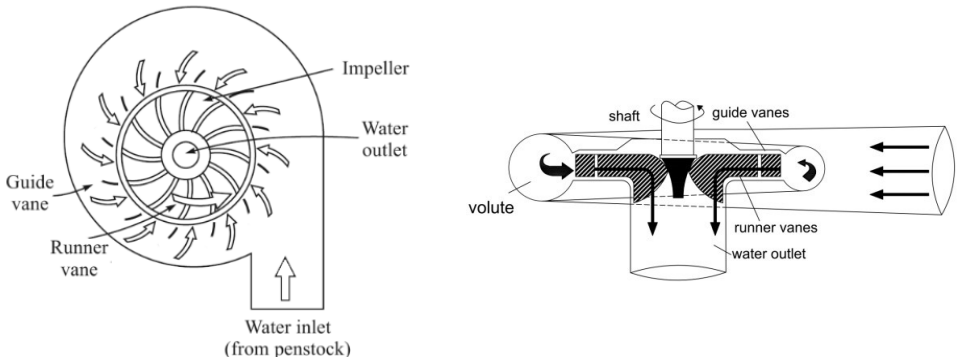


**Fig. 3.1 Schematic flow and cross section for Francis turbine**

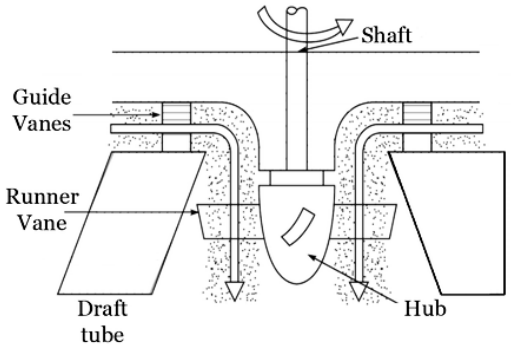


**Fig. 3.2 Schematic flow for Kaplan turbine**

Several applications to real WDNs are actually available. Zakkour et al. (2002) estimated a potential power of about 17 MW obtainable by the Energy Recovery in the UK water industry networks, manageable through the installation of micro-turbines. In Portland (USA) WDN, a micro-turbine with Nominal Power *NP* = 30 kW, able to produce 94 $MWhyear^{-1}$, was installed for pressure management and micro-hydropower generation (Lisk, 2012). The PolyU's Department of Building Services Engineering and the Water Supplies Department (WSD, 2012) of the Hong Kong Special Administrative Region projected the installation of an eight-blade spherical inline turbine for the Hong Kong WDN, estimating a yearly production of 700 $kWhyear^{-1}$. Corcoran et al. (2012) analyzed the hydropower potential of the WDN in the Dublin region, verifying the economical feasibility of installing small hydropower with micro-turbines. A satisfying potential of the network was observed, pointing out the necessity of more accurate

analyses to evaluate both the flow and demand variations and the installation and managing costs.

Analyses about ER in urban areas were also developed by Su and Karney (2014), referred to the installation of a micro-turbine in Vancouver (CA) WDN, pointing out how the economic feasibility of the considered approach was strictly dependent on several factors, related to the hydraulic system and the performances of the considered equipment.

Concerning small-sized urban centers, Sitzenfrei et al. (2015) developed a numerical analysis to estimate the potential ER in an Alpine WDN which supplies about 2000 inhabitants. Installation of PATs or micro-turbines was considered, verifying the capability of reaching mariginal additional profits through the installation of multiple small-scale hydropower systems. Indirect economical benefits were observed when hydropower generation was taken into account in the WDN, as well.

Sammartano et al. (2016b) developed a design procedure to modify a Banki micro-turbine, for determining outlet pressures higher than zero, with the aim of testing its application for both ER and pressure regulation in WDNs. Banki turbine model presented the advantage of reaching efficiencies comparable with Francis one, presenting a simpler geometry, as well. The real application to a water district in Palermo (IT) municipality was tested, showing the capability of the developed approach to convert most of the exceed pressure in electrical energy, in case of effective design flow rates (Sammartano et al., 2016a).

The real case of the large WDN supplying the Fribourg city (SW) was analysed by Samora et al. (2016a), instead. They estimated the hydropower potential derivable from the installation of micro-turbines, specifically developing a model of five-blades tubular propellers (5BTPs). An optimization procedure was applied to detect the optimal turbine location in the network, able to maximize the economical payback. In greater detail, a potential power of about 60.5 $MWhyear^{-1}$ was estimated, by installing a single turbine, whereas a maximum generable energy of 136.2 $MWhyear^{-1}$ was reachable by installing four equal 5BTPs. The energy potential, connected to the installation of a 5BTP, was also evaluated, in reference to a sub-grid of the Lausanne (SW) WDN,

which pointed out a potential ER of about 55 MWhyear$^{-1}$ of the network (Samora et al., 2016b).

## 3.2 Pumps As Turbines for Hydropower Generation in Water Distribution Networks

The use of Pumps As Turbines (PATs) consists in the application of pumps commercially available, operating by inverting the flux direction across the turbo-machine (Fig. 3.3) and using the motor as alternator to generate electrical power (Chapallaz et al., 1992). The opportunity of using pumps operating in reverse mode was firstly considered during the first half of the XX Century (Thoma and Kittredge, 1931), albeit only starting from the last decades several theoretical-experimental investigations have been performed to verify the potentialities related to their application in WDNs (Ramos and Borga, 1999; De Marchis et al., 2014) for hydropower generation.

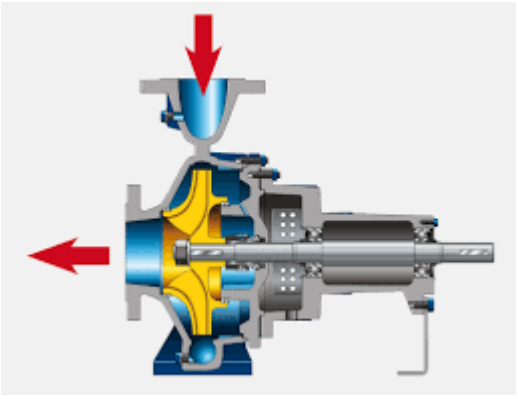

**Fig. 3.3 Cross section of a centrifugal Pump As Turbine (Nautiyal et al., 2010a)**

The ER through PATs and the optimal selection and management of the most appropriate model cannot disregard an in-deep feasibility analysis of the technical and economical sustainability related to the PATs installation. The knowledge of performances, of various pump models commercially available, aims at individuating the allowable operative ranges, compatible with both the available pressure drops $H_t$ and the dynamic operative conditions of the WDNs.

The performance characteristic curves of pumps operating in reverse mode present typical monotonic increasing trends for both head drop $H_t$ (Fig. 3.4a) and produced

power $P_t$ (Fig. 3.4b) at increasing the flow rate $Q_t$, being the subscript $t$ referred to the operations in turbine mode. For the evaluation of the efficiency $\eta_t$ function, a bell-shaped curve is usually determined, instead, showing an increasing branch up the flow rate $Q_{tb}$, correspondent to the Best Efficiency Point (BEP) $\eta_{tb}$ (or maximum efficiency), and a decreasing one for flow rates higher than $Q_{tb}$ (Fig. 3.5).

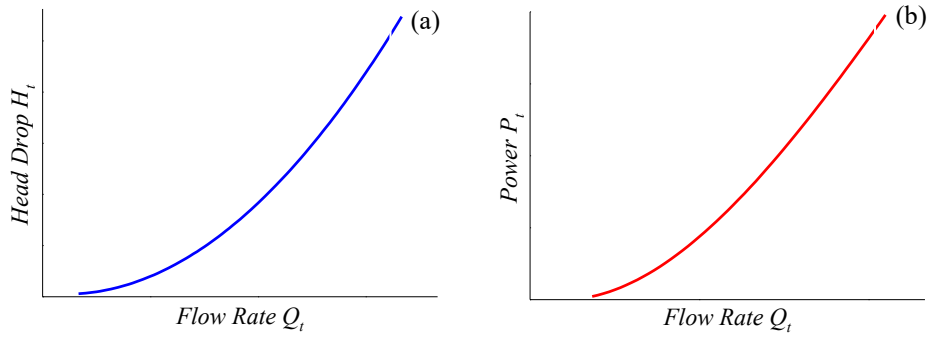


**Fig. 3.4 (a) $H_t(Q_t)$ and (b) $P_t(Q_t)$ PAT characteristic curves**

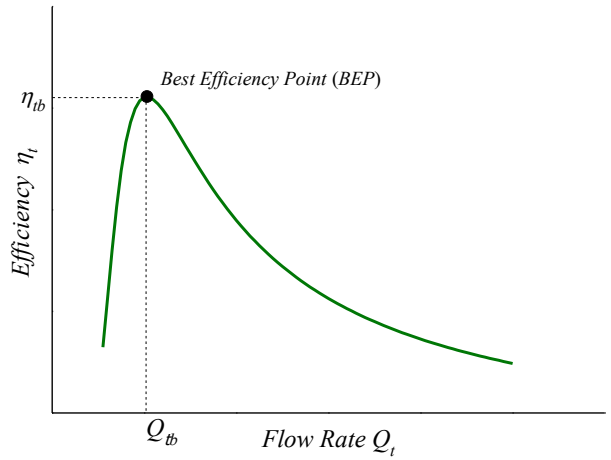


**Fig. 3.5 $\eta_t(Q_t)$ PAT characteristic curve**

Comparison between micro-turbines and PATs efficiency curves (Fig. 3.6) points out that these lasts are usually characterized by lower performances and operative flexibility, due to the internal configuration optimized for the standard use in pump mode. At the same time, the absence of the distributor device represents a limitation for the PATs elasticity, at varying the flowing rate.

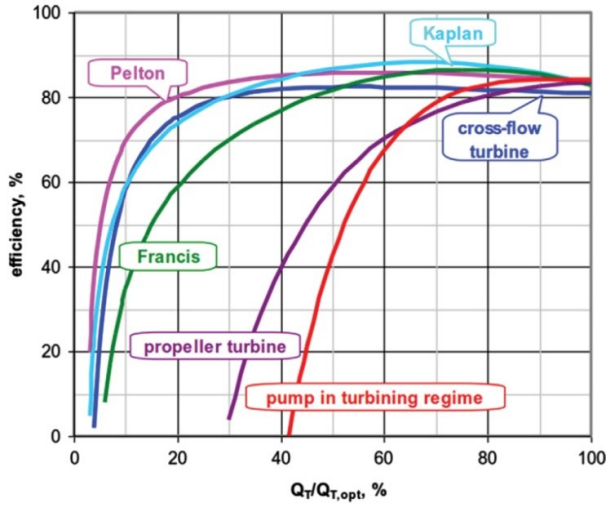


**Fig. 3.6 Performance comparison between PAT and conventional turbines (Jain and Patel, 2014)**

Nevertheless, in WDNs the abovementioned operative limitation can be partially overtaken by arranging specific hydraulic and/or electrical regulations (Par. 3.2.2).

On the contrary, the PAT use requires lower investment and management costs (Nautiyal et al., 2010a) with capital payback periods highly shorter than those required for micro-turbine application. In this regard, Motwani et al. (2013), from an economic analysis on the PAT use for small-hydro generation in India, estimated few years capital payback period, with respect to many years required from the use of micro-turbines. Alatorre-Frenk (1994) carried out a cost analysis to compare the cost benefits of PATs and micro-turbines installation, pointing out, under the hypothesis of the same life cycle, the large cost reduction for PATs, such to widely compensate the lower technical performances (such as lower operative elasticity) than those provided by conventional micro-turbines.

Conversely, as basic issue, the PATs application is usually characterized by limited knowledge about their performances, as a consequence of the lack of information about the characteristic curves, rarely provided by manufacturers (Williams, 1996). Moreover, the actual status of research, about the pump use in reverse mode, results inadequately widespread for predicting the performances of the wide set of pump models, commercially available and useable for running as turbines.

For PAT installation in WDNs, the selection of the effective model has to be accomplished, taking carefully into account the flow rate variations in the system, in order to verify the reliability of the generated head drops $H_t$, with the required set pressure at each delivery point of the network.

In this field, as a preliminary tool to define the pump models useable in reverse operations, the chart in Fig. 3.7 can be considered (Chapallaz et al., 1992). It allows to evaluate the most appropriate model, as a function of both the flow rate $Q_t$ and the head drop $H_t$, this last intended as the difference between the PAT intake and outlet head, minus the head losses generated across the penstock (Isbasoiu et al., 2007).

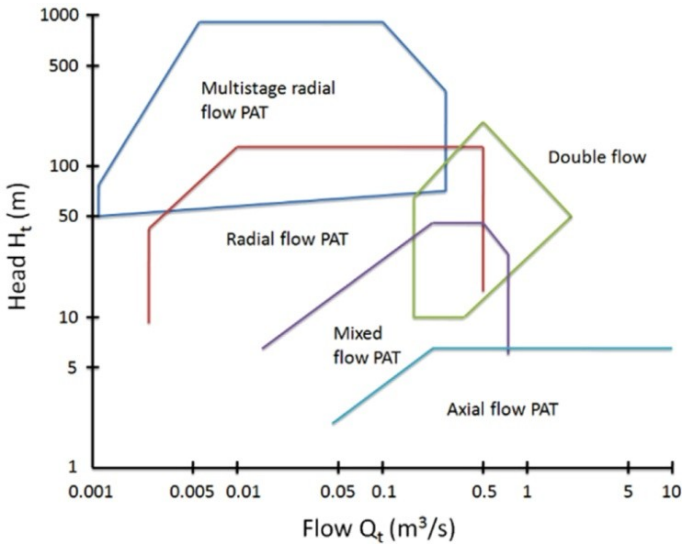


**Fig. 3.7 Operative fields of Pumps As Turbines (Jain and Patel, 2014)**

Hence, for highest $Q_t$ values and lowest $H_t$, the axial flow models are applicable, usually for head drops $H_t$ up to few meters. For higher head drops $H_t$ (in the order of tens of meters), mixed and radial flow models result to be more suitable, whereas the Multi-Stage radial configuration results to be the most appropriate in case of the highest head drops $H_t$.

Concerning the PAT application to WDNs supplying small-medium sized urban and rural centers, the use of radial flow PATs (according to Single-Stage or Multi-Stage configurations) results to be widely considered, because able to combine low-medium flow rates with generated head drops, compatible with the fulfilment of the required

pressure at the delivery points. In greater detail, in the following Par. 3.2.1 several applicative case-studies are reported.

### 3.2.1 PAT Application in Water Distribution Networks

During the last decades, the application of PATs for ER in WDNs is drawing increasing attention. In this regard, several case-studies have been developed to estimate the technical and economic distinctions when PATs are used for both small-scale hydropower generation and pressure regulation.

Maher et al. (2003), from an extensive analysis about the development of sustainable approaches for rural electrification in Kenya, pointed out how the hydropower generation was the low-cost investment approach for procuring and realizing civil works, assuring low environmental impacts, as well. A pico-hydro plant was installed for electrification of about 110 rural households, by applying a centrifugal PAT with modified impeller to guarantee high efficiencies. It was found the PAT installation as the best site-independency solution, with lower investment and maintenance costs (equal to about 15% for each produced kWh) than those connected to solar systems.

Chuenchooklin (2006) carried out an economic analysis for pico-hydropower generation in Thailand by using PATs, to produce electricity for the indoor electrical devices, such as electric lights and some house-ware appliances. An economic recovery period of 6 years was estimated to compensate the initial investment.

A numerical approach was applied by Giugni et al. (2009), instead. They developed a preliminary economic analysis for PAT installation at the "Napoli Est" WDN in Naples (IT), instead of PRVs for both pressure regulation and energy production. Significant profits and attractive capital payback periods were assessed, by guaranteeing improvements, in terms of pressure regulation, comparable with those achievable by using PRVs.

Concerning small sized rural areas, a PAT was installed at the Kinko Village (TZ) water network to generate electrification for about 100 households, financed by the United Nations Industrial Development Organization (UNIDO, 2010). No continuous monitoring was realized to estimate the performances but an overall PAT efficiency, ranging between 64% and 80%, was assessed for the applied hydraulic operations.

Similar approach was considered by Arriaga (2010), who evaluated the application of PATs for hydropower generation in the Lao People's Democratic Republic in South East Asia to furnish electricity to isolated communities with few inhabitants. Their activation was taken into account in case of insufficient energy provided by pico-hydropower turbines and/or too expensive investment costs for traditional turbines. Several solutions were analysed, such as the installation of pico-hydro propeller turbines or cross flow turbines, finding the use of PATs as the most advantageous approach, because able to provide a high-quality service, against both limited costs and long-life operations.

Garcia et al. (2010) verified the installation of PATs in the medium sized WDNs of Murcia and Elche (ES) to realize both the pressure regulation and the hydropower generation, in reference to flow rates between 55 $ls^{-1}$ and 85 $ls^{-1}$. Good experimental-numerical correlations were observed, by applying both the theoretical models of Williams (1994), Fernandez et al. (2004) to quantify the operative conditions at BEP and the Derakhshan and Nourbakhsh (2008a) approach to estimate the characteristic curves of the installed turbo-machines (Par. 3.3.2).

Motwani et al. (2013) performed a cost analysis to compare both the PAT and the Francis turbine installation for hydropower generation in rural areas in India. The annual life cycle cost was assessed for both approaches, defining costs for PATs of about 80% lower than those related to the use of turbines. Payback periods resulted to be shorter, as well, inducting to the choice of PAT installation, because of the lower installation and maintenance costs. Comparable results were observed by Loots et al. (2014), who analyzed the hydropower potential in the Tshwane (SA) WDN, evaluating the high potential of the network to ER, as a consequence of the high pressure level acting on the network. Both micro-turbines and PATs were considered, resulting these lasts the most suitable solution, in terms of both investment and maintenance costs and capital payback periods.

As for Giugni et al. (2009), Tricarico et al. (2013) developed a numerical optimization procedure for pressure regulation and ER in WDNs, by analyzing the overall economical benefits, correlated to the PAT installation on the WDN main pipes.

The Sorrento Peninsula (IT) WDN was tested by using the EPANET 2.0 hydraulic solver, pointing out the advantages derived by the use of PATs, instead of PRVs. Specifically, the energy produced by the PATs was able to cover the energy costs connected to the pumping stations in the Sorrento Peninsula (IT) WSS. Furthermore, Jafari et al. (2015) developed a meta-heuristic optimization procedure to optimize the pressure regulation in WDNs, analysing the feasibility of substituting PRVs with PATs for hydropower generation. The real case of the Andishe (IR) WDN was tested for defining the optimal PATs location, estimanting a daily production of about 7300 kWh, equal to potential benefits (from the electricity sales) of about 133000 $ per year.

Puleo et al. (2014) implemented a steady-state hydraulic model to evaluate the application of PATs in WDNs, by testing it on a Palermo (IT) DMA. The private tanks were considered in the application, by developing three operative scenarios, as a function of the PAT location. The solution with a PAT installed downstream the DMA inlet node, combined with the installation of PATs in further significant links, resulted the best configuration, able to operate at high energy efficiency.

By following the numerical approach, Fecarotta et al. (2015) evaluated the economic benefits connected to the replacement in WDNs of regulation valves with PATs. The WDN by Jowitt and Xu (1990) was taken into account as case study, according to the solution by Araujo et al. (2006). The VOS approach (Carravetta et al., 2012, 2013) was applied to six scenarios, as a function of the number of Pressure Reducing Stations (in which a valve or a PAT could be installed). Significant benefits were reached through the PAT installation, also for low produced powers and variable hydraulic conditions.

Similar approach was followed by Patelis et al. (2016), who estimated the potential ER through PATs in reference to the WDN of Kozani City in West Macedonia Region (GR). Due to the significant geodetic gradients, three different pressure regions were detected in the network. A segmentation approach was considered by dividing the network into 24 DMAs through isolation valves. Simulations using the WaterGems® hydraulic solver were performed, by developing three different operative scenarios: the first provided the network sectorization into DMAs without PRVs or PATs installation; the second was implemented by installing a PRV on the input pipe of the considered

DMA, whereas, in the third scenario, a PAT was installed, instead of the previous PRV. PAT installation on the inlet pipe of a DMA was considered, characterized by both the highest pressure potential and the greatest input flow volume. A PAT with same diameter and nominal power $NP$ = 7.5 kW was taken into account, able to assure a nodal pressure of 20 m at each delivery point of the DMA. Steady-state conditions were considered for both PRVs and PATs, because no daily patterns were set for simulations. The estimation of purchasing, investment and maintenance costs pointed out that PAT installation required more expensive investment costs, however, amortizable in few years, thanks to the annual energy production of about 50000 kWh. The evaluation of total water volume inputted into DMAs defined the reduction of 36.7% with respect to the first scenario, through the PRV application, whereas a decrease of about 28% was reached by simulating the PAT scenario. Simulations pointed out the PAT effectiveness for both Energy Recovery and pressure regulation in WDNs. Their ability to pressure regulation resulted to be lower than that provided by PRVs but still improvable through hydraulic and/or an electrical regulations (Par. 3.2.2).

Aiming at experimentally testing the PAT realibility to real WDNs, Karadirek et al. (2016) installed a pilot study area in Antalya City (TR), in order to evaluate the environmental and economic benefits related to the reduction of physical water losses and pipe burst frequency. Savings from both the lower energy consumption for water extraction and treatment and the reduction of carbon dioxide emissions were also observed.

Rossi et al. (2016) applied an experimental approach, as well. They tested a centrifugal PAT to be installed at the Merano (IT) WDN. The performance analysis and the users' demand estimation pointed out the potentiality connected to the substitution of PRVs with PATs, being able to produce about 340 kWh per each day of operation, with a power peak of about 19.2 kW.

De Marchis et al. (2016) considered the numerical investigation instead. They analysed the reliability of PAT installation at the Misilmeri (IT) WDN to estimate the environmental and economic advantages achievable through the ER in small sized cities. The authors developed a mathematical model to maximize the energy savings in

WDNs. As for Puleo et al. (2014), private tanks, usually installed in Mediterranean cities, were considered for simulations, resulting to be a key factor in the reduction of the potential energy production. Even though, the PAT application was both an economic and an attractive approach for ER, representing a reliable intervention to both reduce the $CO_2$ emission in atmosphere and produce renewable energy.

Lima et al. (2017) proposed an innovative method for PAT selection and location in WDNs, based upon the maximization of both the produced energy and the reduction of leakage volume. A meta-heuristic approach was considered and results from three WDN benchmarks from the literature were analyzed, setting the PAT operation at BEP during the maximum consumption period. The PAT effectiveness was evaluated, as a function of the local electricity tariff.

Parra and Krause (2017) performed an experimental campaign, aimed at combining PRVs and PATs into two WDNs in Germany. A mean power production of 5 kW was evaluated, with mean water losses and pressure reduction of about 8 l/s and 85 m, respectively. A payback period between 8 and 11 years was also estimated.

From the analysis of case-studies referred to PAT application in WDNs supplying small-medium sized, it was found how this approach is resulting intensively applied for hydropower generation in urban and rural areas. Conversely, in order to verify the effectiveness of this approach, either real test applications have required or numerical simulations have been performed, because the predictive models, available in the literature, do not allow to characterize the wide set of PAT models in the market. Specific analyses are thus required to overcome this limitation, aiming at providing more effective instruments to estimate the PAT performarnces for the selection of the most suitable model, among them available in the market.

### 3.2.2 Hydraulic and Electrical Regulation of PATs in Water Distribution Networks

The hydraulic regulation for PATs in WDNs consists in the combined installation of a production line, where the PAT is installed, and of a by-pass one operating in parallel configuration.

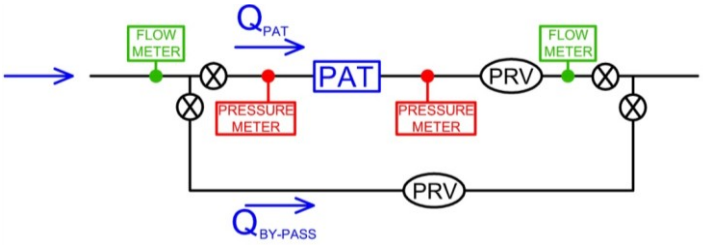


**Fig. 3.8 Hydraulic regulation scheme**

On both lines, two regulation valves (such as PRVs) are installed to modulate the flow through the PAT (Fig. 3.8), in compliance with its performance characteristics (i.e. as a function of the generated head drops at the operative flowing rates), in order to perform a pressure regulation allowable with the required pressure at each delivery point. In the following Fig. 3.9, the PAT and the WDN characteristic curves are plotted. These lasts correlate, at each flow rate $Q_t$, the potential dispersible pressure drop $H_t$ by PAT in the WDN, able to guarantee the required outlet pressure.

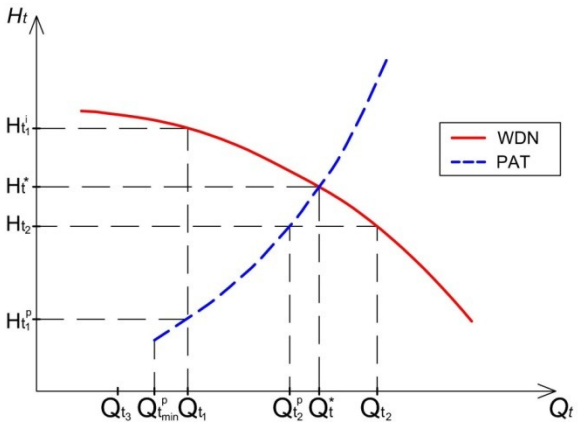


| LEGEND | |
|---|---|
| $Q_{t_3}$ | Flow rate lower than the lower limit of PAT load region |
| $Q^P_{t_{1min}}$ | Lower Limit of PAT load region |
| $Q_{t_1}$ | Flow rate corresponding to PAT pressure drops lower than the dispersible ones |
| $Q^P_{t_2}$ | Flow rate compatible with the dispersible pressure drop in the network |
| $Q^*_t$ | Optimal operating point |
| $Q_{t_2}$ | Flow rate higher than the optimal operating point |
| $H^L_{t_1}$ | Network pressure drop corresponding to $Q_{t_1}$ |
| $H^*_t$ | Network and PAT pressure drop corresponding to $Q^*_t$ |
| $H_{t_2}$ | Network pressure drop corresponding to $Q_{t_2}$ |
| $H^P_{t_1}$ | PAT pressure drop corresponding to $Q_{t_1}$ |

**Fig. 3.9 Characteristic curves of WDN and PAT**

The hydraulic regulation consists in the proper activation of the production and the by-pass lines, according to the operative sets, specified as follows:

- *Set 1* $Q_t=Q_t^*$: the flow rate $Q_t$ is equal to $Q_t^*$, which represents the flow rate value with the which the pressure drop $H_t^*$, generated by the PAT, corresponds to the maximum pressure drop $H_{t,av}$ dispersible in the WDN for assuring the set outlet pressure;

- *Set 2* $Q_{t1}<Q_t^*$: at flow rate $Q_{t1}$ the PAT generates the head drop $H_{t1}^P$ lower than the exceed pressure drop $H_{t1}^i$ dispersible in the WDN. Thus, the residual pressure drop ($H_{t1}^i$- $H_{t1}^P$) is dissipated by the regulation valve installed at the production line;
- *Set 3* $Q_{t2}>Q_t^*$: the flow rate $Q_{t2}$ through the PAT induces a pressure drop higher than the allowable dispersible pressure in the WDN $H_{t2}$; hence, the flow repartition between the production and the by-pass lines is assessed. Specfically, a flow rate $Q_{t2}^P$ passes across the production line, able to generate the pressure drop $H_{t2}$, whereas the residual rate ($Q_{t2}$-$Q_{t2}^P$) flows towards the by-pass one;
- *Set 4* $Q_{t3}<Q_t^P{}_{\min}$: the flow rate $Q_3$ appertains to the PAT no-load region, being lower than the minimum value compatible with its performance characteristics. The whole flow rate $Q_{t3}$ passes towards the by-pass line, acting the pressure regulation through the regulation valve installed at the by-pass line.

The use of hydraulic regulation in WDNs is strictly connected to the application of proper RTCs, useful to regulate the system operations as a function of the dynamic conditions in the network. Specifically, the pressure and flow regulations are based on the capability of maintaining the required pressure at each delivery point, aiming at assuring the required level of service to fulfil the users' requirements. In WDNs, being the hydraulic parameters strongly variable as a consequence of the users' demand patterns, effective control settings can be adopted by using SCADA systems, widely applied in the field of water systems management (Par. 2.5.6).

Concerning the hydraulic regulation in WDNs for pressure control and hydropower generation, Fontana et al. (2016) proposed a hierarchic RTC system algorithm, in presence of by-pass systems, equipped as depicted in Fig. 3.8. The algorithm was tested on a WDN laboratory prototype at the University of Naples (IT) Federico II. A high-level controller was introduced to distribute the head drop $H_t$ and the flow $Q_t$ between the production and the by-pass line and low-level controllers were implemented to regulate the single control valve, according to the set valve outlet pressure. A switching control strategy was applied to operate on the two control valves installed at the production and by-pass lines, according to two alternative steps. The first step implies the fulfilment of the set outlet pressure at the node downstream the by-pass

configuration, obtained by modulating the control valve on the by-pass line. The second step searches for the maximization of the power production, by regulating the control valve at the production line, instead. The RTC convergence was strictly influenced by the non-linear behaviour of the needle valves applied for regulation. As an example, in the following Fig. 3.10, the total flow rate $Q_{tot}$, the flow rate through the production link $Q_2$, the downstream head $H$, the produced power $P_t$ and the opening degrees of control valves on the by-pass and the production lines ($OD_1$ and $OD_2$) are plotted, in reference to the considered RTC model.

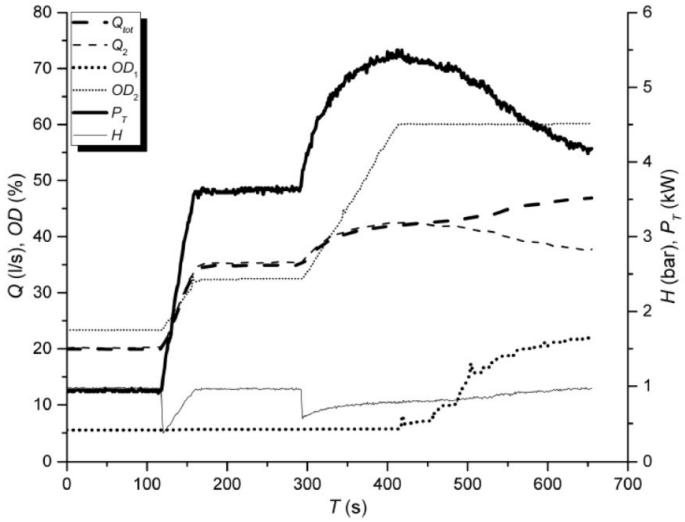


**Fig. 3.10 Pressure regulation at control node for RTC control (Fontana et al., 2016)**

The electrical regulation of PATs consists in the modulation of PAT runner rotational speed $N$ through the electrical connection to a frequency modulator or inverter, instead.

The electrical regulation, combined with SCADA systems, allows to adequate the rotational speed $N$, as a function of the flowing rate $Q_t$, in order to optimize the energy production at the different operative conditions, at the same time, guaranteeing high efficiencies (Fontana et al., 2012; Dannier et al., 2015).

In presence of pumps operating in direct mode, a frequency modulator converts the normal power supply to another frequency power, to control the electric motors in variable speed operations. In presence of PATs, a frequency modulator operates in reverse mode, by converting the input frequency $f$ to Direct Current (DC) and then

reconverting it into the set frequency output *f*. Thus, from the frequency modulation, the rotational speed *N* is regulated according to the following Eq. (3.2) for electric induction motors:

$$N = \frac{60 f}{p^*} \tag{3.2}$$

being *N* the rotational speed, *f* the grid frequency, equal to 50 Hz in the European Union and to 60 Hz in the USA, and $p^*$ the number of pole pairs.

Operating according to the electrical regulation, Joshi et al. (2005a) realized a stand-alone system (Fig. 3.11) by electrically connecting an unregulated PAT, coupled with a Self-Excited Induction Generator (SEIG), to a frequency modulator for hydropower generation in small-sized communities. The improvement of PAT regulation and the stabilization of electric current insertion into the local electrical grid was achieved by using the frequency modulator.

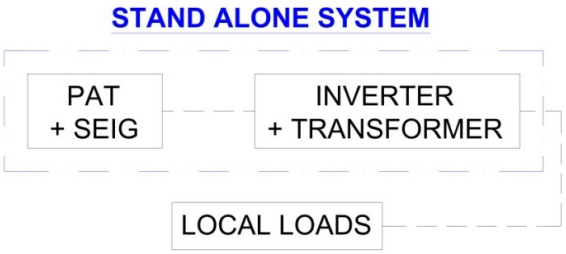


**Fig. 3.11 Block diagram of stand alone system (Joshi et al. 2005a)**

In the RTC systems for WDNs, the application of the electrical regulation is strictly correlated to the hydraulic regulation (Fig. 3.12), because the single electrical approach does not assure the set backpressure during the transient phases. Indeed, the hydraulic regulation implies better modulations during the transient conditions, allowing the swift achievement of the set backpressure.

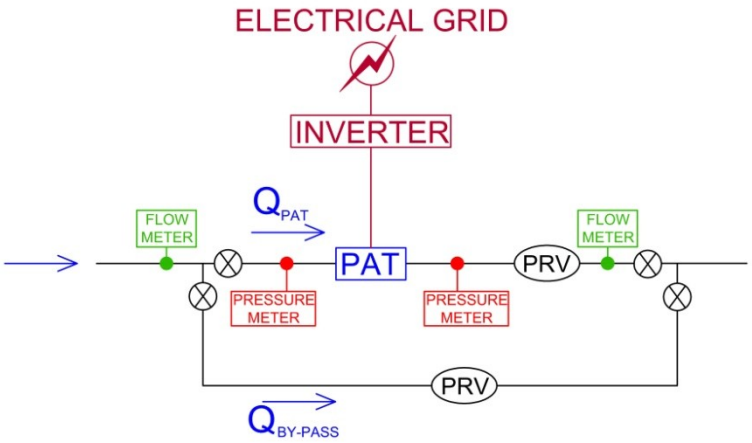


**Fig. 3.12 Hydraulic and electrical regulation in WDNs**

## 3.3 Prediction of PAT Performances through Experimental and Theoretical Approaches

One of the most critical issue, concerning the PAT application, regards the generally limited knowledge, in the selection phase, about the performances of pump models, commercially available, operating as turbines.

Indeed, characteristic curves are rarely made available by manufactures and, at this stage, the performed experimental, numerical and theoretical analyses do not give exhaustive instruments to estimate the PAT performances for the wide set of available pump models.

The acquisition of specific knowledge about the geometric internal configuration of turbo-machines, rarely provided by manufactures, leads the users to test many models before selecting the most appropriate for the WDN requirements, with significant economic and time-consuming efforts. Indeed, the geometric parameters, usually made available from manufacturers, do not assure the required accuracy to carefully reproduce the hydraulic and mechanic phenomena inducted into the turbo-machine. Furthermore, possible characteristic curves from manufactures do not provide dependable reliability, as a consequence of the definition procedures, often based upon predictive and regressive techniques, instead of effective laboratory tests (Pelton, 1988).

### 3.3.1 The Affinity Laws

A basic approach to predict the turbo-machine performances regards to the application of the Affinity Laws (ALs) (Stepanoff, 1948) which analytically convey the concept of similitude for turbo-machines. Specifically, a set of machines operates in similitude when the following conditions are satisfied:

- *Geometric Similitude*: homologous linear entities (i.e the runner diameter, the blade length and thickness) have the same ratio;
- *Kinematic Similitude*: all velocity components, in corresponding points, have the same ratio, determining similar velocity triangles at the machine inlet and outlet zones;
- *Dynamic Similitude:* ratios of all forces acting on corresponding fluid particles and on boundary surfaces are constant.

In reference to geometrically similar runners, the ALs were found out under the hypothesis of flow rate and head depending on the velocity triangles, according to the schemes in Fig. 3.13. In it, *u* and *c* are the peripheral and the meridional velocities, whereas the subscripts 1 and 2 refer to the runner inlet and outlet, respectively.

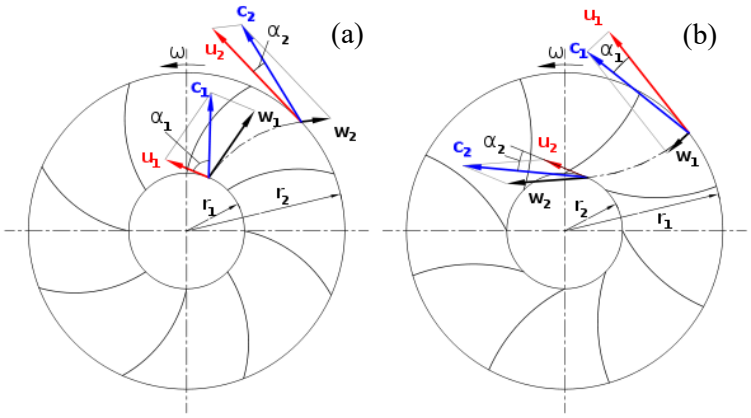


**Fig. 3.13 Velocity triangles at impeller inlet at outlet in (a) pump mode, (b) turbine mode**

By considering the continuity equation and the Euler's rotor dynamics equation, following dependences can be established to evaluate the flow rate $Q$, the head $H$ and the power $P$:

$$Q \propto ND^3 \tag{3.3}$$

$$H \propto (ND)^2 \tag{3.4}$$

$$P \propto (ND)^3 \tag{3.5}$$

From the abovementioned Eqs. (3.3), (3.4) and (3.5), flow rate $Q$, head $H$ and power $P$ are explainable, in dimensionless terms, as a function of the rotational speed $N$ and the runner diameter $D$, according to the **flow rate number $\phi$**, the **head number $\psi$** and the **power number $\pi$**:

$$\phi = \frac{Q}{ND^3} \tag{3.6}$$

$$\psi = \frac{gH}{N^2 D^2} \tag{3.7}$$

$$\pi = \frac{P}{\rho N^3 D^5} \tag{3.8}$$

where $g$ is the acceleration of gravity ($ms^{-2}$) and $\rho$ ($kgm^{-3}$) the fluid density, whereas the flow rate $Q$ is in $m^3s^{-1}$, the rotational speed $N$ in rps, the runner diameter $D$ and the specific head $H$ in m, and the power $P$ in W.

According to the Eqs. (3.6), (3.7) and (3.8), the dimensionless $\phi$, $\psi$ and $\pi$ parameters are constant for similar machines operating at the same overall efficiency $\eta$, in turn calculated as:

$$\eta = \eta_{h^*} \eta_{v^*} \eta_{i^*} \tag{3.9}$$

being $\eta_{h^*}$ the hydraulic efficiency, $\eta_{v^*}$ the volumetric efficiency and $\eta_{i^*}$ the internal efficiency.

To directly quantify the $Q$, $H$ and $P$ parameters, the ALs are represented as follows:

$$\frac{Q_{b^*}}{Q_{a^*}} = \left( \frac{N_{b^*}}{N_{a^*}} \frac{D_{b^*}}{D_{a^*}} \right) \tag{3.10}$$

$$\frac{H_{b^*}}{H_{a^*}} = \left( \frac{N_{b^*}}{N_{a^*}} \frac{D_{b^*}}{D_{a^*}} \right)^2 \tag{3.11}$$

$$\frac{P_{b^*}}{P_{a^*}} = \left( \frac{N_{b^*}}{N_{a^*}} \frac{D_{b^*}}{D_{a^*}} \right)^3 \tag{3.12}$$

where the subscripts $a^*$ and $b^*$ refer to two turbo-machines operating in similitude.

From Eqs. (3.3), (3.4) and (3.5), the specific speed number $N_s$ is also defined as:

$$N_s = N\frac{Q^{1/2}}{H^{3/4}} \tag{3.13}$$

or similarly

$$N_s = N\frac{P^{1/2}}{H^{5/4}} \tag{3.14}$$

Hence, turbo-machines, operating in similitude and having the same efficiency $\eta$, have the same specific speed $N_s$.

From the abovementioned definitions, the ALs allow to reproduce the performances of similar turbo-machines having different rotational speed $N$ and/or runner diameter $D$, being available data from a prototype model. Similarly, in reference to a single machine, by applying the ALs and having at disposal few experimental data, the characteristic curves at different rotational speeds $N$ are derivable.

In order to overcome the ALs limitation of neglecting the physical parameters which scale with velocity, Simpson and Marchi (2013), in reference to pump machines, proposed corrective factors for the ALs. They experimentally tested the corrective Eq. (3.15) proposed by Sarbu and Borza (1998) to estimate the efficiency correlations for similar turbo-machines:

$$\eta_{b^*} = 1-\left(1-\eta_{a^*}\right)\cdot\left(\frac{N_{a^*}}{N_{b^*}}\right)^{0.1} \tag{3.15}$$

The above formulation gave significant results for pumps running at speeds not lower than the 70% of the nominal value.

Regarding the PAT application, Carravetta et al. (2014), by analysing experimental data from a manufacturer, stated that the maximum efficiency resulted to be not constant at varying the rotational speed $N$. Conversely, it reached the highest value $\eta_{tb}^{\max}$ for a specific rotational speed $N^{\max}$, to be properly assessed for each PAT model. Thus, Modified Affinity Laws formulations (MALs) for PATs were proposed, according to the following dependencies:

$$\frac{Q_{tb}}{Q_{tb}^{\max}} = f_1\left(\frac{N_b}{N^{\max}}\right) \tag{3.16}$$

$$\frac{H_{tb}}{H_{tb}^{\max}} = f_2\left(\frac{N_b}{N^{\max}}\right) \tag{3.17}$$

$$\frac{P_{tb}}{P_{tb}^{\max}} = f_3\left(\frac{N_b}{N^{\max}}\right) \tag{3.18}$$

$$\frac{\eta_{tb}}{\eta_{tb}^{\max}} = f_4\left(\frac{N_b}{N^{\max}}\right) \tag{3.19}$$

where $Q_{tb}^{\max}$, $H_{tb}^{\max}$, $P_{tb}^{\max}$ and $\eta_{tb}^{\max}$ are the flow rate, the head drop, the power and the efficiency related to the rotational speed $N^{\max}$, respectively, whereas $f_1$, $f_2$, $f_3$ and $f_4$ are the polynomial functions to be calibrated as a function of the considered PAT model.

Fecarotta et al. (2016) explicated the Eq. (3.20) to calculate the rotational speed $N^{\max}$:

$$N^{\max} = \alpha^* D^{\beta^*} \varphi^{\gamma^*} F^{\delta^*} \tag{3.20}$$

with $D$ the runner diameter, $\varphi$ the stator diameter and $F$ the stator height. The authors experimentally calibrated the $\alpha^*$, $\beta^*$, $\gamma^*$ and $\delta^*$ coefficients for five semi-axial, submersible and Single-Stage PATs, running at specific speeds $N_s$ between 120 and 162. Thus, following coefficients were derived: $\alpha^* = 5.970 \cdot 10^{18}$, $\beta^* = -0.4856$, $\gamma^* = 31.11$ and $\delta^* = -38.6$.

Conversely, Pugliese et al. (2016) experimentally verified the ALs applicability to both a Single-Stage and a Multi-Stage centrifugal PAT, tested at 91 rotational speeds $N$ between 300 and 3000 rpm, achieving significant correlations between the experimental data and those calculated with the ALs.

From the similitude of turbo-machines, the Suter (1966) model was also derived, basing the calculation on the following parameters:

$$WH = \frac{h}{q^2(\theta+1)} \tag{3.21}$$

$$WT = \frac{t^*}{q^2(\theta+1)} \tag{3.22}$$

with

$$\theta = \frac{\omega^*}{q} \tag{3.23}$$

and

$$h = \frac{H}{H_b} \qquad \omega^* = \frac{N}{N_b} \qquad q = \frac{Q}{Q_b} \qquad t^* = \frac{T}{T_b} \tag{3.24}$$

where $T$ is the torque applied to the runner. The model sets the $WH(\theta)$ and $WT(\theta)$ constancy for turbo-machines operating in similitude, allowing the performance estimation of the whole machines operating in similitude, when data sets of a single model are available.

Relations for head $H$ and efficiency $\eta$ curves were also proposed as a function of the operation at BEP:

$$H = \left[q^2\left(\theta^2 + 1\right)WH\right]H_b \tag{3.25}$$

$$\eta = \theta\frac{WT}{WH} \tag{3.26}$$

Basing the PAT performance prediction on the application of both the ALs (Stepanoff, 1948) and the Suter (1966) model, Carravetta et al. (2012) proposed the Variable Operating Strategy (VOS), to evaluate the overall plant efficiency $\eta_{P*}$:

$$\eta_{P*} = \frac{\sum_{i=1}^{n} H_i^T Q_i^T \eta_i^T \Delta t_i}{\sum_{i=1}^{n} H_i \, Q_i \, \eta_i \, \Delta t_i} \tag{3.27}$$

where $\eta_{P*}$ is the overall plant efficiency, $n$ the number of available operating points, $H_i^T$ and $Q_i^T$ the head drop and the flow through the PAT, $\eta_i^T$ the PAT efficiency, $H_i$ and $Q_i$ the available head drop and flow rate, respectively and $\Delta t_i$ the time interval of flow rate-head drop pattern. The approach was based upon the determination of the flow rate and the pressure patterns, as a function of the required backpressure, the PAT typology and the analysis of a wide set of PAT characteristic curves in order to calculate, for each curve, the overall plant efficiency $\eta_{P*}$. Starting from these assumptions, the selection of the PAT model, able to maximize the produced power, was suggested. The VOS

strategy was also extended to WDNs, equipped with an electrical regulation (Par. 3.2.2) for PATs through a frequency regulator (Carravetta et al., 2013).

### 3.3.2 Prediction of PAT Performances at Best Efficiency Point

Several models are available in the literature to predict the PAT performances, as a function of the pump characteristics in pump operation. Most of them are based upon mono-dimensional formulations to estimate the ratios between reverse and direct operations at BEP, for a fixed rotational speed *N*.

Among them, Stepanoff (1957) correlated the flow rate and head ratios to the pump hydraulic efficiency $\eta_{hpb}$, defined, in a simplified form, as:

$$\eta_{hpb} = \sqrt{\eta_{pb}} \tag{3.28}$$

obtaining:

$$\frac{Q_{tb}}{Q_{pb}} = \frac{1}{\sqrt{\eta_{pb}}} \tag{3.29}$$

$$\frac{H_{tb}}{H_{pb}} = \frac{1}{\eta_{pb}} \tag{3.30}$$

where the subscript *b* refers to the BEP condition and subscripts *p* and *t* to the pump and PAT modes, respectively.

Childs (1962) set the equivalence of pump efficiencies at BEP in direct and reverse operations and of the input power in pump mode $P_{pb}$ and the produced power in reverse one $P_{tb}$, obtaining:

$$P_{tb} = \rho g Q_{tb} H_{tb} \eta_{tb} = \frac{\rho g Q_{pb} H_{pb}}{\eta_{pb}} = P_{pb} \tag{3.31}$$

The model was developed under the hypothesis of flow rate and head ratios constancy at BEP, setting them equal to the inverse of the pump efficiency at BEP:

$$\frac{Q_{tb}}{Q_{pb}} = \frac{H_{tb}}{H_{pb}} = \frac{1}{\eta_{pb}} \tag{3.32}$$

Thus, the Eq. (3.32) is equal to the Stepanoff (1957) Eq. (3.30) to predict the head ratio.

McClaskey and Lundquist (1976) and Lueneburg and Nelson (1985) validated the Childs (1962) approach, specifying, at the same time, its applicability exclusively as a preliminary criterion. More accurate analyses and experimental tests were essential for defining effective estimations.

Hancock (1963), under the same hypothesis of flow rate and head ratios constancy, stated that both ratios were equal to the inverse of the efficiency at BEP in turbine mode. This assumption was based upon the hypothesis of quite similar BEP efficiency in direct and reverse operations, because slight discrepancies (in the order of ±2%) between pump and turbine mode at BEP, were experimentally observed:

$$\frac{Q_{tb}}{Q_{pb}} = \frac{H_{tb}}{H_{pb}} = \frac{1}{\eta_{tb}} \tag{3.33}$$

Sharma (1985), in compliance with the Childs hypothesis, assumed the power and the efficiency equivalence at BEP in pump and turbine mode, defining:

$$\frac{Q_{tb}H_{tb}}{Q_{pb}H_{pb}} = \frac{1}{\eta_{pb}^2} \tag{3.34}$$

The Stepanoff approximation in Eq. (3.28) and the Engel (1931) formulation, to correlate the specific speeds $N_s$ in direct and reverse mode, were used:

$$N_{st} = N_{qt}\sqrt{\eta_{pb}} \tag{3.35}$$

and the following formulations, to predict the flow rate and the head ratios, were proposed:

$$\frac{Q_{tb}}{Q_{pb}} = \frac{1}{\eta_{pb}^{0.8}} \tag{3.36}$$

$$\frac{H_{tb}}{H_{pb}} = \frac{1}{\eta_{pb}^{1.2}} \tag{3.37}$$

However, the validation of the abovementioned equations necessitates of wide experimental analyses of the several pump models commercially available (Engeda, 1987). With this aim, Sharma (1998) accounted for data sets from several pump models operating in reverse mode for hydropower generation, considering the pump and turbine characteristic curves introduced by Grant and Bain (1985). In turbine mode, the

BEP was achieved at higher flow rates and heads than those from pump operation. Thus, the following equations were introduced:

$$\frac{Q_{tb}}{Q_{pb}} = \frac{N_{g*}}{N_{m*}} \frac{1.1}{\eta_{pb}^{0.8}} \tag{3.38}$$

$$\frac{H_{tb}}{H_{pb}} = \left( \frac{N_{g*}}{N_{m*}} \right)^2 \frac{1.1}{\eta_{pb}^{1.2}} \tag{3.39}$$

with $N_{g*}$ and $N_m$ the motor and the generator rotational speeds in rpm, respectively.

Schmiedl (1988) defined the aforementioned ratios, as a function of the following approximated hydraulic efficiency $\eta_{hp}$:

$$\eta_{hp} = \sqrt{\eta_{pb}^{0.5} \eta_{tb}^{0.5}} \tag{3.40}$$

proposing the Eqs. (3.41) and (3.42) for flow rate and head drop estimation, respectively:

$$\frac{Q_{tb}}{Q_{pb}} = -1.4 + \frac{2.5}{\eta_{hp}} \tag{3.41}$$

$$\frac{H_{tb}}{H_{pb}} = -1.5 + \frac{2.4}{\eta_{hp}^2} \tag{3.42}$$

Alatorre-Frenk and Thomas (1990), from an experimental analysis, derived analytic correlations to calculate both the flow rate and the head ratios, according to the following equations:

$$\frac{Q_{tb}}{Q_{pb}} = \frac{0.85\eta_{pb}^5 + 0.385}{2\eta_{pb}^{9.5} + 0.205} \tag{3.43}$$

$$\frac{H_{tb}}{H_{pb}} = \frac{1}{0.85\eta_{pb}^5 + 0.385} \tag{3.44}$$

Further approaches, available in the literarature, were developed by correlating the flow rate and the head ratios to the specific speed in pump mode $N_{sp}$ or in turbine mode $N_{st}$. Referring to machines with specific speeds in pump operations $N_{sp}$ in the range 10÷54, Buse (1981) introduced corrective factors to estimate the performances of pumps running in reverse mode, as a function of the characteristics at BEP in direct

operations. Analytic formulations were not provided; nevertheless, the author assessed the $Q_{tb}/Q_{pb}$ and $H_{tb}/H_{pb}$ ratios between 1.1 and 2.2, whereas the range between 0.92 and 0.99 was suggested to estimate the efficiency ratio $\eta_{tb}/\eta_{pb}$.

Grover (1980) set the flow rate and the head ratios, as a function of the specific speed in reverse operations $N_{st}$, for $N_{st}$ varying between 10 and 50:

$$\frac{Q_{tb}}{Q_{pb}} = 2.379 - 0.0264\, N_{st} \tag{3.45}$$

$$\frac{H_{tb}}{H_{pb}} = 2.693 - 0.0229\, N_{st} \tag{3.46}$$

Hergt (1982) introduced a band for flow rate and head ratios respectively, both correlated to the rotational speed in turbine mode $N_{st}$. By applying a mean calibration approach, following analytic correlations were derived:

$$\frac{Q_{tb}}{Q_{pb}} = 1.3 - \frac{1.6}{N_{st} - 5} \tag{3.47}$$

$$\frac{H_{tb}}{H_{pb}} = 1.3 - \frac{6}{N_{st} - 3} \tag{3.48}$$

Williams (1994) applied the abovementioned formulations to an experimental data set of 35 PATs. The Sharma (1985) model resulted to be the most reliable, by obtaining significant correlations with Stepanoff (1957), Hancock (1963), Hergt (1982) and Alatorre-Frenk and Thomas (1990) models, as well. In order to compensate the discrepancies between the experimental data and the calculated ones, Williams (1994) proposed a prediction coefficient $C'$, acting as an analytic corrective factor. Saini (1993) provided a nomogram to evaluate the PAT performances in terms of flow rate and head ratios, as a function of the specific speed in pump mode $N_{sp}$.

Moreover, Amelio et al. (2000) carried out a laboratory analysis on six centrifugal pumps operating in both direct and reverse mode; efficiencies in turbine operations were lower than those in pump mode for both specific speeds $N_{sp} \leq 16$ and $N_{sp} > 56$. Conversely, for $N_{sp}$ between 16 and 56, an opposite trend was observed in compliance with Boccazzi et al. (1997)'s results. Furthermore, analytic correlations to estimate the

flow rate (Eq. 3.49), the head (Eq. 3.50) and the specific speed ratios (Eq. 3.51) were proposed, as a function of the specific speed $N_{sp}$ in pump mode:

$$\frac{Q_{tb}}{Q_{pb}} = 1.80 \cdot 10^{-4} N_{sp}^2 + 2.235 \cdot 10^{-2} N_{sp} + 1.9907 \tag{3.49}$$

$$\frac{H_{tb}}{H_{pb}} = -4.0 \cdot 10^{-5} N_{sp}^3 + 5.41 \cdot 10^{-3} N_{sp}^2 - 0.2381 N_{sp} + 4.79679 \tag{3.50}$$

$$\frac{N_{st}}{N_{sp}} = 0.9329 - 2.6814 N_{sp}^{-1} \tag{3.51}$$

The experimental analysis of centrifugal PAT performances was also taken into account by Fernandez et al. (2004), who arranged the laboratory set-up sketched in the following Fig. 3.14.

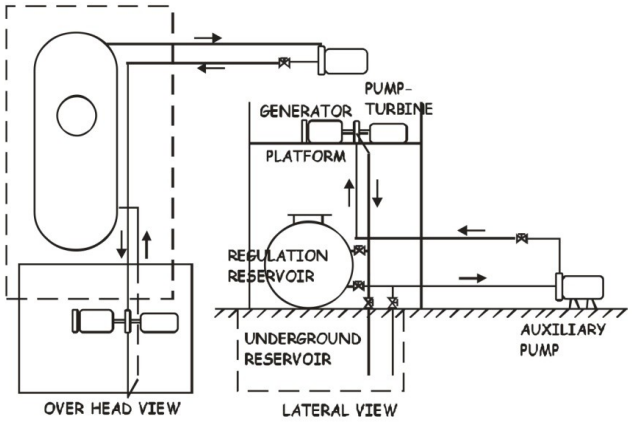


**Fig. 3.14 Laboratory set-up for Fernandez et al. (2004) experiments**

The authors tested a Horizontal Axis Single-Stage centrifugal pump with impeller diameter $D$ = 200 mm (Fig. 3.15), by reproducing the characteristic curves in direct and reverse operations, in reference to rotational speeds $N$ from 1250 to 2500 rpm.

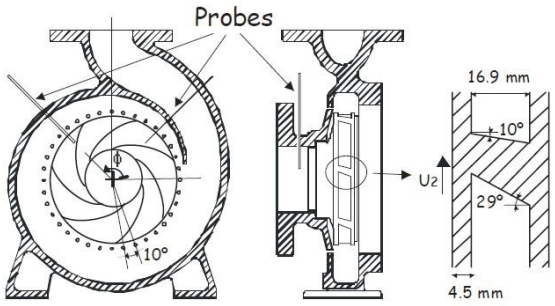


**Fig. 3.15 Tested pump for Fernandez et al. (2004) experiments**

In PAT mode, efficiencies $\eta_t$ of about 15% lower than those in pump mode were observed for higher flow rates. By comparing the velocity triangles at pump outlet and at turbine inlet, a slip at the impeller outlet was observed in direct operations, whereas, in turbine mode at BEP, the relative flow angle at the inlet was close to the blade angle of the impeller. From these considerations, they proposed the Eq. (3.52) to estimate the head ratio at BEP:

$$\frac{H_{tb}}{H_{pb}} = 1.73 \tag{3.52}$$

By elaborating the Swanson (1953) experimental results on a centrifugal, a mixed flow and an axial flow pump, Joshi et al. (2005b) derived the flow rate, head, power and efficiency ratios in reverse and direct operation, as summarized in Tab. 3.2.

| | | Centrifugal Pump | Mixed Flow Pump | Axial Flow Pump |
|---|---|---|---|---|
| $\mathbf{Q_{tb}/Q_{pb}}$ | [-] | 1.5 | 1.6 | 1.6 |
| $\mathbf{H_{tb}/H_{pb}}$ | [-] | 1.6 | 1.5 | 1.7 |
| $\mathbf{P_{tb}/P_{pb}}$ | [-] | 1.3 | 1.5 | 1.6 |
| $\boldsymbol{\eta_{tb}/\eta_{pb}}$ | [-] | 0.57 | 0.69 | 0.60 |

**Tab. 3.2 Flow rate, head, power and efficiency ratios (Joshi et al., 2005b)**

In addition, they explicated the Eq. (3.53) to correlate the specific speeds $N_s$ at BEP in reverse $N_{st}$ and direct mode $N_{sp}$:

$$\frac{N_{st}}{N_{sp}} = \frac{\left(N\sqrt{bhp}/H^{5/4}\right)_t}{\left(N\sqrt{Q}/H^{3/4}\right)_p} \tag{3.53}$$

where *bhp* is the power in horsepower produced by turbine at BEP, $H$ the head in ft and $Q$ the flow rate in usgpm.

However, one of the most applied approach for predicting the performances of centrigual PATs was developed by Derakhshan and Nourbakhsh (2008a), who experimentally investigated four centrifugal PATs running at specific speeds $N_{sp}$ from 14 and 56, at the mini-hydropower plant depicted in Fig. 3.16.

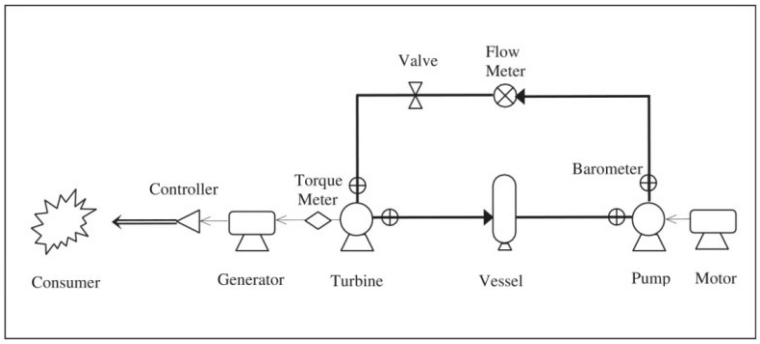


**Fig. 3.16 Experimental set-up for Derakhshan and Nourbakhsh (2008a) experiments**

An analytic criterion to predict the BEP in turbine operations was proposed, as a function of the performances at BEP in direct mode. The model requires the calculation of the following parameters:

$$\bar{\gamma} = 0.0233\,\bar{\alpha}_p + 0.6464 \tag{3.54}$$

$$\bar{\alpha}_t = 0.9413\,\bar{\alpha}_p - 0.6045 \tag{3.55}$$

$$\bar{\beta}_t = 0.849\,\bar{\beta}_p - 1.2376 \tag{3.56}$$

being $\bar{\alpha}_p$ and $\bar{\beta}_t$ the specific speeds at BEP in pump and turbine mode, respectively, obtainable as:

$$\bar{\alpha}_p = \frac{N_p Q_{pb}^{0.5}}{\left(gH_{pb}\right)^{0.75}} \tag{3.57}$$

$$\bar{\beta}_t = \frac{N_{tb} P_{tb}^{0.5}}{\rho^{0.5}\left(gH_{tb}\right)^{1.25}} \tag{3.58}$$

Hence, $\gamma$, $\alpha_t$ and $\beta_t$ parameters were introduced:

$$\bar{\gamma} = \left(\frac{H_{tb}}{H_{pb}}\right)^{-0.5} \frac{N_t}{N_p} \tag{3.59}$$

$$\overline{\alpha}_t = \frac{N_{tb} Q_{tb}^{0.5}}{\left(gH_{tb}\right)^{0.75}} \tag{3.60}$$

$$\overline{\beta}_p = \frac{N_{pb} P_{pb}^{0.5}}{\rho^{0.5}\left(gH_{pb}\right)^{1.25}} \tag{3.61}$$

Knowing the operative conditions at BEP in pump mode, by properly combining the Eqs. (3.54)-(3.61), the head drop $H_{tb,}$ the flow rate $Q_{tb}$ and the produced power $P_{tb}$ in turbine mode at BEP are derived.

The authors also provided analytic formulations to represent the characteristic curves in turbine mode, as a function of the operative conditions at BEP, for specific speeds $N_{st}$ up to 150 and flow rate numbers $\phi \leq 0.40$. By interpolating the available experimental data for $N$ = 1500 rpm, the following Eqs. (3.62) and (3.63) were proposed to predict the head drop $H_t$ and the produced power $P_t$, respectively:

$$\frac{H_t}{H_{tb}} = 1.0283\left(\frac{Q_t}{Q_{tb}}\right)^2 - 0.5468\left(\frac{Q_t}{Q_{tb}}\right) + 0.5314 \tag{3.62}$$

$$\frac{P_t}{P_{tb}} = -0.3092\left(\frac{Q_t}{Q_{tb}}\right)^3 + 2.1472\left(\frac{Q_t}{Q_{tb}}\right)^2 - 0.8865\left(\frac{Q_t}{Q_{tb}}\right) + 0.0452 \tag{3.63}$$

By combining the Eqs. (3.62) and (3.63) with the Eq. (3.1) for the estimation of the efficiency $\eta_t$, the Eq. (3.64) was derivable to estimate the efficiency curve $\eta_t$:

$$\frac{\eta_t}{\eta_{tb}} = \frac{-0.3092\left(\frac{Q_t}{Q_{tb}}\right)^3 + 2.1472\left(\frac{Q_t}{Q_{tb}}\right)^2 - 0.8865\left(\frac{Q_t}{Q_{tb}}\right) + 0.0452}{1.0283\left(\frac{Q_t}{Q_{tb}}\right)^3 - 0.5468\left(\frac{Q_t}{Q_{tb}}\right)^2 + 0.5314\left(\frac{Q_t}{Q_{tb}}\right)} \tag{3.64}$$

Singh and Nestmann (2010) introduced an optimization routine (Fig. 3.17) for the optimal selection and performance prediction of PATs, by developing a theoretical-experimental approach. Nine radial end-suction pumps were experimentally investigated, operating at rotational speeds $N$ between 20 and 80 rpm and the experimental data from Derakhshan and Nourbakhsh (2008a) were considered to calibrate an analytic model for assessing the specific speed $N_{st}$ in reverse mode:

$$N_{st} = 0.94 N_{sp} - 3.12 \tag{3.65}$$

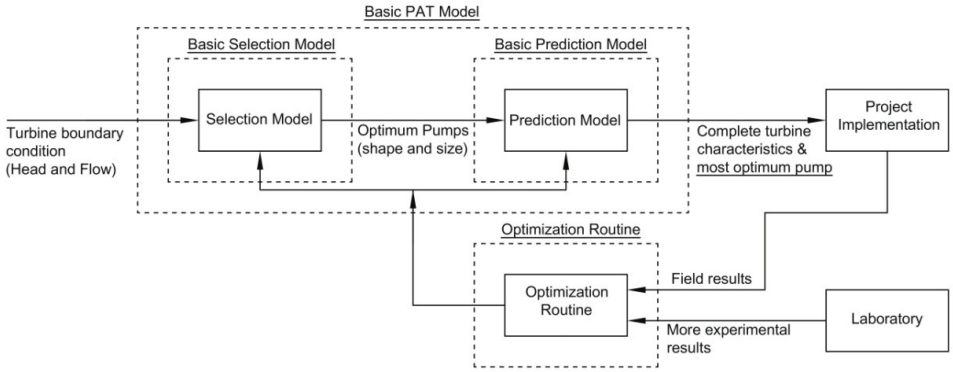


**Fig. 3.17 Optimization routine for PAT selection and prediction (Singh and Nestmann, 2010)**

The Hermite spline interpolation technique was applied to reproduce the characteristic curves of PATs in dimensionless terms, by comparing the numerical results with experiments on three PATs running at rotational speeds $N$ = 18, 20 and 44.5 rpm. Errors in the order of ±4% were estimated, for flow rates in the operative region of pump functioning, whereas numerical-experimental differences of about 10-20% were evaluated in the no-load region. Neverthless, the proposed optimization procedure was mainly focused on the consideration of a single operative condition, overlooking the evaluation of the most appropriate model, at varying flow rates and head drops, as it is determined in WDNs.

Nautiyal et al. (2011) tested a Horizontal Axis Single-Stage PAT operating at specific speed $N_{sp}$ = 18 and rotational speed $N$ = 1500 rpm. By matching the experimental results with data sets from PATs running at $N_{sp}$ = 14.6, 24.5, 35.3 and 46.1, following formulations were proposed:

$$\frac{Q_{tb}}{Q_{pb}} = 30.303 \chi - 3.424 \tag{3.66}$$

$$\frac{H_{tb}}{H_{pb}} = 41.667 \chi - 5.042 \tag{3.67}$$

being the $\chi$ parameter depending on the specific speed $N_{sp}$ and the efficiency $\eta_{pb}$ at BEP in pump mode:

$$\chi = \frac{\eta_{pb} - 0.212}{\ln\left(N_{sp}\right)} \tag{3.68}$$

From a numerical-experimental comparison, differences in the order of ±11% were estimated, with respect to discrepancies of about 40% assessed by applying further models from literature, such as the Alatorre-Frenk and Thomas (1990) and the Grover (1980) ones.

As for Fernandez et al. (2004), Yang et al. (2012a) developed a theoretical approach based upon the analysis of velocity triangles in direct and reverse operations. They stated that the head in pump and turbine mode resulted to be almost equivalent because, in reverse operations, the fluid inlet angle to the impeller corresponds to the volute angle, whereas the outlet angle from impeller is equal to the impeller inlet angle. From this assumption, they introduced the Eqs. (3.69) and (3.70) to predict the flow rate and the head ratios at BEP:

$$\frac{Q_{tb}}{Q_{pb}} = c^* \frac{b^{*0.5}}{\eta_{pb}^{a^*/2}} \tag{3.69}$$

$$\frac{H_{tb}}{H_{pb}} = \frac{b^*}{\eta_{pb}^{a^*}} \tag{3.70}$$

where $a^*$, $b^*$ and $c^*$ are coefficients depending on the pump specific speed $N_{sp}$, the pump size, the mechanical tolerances and the manufacturing accuracies. By calibrating the above introduced parameters with the experimental data from Williams (1992), Singh (2005) and Joshi et al. (2005b) referred to pumps running at different specific speeds and sizes, the authors proposed the following formulations to estimate the flow rate and the head ratios:

$$\frac{Q_{tb}}{Q_{pb}} = \frac{1.2}{\eta_{pb}^{0.55}} \tag{3.71}$$

$$\frac{H_{tb}}{H_{pb}} = \frac{1.2}{\eta_{pb}^{1.1}} \tag{3.72}$$

Furthermore, they linearly correlated the specific speeds in direct and reverse operations $N_{sp}$ and $N_{st}$, according to the following Eq. (3.73):

$$N_{sp} = 1.125\, N_{st} + 1.73 \tag{3.73}$$

Similar approach was followed by Tan and Engeda (2016), who proposed a prediction criterion to represent the PAT characteristic curves, correlating the characteristic parameters with the specific diameter $D_s$ parameter, defined, in dimensional form, as:

$$D_s = \frac{D H_{tb}^{0.25}}{Q_{tb}^{0.5}} \tag{3.74}$$

with $D$ (m) the impeller diameter and $H_{tb}$ (m) and $Q_{tb}$ ($m^3s^{-1}$) the head and the flow rates at BEP, respectively.

The authors experimentally interpolated linear functions between the specific speeds $N_s$ (calculated as a function of the angular velocity $\omega$) and the specific diameter $D_s$ in direct and reverse operations, according to the following formulations:

$$N_{st} = 0.7520\, N_{sp} + 0.0883 \tag{3.75}$$

$$D_{st} = 1.072\, D_{sp} - 0.1419 \tag{3.76}$$

A linear correlation was also derived between the specific speed in direct mode $N_{sp}$ and the efficiency ratio in direct and reverse mode at BEP, as follows:

$$\frac{\eta_{pb}}{\eta_{tb}} = 0.2267\, N_{sp} + 0.8057 \tag{3.77}$$

As a function of $N_{st}$, $D_{st}$ and $\eta_t$, the head drop $H_{tb}$, the flow rate $Q_{tb}$ and the generated power $P_{tb}$ at BEP in turbine mode were calculated by using the Eqs. (3.78), (3.79) and (3.80), respectively:

$$H_{tb} = \left( \frac{\omega D}{N_{st} D_{st} g^{\frac{3}{4}}} \right)^2 \tag{3.78}$$

$$Q_{tb} = \frac{\omega D^3}{N_{st} D_{st}^3 g^{\frac{3}{4}}} \tag{3.79}$$

$$P_{tb} = \eta_{tb} Q_{tb} \rho g H_{tb} \tag{3.80}$$

where $\omega$ is the angular velocity in $s^{-1}$, $g$ the gravitational acceleration, $\rho$ the fluid density. By comparing the experimental results with models in the literature, relative errors in the order of ±5% were observed for low specific speeds $N_{sp}$ with Stepanoff (1957) and Sharma (1985) formulations; for medium specific speeds $N_{sp}$, the Yang et al. (2012a) model resulted to be the most reliable, instead.

The analysis of the geometrical configuration of PATs was specifically considered by Barbarelli et al. (2016) to develop a operative procedure for optimal PAT selection. It consisted in the evaluation of six parameters: the head $H_{tb}$ and flow rate $Q_{tb}$ at BEP, the maximum power, the head at the shut off, the impeller diameter $D$ and the dimensional size of pump. The approach was composed of four phases (Fig. 3.18), requiring, as input parameters, both the specific speed in direct operation $N_{sp}$ and the impeller diameter $D$.

In the first phase, the impeller width was determined, as a function of both the impeller eye diameter and the blade inclination with respect to the radial direction. In the second phase, the number of blades and the vane angle were calculated, whereas in the third phase the impeller width, in the portion close to the volute, was assessed. Finally, the last phase allowed to design the volute area. The authors experimentally tested six centrifugal PATs with specific speeds $N_{sp}$ between 9 and 65. The reliability of the proposed model was experimentally verified, in reference to three configurations: the *design mode*, applied when the geometry was unknown, the *geometry known mode*, used when the geometric parameters were known, and the *mixed mode*, in presence of the partial knowledge about the geometric parameters. The comparison with experimental data pointed out the model reliability to predict the BEP conditions, whereas higher discrepancies were estimated for head and efficiency forecasting, in reference to operative conditions far from the BEP. In greater detail, generally higher efficiencies than the experimental data were estimated. Furthermore, lower errors were observed for the *geometry known mode* configuration, drawing attention to the high importance of an in-deep knowledge about the geometric pump sizing to make the applied models effectively suitable.

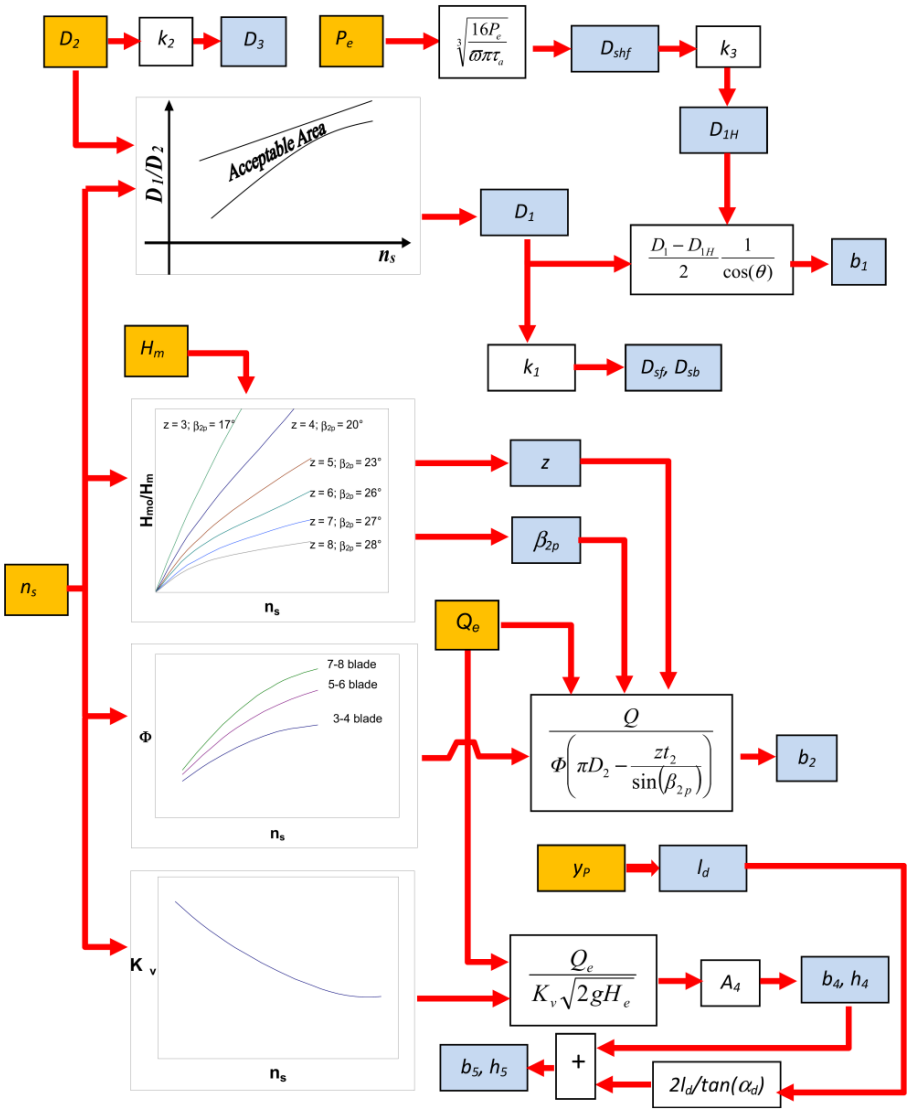


**Fig. 3.18 Flow chart of selection and design model (Barbarelli et al., 2016)**

From the abovementioned approaches, it can be found how the actual instruments available in the literature to predict the PAT performances are not completely suitable for the wide set of centrifugal pump models, commercially available and to the vast operative conditions definable in the WDNs, because devoted to limited operative fields, mainly referred to the BEP conditions. Indeed, very few models allow to reproduce the PAT characteristic curves, far from BEP. Among them, the analytic formulations proposed by Derakhshan and Nourbakhsh (2008a) are validated for

limited flow rate numbers ($\phi \leq 0.40$), resulting specifically applicable for Horizontal Axis Single-Stage PATs.

In this regard, experimental and numerical analysis of different PAT configurations are thus required to both verify the applicability of the abovementioned models to wider operative fields and PAT models (Chapter 4) and develop further approaches having applicability to greater operative fields and PAT models.

### 3.3.3 Cavitation Analysis of PATs

Cavitation in PATs is generated when the pressure drop, caused by the water acceleration across the runner, is such to determine a downstream pressure lower than the vapor pressure at the operating temperature. It causes the formation of vapor pockets or cavities in the moving fluid, implicating both hydraulic and mechanical effects. In presence of cavitation, the efficiency reduction is observed, due to the flow instability, causing dangerous effects on the physical components, such as surface damages, vibrations and noises. The formation of surface erosions could cause, after many years of operations, increasing failures up to the total breaking of the machine (Arndt, 1981).

Gantar (1988), from an experimental investigation on a propeller PAT, pointed out that the probability of cavitation formation for PATs results to be lower than that in pump operation, allowing to place the runner at a lower submergence than that required in direct mode.

Alatorre-Frenk (1994) performed experimental tests on an end-suction PAT, for different values of the dimensionless cavitation parameter $\sigma_t$, defined as the ratio between the Net Positive Suction Head NPSH $H_\Delta$ and the head absorbed by the PAT:

$$\sigma_t = \frac{H_\Delta}{H} \tag{3.81}$$

where

$$H_\Delta = -z_t - \frac{P_v}{\gamma_w} \tag{3.82}$$

with $z_t$ the suction static head (Fig. 3.19) and $P_v$ the vapor pressure, in relative terms with respect to the atmospheric pressure.

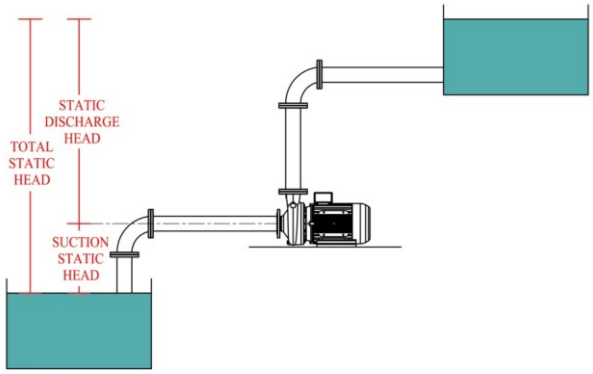


**Fig. 3.19 Cavitation Scheme for PAT**

A constancy in efficiency evaluation was established for $\sigma_t > 0.3$, reaching values in the range 79±0.5%. Conversely, for lower $\sigma_t$, the formation of a vapour layer on the runner blades was generated, causing the decrease of skin friction. A critical value $\sigma_{tcr} = 0.25$ was estimated, which resulted to be higher than that predicted for conventional turbines, operating at the same specific speed $N_{st}$. Starting from this consideration, a susceptibility of PATs to the formation of cavitation phenomena, greater than that for the conventional turbines, was highlighted.

Singh (2005) developed two approaches to evaluate the cavitation formation in PATs: the first, based upon the machine characteristics and the second developed by combining the system properties with the geometric configuration of the machine (i.e. runner geometric configuration). A dimensionless Combined Suction Head Number (CSHN) was proposed to predict the pressure close to the suction eye region, at varying the rotational speed $N$ and the geometric settings:

$$CSHN = \frac{z_t + \frac{P_r}{\gamma_w}}{N^2 D^2} \tag{3.83}$$

where $z_t$ is the suction static head, $P_r$ the pressure, $\gamma_w$ the specific weight, $N$ the rotational speed and $D$ the impeller diameter.

Hence, the critical $CSHN$ represented the pressure value, starting from which the cavitation phenomena begun. From an experimental application of the CSHN model to radial flow PATs, the critical value was individuated for higher flow rates than $Q_{tb}$, whereas flow rates lower than $Q_{tb}$ were established for mixed flow PATs.

Prasad et al. (2006) performed cavitation tests on two end-suction mixed and axial flow PATs, correlating the efficiency with the variation of the cavitation coefficient $\sigma_t$. An increase of PAT efficiency was also observed by reducing $\sigma_t$, up to an operative condition which generated a sudden drop, making the efficiency null.

Different approach was undertaken by Gonzalez et al. (2009) to investigate the cavitation phenomena of PATs. Indeed, they performed a numerical analysis on a double-end suction centrifugal PAT, observing the formation of cavitation regions at the blade inlet section, at running low flow rate values.

### 3.3.4 CFD Simulations of PAT Performances

The development of Computational Fluid Dynamics (CFD) models is widely contemplated to evaluate the turbo-machine performances. This approach is based upon the application of numerical analyses and algorithms to reproduce and solve the fluid flow fields, by considering the fluid interaction with the adjoining surfaces.

As a consequence of the highly time-demanding and expensive approaches related to the application of experimental researches (Jain and Patel, 2014), CFD models result to be strongly suitable to both simulate the complex flow behaviour internal to the turbo-machines and reproduce the turbulence phenomena, by taking into account the generation of secondary flows and physical phenomena, such as cavitation, internal head losses and force analysis (Agarwal, 2012). However, to perform an effective calibration and validatation of CFD models, the availability of wide sets of experimental data is unavoidable (Tamm et al., 2000).

The use of CFD for turbo-machines is generally based upon the application of Finite Element Methods (FEMs), applied to 2D or 3D configurations and numerical models. These often consist in the solution of the Reynolds-Averaged Navier-Stokes (RANS) equations in steady and transient states, combined with turbulence models.

The RANS equations are widely applied in CFD models because they derive from the application of the Navier-Stokes equations, according to a time-averaged approach. In the conservation form, they are analytically expressed as:

$$\frac{\partial v_i}{\partial x_i} = 0 \tag{3.84}$$

$$\rho \frac{\partial v_i}{\partial t} + \rho \frac{\partial v_i}{\partial x_j}\left(v_j v_i\right) = -\frac{\partial p_r}{\partial x_i} + \frac{\partial}{\partial x_j}\left(2\mu S_{ij}\right) \tag{3.85}$$

where $\rho$ is the fluid density, $\mu$ the fluid dynamic viscosity, $p_r$ the pressure and $S_{ij}$ represents the *strain-rate tensor* for the *i-th* and *j-th* components, equal to:

$$S_{ij} = \frac{1}{2}\left(\frac{\partial v_i}{\partial x_j} + \frac{\partial v_j}{\partial x_i}\right) \tag{3.86}$$

The RANS explicate the velocity $v_i$ and pressure $p$ terms, through a linear combination of a time-averaged part and a fluctuating one:

$$v_i = \overline{v_i} + v'_i \qquad p_r = \overline{p}_r + p_r' \tag{3.87}$$

where the marked terms represent the mean values, whereas the signed terms individuate the fluctuating ones. The mean terms are calculated in reference to a fixed position in the space and averaged in a time interval, large enough to make the mean values independent from it. According to the above definition, the time-averaged of the fluctuating terms results to be equal to 0, modifying the Eqs. (3.84) and (3.85) as:

$$\frac{\partial \overline{v'}}{\partial x_i} = 0 \tag{3.88}$$

$$\rho \frac{\partial \overline{v_i}}{\partial t} + \rho \frac{\partial}{\partial x_j}\left(\overline{v'_i}\,\overline{v'_j}\right) = -\frac{\partial \overline{p}_r}{\partial x_i} + \frac{\partial}{\partial x_j}\left(2\mu S_{ij} - \rho \overline{v'_i\, v'_j}\right) \tag{3.89}$$

being $S_{ij}$ the *mean strain-rate tensor*

$$S_{ij} = \frac{1}{2}\left(\frac{\partial \overline{v_i}}{\partial x_j} + \frac{\partial \overline{v_j}}{\partial x_i}\right) \tag{3.90}$$

whereas the product $\tau_{ij} = -\overline{\rho v'_i\, v'_j}$ is the *Reynolds stress tensor*.

Widely applied approaches are based upon the Boussinesq hypothesis to correlate the Reynolds stress tensor to the mean velocity gradients:

$$-\overline{v'_i\, v'_j} = 2\upsilon_T S_{ij} - \frac{2}{3} k \delta_{ij} \tag{3.91}$$

being $v_T$ the *kinetic eddy viscosity* and $k$ the *turbulence kinetic energy*, defined as:

$$k = \frac{1}{2}\overline{v'_i v'_j} \tag{3.92}$$

The CFD models operate by combining the RANS equations with turbulence models. Among them, the most common are:

- **Standard *k-ε* turbulence model**: semi-empirical approach which reproduces the transportation equations for the turbulence kinetic energy $k$ and the turbulence dissipation rate $\varepsilon$ (Launder and Spading, 1974). Based upon the hypothesis of fully turbulent flow and negligible effects of molecular viscosity, it is explicated by two differential Eqs. (3.93) and (3.94) which represent the turbulence kinetic energy and the specific dissipation rate, respectively:

$$\frac{\partial(\rho k)}{\partial t} + \frac{\partial(\rho k v_i)}{\partial x_i} = \frac{\partial}{\partial x_j}\left[\left(\mu + \frac{\mu_t}{\sigma_k}\right)\frac{\partial k}{\partial x_j}\right] + G_k + G_b - \rho\varepsilon - Y_M \tag{3.93}$$

$$\frac{\partial(\rho\varepsilon)}{\partial t} + \frac{\partial(\rho\varepsilon v_i)}{\partial x_i} = \frac{\partial}{\partial x_j}\left[\left(\mu + \frac{\mu_t}{\sigma_\varepsilon}\right)\frac{\partial \varepsilon}{\partial x_j}\right] + C_{1\varepsilon}\frac{\varepsilon}{k}\left(G_k + C_{3\varepsilon}G_b\right) - C_{2\varepsilon}\rho\frac{\varepsilon^2}{k} \tag{3.94}$$

in which $G_k$ and $G_b$ are the turbulent kinetic energy increasing, caused by the velocity gradients and the buoyancy, respectively. $Y_M$ is the fluctuating dilation in compressible turbulence which determines the overall dissipation rate, whereas $C_{1\varepsilon}$, $C_{2\varepsilon}$, $C_{3\varepsilon}$ and $C_\mu$ are experimental constant values equal to 1.44, 1.92, 0.98 and 0.09, respectively. $\sigma_k$ and $\sigma_\varepsilon$ represent the turbulent Prandtl numbers for the kinetic energy and the related dissipation rate. Their derivation is experimental, as well, and they are set equal to 1.0 and 1.3, respectively. For each point of the motion field, the turbulent or *eddy viscosity* is intended as a function of the local values of the turbulent kinetic energy $k$ and of the dissipation rate $\varepsilon$ through the equation:

$$\mu_t = \rho C_\mu \frac{k^2}{\varepsilon} \tag{3.95}$$

where $C_\mu$ is the abovementioned constant.

The parameter $G_k$ and the modulus of the strain-rate tensor $S$ are calculated as follows, instead:

$$G_k = -\rho\overline{v'_i v'_j}\frac{\partial v_j}{\partial v_i} \tag{3.96}$$

$$S = \sqrt{2S_{ij}S_{ij}} \tag{3.97}$$

- **RNG *k-ε* turbulence model:** this model results to be more accurate than the Standard *k-ε* model, being derived by the application of the Renormalization Group Theory approach (Yakhot and Orszag, 1986). It differs from the Standard *k-ε* model for both different constants and the introduction of transport equations for the turbulent kinetic energy *k* and its dissipation rate *ε*. A differential formulation is also introduced to define the effective turbulent viscosity, in reference to flows with low Reynolds numbers;
- **Realizable *k-ε* turbulence model:** it presents significant differences from the abovementioned two *k-ε* models because based on both different turbulent viscosity and dissipation rate transport equations, derived as a function of the mean-square vorticity fluctuation (Shih, 1995);
- **Standard *k-ω*$^I$ turbulence model:** empirical-based model which analytically reproduces the turbulent kinetic energy *k* and its specific dissipation rate $\omega^I$ (Wilcox, 1998), through the equations:

$$\frac{\partial(\rho k)}{\partial t} + \frac{\partial(\rho k v_i)}{\partial x_i} = \frac{\partial}{\partial x_j}\left[\left(\mu + \frac{\mu_t}{\sigma_k}\right)\frac{\partial k}{\partial x_j}\right] + G_k - Y_k \tag{3.98}$$

$$\frac{\partial(\rho \omega)}{\partial t} + \frac{\partial(\rho \omega^I v_i)}{\partial x_i} = \frac{\partial}{\partial x_j}\left[\left(\mu + \frac{\mu_t}{\sigma_\omega}\right)\frac{\partial \omega^I}{\partial x_j}\right] + G_\omega - Y_\omega \tag{3.99}$$

in which $G_\omega$ is the generation of the specific dissipation rate $\omega^I$, whereas $Y_k$ and $Y_\omega$ represent the dissipation generated by the turbulence, for *k* and $\omega^I$, respectively. $\sigma_k$ and $\sigma_\varepsilon$, in conformity with the *k-ε* model, are the turbulent Prandtl numbers. The *eddy viscosity* $\mu_t$ is defined as a function of a damping coefficient $\alpha^{**}$;

- **SST *k-ω*$^I$ turbulence model:** the Shear Stress Transport *k-ω*$^1$ model (Menter, 1994) derives from the combination of a Standard *k-ω*$^I$ model and a transformed *k-ε* one. It differs from the Standard *k-ω*$^I$ model for the turbulent viscosity calculation, evaluated as a function of the transport of the principal turbulent shear stress. A cross-diffusion term in the $\omega^I$ equation and a blending function are also introduced to improve the calculation on the near-walls and far-field areas.

In the field of the CFD applications, several researches were carried out to simulate the internal kinematic and dynamic fields of PATs. Specifically, Tamm et al. (2000) showed the results of a preliminary CFD application on PATs, pointing out the necessity of improving the performed research with experimental data, in order to test and validate the developed approach. Natanasabapathi and Kshirsagar (2004) applied the ANSYS® CFX™ commercial software to simulate the behaviour of a centrifugal PAT. An unstructured mesh was generated by applying the Multiple Reference Frame (MRF) solution with frozen rotor interface to model the relative motion between impeller and volute. Total pressure and mass flow rate were set as boundary conditions for inlet and outlet, respectively. The comparison with experimental data pointed out great differences, in terms of efficiency estimation, when operative conditions far from the BEP were running. Improvements were observed when two rings were geometrically inserted between volute and runner, defining better experimental-numerical correlations.

Rawal and Kshirsagar (2007) applied a CFD model to a mixed-flow pump running in both direct and reverse mode. The geometric CFD model was composed of casing, runner and draft tube, by generating a tetrahedral unstructured mesh (Fig. 3.20). As for Natanasabapathi and Kshirsagar (2004), a frozen rotor approach was applied to define the correlation between stationary and rotating parts. Hence, a steady-state method was applied, by considering the MRF approach to convert inherently transient conditions into steady-state ones.

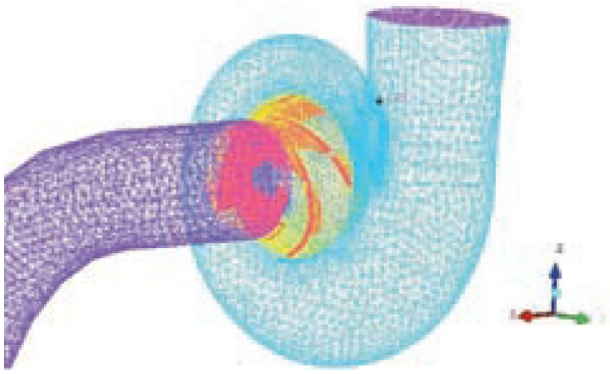

**Fig. 3.20 CFD modelling mesh (Rawal and Kshirsagar, 2007)**

Total pressure and mass flow rate were set as boundary conditions at inlet and outlet, respectively. From an experimental-numerical comparison, the modelled output power resulted to be higher than the measured one, as a consequence of the frictional losses (such as bearing and bushing), which were not considered in the modelling. Higher discrepancies were shown for lower flow rate values, whereas good performances were achieved for operative conditions near the BEP. The observed differences were specifically due to the geometric approximation and the necessity of proper mesh refinements. Similar results were achieved by Shukla (2008), who analysed the flow field across the inner parts of a centrifugal PAT, by using the ANSYS® Fluent™ MRF approach. Simulated results were compared with experimental data in both direct and reverse operations, observing good correlation in pump mode, whereas greater discrepancies were determined when the turbine mode was running. The model reliability was particularly observed for flow rates close to the BEP, relating to which low physical losses through the volute and the draft tube were shown, whereas the loss increase was observed for the furthest regions.

A different CFD commercial code was used by Derakhshan and Nourbakhsh (2008b). They applied the Numeca® FineTurbo™ software to simulate the centrifugal PAT motion. The MRF option with standard $k$-$\varepsilon$ turbulence model was considered, setting, as boundary conditions, the mass flow rate and the static pressure for inlet and outlet, respectively. A PAT, with specific speed $N_{sp}$ = 23.5, was modelled at rotational speeds $N$ between 750 and 3000 rpm, by comparing the numerical results with the experimental data. Differences in the order of ±5% for flow rate, head, power and efficiency were estimated for pump running in direct operations, whereas, in compliance with Shukla (2008), higher differences were assessed in reverse mode, up to about -3% for head and -16.5% for produced power. However, in turbine mode, simulations gave lower heads and powers than the experimental ones, probably as a result of the geometric simplification which neglected the physical interaction between the impeller, the hub and shroud and the casing. With respect to the Shukla (2008) approach, not negligible differences between numerical and experimental results were determined at BEP, as well.

Different approach was followed by Gonzalez et al. (2009), who pointed their attention on a double-suction centrifugal pump operating in turbine mode, aiming at analysing the formation of cavitation phenomena, generated in presence of high flow rates. A six-blade double aspirating impeller was considered with a vaneless spiral volute casing (Fig. 3.21).

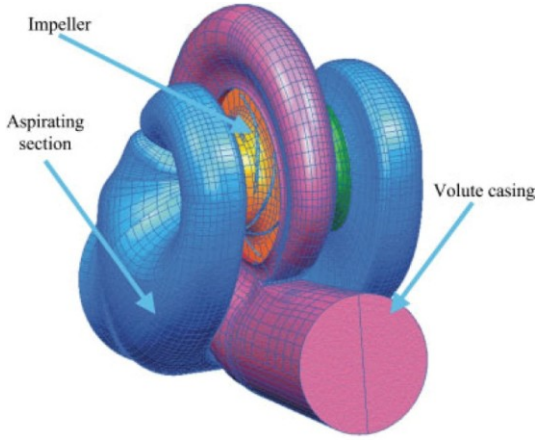


**Fig. 3.21 CFD model of a double-suction centrifugal PAT (Gonzalez et al., 2009)**

As per Shukla (2008) approach, Gonzalez et al. (2009) used the ANSYS® Fluent™ code, taking advantage from the geometric symmetry to analyse a halved pump. An unstructured mesh of tetrahedral cells was implemented for impeller, volute, inlet and outlet regions and a proper refinement across the tongue zone was arranged to characterize the velocity field of the region around the volute tongue. The Sliding Mesh (SM) technique was considered to simulate the relative motion between the impeller and the confining static elements. In turbine operations, the boundary conditions were set equal to the total pressure at inlet and static pressure at outlet; a logarithm law was also selected on both the blades and the volute walls. By analysing three flow rates, a slightly constant velocity field for lowest and normal flow rates was individuated, whereas a significant velocity gradient was observed for the higher flow rate value. However, high efficiencies were calculated in PAT operations, reaching values in the order of 80% for operative conditions close to the BEP.

Conversly, Sedlar et al. (2009) numerically drew the attention to a Multi-Stage pump with specific speed $N_s$ = 23, pointing out how, in reference to models with

number of stages higher than 3, the influence of casing could be neglected, allowing to exclusively model the middle stage. The ANSYS® CFX™ CFD code was applied to model two complete stages, by adding a straight pipe above the first impeller and a vaneless with counter-rotating walls. A structured grid was considered, composed of about 1.4 million elements, setting, as boundary conditions, the mass flow rate and the static pressure at inlet and outlet, respectively. Comparisons between experimental and numerical results showed, in both direct and reverse operations, high correlation for the flow rate-head curve reproduction, whereas greater differences, in the order of 13%, were assessed to estimate the efficiency. With the aim of simplifying the connection between stages, two planes, orthogonal to the shaft axis, were introduced, located at the mid-height of the return guide channel of the first impeller and between the hub and the shroud of the second impeller (Fig. 3.22), respectively.

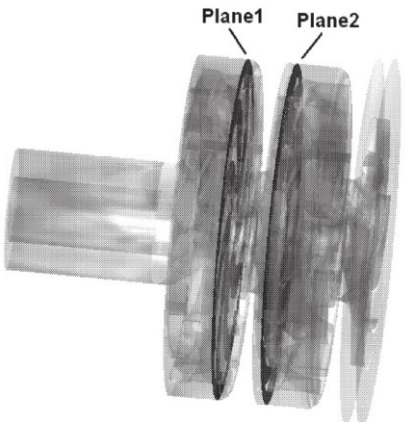


**Fig. 3.22 CFD model reproduction of a multi-stage centrifugal pump (Sedlar, 2009)**

In reverse mode, for the whole set of simulated flow rates, the velocity streamlines did not result to be detached by the impeller passages; conversely, for flow inside the channel stator and flow rates close to the BEP, the local separation from the stator was shown, both causing relevant energy losses and generating secondary flows.

Barrio et al. (2010) numerically simulated a Horizontal Axis Single-Stage centrifugal pump, operating in both direct and reverse mode, having impeller diameter $D$ = 200 mm and seven blades with logarithmic profile. The ANSYS® Fluent™ code was applied, by setting a constant total pressure at inlet and a variable static pressure at outlet as boundary conditions in pump mode. A constant total pressure at inlet and a

constant static pressure at outlet were applied in reverse operations, instead. The relative motion between the impeller and the stationary surrounding elements was reproduced by introducing interfaces between fluid regions, according to a Sliding Mesh (SM) technique. Steady and transient states were simulated, considering, during the transient simulations, at least five complete impeller revolutions, required to achieve the periodicity of the flow variables.

Performance curves were reproduced in reference to rotational speed $N$ = 1750 rpm and comparison with collected experimental data was presented, reaching good correlations, for head prediction, in both direct and reverse operations (Fig. 3.23).

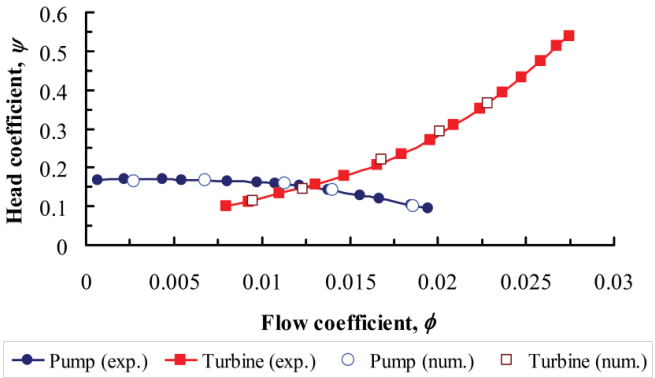


**Fig. 3.23 Experimental-numerical comparison for head prediction (Barrio et al., 2010)**

The analysis of the pressure across the impeller highlighted the pressure decrease from the external to the internal parts, as a consequence of the fluid impact on the blades. The generated head drop resulted to be higher at increasing the flow rate, whereas, for lower flow rates, the pressure resulted to be almost constant in the whole region near the tongue. Conversely, for higher flow rates, a region at lower pressure was detected between the impeller and the tongue.

The analysis of the velocity field pointed out the determination of a re-circulation zone close to the blades edges (Fig. 3.24), which caused the efficiency decrease. For higher flow rates, the re-circulating area moved forward the blade suction side, generating the fluid shifting across the blades.

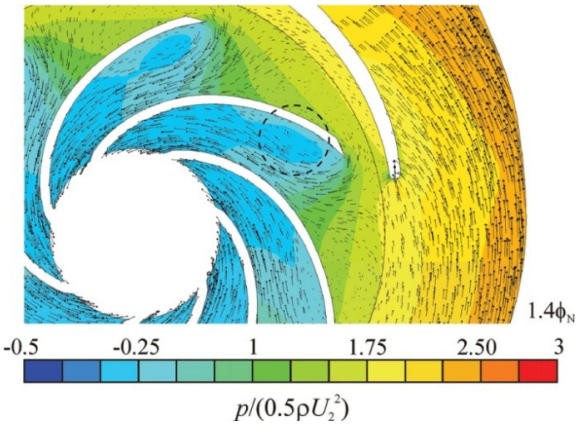


**Fig. 3.24 Impeller velocity field in PAT operation (Barrio et al., 2010)**

In addition, in PAT simulations, a monotonic increasing trend of the radial load was observed, however, resulting to be lower than the radial load assessed in pump mode.

As pointed out by the previous models, one of the critical points of CFD simulations of turbo-machines regards the geometric simplification, which causes relevant errors (Nautiyal et al., 2010b). With the aim of overcoming this limitation, Silva et al. (2010) numerically simulated a centrifugal pump operating in direct and reverse mode by using 3D cad files from manufacturer. The ANSYS® Fluent™ code was applied, referring to a fluid domain composed of more than 2 million elements, in reference to a horizontal axis Single-Stage centrifugal pump with impeller diameter $D$ = 265 mm and 8 blades, operating at rotational speed $N$ = 2900 rpm. A MRF approach was applied to reproduce the relative motion between impeller and volute, whereas total and static pressures were set as inlet and outlet boundary conditions, respectively. In direct operations, simulated results were compared with the experimental data, determining numerical characteristic curves, in terms of flow rate-head correlation, however, lower of about 5% than the experimental ones. On the other hand, in turbine mode, they compared the simulated results with theoretical data calculated with Williams (1996) model, by determining low discrepancies in the whole set of considered flow rates.

According to Sedlar et al. (2009) approach, Carravetta et al. (2010) numerically investigated a Multi-Stage PAT, using the ANSYS® CFX™ code. At first, a simulation level in pump mode was run, considering a mesh resolution of about 5 million elements for each stage, in both transient and steady-state operations. By comparing the

simulated data with experimental results from manufacturer, a good experimental-numerical correlation was shown for the transient-state simulations, in terms of head drop curve. Conversely, the steady-state simulations gave better results for the power curve prediction. Furthermore, a sensitivity analysis was performed, for a fixed flow rate value, by varying the mesh resolution according to 24 levels of simulation. A head increase was noticed for lower number of elements, defining a maximum error of about 7.5% with respect to the resolution of 5 million elements. However, the efficiency presented similar trends, with errors in the order of 19% for lower resolutions. Hence, a mesh configuration with 2.5 million elements was simulated in turbine mode by comparing numerical results with Suter (1966) and Derakhshan and Nourbakhsh (2008a) models. In this case, an overestimation of both head drop and power was determined, for both steady and transient state configuration.

In compliance with the Barrio et al. (2010) criterion, Fernandez et al. (2010) considered a single-suction centrifugal pump running at $N$ = 1750 rpm, by comparing experimental data with numerical simulations with ANSYS® Fluent™. A uniform velocity distribution at inlet and a constant static pressure at outlet were set as boundary conditions, whereas, as a result of a sensitivity analysis on several turbulence models implemented in ANSYS® Fluent™, the $k$-$\varepsilon$ turbulence model was applied, with standard wall functions across the wall regions. The SM technique was used to reproduce the relative motion between impeller and volute and two simulation procedures were performed: with frozen-rotor interface and with unsteady simulations. Comparison between experimental data and numerical simulations showed good agreements for both head and power, evaluating relative errors not higher than 10%. Specifically, the power was slightly overestimated, probably due to the neglecting of casing front and back sides. Thus, a hydraulic efficiency overestimation was assessed with the relative shifting of the BEP location. The existence of a tangential velocity component at the impeller exit was also observed, by causing, in presence of low flow rates, a fluid rotation with same direction of the impeller movement. Instead, for high flow rates, the opposite rotation was established.

In reference to the analysis of a radial flow PAT at a single rotational speed N = 1500 rpm, Morros et al. (2011) applied special refinements to the mesh generation, in the region between the volute tongue and the impeller blades and passages. Specifically, structured hexahedral cells were set for inlet and outlet domains, whereas unstructured tetrahedral cells were applied to both the impeller and the volute. A sensitivity analysis was also performed to evaluate the mesh resolution dependency, choosing a resolution rate able to give results, in terms of overall efficiency, comparable with those reached with a halved resolution. The ANSYS® Fluent™ code was applied for simulations, considering the SM technique to generate the grid interfaces. The *k-ε* turbulence model was used and the wall refinement was set through logarithmic law wall functions. Static pressure at inlet and total pressure at outlet were set as boundary conditions, with a rotor-frozen simulation approach. Comparison between numerical results and experimental data highlighted the model reliability to reproduce the head drop and efficiency performance curves, by determining increasing differences just at higher flow rates. The asymmetrical distribution of the velocity field across the impeller, caused by the volute tongue, was pointed out, so to direct to a specific evaluation of the circumferential pressure gradients on the blades. Starting from these results, the PAT capability to determine acceptable efficiencies, at different flow rates, was highlighted.

By following the Carravetta et al. (2010) analysis, Fecarotta et al. (2011) drew the attention on the evaluation of the dependency of CFD results from the mesh resolution, in reference to a Multi-Stage centrifugal pump operating in both direct and reverse mode. It was found that a reduction of elements of 54% was able to limit the computational times of about 90% with a lower Random Memory Access (RAM) occupation of about 84%, at the same time, guaranteeing discrepancie not higher than 10% for both head and efficiency estimation.

Furthermore, Yang et al. (2012a) applied the ANSYS® CFX™ code to reproduce the internal flow for a centrifugal PAT at rotational speed $N$ = 1500 rpm. A structured hexahedral grid was generated to model five elements: the inlet pipe, the front and the back chambers, the impeller and the volute. The Standard *k-ε* model was set as

turbulence model, whereas the static pressure and the mass flow rate were considered as inlet and outlet boundary conditions, respectively. A MRF approach was applied to reproduce the relative motion between the impeller and the adjacent static elements, introducing rotor-stator interfaces. Pump simulations, in direct operations, showed theoretical-experimental discrepancies at BEP for head $H_p$, power $P_p$ and efficiency $\eta_p$ of -0.8%, -0.8% and -3.0%, respectively. Higher differences were assessed far from the BEP, in the range 0.7-1.3$Q_{tb}$, equal to -3.9%, -6.0% and -2.5%, respectively. Simulations in PAT mode showed the overestimation of both head drop $H_t$ and power $P_t$ in the order of 5%. Higher differences were ascribable to the leakages through the balancing holes (introduced to equalize the pressure on the impeller suction and the back sides) and to the losses generated by mechanical seal and bearings, which were neglected into the computational modelling.

Different CFD commercial software was considered by Bozorgi et al. (2013), who applied the Numeca® Fineturbo™ code to an axial PAT, instead. A mesh with 2 million elements was generated and comparison with experimental tests was performed for rotational speed $N$ = 750 rpm. Results showed the satisfying correlation for head drop $H_t$, power $P_t$ and hydraulic efficiency $\eta_{ht}$, highlighting the capability of the considered axial pump of assuring a slightly constant high efficiency for a wide range of operative flow rates. Baburaj et al. (2013) simulated the behaviour of a Single-Stage centrifugal pump with specific speed $N_s$ = 23.9 operating in direct and reverse mode, by using the ANSYS® CFX™ software, instead. A single rotational speed $N$ = 2880 rpm was considered and an unstructured mesh was applied, composed of quadrilateral and triangular elements. Boundary conditions were set equal to the total pressure at inlet and to the mass flow rate at outlet and the characteristic curves, in PAT operations, were found out, evaluating a BEP efficiency $\eta_{tb}$ of about 70%, which resulted to be lower than that in pump operations.

Su et al. (2016) applied the ANSYS® CFX™ software to simulate a Single-Stage centrifugal PAT running at 1480 rpm. The turbulence SST $k$-$\omega^I$ model was set and total pressure at the inlet and flow rate at the outlet were considered as boundary conditions, respectively. Unsteady-state simulations were performed with the aim of analyzing the

periodicity of both the internal velocity and the pressure fields. By comparing the simulations with experimental data, good correlations were observed by both reproducing the whole geometrical configuration of the PAT and neglecting the bilateral chambers.

Frosina et al. (2017) applied the Simerics® PumpLinx® code to simulate three centrifugal PATs, running in transient conditions, in order to account for the relative motion between impeller and volute. The standard $k$-$\varepsilon$ turbulence model, defining the high experimental-numerical correlation to reproduce the characteristic curves of the whole set of investigated machines.

From the analysed review about the CFD application for PAT simulations, it is pointed out how the use of numerical models could result to be significantly relevant to both define the performances and reproduce the velocity and pressure fields for turbo-machines. However, the reliability of achieved results is strictly correlated with several modelling aspects, such as the considered simulation state, the applied turbulence model and the set boundary conditions. Specifically, more models were based on the application of the Standard $k$-$\varepsilon$ turbulence model, because able to provide effective results in shorter computational times. Moreover, to set the boundary conditions, several approaches were considered, as summarized in the following Tab. 3.3. Among them, the combination of pressure paramenters with velocity ones (in terms of velocity field and mass flow rate) at inlet and outlet or vice versa, usually resulted the most reliable, because more suitable for achieving the model convergence through the decoupled RANS equations.

A significant consideration should be also given to both the accuracy of the internal geometric configuration and the mesh generation, in terms of resolution and specific refinements, in order to properly reproduce the flow field across turbo-machines having complex configurations. Some models from literature neglected physical component of the PAT geoemetric model, such as the impeller hub and shrouds, making th interaction between the several parts less reliable. Furthermore, the analysis was generally focused on limited flow rate and rotational speed ranges, defining a restriction in the significance of the achieved results.

The characteristic analysis of CFD models for PATs in the literature, briefly summarized in the following Tab. 3.3, has represented the preliminary step for the implementation of the numerical approach, developed in the ambit of this Ph.D. work, extensively introduced and discussed in Chapter 5. In this ambit, the exhaustive characterization of a centrifugal Horizontal Axis Single-Stage PAT was performed, by both accurately reproducing its geometrical configuration and verifying the operations at several rotational speeds and flow rates.

| | **Code** | **PAT Model** | **Simulation** | **Inlet Boundary Condition** | **Outlet Bounday Condition** | **Turbulence Model** |
|---|---|---|---|---|---|---|
| Natanasabapathi and Kshirsagar (2004) | ANSYS® CFX™ | Centrifugal | MRF | Total Pressure | Mass Flow Rate | - |
| Rawal and Kshirsagar (2007) | - | Mixed Flow | MRF | Total Pressure | Mass Flow Rate | Standard $k$-$\varepsilon$ |
| Derakhshan and Nourbakhsh (2008b) | Numeca® FineTurbo™ | Centrifugal | Periodic B.C. | Mass Flow Rate | Static Pressure | Standard $k$-$\varepsilon$ |
| Gonzalez et al. (2009) | ANSYS® Fluent™ | Double-Suction Centrifugal | SM | Total Pressure | Static Pressure | Standard $k$-$\varepsilon$ |
| Sedlar et al. (2009) | ANSYS® CFX™ | Multi-Stage | MRF | Mass Flow Rate | Static Pressure | SST $k$-$\omega^{I}$ |
| Barrio et al. (2010) | ANSYS® Fluent™ | Centrifugal | SM | Total Pressure | Static Pressure | Standard $k$-$\varepsilon$ |
| Silva et al. (2010) | ANSYS® Fluent™ | Centrifugal | MRF | Total Pressure | Static Pressure | |
| Fernandez et al. (2010) | ANSYS® Fluent™ | Centrifugal | SM | Uniform Velocity | Static Pressure | Standard $k$-$\varepsilon$ |
| Morros et al. (2011) | ANSYS® Fluent™ | Centrifugal | SM | Static Pressure | Total Pressure | Standard $k$-$\varepsilon$ |
| Fecarotta et al. (2011) | ANSYS® CFX™ | Centrifugal | MRF | Static Pressure | Mass Flow Rate | Standard $k$-$\varepsilon$ |
| Baburaj et al. (2013) | ANSYS® CFX™ | Centrifugal | - | Total Pressure | Mass Flow Rate | - |
| Su et al. (2016) | ANSYS® CFX™ | Centrifugal | Trans. Mode | Total Pressure | Mass Flow Rate | SST $k$-$\omega^{I}$ |
| Frosina et al. (2017) | Simerics® PumpLinx® | Centrifugal | Trans. Mode | - | - | Standard $k$-$\varepsilon$ |

**Tab. 3.3 CFD PAT models in the literature**

### 3.3.5 PAT Geometric Modification for Efficiency Improvement

The performance improvement of a PAT, by modifying the pump geometric configuration, has been mainly directed to the impeller and the blade modifications, aiming at reducing the shock losses generated by the fluid impact against the blade tips (Lobanoff and Ross, 1992).

In this regard, results deriving by the blade rounding have been widely analysed both with experimental and numerical approaches. Among them, Lueneburg and

Nelson (1985) experimentally verified the efficiency improvement obtainable by rounding the impeller blades, estimating an increase of about 2.5% for flow rates close to the BEP. Furthermore, Suarda et al. (2006) analysed the benefits connected to the rounding of the impeller inlet ends (Fig. 3.25), in reference to centrifugal PATs applied for hydropower generation in Thailand.

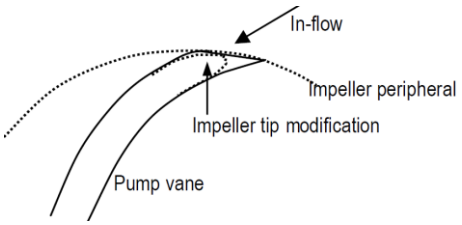


**Fig. 3.25 Rounding of the impeller tips (Suarda et al., 2006)**

As a result of the tested modification, a slight efficiency increase was estimated, able to make the flow rate range, having efficiency close to the BEP, wider. Benefits from tips rounding were remarkable for high capacity centrifugal PATs, whereas low improvements were achieved for small-sized models.

In this field, Derakhshan et al. (2009) applied an optimization procedure to redesign the blade shape with the aim of improving the pumps efficiency when operating as turbines. The model was based upon the consideration that the performance of radial turbo-machines is closely dependent on the blade angles, whereas the independency from the blade thickness was assigned. As a result of the optimization procedure, in a first phase, the rounding of blade leading edges (Fig. 3.26a) was both numerically and experimentally taken into account, whereas the rounding of hub and shroud inlet edges (Fig. 3.26b) was applied later. The proposed procedure was tested on a centrifugal PAT, running at rotational speed $N$ = 1500 rpm for several operating flow rates.

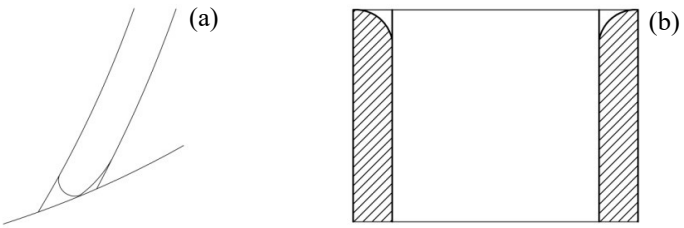


**Fig. 3.26 Rounding of (a) impeller blades and (b) hub/shroud (Derakhshan et al., 2009)**

Efficiency improvements were observed for the whole set of tested data, determining, by rounding the blade tips, an averaged head drop decrease of about 3%, whereas the power and efficiency increase of 9% and 3% were observed, respectively. Higher benefits were also reached by modifying the hub and shroud, through the which the power and efficiency improvement of about 36% and 5.5% were achieved, respectively.

Similar experimental approach was followd by Singh and Nestmann (2011), analysing the benefits of the impeller rounding for 9 centrifugal PATs operating at rotational speeds $N$ between 20 and 94 rpm. The rounding was carried out at half of both the blade and shroud thickness, at blade inlets and at shroud inlet (Fig. 3.27), respectively. An efficiency improvement of about 2% was shown for the whole set of investigated PATs.

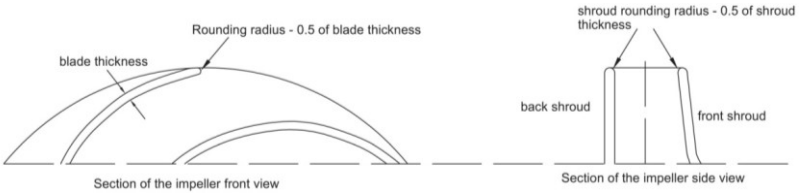


**Fig. 3.27 Rounding of impeller blades and hub/shroud (Singh and Nestmann, 2011)**

Aiming at combining numerical analyses with experimental results, Yang et al. (2012b) considered two impeller configurations of a Single-Stage centrifugal pump: with and without the splitter blades, respectively. The numerical approach pointed out the efficiency increase for impeller with splitter blades, as a consequence of both the lower head drop and the constant shaft power. By analysing the pressure field into the machine for the splitter blades adding, the maximum pressure pulsation was strongly lower than that observed for impeller without splitting. In both cases, as a consequence of the energy transfer to the shaft power, the pressure within the impeller was strongly reduced, across the impeller flow passage. Furthermore, the effects of the blade wrap angle, in terms of efficiency improvement, was investigated for three centrifugal PATs (Yang et al. 2012c). Blade wrap angles from 110° to 70° were accounted for experiments and simulations. Results showed the drop of flow rate-head and flow rate-power curves, at decreasing the blade wrap angle; the flow rate increase at BEP was

observed, instead. Thus, an optimal blade wrap angle was defined, able to maximize the efficiency, resulting to be lower for higher specific speeds $N_{sp}$. The numerical analysis gave head, power and efficiency values higher than the experimental ones, due to the neglecting of mechanical losses on seal and bearings.

Different approach was undertaken by Williams and Rodrigues (2013), instead. Indeed, they evaluated the head drop reduction, obtainable by enlarging the impeller suction eye. A head drop decrease was specifically achieved, whereas the shaft power did not vary, so to determine the efficiency increase.

Patel et al. (2013), in order to overcome the PAT limitation in flow regulation, due to the absence of the distributor device, numerically developed a physical modification of machine, by introducing fixed guide vanes in the casing. They assessed the angle of 75° as the one able to minimize the losses in kinetic energy. This configuration assured a tangential fluid entry across the impeller blades. Two reducers were also considered, a shorter and a longer one, by determining a loss decrease of about 55% at PAT inlet, by using the longer reducer.

Yang et al. (2014) combined numerical and experimental investigations on three centrifugal PATs with different blade thickness. Results showed the efficiency reduction, due to the simultaneous increment of head drop and shaft power and the increase of hydraulic losses within the impeller, as a consequence of the increase of velocity magnitude.

Finally, Doshi et al. (2017) experimentally analysed the benefits, in terms of efficiency increasing, obtainable by rounding the blades and the inner shrouds. For blades, a rounding radius equal to half blade thickness was applied, whereas a radius of half shroud thickness was taken into account for the inner sharp edges. The experimental results, performed on 9 PATs, pointed out the decrease of internal energy losses at PAT inlet. Experimental tests, by varying the rotational speed $N$ from 18 to 54 rpm, were performed, from which the loss reduction was achieved for lower rotational speeds. For higher $N$, greater variation in torque was observed, instead. Therefore, an overall improvement in efficiency, from 1% to 2.5%, was assessed, pointing out the possibility of further improvements, by enlarging the volute entry.

# References


- Agarwal T. (2012). Preview of Pump As Turbine (PAT) for micro-hydropower. *International Journal of Emerging Technology and Advanced Engineering*, 2(11).
- Alatorre-Frenk C., Thomas T.H. (1990). The pumps as turbines approach to small hydropower. *World Congress on Renewable Energy* (reading).
- Alatorre-Frenk C. (1994). Cost minimization in micro hydro systems using pumps-as-turbines. *Ph.D. Thesis*, University of Warwick, England.
- Amelio M., Barbarelli S., Scornaienchi N.M. (2000). Caratterizzazione al banco prova di pompe centrifughe utilizzate come turbine. *Proceedings of 55th National Congress ATI*, Bari and Potenza, Italy, 2000 (in Italian).
- Araujo L.S., Ramos H.M., Coelho S.T. (2006). Pressure control for leakage minimization in water distribution systems management. *Journal of Water Resources Planning & Management*, 20(1), 133-149.http://dx.doi.org/10.1007/s11269-006-4635-3
- Arndt R.E.A. (1981). Cavitation in fluid machinery and hydraulic structures. *Annual Review Fluid Mechanics*, 13, 273-326. http://dx.doi.org/10.1146/annurev.fl.13.010181.001421
- Arriaga M. (2010). Pump As Turbine – A pico-hydro alternative in Lao People's Democratic Republic. *Renewable Energy*, 35, 1109-1115. http://dx.doi.org/10.1016/j.renene.2009.08.022
- Baburaj E., Sivaprakasam R., Manikandan C., Sudha K. (2013). CFD analysis of Pump As Turbine for micro-hydro schemes. *International Journal of Innovative Research in Science, Engineering and Technology*, 2(3), 590-594.
- Barbarelli S., Amelio M., Florio G. (2016). Predictive model estimating the performances of centrifugal pumps used as turbines. *Energy*, 107, 103-121. http://dx.doi.org/ 10.1016/j.energy.2016.03.122
- Barrio R., Fernandez J., Parrondo J., Blanco E. (2010). Performance prediction of a centrifugal pump working in direct and reverse mode using Computational Fluid Dynamics. *Proceedings of the International Conference on Renewable Energies and Power Quality ICREPQ '10*, 23rd-25th March 2010, Granada, Spain.
- Boccazzi A., Pallabazzer R., Sebbit A. (1997). Pumps as Turbines for micro-hydropower. *Proceedings of the International Symposium on Alternative/Renewable Energy ISAAE '97*, 22nd -24th July 1997, Malaysia.
- Bozorgi A., Javidpour E., Riasi A., Nourbakhsh A. (2013). Numerical and experimental study of using axial Pump As Turbine in Pico hydropower plants. *Renewable Energy*, 53, 258-64. http://dx.doi.org/10.1016/j.renene.2012.11.01
- Buse F. (1981). Using centrifugal pumps as hydraulic turbines. *Chemical Engineering*, 113-117.
- Carravetta A., Fecarotta O., Ramos H.M. (2010). Numerical simulation on Pump As Turbine: mesh reliability and performance concerns. *Proceedings of the International Conference on Clean Electrical Power ICCEP 2011*, 14th-16th June 2011, Ischia, Italy. http://dx.doi.org/10.1109/ICCEP.2011.6036260

- Carravetta A., Del Giudice G., Fecarotta O., Ramos H.M. (2012). Energy production in Water Distribution Networks: a PAT design strategy. *Water Resources Management*, 26, 3947-3959. http://dx.doi.org/10.1007/s11269-012-0114-1
- Carravetta A., Del Giudice G., Fecarotta O., Ramos H.M. (2013). PAT design strategy for energy recovery in water distribution networks by electrical regulation. *Energies*, 6(1), 411-424. http://dx.doi.org/10.3390/en6010411
- Carravetta A., Conte M.C., Fecarotta O., Ramos H.M. (2014). Evaluation of PAT performances by Modified Affinity Laws. *Procedia Engineering*, 89, 581-587. http://dx.doi.org/10.1016/j.proeng.2014.11.481
- Chapallaz J.M., Eichenberger P., Fisher G. (1992). Manual on Pumps used As Turbines. Vieweg, Braunschweig, Germany, Chapter 1.
- Childs S.M. (1962). Convert pumps to turbine and recover HP. In: *Hydrocarbon Processing and Petroleum Rejner*, 41(10), 173-174.
- Chuenchooklin S. (2006). Development of pico-hydropower plant for farming village in upstream Watershed, Thailand. *Proceedings of Conference on Prosperity and Poverty in a Globalised World – Challenges for Agricultural Research*, Tropentag, Bonn, Germany.
- Corcoran L., McNabola A., Coughlan P. (2012). Energy recovery potential of the Dublin region water supply network. *Proceedings of the World Congress on Water Climate and Energy*, 13th-18th May 2012, Dublin, Ireland.
- Dannier A., Del Pizzo A., Giugni M., Fontana N., Marini G., Proto D. (2015). Efficiency evaluation of a micro-generation system for energy recovery in water distribution networks. *Proceedings of the 5th International Conference on Clean Electrical Power. Renewable Energy Resources Impact ICCEP15*, 16th-18th June 2015, Taormina, Italy, http://dx.doi.org/10.1109/ICCEP.2015.7177566
- De Marchis M., Fontanazza C.M., Freni G., Messineo A., Milici B., Napoli E., Notaro V., Puleo V., Scopa A. (2014). Energy recovery in water distribution networks. Implementation of Pumps As Turbines in a dynamic numerical model. *Procedia Engineering*, 70, 439-448. http://dx.doi.org/10.1016/j.proeng.2014.02.049
- De Marchis M., Milici B., Volpe R., Messineo A. (2016). Energy saving in water distribution network through Pump As Turbine generators: economic and environmental analysis. *Energies*, 9(11), 877. http://dx.doi.org/10.3390/en9110877
- Derakhshan S., Nourbakhsh A. (2008a). Experimental study of characteristic curves of centrifugal pumps working as turbines in different specific speeds. *Experimental Thermal and Fluid Science*, 32, 800-807. http://dx.doi.org/10.1016/j.expthermflusci.2007.10.004
- Derakhshan S., Nourbakhsh A. (2008b). Theoretical, numerical and experimental investigation of centrifugal pumps in reverse operation. *Experimental Thermal and Fluid Science*, 32, 1620-1627. http://dx.doi.org/10.1016/j.expthermflusci.2008.05.004
- Derakhshan S., Mohammadi B., Nourbakhsh A. (2009). Efficiency improvement of centrifugal reverse pumps. *Journal of Fluids Engineering. Transactions of the ASME*, 131(2). 0211031-0211039. http://dx.doi.org/10.1115/1.3059700

- Doshi A., Channiwala S., Singh P. (2017). Inlet impeller rounding in Pumps As Turbines: an experimental study to investigate the relative effects of blade and shroud rounding. *Experimental Thermal and Fluid Science*, 82, 333-348. http://dx.doi.org/10.1016/j.expthermflusci.2016.11.024
- Engeda A. (1987). Untershungen an Kreisle pumpen mit offenen und geschlossenen Laufradern im pumpen- und Turbinenbetrieb. *Ph.D. Thesis*. University of Hannover, DH (in German).
- Engel L. (1931). Die Rücklaufdrehzahlen der Kreiselpumpen. *Ph.D. Thesis*, Tech. Hochschule Braunschweig, Germany (in German).
- European Small Hydropower Association (2005). Small Hydropower for developing Countries, European Small Hydropower Association, IT Power website: https://kunaifien.files.wordpress.com/2008/12/small-hydropower-for-developing-countries1.pdf
- Fecarotta O., Carravetta A., Ramos H.M. (2011). CFD and comparisons for a Pump As Turbine: mesh reliability and performance concerns. *International Journal of Energy and Environment*, 2(1), 39-48.
- Fecarotta O., Aricò C., Carravetta A., Martino R., Ramos H.M. (2015). Hydropower potential in Water Distribution Networks: pressure control by PATs. *Water Resources Management*, 29, 699-714. http://dx.doi.org/10.1061/10.1007/s11269-014-0836-3
- Fecarotta O., Carravetta A., Ramos H.M., Martino R. (2016). An improved affinity model to enhance variable operating strategy for Pumps used As Turbines. *Journal of Hydraulic Research*, 54(3), 332-341. http://dx.doi.org/10.1080/00221686.2016.1141804
- Fernandez J., Blanco E., Parrondo J., Stickland M.T., Scanlon T.J. (2004). Performance of a centrifugal pump running in inverse mode. P*roceedings of the Institution of Mechanical Engineers, Part a: Journal of Power and Energy*, 218(4), 265-271. http://dx.doi.org/10.1243/0957650041200632
- Fernandez J., Barrio R., Blanco E., Parrondo J., Marcos A. (2010). Numerical investigation of a centrifugal pump running in reverse mode. *Proceedings of the Institution of Mechanical Engineers, Part a: Journal of Power and Energy*, 224(3), 373-381. http://dx.doi.org/10.1243/09576509JPE757
- Filion Y.R., MacLean H.L., Karney B. (2004). Life-cycle energy analysis of a water distribution system. *Journal of Infrastructure Systems*, 10, 120-130. http://dx.doi.org/10.1061/(ASCE)1076-0342(2004)10:3(119)
- Fontana N., Giugni M., Portolano D. (2012). Losses reduction and energy production in water distribution networks. *Journal of Water Resources Planning and Management*, 138(3), 237-244. http://dx.doi.org/10.1061/(ASCE)WR.1943-5452.0000179
- Fontana N., Giugni M., Glielmo L., Marini G. (2016). Real time control of a prototype for pressure regulation and energy production in water distribution networks. *Journal of Water Resources Planning and Management*, 142(7), 04016015, 1-9. http://dx.doi.org/10.1061/(ASCE)WR.1943-5452.0000651
- Frosina E., Buono D., Senatore A. (2017). A performance prediction method for Pumps As Turbines (PATs) using a Computational Fluid Dynamics (CFD) modelling approach. *Energies*, 10(103), 1-19. http://dx.doi.org/10.3390/en10010103

- Gantar M. (1988). Propeller pump running as turbines. *Conference on Hydraulic Machinery*, Ljubljana, Slovenia, 237-248.
- Garcia J.P., Marco A.C., Santos S.N. (2010). Use of centrifugal pumps operating as turbines for energy recovery in water distribution networks. Two case study. *Advanced Material Research*, 107, 87-92. http://dx.doi.org/10.4028/www.scientific.net/AMR.107.87
- Giugni M., Fontana N., Portolano D. (2009). Energy saving policy in water distribution networks. *Proceedings of the International Conference on Renewable Energies and Power Quality ICREPQ'09*, 15th-17th April 2009, Valencia, Spain.
- Gonzalez J., Fernandez Oro J.M., Arguelles-Diaz K.M., Santolaria C. (2009). Flow analysis for a double suction centrifugal machine in the pump and turbine operation modes. *International Journal for Numerical Methods in Fluids*, 61, 220-236. http://dx.doi.org/10.1002/fld.1951
- Grant A., Bain J.M. (1985). Pump turbine – the economic answer. *Proceedings of the International Conference on Small Hydropower – a developing asset.*
- Grover K.M. (1980). Conversion of Pumps to Turbines. GSA Inter Corp, Katonah, New York, USA.
- Hancock J.W. (1963). Centrifugal pump or water turbine. *Pipe Line News*, 25-27.
- Hergt P. (1982). The influence of the volute casing on the position of the best efficiency point. *Proceedings of the 11th IAHR Symposium*, Amsterdam, Holland, 3, 69.
- Isbasoiu E.C., Bucur D.M., Ghergu C.M., Dunca G. (2007). Using standard pumps as turbines. *Proceedings of the International Conference CEEX 2007*, Technical Publishing House, 24th –26th October 2007, Brasov, Romenia.
- Jafari R., Khanajani M.J., Esmaeilian H.R. (2015). Pressure management and electric power production using Pumps As Turbines. *Journal American Water Works Association*, 107(7), E351-E363. http://dx.doi.org/10.5942/jawwa.2015.107.0083
- Jain S.V., Patel R.N. (2014). Investigations on pump running in turbine mode: a review of the state-of-the-art. *Renewable and Sustainable Energy Reviews*, 30, 841-868. http://dx.doi.org/10.1016/j.rser.2013.11.030
- Joshi S., Holloway A.G.L., Chang L., Kojabadi H.M. (2005a). Development of a stand alone micro-hydro system using pump as turbine technology for low head sites in remote areas. *Proceedings of the 20th International Power System Conference PSC2005*, 14th-16th November 2004, Tehran, Iran.
- Joshi S., Gordon A., Holloway L., Chang L. (2005b). Selecting a high specific speed pump for low head hydro-electric power generation. *Canadian Conference on Electrical and Computer Engineering*. http://dx.doi.org/10.1109/CCECE.2005.1557003
- Jowitt P.W., Xu C. (1990). Optimal valve control in water-distribution networks. *Journal of Water Resources Planning and Management ASCE*, 116(4), 455–472. http://dx.doi.org/10.1061/(ASCE)0733-9496(1990)116:4(455)
- Karadirek E., Kara S., Ozen O., Gulaydin O., Bestas E., Boyacilar M., Muhammetoglu A., Gungor A., Muhammetoglu H. (2016). Energy recovery potential from excess pressure in water supply and distribution systems. *Mugla Journal of Science and Technology*, 2(1), 70-76.

- Launder B., Spalding D.B. (1974). The numerical computation of turbulent flow computer methods. *Computer Methods in Applied Mechanics and Engineering*, 3(2), 269-289. http://dx.doi.org/10.1016/0045-7825(74)90029-2
- Lima G.M., Luvizotto E.Jr., Brentan B.M. (2017). Selection and location of Pumps As Turbines substituting Pressure Reducing Valves. *Renewable Energy*, in press. http://dx.doi.org/10.1016/j.renene.2017.03.056
- Lisk B., Greenberg E., Bloetscher F. (2012). Implementing renewable energy at water utilities. Case studies. *Water Research Foundation*, Denver, USA.
- Lobanoff V.S., Ross R.R. (1992). Centrifugal pumps: design and applications. 2nd ed. Texas: Gulf publishing company.
- Loots I., Van Dijk M., Van Vuuren S.J., Bhagwan J.N., Kurtz A. (2014). Conduit-hydropower potential in the City of Tshwane water distribution system: a discussion of potential applications, financial and other benefits. Journal of the South African Institution of Civil Engineering, 56(3), 2-13.
- Lueneburg R., Nelson R.M. (1985). Hydraulic power recovery turbines. *Centrifugal pumps: design and applications*. Lobanoff VS, Ross RR editors. Texas: Gulf Publishing Company, 246-285.
- Maher P., Smith N.P.A., Williams A.A. (2003). Assessment of pico-hydro as an option for off-grid electrification in Kenya. *Renewable Energy*, 28(9), 1357-1369. http://dx.doi.org/ 10.1016/S0960-1481(02)00216-1
- McClaskey B.M., Lundquist J.A. (1976). Hydraulic power recovery turbines, ASME Conference, 76(65).
- Menter F.R. (1994). Two-Equation eddy-viscosity turbulence models for engineering applications. *American Institute of Aeronautics and Astronautics AIAA Journal*, 32(8), 1598-1605.
- Morros C.S., Fernandez Oro J.M., Arguelles Diaz K.M. (2011). Numerical modelling and flow analysis of a centrifugal pump running as a turbine: Unsteady flow structures and its effects on the global performance. *International Journal for Numerical Methods in Fluids*, 65, 542-562. http://dx.doi.org/10.1002/fld.2201
- Motwani K.H., Jain S.V., Patel R.N. (2013). Cost analysis of Pump As Turbine for pico hydropower plants – a case study. *Procedia Engineering*, 51, 721-726. http://dx.doi.org/10.1016/j.proeng.2013.01.103
- Natanasabapathi S.R., Kshirsagar J.T. (2004). Pump As Turbine – An experience with CFX-5.6. Corporate Research and Eng. Division, Kiloskar Bros. Ltd.
- Nautiyal H., Varun, Kumar A. (2010a). Reverse running pumps analytical, experimental and computational study: a review. *Renewable and Sustainable Energy Reviews*, 14, 2059-2067. http://dx.doi.org/10.1016/j.rser.2010.04.006
- Nautiyal H., Varun, Kumar A. (2010b). CFD analysis on Pumps working As Turbines. *Hydro Nepal Journal of Water Energy and Environment*, 6, 35-37. http://dx.doi.org/ 10.3126/hn.v6i0.4191

- Nautiyal H., Varun Kumar A., Yadav S. (2011). Experimental investigation of centrifugal Pump working As Turbine for small hydropower systems. *Energy Science and Technology*, 1(1), 79-86.
- Paish O. (2002). Small hydro power: technology and current status. *Renewable and Sustainable Energy Reviews*, 6(6), 537-556. http://dx.doi.org/10.1016/S1364-0321(02)00006-0
- Parra S., Krause S. (2017). Pressure management by combining Pressure Reducing Valves and Pumps As Turbines for water loss reduction and energy recovery. *International Journal of Sustainable Development and Planning*, 12(1), 89-97. http://dx.doi.org/10.1016/10.2495/SDP-V12-N1-89-97
- Patel V.A., Jain S.V., Motwani K.H., Patel R.N. (2013). Numerical optimization of guide vanes and reducer in pump running in turbine mode. *Procedia Engineering*, 51, 797-802. http://dx.doi.org/10.1016/j.proeng.2013.01.114
- Patelis M., Kanakoudis V., Gonelas K. (2016). Pressure management and energy recovery capabilities using PATs. *Procedia Engineering,* 162, 503-510. http://dx.doi.org/ 10.1016/j.proeng.2016.11.094
- Pelton A.D. (1988). A database and sublattice model for molten salts. *Calphad*, 12(2), 127-142.
- Prasad V., Shukla S.N., Joshi S.G. (2006). Performance characteristics of Pump As Turbine. *Indian Pumps*, 5-9.
- Pugliese F., De Paola F., Fontana N., Giugni M., Marini G. (2016). Experimental characterization of two Pumps As Turbines for hydropower generation. *Renewable Energy*, 99, 180-187. http://dx.doi.org/10.1016/j.renene.2016.06.051
- Puleo V., Fontanazza C.M., Notaro V., De Marchis M., Freni G., La Loggia G. (2014). Pumps As Turbines (PATs) in water distribution networks affected by intermittent service. *Journal of Hydroinformatics*, 162(2): 259-271. http://dx.doi.org/10.2166/hydro.2013.200
- Ramos H.M., Borga A. (1999). Pumps As Turbines: an unconventional solution to energy production. *Urban Water*, 1, 261-263. http://dx.doi.org/10.1016/S1462-0758(00)00016-9
- Rawal S., Kshirsagar J.T. (2007). Numerical simulation on a pump operating in a turbine mode. *Proceedings of the 23rd International Pump Users Symposium*, 5th-8th March 2007, Houston, Texas, USA.
- Rossi M., Righetti M., Renzi M. (2016). Pump-As-Turbine for energy recovery applications: the case of an aqueduct. *Energy Procedia*, 101, 1207-1214. http://dx.doi.org/10.1016/j.egypro.2016.11.163
- Saini R.P., Ahmad N. (1993). Selection procedure of centrifugal pump to use as turbine for small hydro power stations. *Proceedings of National Seminar on Small Hydro Power Project CIVSEM'93*, 64-71, Coimbatore, India.
- Sammartano V., Sinagra M., Spada E., Tucciarelli T. (2016a). Regolazione delle pressioni mediante produzione di energia idroelettrica nelle reti di distribuzione. *Proceedings of the 35th Convegno Nazionale di Idraulica e Costruzioni Idrauliche*, 14th-16th September 2016, Bologna, Italy. http://dx.doi.org/10.6092/unibo/amsacta/5400

- Sammartano V., Aricò C., Sinagra M., Tucciarelli T. (2016b). Banki-Mitchell micro-turbines for energy production in water distribution networks. Proceedings of the 4th IAHR Europe Congress, 27th-29th July 2016, Liegi, Belgium. http://dx.doi.org/10.1201/b21902-159
- Samora I., Manso P., Franca M.J., Schleiss A.J., Ramos H.M. (2016a). Energy recovery using micro-hydropower technology in Water Supply Systems: the case study of the city of Fribourg. *Water*, 8(8), 344-359. http://dx.doi.org/10.3390/w8080344
- Samora I., Hasmatuchi V., Munch-Alligne C., Franca M.J., Schleiss A.J., Ramos H.M. (2016b). Energy production with a tubular propeller turbine. *Proceedings of the 28th IAHR Symposium on Hydraulic Machinery and Systems*, 4th-8th July 2016, Grenoble, France.
- Sarbu I., Borza I. (1998). Energetic optimization of water pumping in distribution systems. *Periodica Polytechnica Mechanical Engineering*, 42(2), 141-152.
- Schmiedl E. (1988). Serien-Kreiselpumpen im Turbinenbetrieb. *Pumpentagung Karlsruhe*, A6 (in German).
- Sedlar M., Soukal J., Komarek M. (2009). CFD analysis of middle stage of multistage pump operating in turbine regime. *Engineering Mechanics*, 16(6), 413-421.
- Sharma K.R. (1985). Small Hydroelectric Project-use of Centrifugal Pumps as Turbines, Kirloskar Electric Co, Bangalore, India.
- Sharma R.L. (1998). Pumps as turbines (PAT) for small hydro. *Proceedings of the International Conference on Hydropower Development in Himalayas*, 137-146.
- Shih T., Liou W., Shabbir A., Yang Z., Zhu J. (1995). A new k–e eddy viscosity model for high Reynolds number turbulent flows – Model development and validation. *Journal Computer Fluids*, 24, 227-238.
- Shukla A. (2008). Performance evaluation of Pump As Turbine. *Ph.D. Thesis*. Indian Institute of Technology Roorkee, India.
- Silva F.J., Pascoa J.C., Pinheiro J.S., Martins D.J. (2010). Turbulent flow structure computation inside a pump-PAT using an industrial benchmark test case. *Proceedings of the European Conference on Computational Fluid Dynamics ECCOMAS CFD 2010*, 14th-17th June 2010, Lisbon, Portugal.
- Simpson A.R., Marchi A. (2013). Evaluating the approximation of the Affinity Laws and improving the efficiency estimate for variable speed pumps. *Journal of Hydraulic Engineering*, 139, 1314-1317. http://dx.doi.org/10.1061/(ASCE)HY.1943-7900.0000776
- Singh P. (2005). Optimization of internal hydraulics and of system design for Pumps As Turbines with field implementation and evaluation. *Ph.D. Thesis*, Universitat Fridericiana zu Karlsruhe (TH), Karlsruhe, German.
- Singh P., Nestmann F. (2010). An optimization routine on a prediction and selection model for the turbine operation of centrifugal pumps. *Experimental Thermal and Fluid Science*, 34, 152-164. http://dx.doi.org/10.1016/j.expthermflusci.2009.10.004
- Singh P., Nestmann F. (2011). Internal hydraulic analysis of impeller rounding in centrifugal Pumps As Turbines. *Experimental Thermal and Fluid Science*, 35(1), 121-134. http://dx.doi.org/10.1016/j.expthermflusci.2010.08.013

- Sitzenfrei R., Berger D., Rauch W. (2015). Design and optimization of small hydropower systems in water distribution networks under consideration of rehabilitation measures. Urban Water Journal, 1-9. http://dx.doi.org/10.1080/1573062X.2015.1112410
- Stepanoff A.J. (1948). Centrifugal and Axial Flow Pumps: Theory, Design and Application, John Wiley & Sons, Inc, New York, USA.
- Stepanoff A.J. (1957). Centrifugal and Axial Flow Pumps, 2nd ed., John Wiley & Sons, Inc, New York, USA, 276.
- Su P-A., Karney B. (2014). Micro hydroelectric Energy recovery in municipal water systems: a case study for Vancouver. *Urban Water Journal*, 12(8), 678-690. http://dx.doi.org/10.1080/1573062X.2014.923919
- Suarda M., Suarnadwipa N., Adnyana W.B. (2006). Experimental work on modification of impeller tips of a centrifugal Pump As a Turbine. *Proceedings of the 2nd Joint International Conference on "Sustainable Energy and Environment* (*SEE 2006*), 21st-23rd November 2006, Bangkok, Thailand.
- Suter P. (1966). Representation of pump characteristics for calculation of water hammer. *Sulzer Technical Review Research Issue*, 45-48.
- Su X., Huang S., Zhang X., Yang S. (2016). Numerical research on unsteady flow rate characteristics of Pump As Turbine. Renewable Energy, 94, 488-495. http://dx.doi.org/ 10.1080/10.1016/j.renene.2016.03.092
- Swanson M.M. (1953). Complete characteristics circle diagram for turbo-machinery. *Transactions of American Society of Mechanical Engineering ASME*, 75, 816-826.
- Tamm A., Braten A., Stoffel B., Ludwig G. (2000). Analysis of a standard pump in reverse operation using CFD. *Proceedings of the 20th IAHR Symposium: Hydro, Technology, and the Environment for the New Century*, 6th-9th August 2000, Charlotte, North Carolina, USA.
- Tan X., Engeda A. (2016). Performance of centrifugal Pumps running in reverse As Turbine: Part II – systematic specific speed and specific diameter based performance prediction. *Renewable Energy*, 99, 188-197. http://dx.doi.org/10.1016/j.renene.2016.06.052
- Thoma D., Kitteredge C.P. (1931). Centrifugal pumps operated under abnormal conditions. *Power*, 73, 881–4.
- Tricarico C., Morely M.S., Gargano R., Kapelan Z., de Marinis G., Savic D., Granata F. (2014). Integrated optimal cost and pressure management for water distribution networks. Procedia Engineering, 70, 1659-1668. http://dx.doi.org/10.1016/j.proeng.2014.02.183
- United Nations Industrial Development Organization (2010). Projects for the promotion of small hydro power for productive use. Technical report, Vienna, Austria.
- Water Supply Department of the Hong Kong Administrative Region (2012). Novel Inline Hydropower System for Power Generation from Water Pipelines. http://phys.org/news/2012-12-inline-hydropower-power-pipelines.html
- Wilcox D.C. (1998). Turbulence modeling for CFD. 2nd ed. DCW Industries, Inc., La Canada CA.
- Williams A. (1992). Pumps As Turbines used with induction generations of stand-alone micro-hydroelectric power plants. *Ph.D. Thesis*. Nottingham Polytechnic, England.

- Williams A. (1994). The turbine performance of centrifugal pumps: a comparison of prediction methods. *Proceedings of the Institution of Mechanical Engineers Part A*: *Journal of Power Energy*, 208(1), 59-66.
- Williams A. (1996). Pump As Turbines for low cost micro hydropower. *Renewable Energy*, 9(1–4), 1227-1234.
- Williams A., Rodrigues A. (2013). The performance of centrifugal Pumps As Turbines and influence of pump geometry. http://ebookbrowse.com/3-arthur-williams-the-performance-of-centrifugal-pumps-as-turbines-and-influence-of-pump-geometry-pdf-d73005868
- Yakhot V., Orszag S.A. (1986). Renormalization group analysis of turbulence. I. Basic of theory. *Journal of Scientific Computing*, 1(1), 3-51. http://dx.doi.org/10.1007/BF01061452
- Yang S-S., Derakhshan S., Kong F-Y. (2012a). Theoretical, numerical and experimental prediction of Pump As Turbine performance. *Renewable Energy*, 48, 507-513. http://dx.doi.org/10.1016/j.renene.2012.06.002
- Yang S-S., Kong F-Y., Jiang W-M., Qu X-Y. (2012b). Effects of impeller trimming influencing Pump As Turbine. *Computers & Fluids*, 67, 72-78. http://dx.doi.org/10.1016/j.compfluid.2012.07.009
- Yang S-S., Kong F-Y., Chen H., Su X-H. (2012c). Effects of blade wrap angle influencing a Pump As Turbine. *Journal of Fluids Engineering, Transactions of the ASME*, 134(2), 0611021-0611021-0611028. http://dx.doi.org/10.1115/1.4006677
- Yang S-S., Wang C., Chen K., Yuan X. (2014). Research on blade thickness influencing Pump As Turbine. *Advances in Mechanical Engineering*, 2014, 1-8. http://dx.doi.org/10.1155/2014/190530
- Zakkour P.D., Gaterell M.R., Griffin P., Gochin R.J., Lester J.N. (2002). Developing a sustainable energy strategy for a water utility. Part II: a review of potential technologies and approaches. *Journal of Environmental Management*, 66, 114-125. http://dx.doi.org/10.1006/jema.2002.0567

# Chapter 4

# Experimental Investigation of Centrifugal Pumps As Turbines

From the analysis of the literature approaches introduced in Chapter 3, the necessity of extending the experimental knowledge about several centrifugal pump models, available on the market, and useful for running as turbines, was deduced. Specifically, by verifying the analytic relationships in the literature, it was found that very few tools were available to predict the PAT performances far from BEP, however, resulting limited to narrow operative conditions (Par. 3.3.2).

With the aim of overcoming the limitation about the knowledge of PAT perfomances of different centrifugal PAT models, realiable for hydropower generation in WDNs, an experimental analysis was carried out at the Hydraulic Laboratory of the Department of Civil, Architectural and Environmental Engineering (DICEA) of University of Naples Federico II (IT).

The laboratory WDN prototype in Fig. 4.1, installed with the grants of Projects PON01_01596 "WaterGRID" and PON04a2_F "BE&SAVE – AQUASYSTEM – SIGLOD", was used for experiments, because able to provide the equipments and the flexibility, required to perfom an intensive experimental campaign on PAT models, having different geometric characteristics and working at wide operative conditions, both in terms of flow rates and rotational speeds.

**Fig. 4.1 WDN laboratory prototype at DICEA Hydraulic Laboratory**

In greater detail, the perfomed analysis was focused on the characterization of four PAT models with different geometric configuration and performances, aiming at extending the experimental knowledge about the characteristics of centrifugal pumps running in reverse mode, in reference to typical flow rate ranges for WDNs of small-medium sized urban and rural centers supplying up to about 20000 inhabitants.

The attention was specifically drawn to a classical Single-Stage Horizontal Axis centrifugal pump and to three Single-Stage and Multi-Stage Vertical Axis centrifugal pumps, having different number of stages and motor equipment.

The reliability of prediction tools for PAT performances available in the literature was verified and new analytic relationships were proposed for wider sets of both centrifugal PAT models and operations. Basing on the experimental results, a procedure for the optimal selection of centrifugal PATs in WDNs was developed, with the aim of furnishing a basic tool of a Decision Support System (DSS) for hydropower generation in urban and rural areas.

## 4.1 Experimental Laboratory Set-Up

The laboratory prototype, used for the experimental analysis, reproduced a four loops WDN, composed of cast iron and steel pipes with diameter DN150. Several devices were installed to monitor, record and regulate the physical and mechanical parameters

in the system. In greater detail, the prototype allowed the simultaneous installation of two PATs, at Nodes SS and MS, as sketched in the following Fig. 4.2.

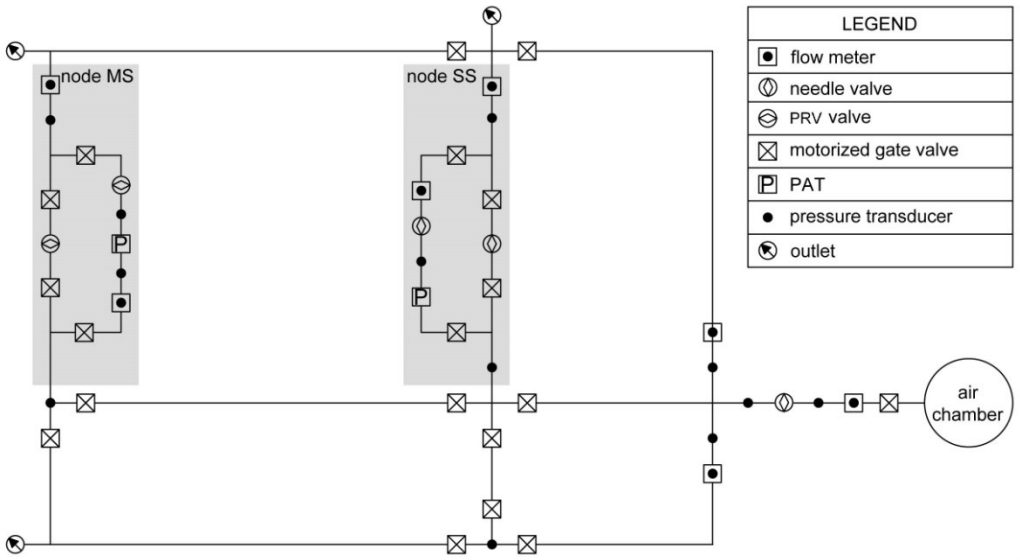


**Fig. 4.2 Layout of laboratory network at DICEA Hydraulic Laboratory (Pugliese et al., 2016)**

The laboratory model was supplied by an air chamber (Fig. 4.3) which set an inlet pressure up to 100 m for flow rates up to 50 $ls^{-1}$. The air chamber was, in turn, supplied by water volumes stored into the water tanks placed at the laboratory basement level through the pump in Fig. 4.4 (model KSB Omega 080-270), manageable by means of the electrical control panel depicted in Fig. 4.5. The pump electrical connection to a frequency modulator allowed the regulation of the pump rotational speed $N$, as a function of the flow rate $Q_t$ required during the experiments. The reduction of pump rotational speed $N$, with respect to the nominal value of 2980 rpm, was specifically adopted for flow rates outer the pump load region, declared by manufacturer equal to flow rates lower than 17 $ls^{-1}$. In greater detail, for $Q_t < 17$ $ls^{-1}$, the Affinity Laws (Par. 3.3.1) were applied to regulate the pump rotational speed $N$ to set points corresponding to high efficiencies of the pump station.

**Fig. 4.3 Air chamber**

**Fig. 4.4 Pump station**

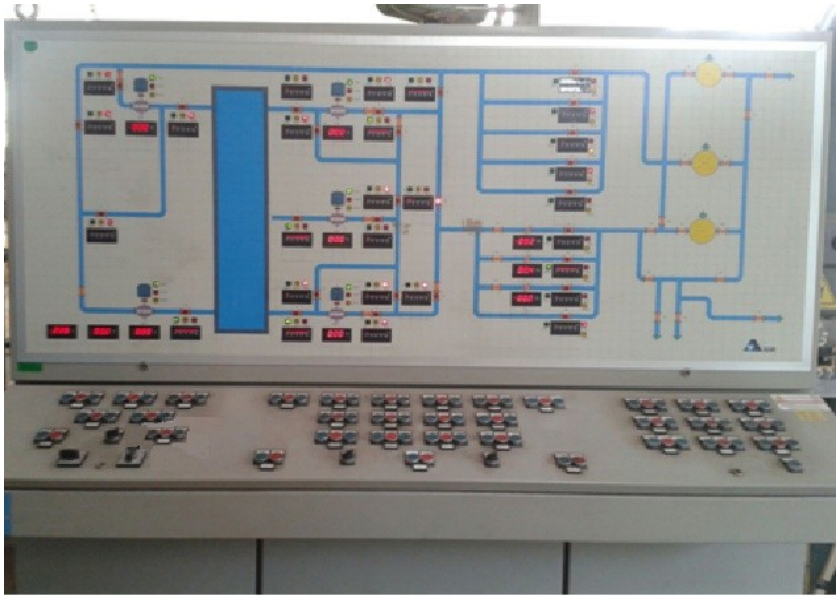

**Fig. 4.5 Control panel of the pump station**

The flow regulation at the required flow set points was carried out by varying the opening degree of the outlets depicted in Fig. 4.2 and the regulation refinement was achieved through motorized gate valves, installed at relevant points of the WDN prototype.

In greater detail, following devices were installed at the WDN prototype:

- **7 Electromagnetic Flowmeters** placed at the inlet pipe of the network to monitor and record the total flow conveyed into the WDN, at the production and by-pass lines of Node SS (model SIEMENS Sitrans Maddalena MAG 5100W) and Node MS (model ABB Watermaster FER111) and on further pipes, as sketched in Fig.

4.2. Installed electromagnetic flowmeters had the following technical specifications:

- Electromagnetic flowmeter SIEMENS Sitrans Maddalena MAG 5100W (Fig. 4.6a): velocity range $v$ = 0÷20 $ms^{-1}$; accuracy 0.2% ± 2.5 $mms^{-1}$ of full-scale equal to 140 $ls^{-1}$; max operative pressure $P_{r\,max}$ = 160 m;
- Electromagnetic flowmeter ABB Watermaster (Fig. 4.6b): velocity range $v$ = 0÷22 $ms^{-1}$; accuracy 0.2% ± 0.9 $mms^{-1}$ of full-scale of 140 $ls^{-1}$; max operative pressure $P_{r\,max}$ = 160 m.

(a)

(b)

**Fig. 4.6 Electromagnetic flowmeters installed at (a) Node SS, (b) Node MS**

- **12 Pressure Transducers** deployed upstream and downstream the needle valve on the network inlet pipe and in further measurement points (Fig. 4.2) to monitor the pressure at each characteristic point. In greater detail, at Nodes SS and MS, the pressure transducers were installed upstream and downstream the PATs, to estimate the head drop $H_t$ generated by the tested PATs. Installed pressure transducers were WIKA S-11 model (Fig. 4.7), operating at the pressure range 0÷10 bar and having accuracy equal to 0.25% of the full-scale of 10 bar.


**Fig. 4.7 WIKA S-11 pressure transducers installed at the laboratory prototype**

- **19 Motorized gate valves** installed at each link, in order to modulate the flow patterns in the network, allowing to either connect or disconnect the continuity of flow links;
- **5 Regulation valves**, deployed for flow and pressure regulation, installed at the network inlet pipe and at the production and by-pass lines of Nodes SS and MS (Fig. 4.2). Specifically, at Node SS needle valves were installed on both the inlet pipe and the production and by-pass links. They operated following the high no-linearity between the opening degree and the inflow rate. Fontana et al. (2016) provided the experimental characteristic curves for needle valves at production and by-pass links at Node SS (Fig. 4.8a), observing significant deviations from the characteristic curves provided by the manufacturer.

  At Node MS, two electrically actuated PRVs with manual over-ride (model RACI PCM93D-36C/P9) were installed, at both the production and the by-pass lines (Fig. 4.8b). They operated through a pilot control, composed of a hydraulic pilot and an integral controller; this last allowed the acquisition of a remote set-point command input to generate smooth set-point adjustments through the pilot.

  During the experiments, the needle valve installed at the production line of Node SS was applied to sharpen the flow modulation to the required set point, by using an implemented automatic algorithm. The electrically actuated PRVs at Node MS were deactived during the tests, working in full open configuration, instead.


(a)


(b)

**Fig. 4.8 Regulation valves in the network: (a) needle valve at Node SS and (b) PRV at Node MS**

- **Programmable Logic Controllers (PLCs)**, located at each node of the network and communicating with a master PLC through a wired connection with Ethernet/IP protocol. At each node, the electrical communication with motorized and regulation valves and with flowmeters and transducers allowed the valve activation and the data collection, respectively.
- **SCADA system**, implemented in-house under the abovementioned PON projects, was based on the Progea Movicon™ software. It was structured with a Main Page (Fig. 4.9) for monitoring and managing the hydraulic and technical parameters of the whole WDN prototype. The in-continuous monitoring and recording, with sampling frequency of 1 Hz, of the hydraulic and physical parameters (such as flow rates, pressures, opening degrees of regulation valves) was applied; recorded data were collected on an external database for further analyses and elaborations. Moreover, the SCADA system allowed the remote setting of the PATs rotational speed $N$, by using their electrical connection to a frequency modulator. Monitoring and recording of power $P_t$, produced by PATs and returned by the frequency modulator, was also carried out taking advantage of the SCADA system.

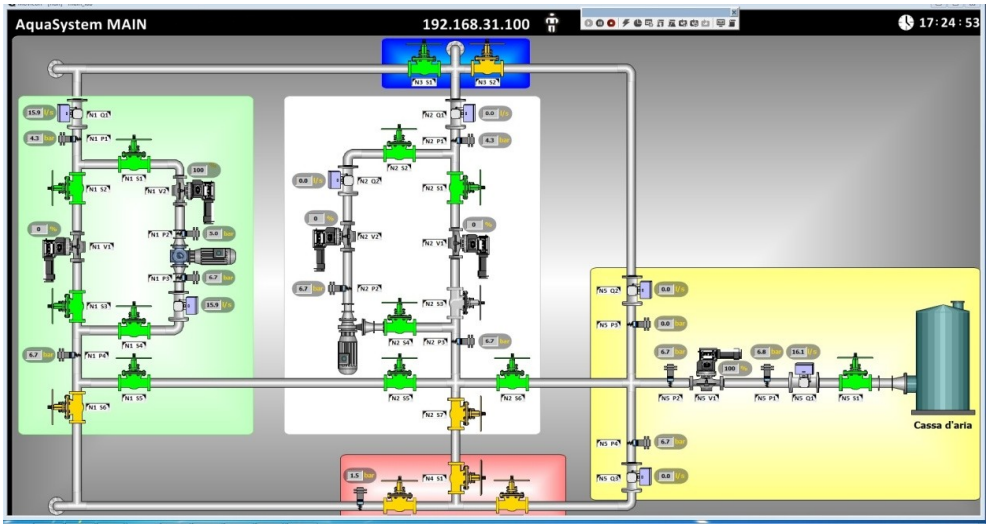


**Fig. 4.9 SCADA Main Page**

Furthermore, the SCADA was composed of dedicated pages, for each network node, for the specific visualization, control and setting of each device installed at node. In the following Fig. 4.10 and Fig. 4.11 the dedicated pages for Node SS and Node MS are pictured, respectively.

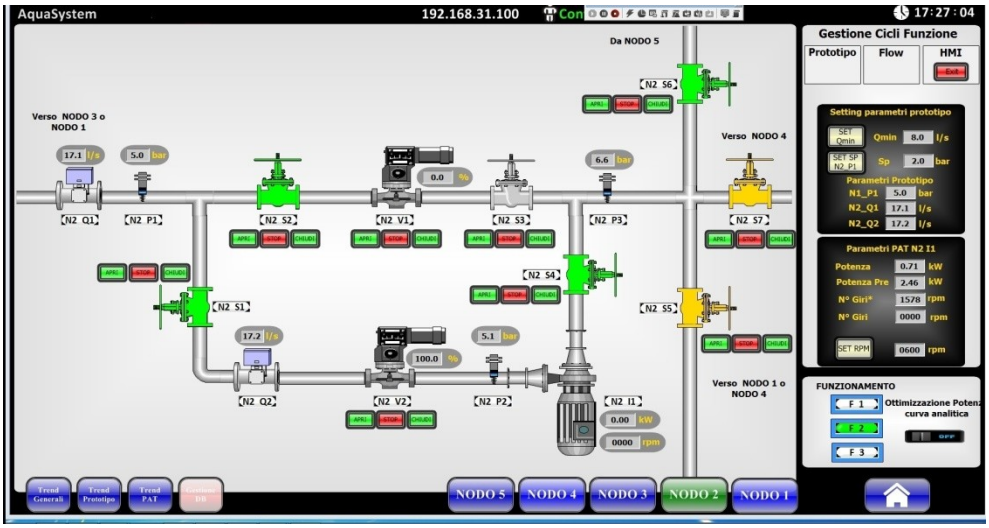


**Fig. 4.10 SCADA Node SS Page**

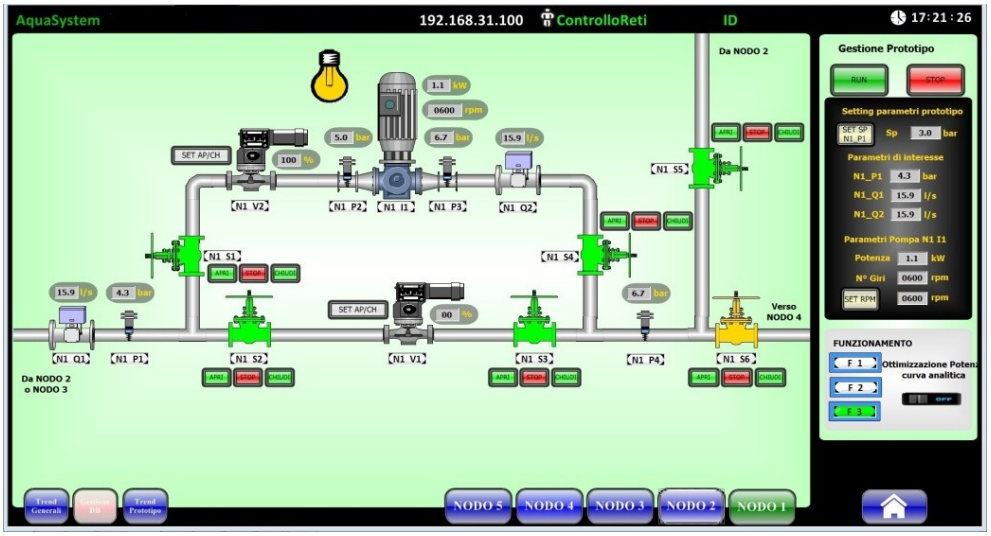


**Fig. 4.11 SCADA Node MS Page**

- **Frequency Modulator**, corresponding to the regenerative converter (model ABB ACS800-11-00250-3) depicted in Fig. 4.12. It was composed of two Insulated-Gate Bipolar Transistor (IGBT) converters: a line-side and a motor-side converter. The first operated as a Voltage-Source Inverter (VSI) to generate a regulated Alternative Current (AC) at the output, whereas the second one acted as a Voltage Sensitive Relay (VSR), according to the electrical scheme in Fig. 4.13 (Dannier et al., 2015).

**Fig. 4.12 ABB ACS800-11-00250-3 regenerative frequency modulator**

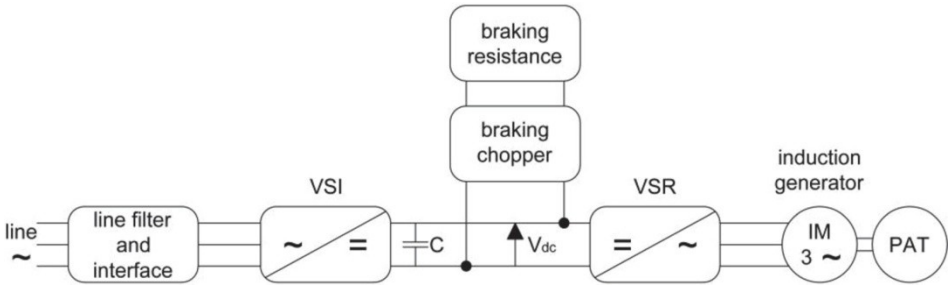


**Fig. 4.13 Electrical connection diagram of the frequency modulator (Dannier et al., 2015)**

The frequency modulator worked in agreement with the following settings: input ratings = 380÷415 V, 44 A, 48÷63 Hz; output ratings = 0÷415 V, 47 A, 0÷300 Hz; power rating: 5.5÷110 kW; accuracy = 1.00%. According to the first configuration, the frequency modulator was composed of both a braking chopper (ABB NBRA-653C) and a braking resistor (ABB 15RE13), able to dissipate the power produced by the electric generators of PATs, up to 3 kW. In greater detail, in presence of low produced power, the generated energy was adsorbed as self-consumption of the frequency modulator, whereas, for higher powers, the DC-link increase was determined, up to activate the chopper operations. It was able to dissipate the produced energy, starting from a reference voltage value of about 650 V. A frequency modulator self-consumption of about 0.04 kW was measured and accounted for estimating the effective produced power $P_t$ from PAT generators.

During the second phase of experiments, due to the capability of the investigated PATs to generate higher powers than the abovementioned limit of $P_t$ = 3 kW, an electrical system improvement was adopted, by installing 6 external resistors (Fig. 4.14), operating in parallel electrical connection and able to dissipate powers $P_t$ up to 24 kW. The power dissipation, through both the braking resistor and the additional resistors, was adopted to avoid the insertion of the produced power into the municipal electric grid, because of the absence of covenants with the local energy provider.

The frequency regulator fulfilled a double function: both to modulate the PATs rotational speed $N$, by varying the inputted frequency $f$ in compliance with the required set value, and to give back the produced power $P_t$ from PAT generators. This last was

measured in terms of both current intensity $I$ and percentage of the tested pump Nominal Power $NP$.

**Fig. 4.14 External resistors for power dissipation**

As abovementioned, in the ambit of this Ph.D. work, the considered laboratory prototype was applied to experimentally characterize four centrifugal PATs, having different geometric configurations, performances and motor equipment.

## 4.2 Experimental Analysis of Centrifugal PATs

The experimental analysis was carried out, for each investigated PAT model, in reference to a wide flow rate $Q_t$ range, compatible with both the prototype capability and the purpose of reproducing the operative conditions of WDNs supplying small-medium sized urban centers. Cavitation phenomena were not considered during the experimental analysis because the investigated flow rate range assured a PAT outlet pressure of at least 1.5 bar for each operational condition.

During each test, the flow rate $Q_t$ was maintained almost constant by varying the rotational speed $N$ through the frequency modulator and settable by remote through the SCADA system described in Par. 4.1. The rotational speed $N$ was varied from a minimum value of 300 rpm (evaluated as the lower allowable operative value) to the maximum compatible with the effective flow rate $Q_t$ through the PAT, with increasing steps $\Delta N$ = 30 rpm. However, a maximum $N$ = 3000 rpm was accounted for experiments, being equal, according to the Eq. (3.2), to the rotational speed of a turbo-

machine having 1 pole pair, as for the tested PATs. In order to adequate the flow rate $Q_t$ at varying $N$, an automatic control was used to guarantee low variations (with respect to the set flow rate value) in the order of $\pm 0.1 \div 0.2$ $ls^{-1}$. This dead band caused low oscillations for both the data recording and the representation of the characteristic curves. During the experiments, the flow modulation was performed by varying the opening degrees of outlets depicted in Fig. 4.2.

The measurements consisted in the calculation of the flowing rate $Q_t$ through the PATs, recorded by the electromagnetic flowmeters (Par. 4.1) installed at the production lines of Nodes SS and MS, respectively (Fig. 4.2). The head drop $H_t$ generated by PATs was evaluated as difference between the pressure, provided by pressure transducers, at measurement points located upstream and downstream the PATs, whereas the produced power $P_t$ was given as an output data by the regenerative frequency modulator. Thus, the PAT overall efficiency was estimated as:

$$\eta_t = \frac{P_t}{\gamma_w Q_t H_t} \tag{4.1}$$

being $\gamma_w$ the specific weight of water set equal to 9806 $Nm^{-3}$.

For each investigated point, the sampling frequency was set equal to 1 Hz, considering recording duration not lower than 60 s, starting from the achievement of the steady-state conditions. A time-averaged approach was also taken into account, in order to reduce the sampling random error. In this field, for each test, an uncertainty analysis was carried out to estimate the level of confidence of the collected measurements.

## 4.3 Uncertainty Analysis of Experimental Measurements

The uncertainty analysis to estimate the errors of the experimental measurements was carried out according to the Abernethy et al. (1973) method.

This approach is based upon the calculation of the *Uncertainty U*, considered as composed of a *Fixed Error* or *Bias Error B* and a *Random Error* or *Precision Error R* of the recorded data set.

The *Fixed Error* or *Bias Error B* was intended as the difference between the sample mean value $\bar{x}$ and the true value $x^*$. In repeated measurements of the same entity, the

*Fixed Error* was constant and its estimation could be achieved through instruments with greater precision, in order to quantify the distance between the measured $x$ and the true value $x^*$.

The *Random Error* or *Precision Error R* represents the measurement variation, caused by external effects, which determines disagreements during the measurement repeating.

It varied for repeated measurements, according to a probabilistic distribution function inferred as a Normal Distribution, by estimating the mean $\bar{\mu}$ and the variance $\sigma^*$ through the sample mean value $\bar{x}$ (Eq. 4.2) and the statistic standard deviation $s^*$ (Eq. 4.3), respectively:

$$\bar{x} = \frac{\sum_{i=1}^{N^*} x_i}{N^*} \tag{4.2}$$

$$s^* = \sqrt{\frac{\sum_{i=1}^{N^*} \left(x_i - \bar{x}\right)}{N^* - 1}} \tag{4.3}$$

with $x_i$ the individual measurement, $\bar{x}$ the sample mean value, $N^*$ the number of measurements and $N^*$*-1* the statistical degrees of freedom.

Hence, great $s^*$ values representes large scatters in measurements and vice versa. By increasing the number of measurements, a more reliable estimation of the mean value $\bar{\mu}$ was obtained, as a consequence of the reduction of the standard deviation $s^*$.

In these hypotheses, the uncertainty $U$ was calculated as:

$$U = \pm\left(B + t_{95} s^*\right) \tag{4.4}$$

with $B$ the Fixed Error, $s^*$ the standard deviation and $t_{95}$ the 95$^{th}$ percentile of the two-tailed $t$-Student distribution. In reference to the performed experimental analysis, $t_{95}$ was set equal to 2.00, being, for each measured operative condition, the degrees of freedom higher than 30 (Moffat, 1982). The time-averaged approach, with sampling frequency of 1 Hz and sampling duration of at least 60 s, assured the reliability of the above indicated assumption.

For flow rate $Q_t$ and power $P_t$ measurements, the *Fixed Error B* was estimated as a function of the accuracy of the electromagnetic flowmeters and of the frequency modulator, respectively.

Conversely, the error propagation method (Abernethy et al., 1973) was applied to estimate the *Fixed Error B* of both head drop $H_t$ (as a function of the pressure transducers accuracy) and efficiency $\eta_t$ (through the Eq. 4.1), according to the following Eq. (4.5):

$$B = \sqrt{\sum_{j=1}^{M}\left(\frac{\partial f^*(x)}{\partial x_j} B(x_j)\right)^2} \tag{4.5}$$

where $f^*$ is the function to calculate the required entity, $M$ the number of the $x_j$ measured parameters to calculate $f^*(x)$ and $B(x_j)$ the fixed error of the *j-th* measured parameter $x_j$.

## 4.4 Experimental Characterization of a Horizontal Axis Single-Stage PAT

The first phase of the experiments was focused on the characterization of a Horizontal Axis Single-Stage centrifugal HA SS PAT (model LOWARA FHE 80-200/220) installed at Node SS, according to the sketch in the following Fig. 4.15.

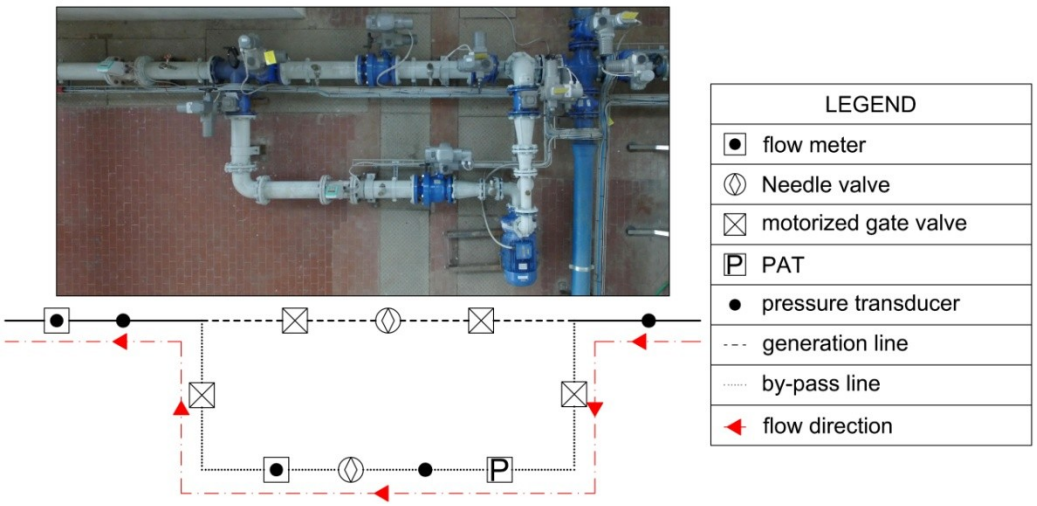


**Fig. 4.15 Detail of equipment and transducers at Node SS (Pugliese et al., 2016)**

Characteristic curves of HA SS PAT in pump operations (Fig. 4.16 and Fig. 4.17) and its properties were inferred from the manufacturer's datasheets, as summarized in Tab. 4.1.

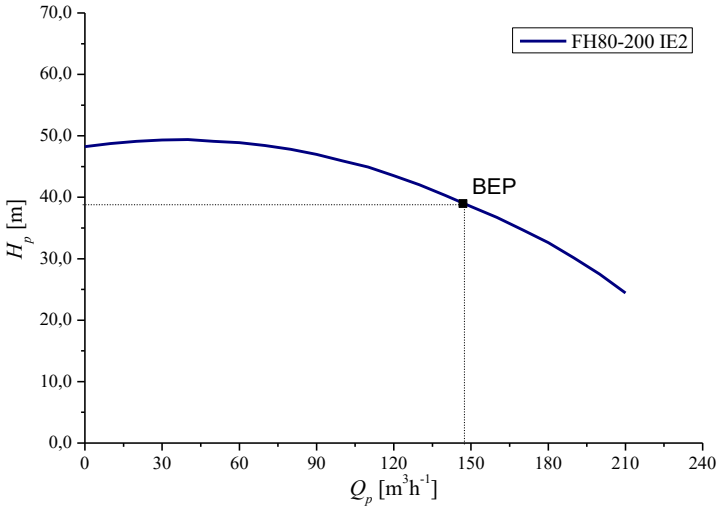


**Fig. 4.16 $H_p(Q_p)$ curve HA SS – Pump mode**

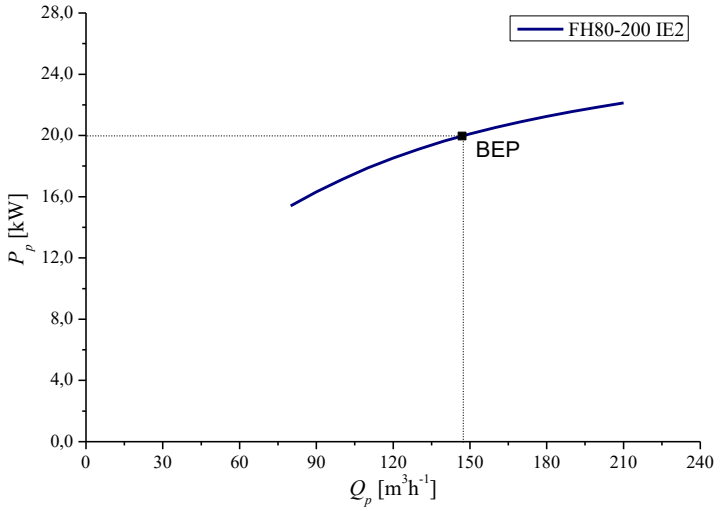


**Fig. 4.17 $P_p(Q_p)$ curve HA SS – Pump mode**

| **LOWARA FH80-200 IE2 Pump Mode** | | |
|---|---|---|
| **No. poles** | [-] | 2 |
| **No. impellers** | [-] | 1 |
| **Motor Efficiency Class** | [-] | IE2 |
| **Impeller diameter *D*** | [m] | 0.189 |
| **Rotational Speed *N*** | [rpm] | 2900 |
| **Motor Nominal Power *NP*** | [kW] | 22.0 |
| **Efficiency at BEP $\eta_{pb}$** | [%] | 78.7 |
| **Flow Rate at BEP $Q_{pb}$** | [$m^3h^{-1}$] | 148.0 |
| **Head at BEP $H_{pb}$** | [m] | 39.0 |
| **Power at BEP $P_{pb}$** | [kW] | 20.0 |
| **Specific Speed $N_{sp}$** | [rpm, $m^3s^{-1}$] | 37.75 |

**Tab. 4.1 LOWARA HA SS properties – Pump mode**

The HA SS PAT was equipped with a IE2 motor efficiency class (IEC 2008, 2014), reaching, at the rotational speed $N$ = 2900 rpm, the BEP at flow rate $Q_{pb}$ equal to about 41.1 $ls^{-1}$ (148 $m^3h^{-1}$).

The experimental tests in PAT mode were carried out, according to the procedure stated in Par. 4.2, in the flow rate range 8-50 $ls^{-1}$ in order to reproduce the typical flow rate range of WDN for small-medium sized urban and rural centers. Rotational speed $N$ was varied from 30 to 3000 rpm (where reachable) with incresing step of 30 rpm; thus 91 different $N$ values were accounted for the experimental characterization. Total 3232 operative points were analysed, defining head drops $H_t$ between 1.2 and 55.8 m, produced power $P_t$ in the range 0.1÷16.3 kW and reaching a maximum efficiency at BEP $\eta_{tb}$ = 61.3%.

The uncertainty analysis in Par. 4.3 was applied, estimating the uncertainy for flow rate $Q_t$, head drop $H_t$, power $P_t$ and efficiency $\eta_t$ measurements equal to ±0.26%, ±2.09%, ±2.93% and ±3.61%, respectively.

As an example, in the following Fig. 4.18, Fig. 4.19 and Fig. 4.20 the experimental results for $N$ = 300, 600, 900, 1200, 1500, 1800, 2100, 2400, 2700 and 3000 rpm are plotted to reproduce the $H_t(Q_t)$, $P_t(Q_t)$ and $\eta_t(Q_t)$ experimental curves, respectively.

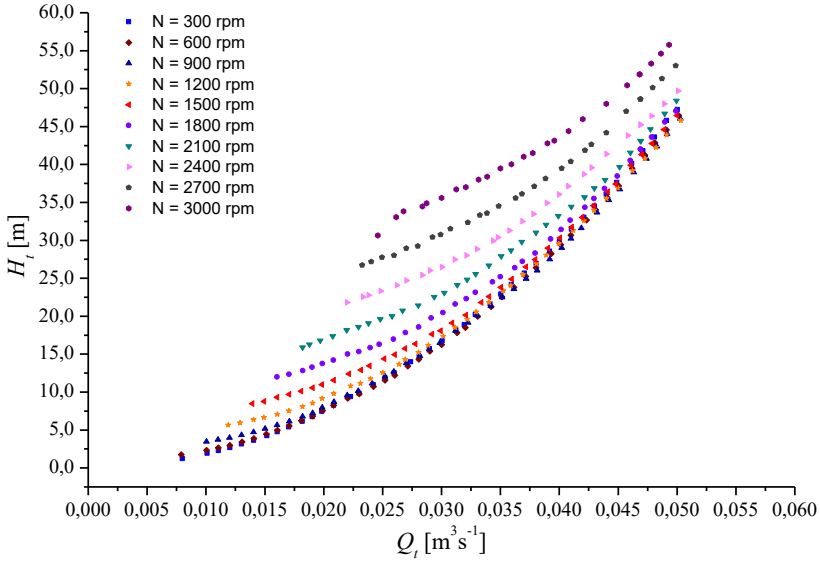


**Fig. 4.18 $H_t(Q_t)$ experimental curves – HA SS PAT**

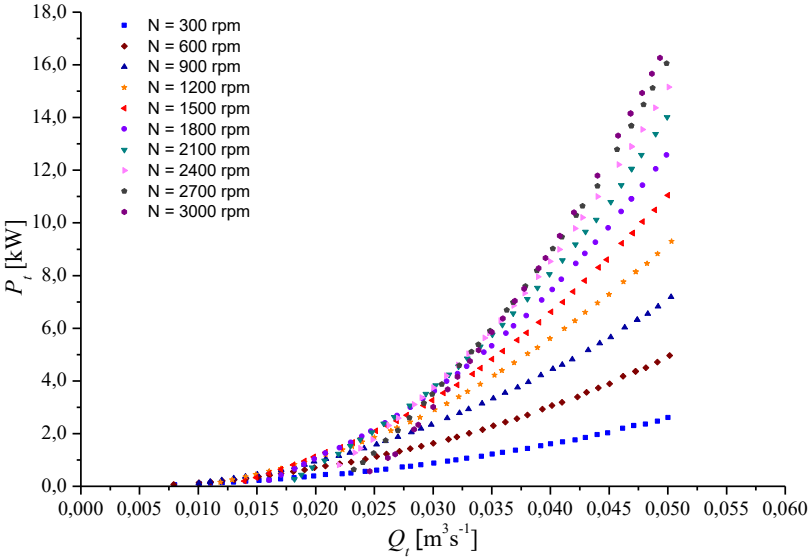


**Fig. 4.19 $P_t(Q_t)$ experimental curves – HA SS PAT**

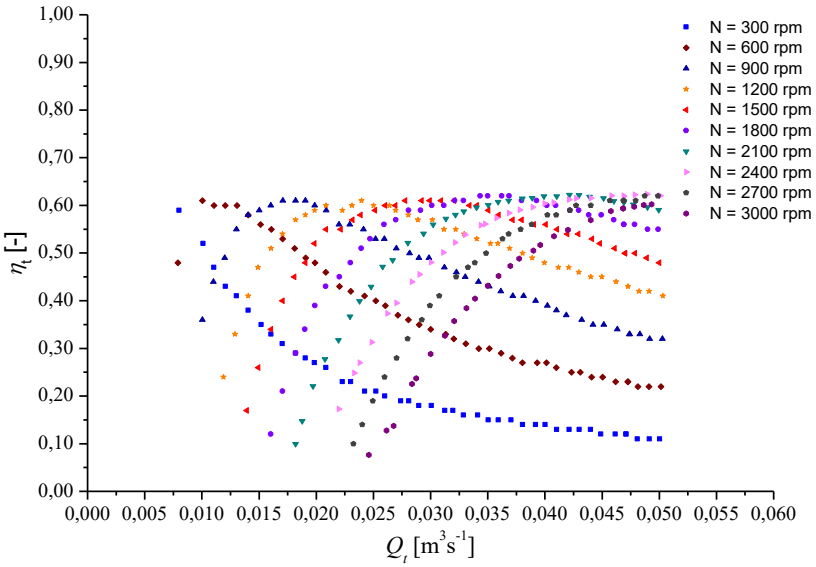


**Fig. 4.20 $\eta_t(Q_t)$ curves – HA SS PAT**

From Fig. 4.18, the upward translation of the head curves $H_t(Q_t)$ was achieved at increasing the rotational speed $N$, noticing, for higher flow rates $Q_t$, the curve approaching with respect to what observed for low $Q_t$ values. Nevertheless, for lower rotational speeds $N$, the head drop $H_t$ did not monotonically increase at raising $N$, defining a minimum $H_{t\min}$, variable as a function of the flow rate $Q_t$ (Fig. 4.21).

In terms of experimental power curve $P_t(Q_t)$, in Fig. 4.19 it is shown that for flow rates $Q_t$ up to 30 ls$^{-1}$, the produced power $P_t$, at varying $N$, was always lower than 4 kW. In this range, for the highest $N$ values low differences were determined, defining, for $N$ > 1500 rpm power $P_t$ values lower than those produced for $N \leq 1500$ rpm. Conversely, for flow rates $Q_t$ higher than 30 ls$^{-1}$, the power $P_t$ raising, at increasing $N$, was observed for each considered rotational speed $N$.

In Fig. 4.20, the efficiency constanscy at BEP, at varying the rotational speed $N$, is plotted, reaching the maximum efficiency $\eta_{tb}$ equal to 61.3%. Specifically, by increasing $N$, the BEP was achieved for higher flow rates $Q_t$, thus defining the translation of the efficiency curve $\eta_t(Q_t)$, in the range experimentally tested, from the decreasing branch, for lower $N$ values, to the increasing one, for higher rotational speeds $N$.

By analysing the head drop $H_t(N)$ curves (Fig. 4.21), for fixed flow rates $Q_t$, a quadratic correlation was observed, in compliance with the dependency defined by the Affinity Laws (Eq. 3.13). For each experimental curve, a minimum head drop $H_{t\min}(N)$ was found, reached for higher $N$ values, at increasing the flow rate $Q_t$.

In Fig. 4.21 the experimental data are plotted with punters, whereas results from the ALs are represented with solid lines. The curve representing the minimum $H_{t\min}$ for fixed $Q_t$, at varying $N$ in rpm, was derived, according to the following equation:

$$H_{t\min} = 2.90 \cdot 10^{-5} N^2 \tag{4.6}$$

The significant correlation between experimental data and results from ALs is observed in Fig. 4.21, where low discrepancies were due to the oscillation of flow rate during the experiments in the dead band ±0.1÷0.2 ls$^{-1}$.

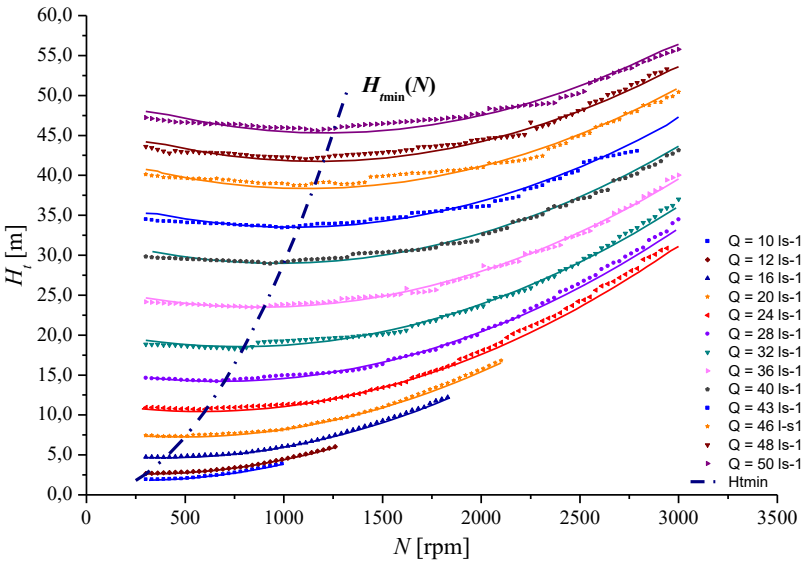


**Fig. 4.21 $H_t(N)$ experimental curves – HA SS PAT**

Power $P_t(N)$ curves, for constant flow rate $Q_t$, are plotted in the following Fig. 4.22. In compliance with the ALs correlations (Eq. 3.14), third order polynomial curves were determined, by reaching the maximum produced power $P_{t\max}(N)$ for higher rotational speed $N$ at increasing the flow rate $Q_t$. Thus, Eq. (4.7) was derived to calculate $P_{t\max}$ at varying $N$:

$$P_{t\max} = 4.63 \cdot 10^{-10} N^3 \tag{4.7}$$

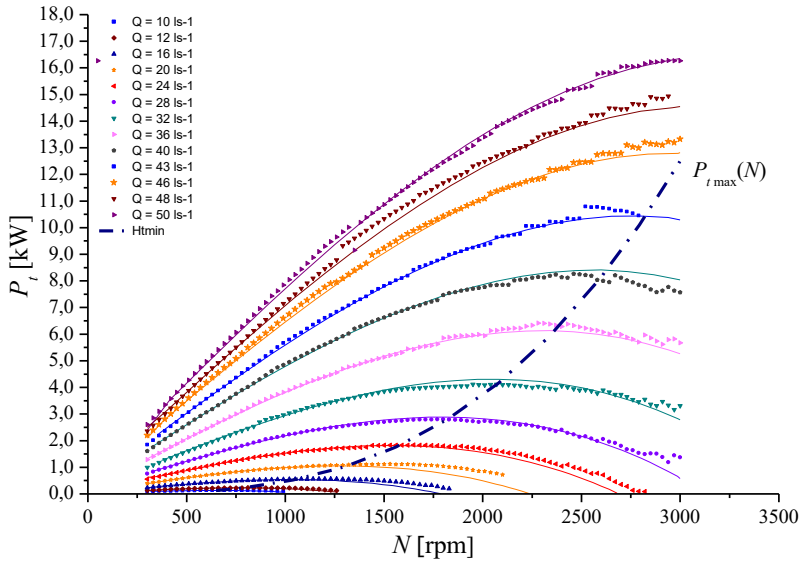


**Fig. 4.22 $P_t(N)$ experimental curves – HA SS PAT**

Operations at BEP in reverse mode are summarized in dimensionless terms in the following Tab. 4.2, by using the flow rate number $\phi$, the head number $\psi$ and the power number $\pi$ parameters, introduced in Eqs. (3.6), (3.7) and (3.8), respectively. The specific speed $N_{st}$ at BEP is also reported.

| $\phi_b$ [-] | $\psi_b$ [-] | $\pi_b$ [-] | $\eta_{tb}$ [%] | $N_{st}$ [rpm, $m^3s^{-1}$] |
|---|---|---|---|---|
| 0.18 | 8.50 | 0.96 | 61.3 | 28.74 |

**Tab. 4.2 Dimensionless parameters at BEP in PAT mode – HA SS PAT**

In the following Tab. 4.3, experimental ranges for $Q_t$, $H_t$, $P_t$ and $\eta_t$ are summarized in dimensional and dimensionless terms.

| $Q_t$ [$ls^{-1}$] | $\phi$ [-] | $H_t$ [m] | $\psi$ [-] | $P_t$ [kW] | $\pi$ [-] | $\eta_t$ [%] |
|---|---|---|---|---|---|---|
| 8 - 50 | 0.07 - 1.48 | 1.24 - 55.80 | 3.37 - 518.83 | 0.06 - 16.28 | 0.01 - 86.61 | 4.0 – 61.3 |

**Tab. 4.3 Experimental ranges in PAT mode – HA SS PAT**

Results from the whole set of experiments are represented, in dimensionless terms, in the following Fig. 4.23, Fig. 4.24 and Fig. 4.25. Characteristic curves (3.62), (3.63) and (3.64) from Derakhshan and Nourbakhsh (2008a) model are also plotted, using a

solid line up to the limit $\phi \leq 0.40$ defined by the authors, whereas a dashed line is applied for $\phi > 0.40$.

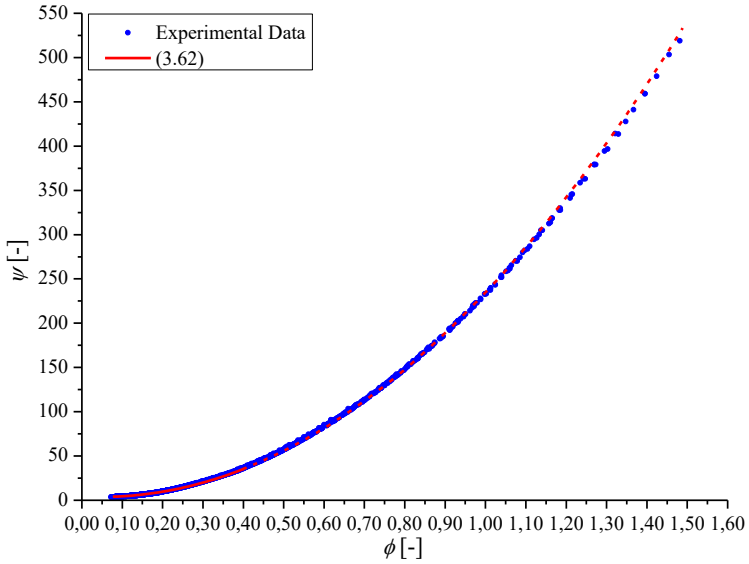


**Fig. 4.23 $\psi(\phi)$ experimental and Eq. (3.62) curves – HA SS PAT**

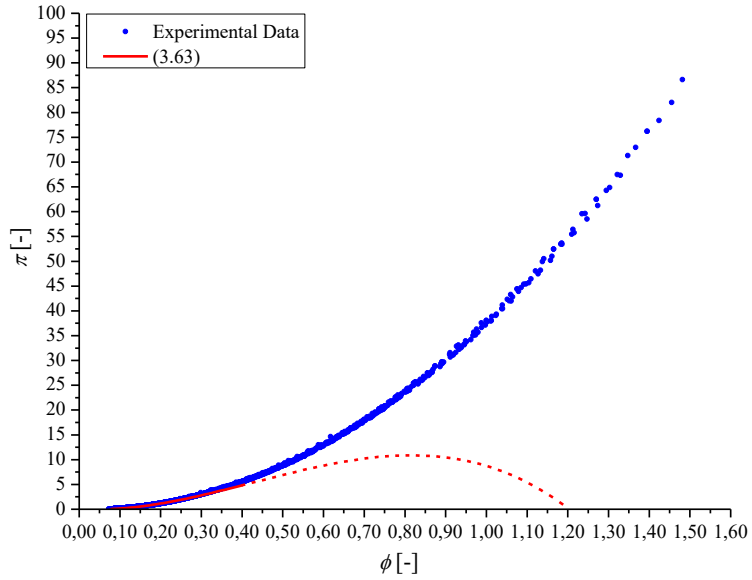


**Fig. 4.24 $\pi(\phi)$ experimental and Eq. (3.63) curves – HA SS PAT**

Regarding the $\psi(\phi)$ function (Fig. 4.23), a significant correlation between experiments and Eq. (3.62) was observed for the whole range of flow rate numbers $\phi$, defining relative scatters utmost of ±10%.

In terms of power number $\pi(\phi)$ curve (Fig. 4.24), the reliability of Eq. (3.63) was observed only for $\phi \leq 0.40$, in reference to which differences in the range ±15% were achieved, whereas significant discrepancies were defined for flow rate numbers $\phi > 0.40$. In effect, the experimental trend was monotonically increasing, whereas Eq. (3.63) showed a maximum power number $\pi = 10.85$ for $\phi = 0.81$, by decreasing for higher $\phi$, up to become zero for $\phi = 1.20$.

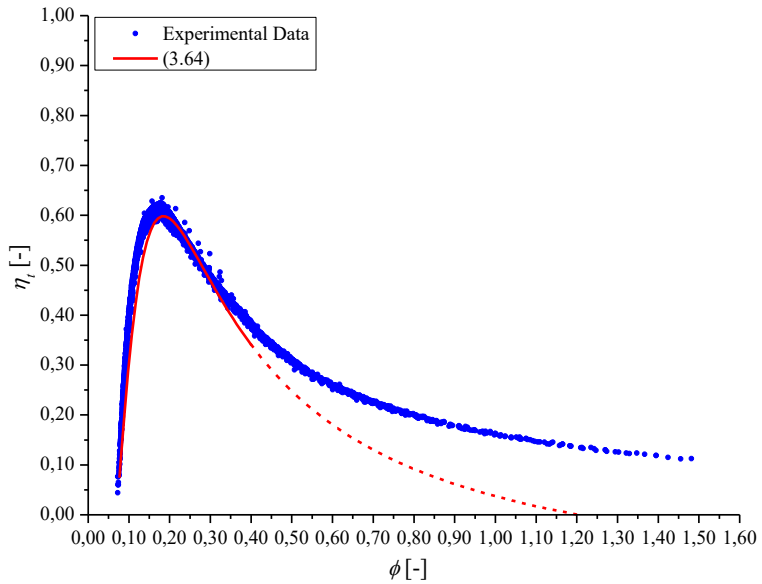


**Fig. 4.25 $\eta_t(\phi)$ experimental and Eq. (3.64) curves – HA SS PAT**

In Fig. 4.25, it is shown how the BEP, for the whole set of considered rotational speeds $N$, was reached at the same flow rate number $\phi_b = 0.18$ (Tab. 4.2), thus resulting to be the reference parameter for the BEP characterization, independently from the rotational speed $N$. In agreement with the $\pi(\phi)$ trend, the Derakhshan and Nourbakhsh (2008a) model well reproduced the efficiency curve $\eta_t(\phi)$ up to $\phi = 0.40$, whereas it fell for higher $\phi$ values. In this regard, being the BEP reached for $\phi \leq 0.40$, it allowed to significantly characterize the BEP operative conditions. Concerning the efficiency curve $\eta_t(\phi)$ in Fig. 4.25, a significant reduction at BEP was observed in PAT operations

being the maximum efficiency $\eta_{tb}$ = 61.3%, with respect to about 79%, declared by manufacturer, in pump mode (Tab. 4.1). This result was in disagreement with Amelio et al. (2000)'s deductions, who individuated, for centrifugal pumps running at specific speeds $N_{sp}$ in the range 16÷56, greater experimental data at BEP in turbine mode than those in pump operations.

## 4.5 Predicting Formulations of Performances for Horizontal Axis Centrifugal PATs

In this field, with the aim of providing an analytic function to predict the power characteristic curve, valid for operative ranges wider than those from the Derakhshan and Nourbakhsh (2008a) approach, following Eq. (4.8) was proposed. In compliance with the analytic form used by Derakhshan and Nourbakhsh (2008a) in Eq. (3.63), a third order polynomial function was applied; coefficients were calibrated by minimizing the standard deviations (Pugliese et al., 2016), being experimentally validated for $\phi$ up to 1.50:

$$\frac{P_t}{P_{tb}} = 4.0 \cdot 10^{-3}\left(\frac{Q_t}{Q_{tb}}\right)^3 + 1.386\left(\frac{Q_t}{Q_{tb}}\right)^2 - 0.390\left(\frac{Q_t}{Q_{tb}}\right) \tag{4.8}$$

By combining the Eq. (4.8) and the Derakhshan and Nourbakhsh Eq. (3.62) with the Eq. (4.1), following relationship was found to predict the overall efficiency $\eta_t$, as a function of the operative conditions at BEP:

$$\frac{\eta_t}{\eta_{tb}} = \frac{4.0 \cdot 10^{-3}\left(\frac{Q_t}{Q_{tb}}\right)^3 + 1.386\left(\frac{Q_t}{Q_{tb}}\right)^2 - 0.390\left(\frac{Q_t}{Q_{tb}}\right)}{1.0283\left(\frac{Q_t}{Q_{tb}}\right)^3 - 0.5468\left(\frac{Q_t}{Q_{tb}}\right)^2 + 0.5314\left(\frac{Q_t}{Q_{tb}}\right)} \tag{4.9}$$

In the following Fig. 4.26 and Fig. 4.27, Eqs. (4.8) and (4.9) are compared with both the experimental data and the Eqs. (3.63) and (3.64) from Derakhshan and Nourbakhsh (2008a) model, drawing a dashed line for $\phi > 0.40$.

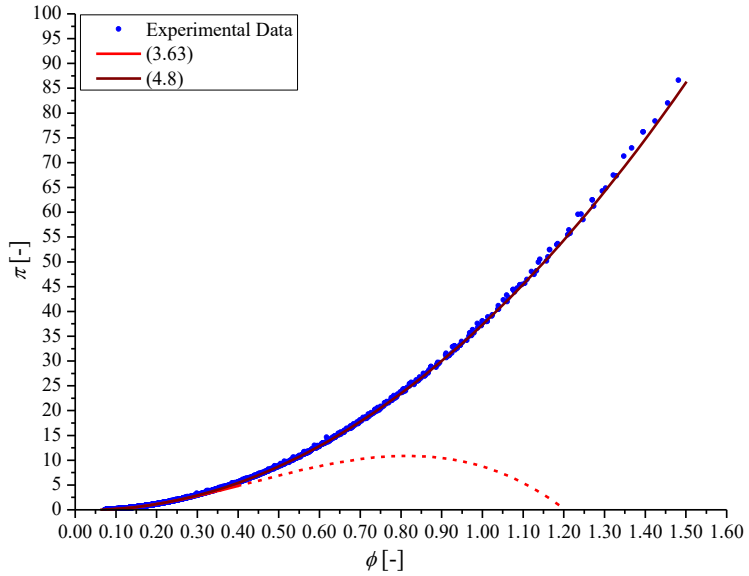


**Fig. 4.26 $\pi(\phi)$ experimental, Eqs. (3.63) and (4.8) curves – HA SS PAT**

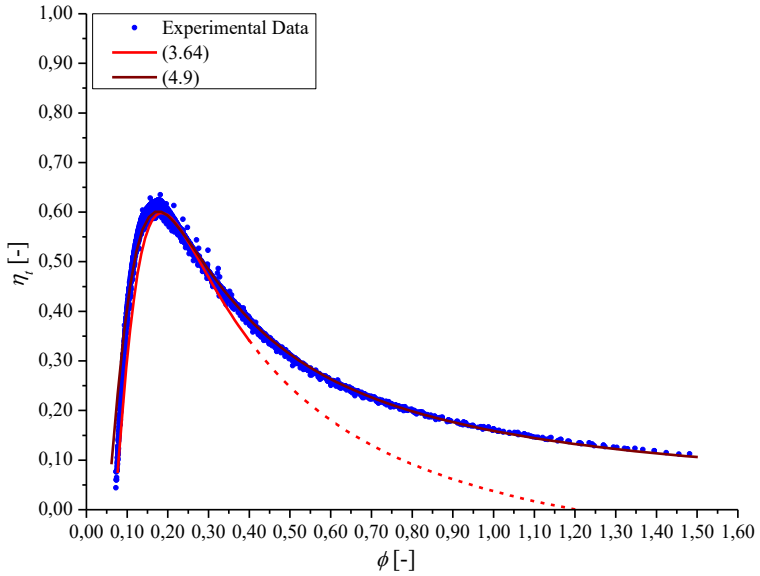


**Fig. 4.27 $\eta_t(\phi)$ experimental, Eqs. (3.64) and (4.9) curves – HA SS PAT**

Thus, Eqs. (4.8) and (4.9) were able to overcome the limitation of Derakhshan and Nourbakhsh (2008a) model, valid up to $\phi$ = 0.40. Indeed, significant correlations were observed for the whole set of investigated ranges, defining discrepancies utmost equal ±10% for power number $\pi$ curve and of the ±15% for the efficiency $\eta_t$ curve.

To predict the BEP in PAT mode, as a function of the BEP in pump mode, mono-dimensional models from the literature were applied in terms of flow rate $Q_{tb}/Q_{pb}$ and head $H_{tb}/H_{pb}$ ratios and comparison with experimental ratios (Tab. 4.4) at rotational speed $N$ = 2900 rpm (according to manufacturer's datasheets) was performed. Results are summarized in the following Tab. 4.5 and the relative scatters are plotted in Fig. 4.28.

| $Q_{tb}/Q_{pb}$ [-] | $H_{tb}/H_{pb}$ [-] | $P_{tb}/P_{pb}$ [-] | $\eta_{tb}/\eta_{pb}$ [-] | $Ns_{tb}/Ns_{pb}$ [-] |
|---|---|---|---|---|
| 1.47 | 1.86 | 1.30 | 0.78 | 0.76 |

**Tab. 4.4 Experimental ratios at BEP – HA SS PAT**

| | $Q_{tb}/Q_{pb}$ [-] | $H_{tb}/H_{pb}$ [-] | $\Delta(Q_{tb}/Q_{pb})$ [%] | $\Delta(H_{tb}/H_{pb})$ [%] |
|---|---|---|---|---|
| Stepanoff (1957) | 1.13 | 1.27 | -23.18% | -31.62% |
| Childs (1962) | 1.27 | 1.27 | -13.41% | -31.62% |
| Hancock (1963) | 1.63 | 1.63 | 11.22% | -12.17% |
| Grover (1980) | 1.62 | 2.04 | 10.44% | 9.51% |
| Hergt (1982) | 1.23 | 1.07 | -16.00% | -42.59% |
| Sharma (1985) | 1.21 | 1.33 | -17.46% | -28.27% |
| Schmiedl (1988) | 1.96 | 1.60 | 33.31% | -13.90% |
| Alatorre-Frenk and Thomas (1990) | 1.56 | 1.56 | 6.52% | -16.13% |
| Amelio et al. (2000) | 3.09 | 1.37 | 110.50% | -26.48% |
| Joshi et al. (2005b) | 1.50 | 1.60 | 2.15% | -13.90% |
| Derakhshan and Nourbakhsh (2008a) | 1.39 | 1.54 | -5.08% | -16.98% |
| Nautiyal et al. (2011) | 1.37 | 1.56 | -6.31% | -16.25% |
| Yang et al. (2012a) | 1.37 | 1.56 | -6.71% | -15.96% |
| Tan and Engeda (2016) | 1.10 | 1.28 | -24.76% | -31.37% |

**Tab. 4.5 Flow rate and head ratios at BEP – HA SS PAT**

In Tab. 4.5, experimental-theoretical differences in the range ±40% were calculated for both flow rate and head drop ratios, by applying the almost whole set of considered literature models. The only exception was the Amelio et al. (2000) Eq. (3.49), which assessed a theoretical flow rate ratio, equal to more than twice the amount of the experimental ratio. Conversely, the Amelio et al. (2000) Eq. (3.50) underestimated the head ratio, defining a relative error of about –26.5%. Grover (1980) method was the only approach to overestimate the head ratio; nevertheless, it defined, for both flow rate and head ratios, differences in the order of +10% (Fig. 4.28).

Furthermore, Fernandez et al. (2004) Eq. (3.52) was considered to estimate the head ratio, resulting of about 7.0% lower than the experimental value.

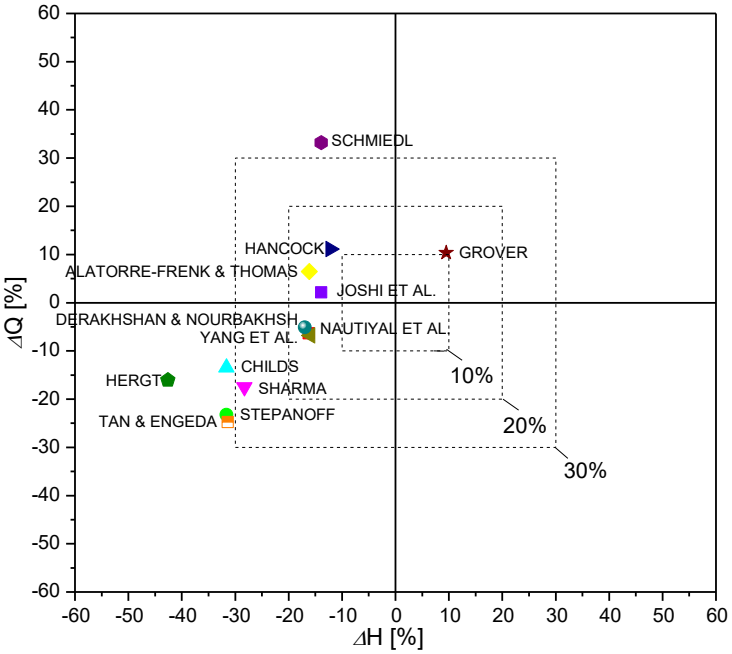


**Fig. 4.28 Flow rate and head ratios scatters at BEP – HA SS PAT**

For the estimation of power ratio $P_{tb}/P_{tp}$ at BEP, the Derakhshan and Nourbakhsh (2008a) approach was satisfactorily reliable, determining a theoretical ratio of 1.40, with respect to the experimental one of 1.30, corresponding to a scatter of +7.5%. The Tan and Engeda (2016) approach gave a power ratio of 1.48, equal to +13.8% higher than the experimental one, instead.

To predict the specific speed ratio $N_{st}/N_{sp}$, the Tan and Engeda (2016) model resulted to be the most reliable, implicating a scatter lower than -1% (Tab. 4.6). Conversely, Amelio et al. (2000) and Yang et al. (2012a) formulations overestimated the experimental ratio of about 13% and 11.5%, respectively.

| **Model** | **$Ns_{tb}/Ns_{pb}$ [-]** | **$\Delta(Ns_{tb}/Ns_{pb})$ [%]** |
|---|---|---|
| Amelio et al. (2000) | 0.86 | 13.20% |
| Yang et al. (2012a) | 0.85 | 11.40% |
| Tan and Engeda (2016) | 0.75 | -0.92% |

**Tab. 4.6 Specific speed ratios at BEP – HA SS PAT**

## 4.6 Experimental Characterization of Vertical Axis Single-Stage and Multi-Stage PATs

The second phase of the experimental analysis was focused on the performance characterization of three Vertical Axis Single-Stage and Multi-Stage models installed at the Node MS of the WDN prototype (Fig. 4.2). Regarding the performances of Vertical Axis PATs, very few evidences are available in the literature, thus resulting to be strongly significant to experimentally investigate their behaviour under the considered wide range of operating flow rates.

The detailed equipment at Node MS is pictured and sketched in the following Fig. 4.29.

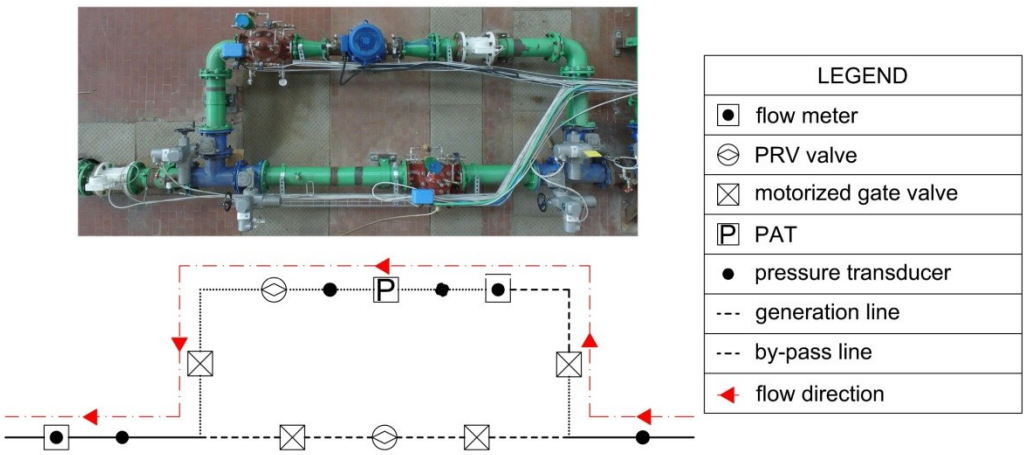


**Fig. 4.29 Detail of equipment and transducers at Node MS (Pugliese et al., 2016)**

In this case, the experimental investigation involved three centrifugal PATs which appertained to the same manufacturer family (LOWARA 92SV family group) but having different number of stages and efficiency motor classes equipment. In particular, the IE2 and IE3 efficiency classes, ruled by the IEC 60034 (IEC, 2004) standard and following updates (IEC, 2008), were considered, in reference to a Single-Stage PAT (model LOWARA 92SV1G75T) equipped with IE3 efficiency class motor (VA SS PAT) and two two-stage PATs (model LOWARA 92SV2G150T) equipped with IE2 (VA $MS_1$ PAT) and IE3 (VA $MS_2$ PAT) efficiency motor class, respectively. The pump characteristics from manufacturer's datasheets are summarized in Tab. 4.7, whereas the characteristic curves in pump operations are represented in Fig. 4.30 and Fig. 4.31, in

reference to the VA SS model. Concerning the VA MS models, the head $H_p(Q_p)$ and the power $P_p(Q_p)$ were doubled, being equal the flow rate $Q_p$, whereas the efficiency curve $\eta_p(Q_p)$ was the same as that for the VA SS PAT model.

| **PAT** | | **VA SS** | **VA $MS_1$** | **VA $MS_2$** |
|---|---|---|---|---|
| **No. poles** | [-] | 2 | 2 | 2 |
| **No. impellers** | [-] | 1 | 2 | 2 |
| **Impeller diameter *D*** | [m] | 0.146 | 0.146 | 0.146 |
| **Rotational Speed *N*** | [rpm] | 2900 | 2900 | 2900 |
| **Motor Efficiency Class** | [-] | IE3 | IE2 | IE3 |
| **Motor Nominal Power *NP*** | [kW] | 7.5 | 15.0 | 15.0 |
| **Efficiency at BEP $\eta_{pb}$** | [%] | 76.5 | 76.5 | 76.5 |
| **Flow Rate at BEP $Q_{pb}$** | [$m^3h^{-1}$] | 88.5 | 88.5 | 88.5 |
| **Head at BEP $H_{pb}$** | [m] | 22.0 | 44.0 | 44.0 |
| **Power at BEP $P_{pb}$** | [kW] | 7.0 | 14.0 | 14.0 |
| **Specific Speed $N_{sp}$** | [rpm, $m^3s^{-1}$] | 44.76 | 44.76 | 44.76 |

**Tab. 4.7 Characteristics of the tested Vertical Axis PATs – Pump Mode**

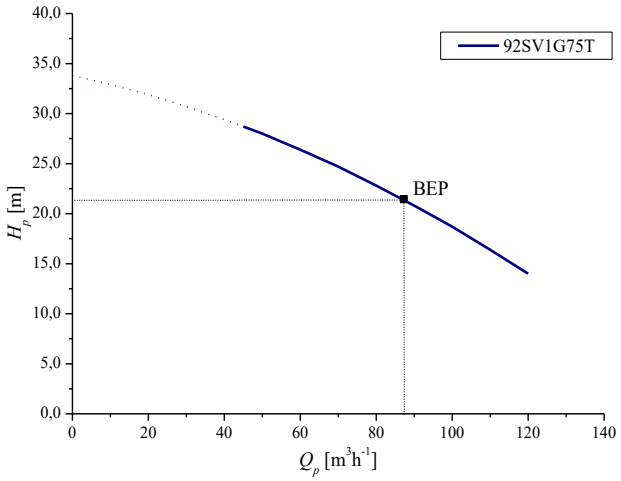


**Fig. 4.30 $H_p(Q_p)$ curve VA SS – Pump mode**

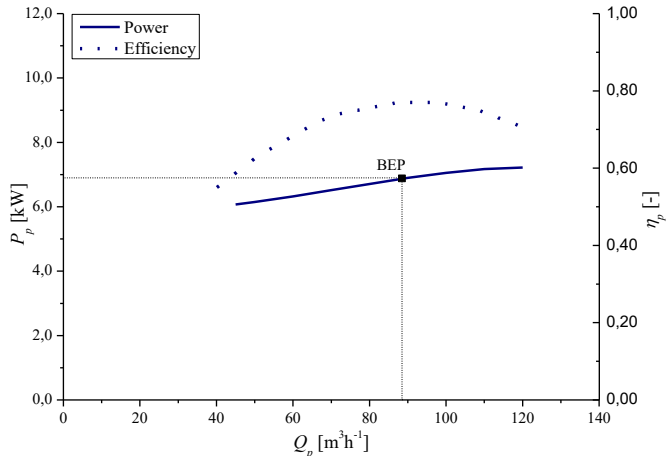


**Fig. 4.31 $P_p(Q_p)$ and $\eta_p(Q_p)$ curves VA SS – Pump mode**

In compliance with the uncertainty analysis in Par. 4.3, the measurement uncertainty was estimated according to the Abernethy et al. (1973) model, setting a 95% confidence interval of the Student's *t*-distribution with $t_{95} = 2.00$ (Moffat, 1982). The uncertainties of flow rate $Q_t$, head drop $H_t$, power $P_t$ and efficiency $\eta_t$, for each tested VA PAT, are reported in the following Tab. 4.8.

| PAT | $Q_t$ [%] | $H_t$ [%] | $P_t$ [%] | $\eta_t$ [%] |
|---|---|---|---|---|
| **VA SS IE3** | ±0.26% | ±1.84% | ±2.48% | ±3.10% |
| **VA MS IE2** | ±0.23% | ±2.01% | ±1.25% | ±2.38% |
| **VA MS IE3** | ±0.25% | ±1.58% | ±2.25% | ±2.76% |

**Tab. 4.8 Experimental uncertainty of VA PATs**

The tests were performed according to the working procedure explained in Par. 4.4 for the characterization of the HA SS PAT. Thus, for a fixed flow rate $Q_t$, the rotational speed $N$ was varied in the range 300÷3000 rpm, by considering 91 different rotational speeds $N$. A total of about 4200 operative conditions was analysed, related to the operative ranges summarized in Tab. 4.9.

| PAT | n° Exp. | $Q_t$ [ls$^{-1}$] | $H_t$ [m] | $P_t$ [kW] | $\eta_t$ [%] |
|---|---|---|---|---|---|
| **VA SS IE3** | 1348 | 9 – 33 | 2.73 – 47.34 | 0.04 –7.40 | 5.0 – 65.5 |
| **VA MS IE2** | 1684 | 8 – 28 | 4.07 – 54.38 | 0.04 – 9.74 | 1.6 – 72.1 |
| **VA MS IE3** | 1166 | 8 – 31 | 4.06 – 72.34 | 0.11 – 13.37 | 3.2 – 72.1 |

**Tab. 4.9 Experimental operative ranges in PAT mode – VA PATs**

In the following Fig. 4.32, Fig. 4.33 and Fig. 4.34, the experimental $H_t(Q_t)$, $P_t(Q_t)$ and $\eta_t(Q_t)$ curves for the VA SS PAT are plotted, respectively, in reference to rotational speeds $N$ = 300, 600, 900, 1200, 1500, 1800, 2100, 2400, 2700, 3000 rpm.

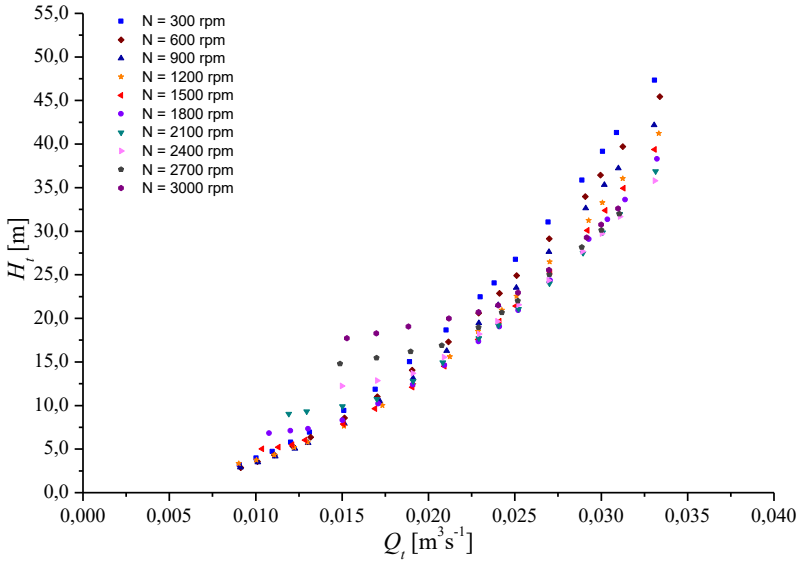


**Fig. 4.32 $H_t(Q_t)$ experimental curves – VA SS PAT**

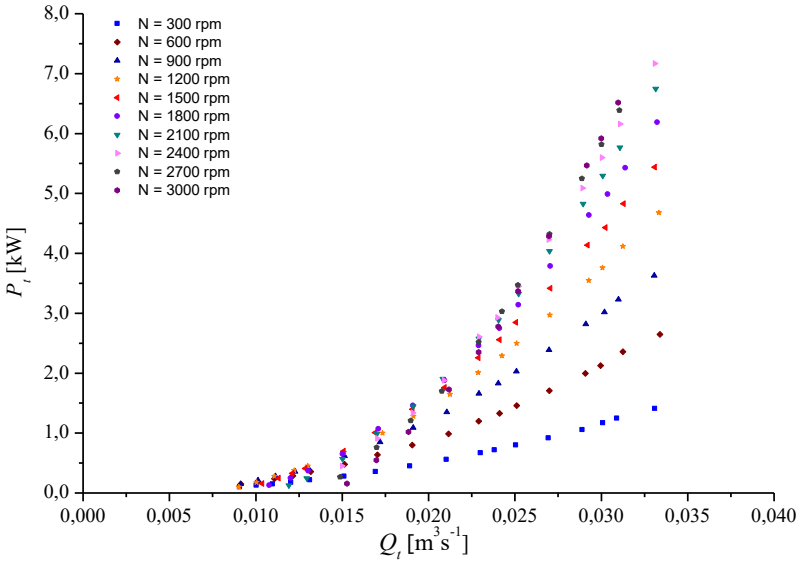


**Fig. 4.33 $P_t(Q_t)$ experimental curves – VA SS PAT**

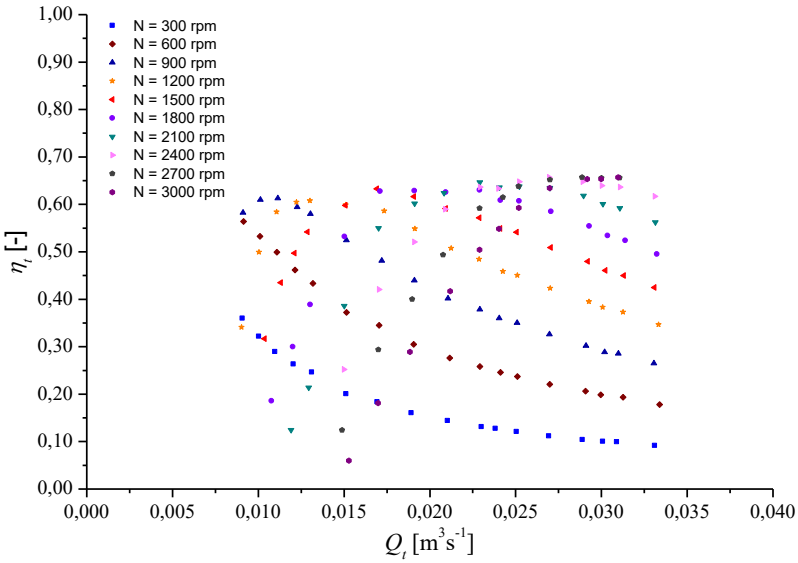


**Fig. 4.34 $\eta_t(Q_t)$ experimental curves – VA SS PAT**

The head drop $H_t$ raising, at increasing the flow rate $Q_t$, was observed (Fig. 4.32), whereas, for a fixed flow rate $Q_t$, the head drop $H_t$ increase, at increasing the rotational speed $N$, was lower than that observed for the HA SS PAT. Furthermore, for rotational speeds $N \leq 2400$ rpm, low head drop increases were determined at increasing the rotational speed $N$, defining almost constant head drops $H_t$ for flow rates $Q_t$ up to 21 ls$^{-1}$. For $Q_t > 21$ ls$^{-1}$, lower $N$ values implicated higher head drops $H_t$, instead. As observed for the HA SS PAT, the head drop $H_t$ did not monotonically increase at varying $N$, showing a minimum $H_{t\min}$ for higher $N$, at raising the flow rate $Q_t$ (Fig. 4.35).

In terms of produced power $P_t$ (Fig. 4.33), an increasing monotonic trend was observed at increasing the flow rate $Q_t$, obtaining for $N \geq 2400$ rpm slight power $P_t$ improvement at rising $N$.

The maximum efficiency $\eta_{tb}$ was almost constant at increasing $N$, equal to 65.5%, being reached, as observed for the HA SS PAT, for higher flow rate $Q_t$ at raising $N$ (Fig. 4.34).

By analysing the head drop $H_t(N)$ correlation (Fig. 4.35), for a fixed flow rate $Q_t$, a second order polynomial function was derived with a minimum $H_{t\min}$, defined by the following Eq. (4.10):

$$H_{t\min} = 4.50 \cdot 10^{-6} N^2 \tag{4.10}$$

For the VA SS PAT, in reference to flow rates $Q_t \leq 21$ ls$^{-1}$, the application of the ALs was reliable only up to a fixed $N$ value, which increased at increasing $Q_t$. Specifically, it varied from 1100 rpm for $Q_t = 9$ ls$^{-1}$ to 2750 rpm for $Q_t = 21$ ls$^{-1}$. For higher $N$, greater slopes of the experimental $H_t(N)$ curves were observed, according to an asymptotic trend, as showed in Fig. 4.35.

Moreover, the third order polynomial function was used to correlate the maximum produced power $P_{t\max}$ to the rotational speed $N$ (Fig. 4.36), according to the Eq. (4.11):

$$P_{t\max} = 2.08 \cdot 10^{-10} N^3 \tag{4.11}$$

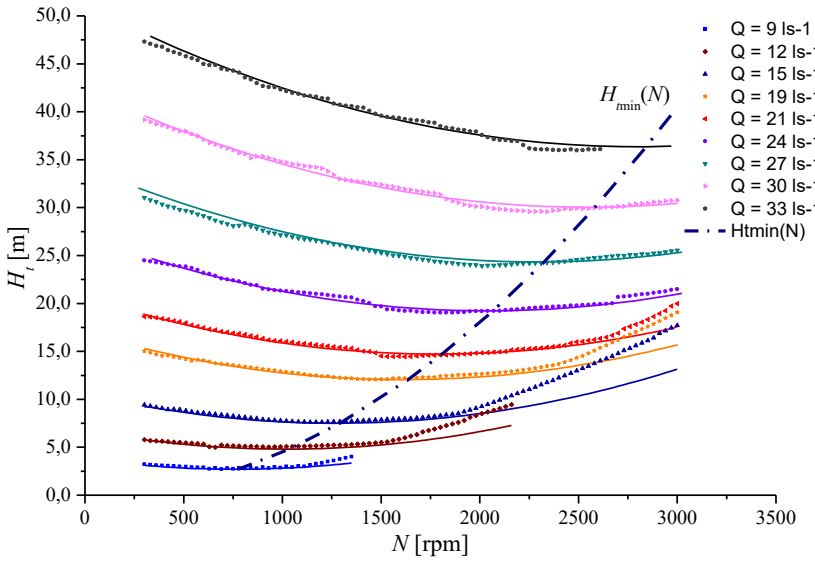


**Fig. 4.35 $H_t(N)$ experimental curves – VA SS PAT**

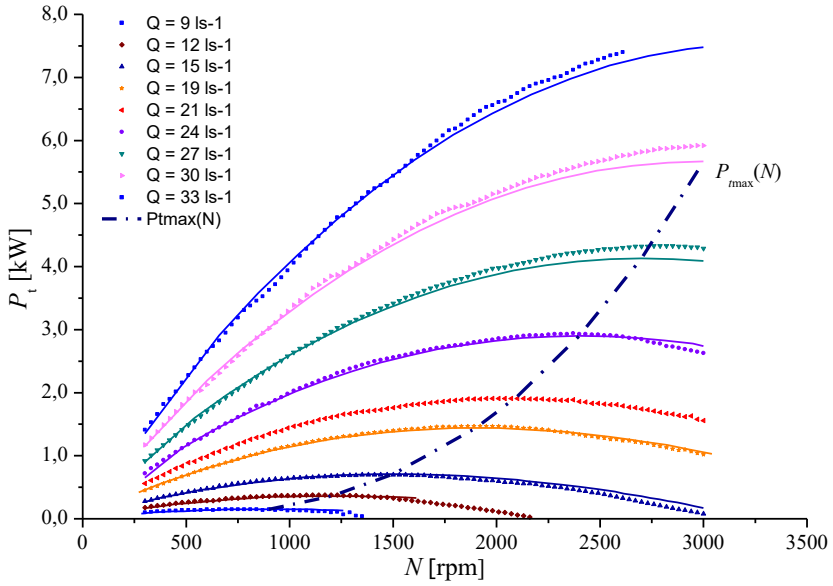


**Fig. 4.36 $P_t(N)$ experimental curves – VA SS PAT**

In the following Fig. 4.37, Fig. 4.38 and Fig. 4.39, the experimental $H_t(Q_t)$, $P_t(Q_t)$ and $\eta_t(Q_t)$ curves for the VA $MS_1$ PAT are plotted, at varying the flow rate $Q_t$, respectively, for $N$ = 300, 600, 900, 1200, 1500, 1800, 2100, 2400, 2700, 3000 rpm.

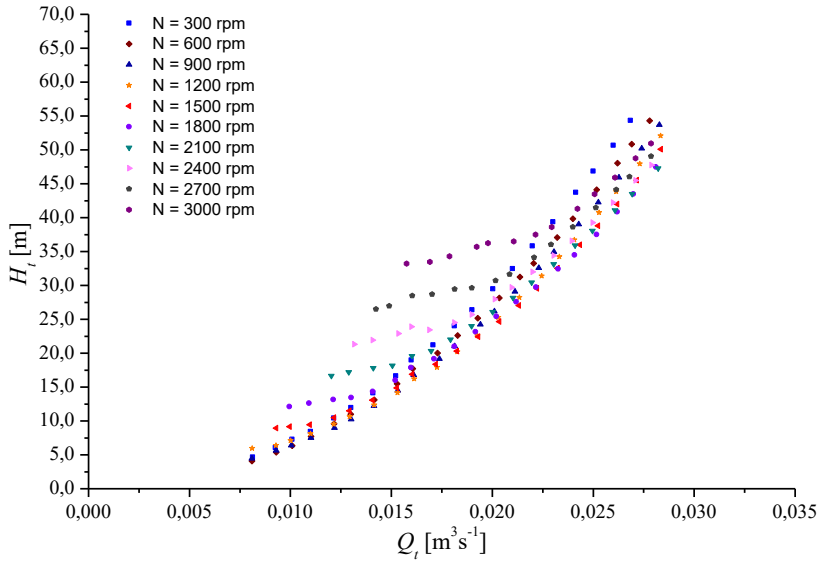


**Fig. 4.37 $H_t(Q_t)$ experimental curves – VA $MS_1$ PAT**

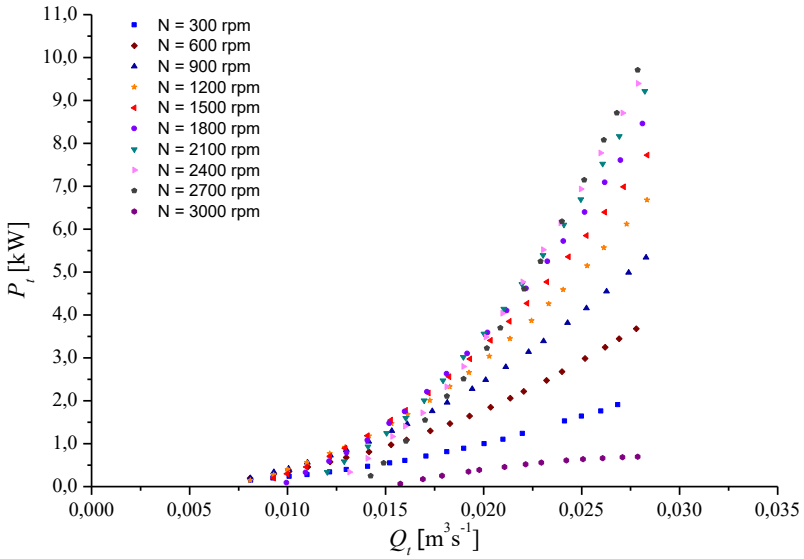


**Fig. 4.38 $P_t(Q_t)$ experimental curves – VA MS$_1$ PAT**

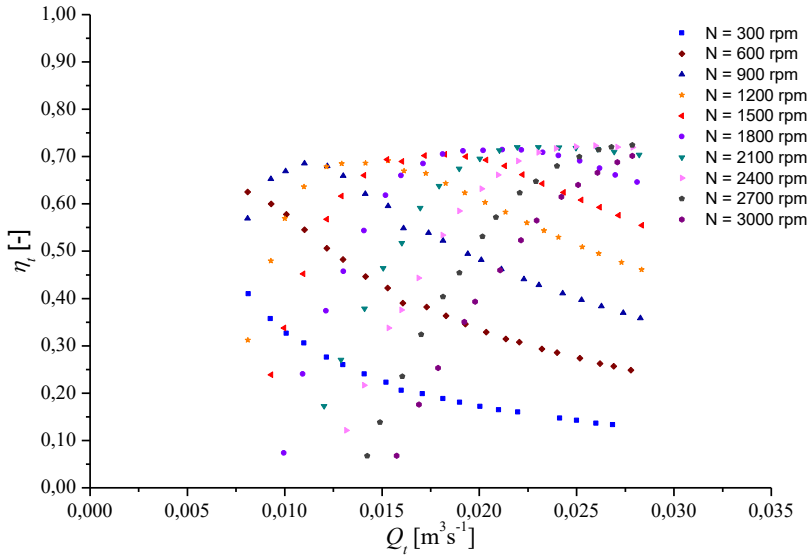


**Fig. 4.39 $\eta_t(Q_t)$ experimental curves – VA MS$_1$ PAT**

Similar trends were determined, with respect to the VA SS PAT model. The head drops $H_t$, for each flow rate $Q_t$, was lower than twice the amount (meanly equal to 1.84 times of the VA SS PAT model), individuating low differences in the generated head drops $H_t$ (Fig. 4.37) for rotational speed $N \leq 1500$ rpm. Conversely, for $N > 1500$ rpm and flow rates $Q_t \leq 22$ ls$^{-1}$, $H_t$ values were widely greater than these generated at low $N$.

Finally, for $Q_t > 22$ ls$^{-1}$, greater head drops $H_t$ corresponded to lower rotational speeds $N$ and vice versa.

The produced power $P_t$ showed a trend similar to the VA SS PAT one, defining, being equal the flow rate $Q_t$ and the rotational speed $N$, power $P_t$ of almost twice its amount (Fig. 4.38). A mean ratio of 2.12 was specifically estimated.

Head drop $H_t$ and power $P_t$ combination assessed greater overall efficiencies $\eta_t$ than the VA SS PAT one, reaching at BEP the maximum efficiency $\eta_{tb}$ = 72.1% (Fig. 4.39). In this case, at $N \leq 1500$ rpm $\eta_{tb}$ was slightly lower (deploying on 69%), of about 3%, than that reached at $N > 1500$ rpm.

For the VA MS$_1$ PAT, the $H_t(N)$ correlation presented, also in this case, a minimum $H_{t\min}$ (Fig. 4.40), definable by applying the Eq. (4.12):

$$H_{t\min} = 1.15 \cdot 10^{-5} N^2 \tag{4.12}$$

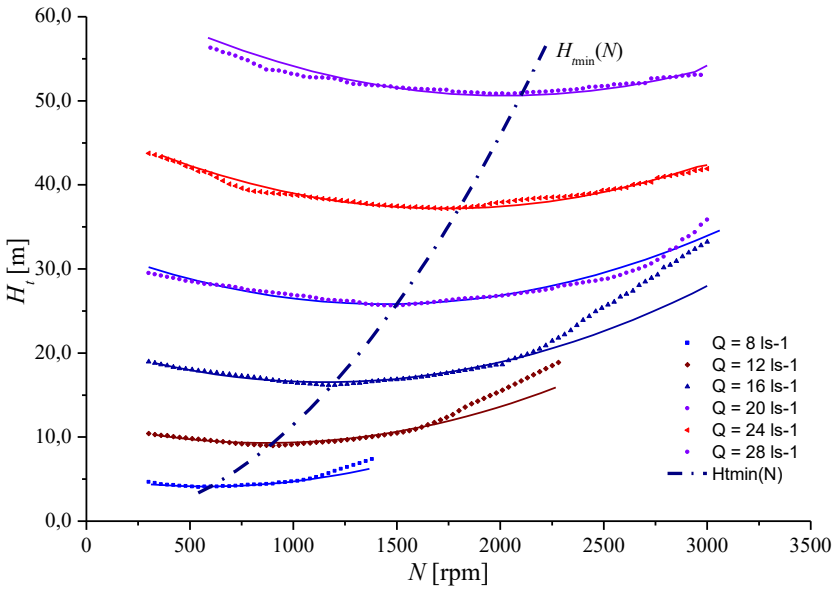


**Fig. 4.40 $H_t(N)$ experimental curves – VA MS$_1$ PAT**

As stated for the VA SS PAT, for $Q_t \leq 20$ ls$^{-1}$ the ALs were reliable only up to fixed $N$ values, definable as a function of the considered flow rate. Being equal $Q_t$, this limit resulted to be substantially similar to that observed for the VA SS PAT (Fig. 4.40), defining greater head drops $H_t$ than those calculated with the ALs for both VA SS and VA MS PATs.

The third order polynomial function to estimate the $P_{t\max}$ curve at varying the rotational speed $N$ (Fig. 4.41), was inferred by using the Eq. (4.13):

$$P_{t\max} = 5.25 \cdot 10^{-10} N^3 \tag{4.13}$$

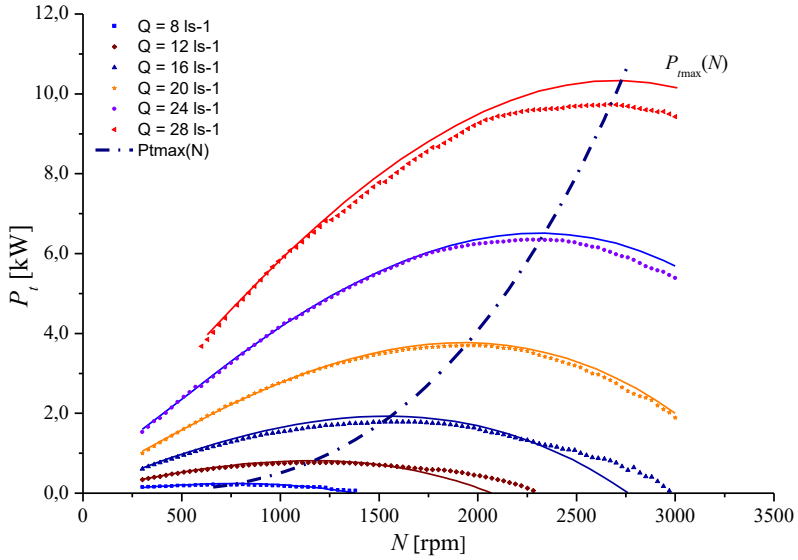


**Fig. 4.41 $P_t(N)$ experimental curves – VA $MS_1$ PAT**

In this case, for $Q_t \leq 16$ $ls^{-1}$ the ALs underestimated the produced power $P_t$ at higher rotational speed $N$, whereas a slight overestimation was reached at higher $Q_t$ and $N$, however, not higher than 6%.

Moreover, the characteristic curves for VA $MS_2$ PAT are plotted in the following Fig. 4.42, Fig. 4.43 and Fig. 4.44 at varying the flow rate $Q_t$. In terms of head drop $H_t$ (Fig. 4.42), the experimental observations were essentially equal to the VA $MS_1$ PAT ones, establishing relative errors utmost of ±6%, being equal the flow rate $Q_t$ and the rotational speed $N$.

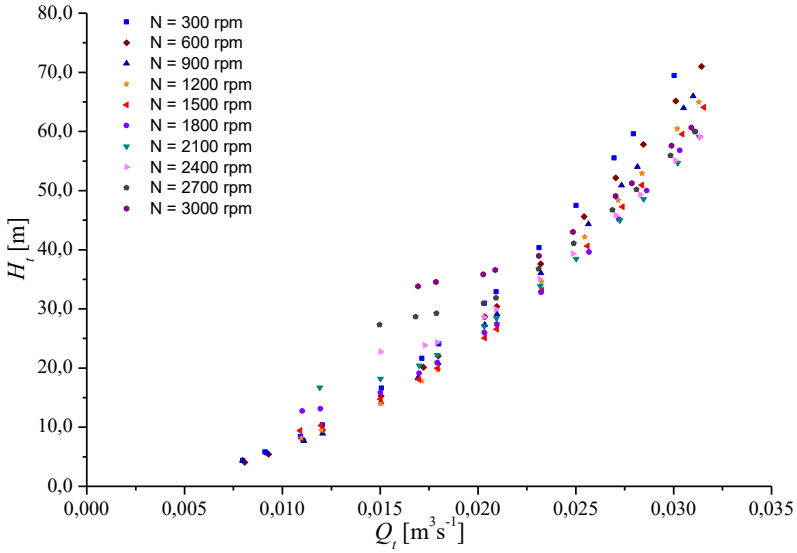


**Fig. 4.42 $H_t(Q_t)$ experimental curves – VA $MS_2$ PAT**

In terms of produced power $P_t$ (Fig. 4.43), the IE3 efficiency motor class equipment entailed higher performances, than those reached with the same PAT model and the IE2 motor equipment, just for rotational speeds $N \leq 1200$ rpm, whereas essentially equivalent trends were observed for $N > 1200$ rpm. From the above considerations, very similar trends to the VA $MS_1$ PAT ones were determined for the efficiency $\eta_t$ curve estimation, reaching the same maximum efficiency at BEP $\eta_{tb}$, equal to 72.1% and 69% for $N > 1200$ rpm and $N \leq 1200$ rpm, respectively (Fig. 4.44).

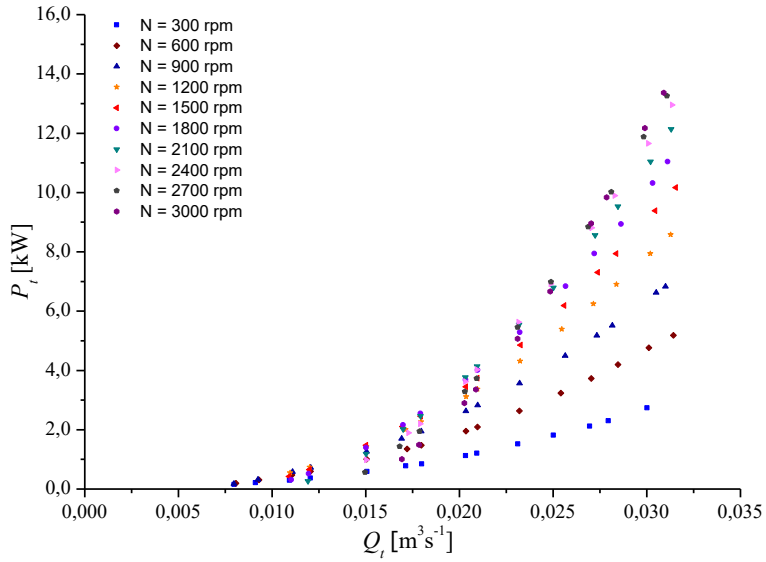


**Fig. 4.43 $P_t(Q_t)$ experimental curves – VA MS$_2$ PAT**

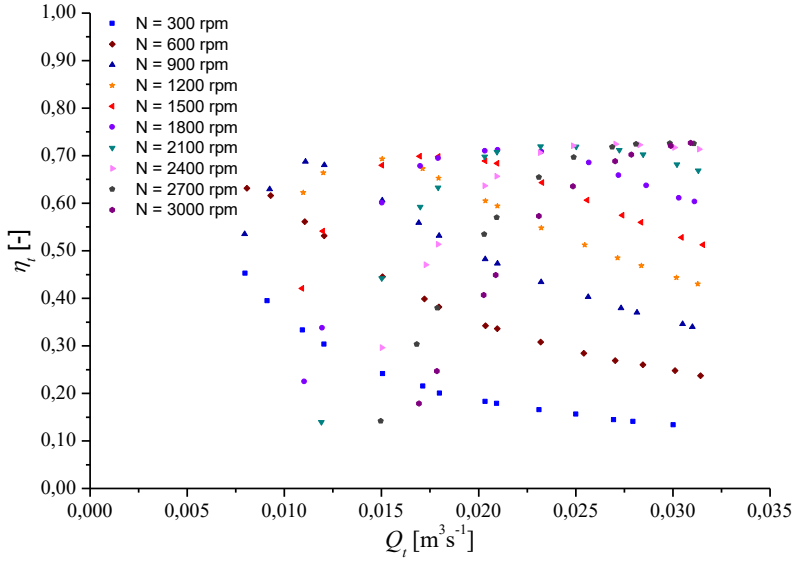


**Fig. 4.44 $\eta_t(Q_t)$ experimental curves – VA MS$_2$ PAT**

In greater detail, for rotational speed $N$ = 300 rpm, a scatter of about +10% was estimated for both power $P_t$ (Fig. 4.45a) and efficiency $\eta_t$ (Fig. 4.45b) at flowing greater $Q_t$, whereas the discrepancy progressively decreased at raising the rotational speed $N$. Finally, for $N$ = 3000 rpm, a scatter of about +1.5% for VA MS$_2$ PAT was assessed.

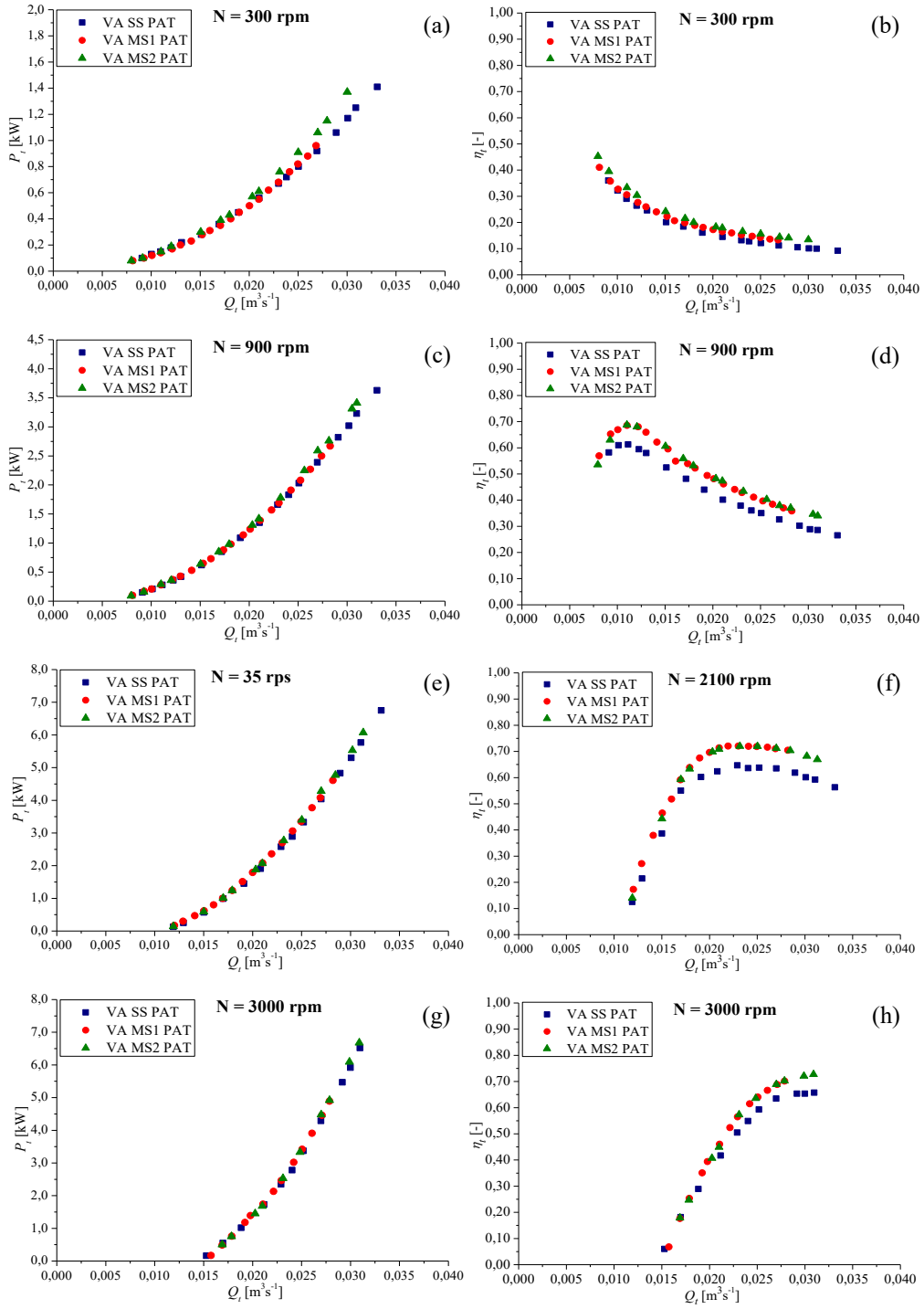


**Fig. 4.45 $P_t(Q_t)$ and $\eta_t(Q_t)$ curves for $N$ = 300 rpm (a,b), 900 rpm (c,d), 2100 rpm (e,f) and 3000 rpm (g,h) – VA SS and MS PATs**

In the previous Fig. 4.45a-h, comparison between the three tested VA PATs was plotted for $N$ = 300, 900, 2100 and 3000 rpm. In these figures, in order to compare experimental data from Single-Stage and Multi-Stage models, the head drop $H_t$ and the power $P_t$ are divided by the number of stages of each PAT.

In them, the improvement of power $P_t$ generation, defined by the IE3 motor equipment, is remarkable only for $N \leq 900$ rpm, whereas no differences are observed for higher $N$ between the two VA MS PATs. This result points out the restricted operative range in which the IE3 equipment generated effective performance improvements, for a pump motor acting as an electrical generator.

With respect to the VA SS model, the differences in terms of efficiency curves were due to the high head drops generated by the VA SS model (for the same number of stages), which caused, being equal the produced power, the efficiency reduction at BEP.

In dimensionless terms, flow rate number $\phi$, head number $\psi$ and power number $\pi$ were varied in the ranges in Tab. 4.10, whereas the BEP operations in PAT mode are summarized in Tab. 4.11. For comparison between Single-Stage and Multi-Stage models, results at BEP in Tab. 4.11 are reported in terms of single stage. In it, the specific speed $N_{st}$ is also introduced.

| PAT | $\phi$ [-] | $\psi$ [-] | $\pi$ [-] |
|---|---|---|---|
| **VA SS IE3** | 0.10 - 2.13 | 3.26 - 871.47 | 0.02 - 170.40 |
| **VA $MS_1$ IE2** | 0.10 - 1.73 | 5.91 - 1000 .88 | 0.01 - 230.33 |
| **VA $MS_2$ IE3** | 0.10 - 1.93 | 6.00 - 1278.67 | 0.02 - 330.91 |

**Tab. 4.10 Dimensionless experimental operative ranges – VA PATs**

| PAT | $\phi_b$ [-] | $\psi_b$ [-] | $\pi_b$ [-] | $\eta_{tb}$ [%] | $N_{st}$ [rpm, $m^3s^{-1}$] |
|---|---|---|---|---|---|
| **VA SS IE3** | | 6.34 | 0.85 | 65.5% | 37.68 |
| **VA $MS_1$ IE2** | 0.21 | 5.91 | 0.87 | 72.1% | 39.77 |
| **VA $MS_2$ IE3** | | 5.91 | 0.87 | 72.1% | 39.77 |

**Tab. 4.11 Dimensionless parameters at BEP – VA PATs**

In reference to the three considered PATs, the BEP was achieved for the almost equal flow rate number $\phi_b$ = 0.21. In particular, at BEP the SS PAT generated a higher head number $\psi$ than the two VA MS PATs, whereas the power number $\pi$ was quite

similar, thus defining lower efficiency at BEP $\eta_{tb}$ than that of two MS models, of about 6.5%. With respect to the efficiency at BEP in pump mode, equal to $\eta_{pb}$ = 76.5% for all the three considered VA PATs, the VA SS PAT showed an efficiency reduction at BEP in turbine mode $\eta_{tb}$ of about 11%, whereas the two VA MS PATs established $\eta_{tb}$ of about 5% lower than $\eta_{pb}$.

Comparison between the experimental data for the three tested VA PATs and the Derakhshan and Nourbakhsh (2008a) Eq. (3.62) is plotted, in terms of $\psi(\phi)$ function, in Fig. 4.46. Eq. (3.62) is represented as a function of the BEP conditions for the VA SS PAT and its extension, over the limit defined by the authors of $\phi$ = 0.40, is plotted with a dashed line.

As above stated, no differences were shown between the two VA MS PATs, for the definition of the head number $\psi(\phi)$ curve, having the same internal geometry and configuration, whereas the VA SS PAT showed higher $\psi$ values with scatters up to 11.6%.

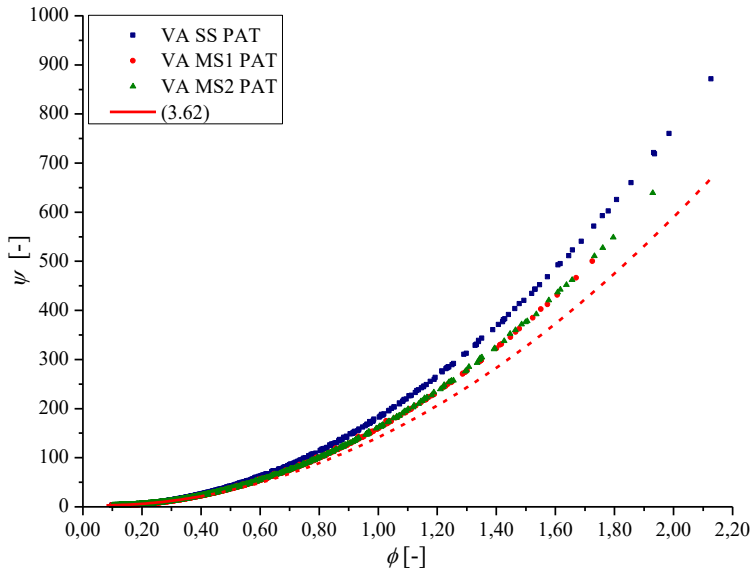


**Fig. 4.46 $\psi(\phi)$ experimental and Eq. (3.62) curves – VA PATs**

In Fig. 4.46, the underestimation of Eq. (3.62) is shown, in terms of head numbers $\psi$, for the whole experimented flow rate range. Indeed, relative scatters up to 23% were

observed for the VA SS PAT, whereas lower discrepancies, not higher than 14%, were measured for both VA MS PAT models.

By comparing the power number $\pi(\phi)$ curves, a significant correspondence between the SS and the VA $MS_1$ PATs was observed for the whole range of $\phi$ values (Fig. 4.47), whereas the VA $MS_2$ PAT, equipped with a IE3 motor efficiency class, presented comparable $\pi$ values for flow rate numbers $\phi$ up to 0.80. For higher $\phi$ values, the VA $MS_2$ PAT showed higher efficiency, by defining $\pi$ values greater than the VA $MS_1$ PAT ones, with discrepancies up to 10%.

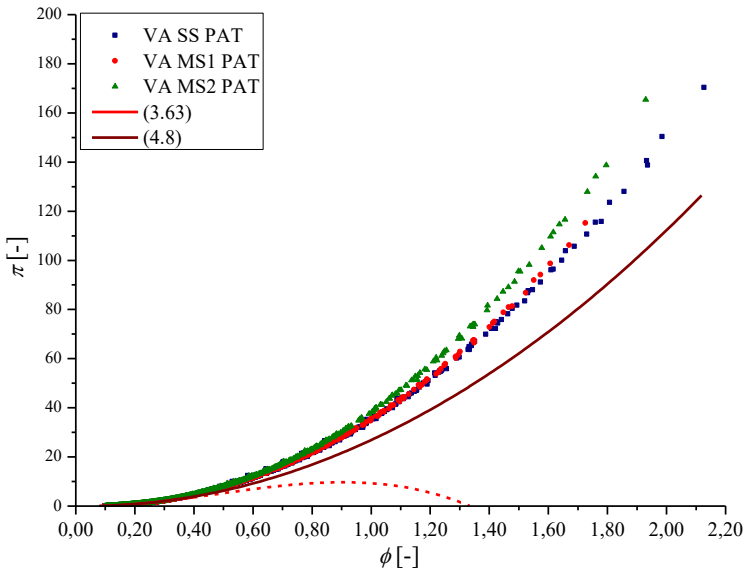


**Fig. 4.47 $\pi(\phi)$ experimental and Eqs. (3.63) and (4.8) curves – VA PATs**

As observed for the HA SS PAT, the Derakhshan and Nourbakhsh Eq. (3.63) was reliable only in the range declared by the authors of $\phi \leq 0.40$, whereas, for greater $\phi$, it returned an unreliable bell curve with maximum $\pi = 9.70$ at $\phi = 0.90$. Indeed, for $\phi >$ 0.90, a decreasing function was assessed, up to its nullification for $\phi = 1.33$.

Conversely, the experimental data showed a monotonic increasing trend, in compliance with the Eq. (4.8). From comparison between the experimental data for VA PATs and the Eq. (4.8), it was shown its good reliability for $\phi \leq 0.60$. For higher $\phi$ increasing discrepancies were determined, defining the numerical underestimation up to 30%, instead.

Concerning the efficiency curve $\eta_t(\phi)$, for the three VA PATs, the BEP was achieved at the almost equal flow rate number $\phi = 0.21$, defining the same $\eta_{tb}$ for the two VA MS PATs. Comparison between experimental data, Derakhshan and Nourbakhsh Eq. (3.64) and Eq. (4.9) are plotted in Fig. 4.48, pointing out, once again, the reliability of Eq. (3.64) only for $\phi \leq 0.40$. Conversely, Eq. (4.9) was able to well represent the experiments in the whole considered experimental range, overestimating the experimental efficiency $\eta_t$ of about 15% for $\phi \leq 0.20$. For $\phi > 0.20$, a significant correlation was found, corresponding to a mean relative error of about 1.5%, instead.

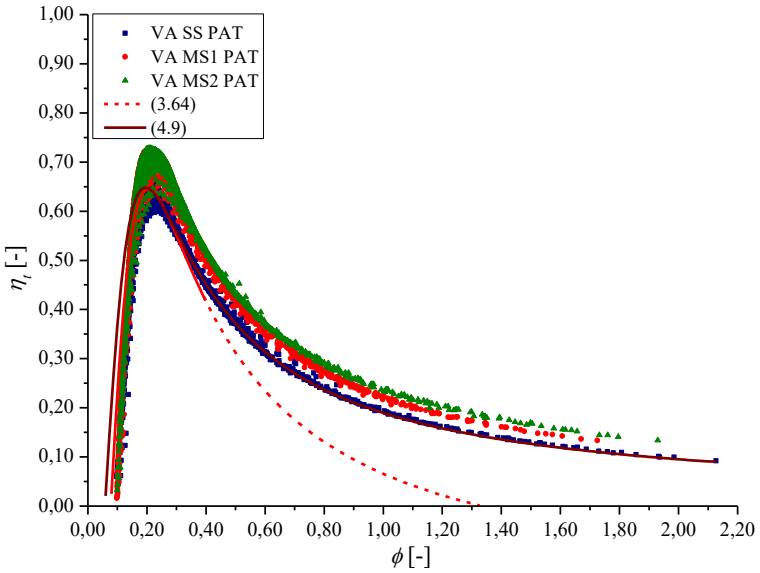


**Fig. 4.48 $\eta_t(\phi)$ experimental and Eqs. (3.64) and (4.9) curves – VA PATs**

As abovementioned, Fig. 4.48 shows that the influence of the motor efficiency class was spotted just for low rotational speeds $N$ (thus for high flow rate numbers $\phi$), as a consequence of slightly higher power numbers $\pi$ for the VA $MS_2$ PAT model and equal head numbers $\psi$ for all the tested VA PATs.

## 4.7 Predicting Formulations of Performances for Vertical Axis Centrifugal PATs

Hence, performed experiments on the VA PATs models, for high flow rate numbers $\phi$, showed significant differences from results reached by applying relationships available

in the literature. Eqs. (4.8) and (4.9), derived in the context of this Ph.D. work for the HA PAT models, resulted to be more reliable than the other models in the literature; however, they fell for greater $\phi$ values.

Therefore, by applying the same analytic forms of second order and third order polynomial functions for head drop $H_t$ and power $P_t$ curves, respectively, alternative formulations were derived for VA PATs, in dimensionless terms with respect to the BEP operations.

Coefficients were calibrated by minimizing the standard deviations between experimental data from the VA SS PAT and the theoretical curves. Results were defined as follows:

$$\frac{H_t}{H_{tb}} = 1.358\left(\frac{Q_t}{Q_{tb}}\right)^2 - 0.847\left(\frac{Q_t}{Q_{tb}}\right) + 0.508 \tag{4.14}$$

$$\frac{P_t}{P_{tb}} = 6.0\cdot 10^{-3}\left(\frac{Q_t}{Q_{tb}}\right)^3 + 1.897\left(\frac{Q_t}{Q_{tb}}\right)^2 - 0.934\left(\frac{Q_t}{Q_{tb}}\right) + 0.003 \tag{4.15}$$

In Fig. 4.49 and Fig. 4.50, the Eqs. (4.14) and (4.15) are represented, in the form of the $\psi(\phi)$ and $\pi(\phi)$ functions, and comparisons with experimental data (plotted as a function of a single-stage) are shown.

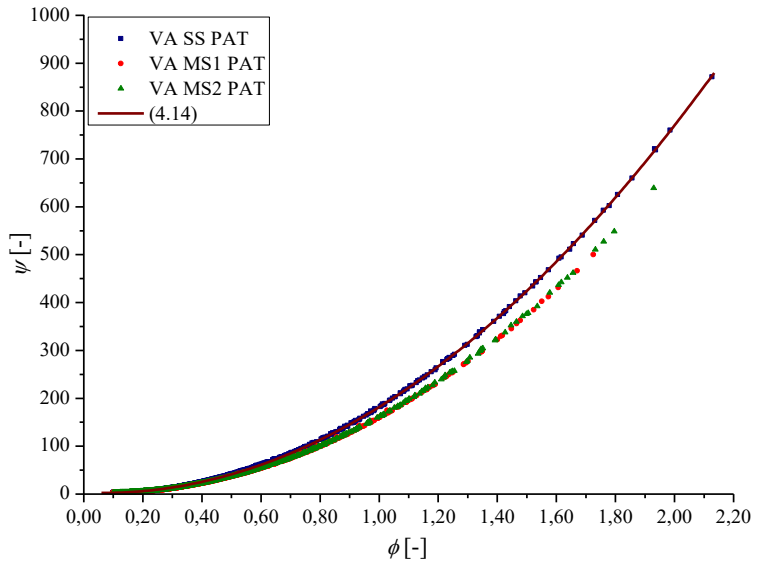


**Fig. 4.49 $\psi(\phi)$ experimental and Eq. (4.14) curves – VA PATs**

Eq. (4.14) presented significant agreement with experiments for the VA SS PAT, whereas it well reproduced the experimental results of the VA MS PATs only for $\phi \leq 0.60$. For $\phi > 0.60$, as a consequence of the difference between the head drops generated by the VA SS PAT and by the VA MS ones, greater discrepancies were established, however, not higher than 10%.

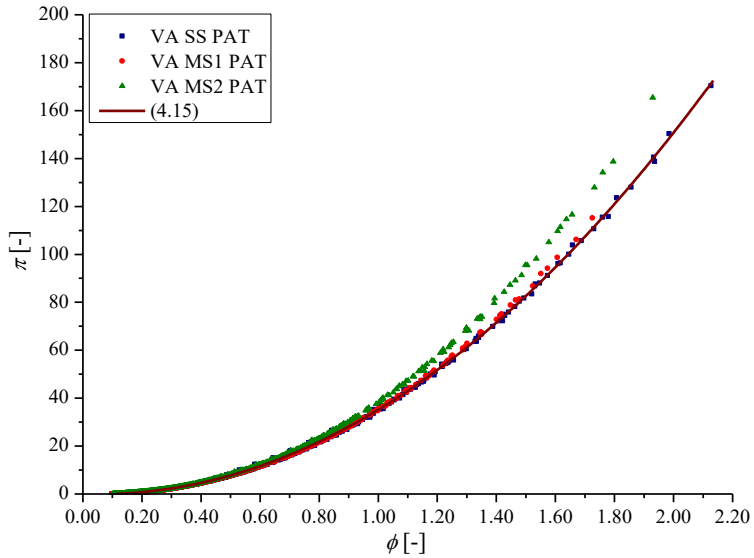


**Fig. 4.50 $\pi(\phi)$ experimental and Eq. (4.15) curves – VA PATs**

Eq. (4.15) significantly reproduced the experiments of both the VA SS PAT and the VA $MS_1$ PAT in the whole set of tested $\phi$ values; for the VA $MS_2$ PAT, it was significantly reliable for $\phi \leq 0.80$. For higher $\phi$ values, an increasing discrepancy was observed for the VA $MS_2$ PAT, because of the power number $\pi$ underestimation in the order of 10%, instead. This scatter was due to the VA $MS_2$ PAT equipment; indeed, it was shown that the IE3 motor efficiency class assured higher efficiencies at low rotational speeds $N$.

Furthermore, by combining the Eqs. (4.14) and (4.15) with Eq. (4.1), the Eq. (4.16) was derived to estimate the efficiency curve $\eta_t$ of VA PATs, as a function of the operative conditions at BEP:

$$\frac{\eta_t}{\eta_{tb}} = \frac{6.0 \cdot 10^{-3}\left(\frac{Q_t}{Q_{tb}}\right)^3 + 1.897\left(\frac{Q_t}{Q_{tb}}\right)^2 - 0.934\left(\frac{Q_t}{Q_{tb}}\right) + 0.003}{1.358\left(\frac{Q_t}{Q_{tb}}\right)^3 - 0.847\left(\frac{Q_t}{Q_{tb}}\right)^2 + 0.508\left(\frac{Q_t}{Q_{tb}}\right)} \tag{4.16}$$

From comparison between the Eq. (4.16) and the experimental results, a good correlation was observed, in reference to the VA SS PAT. Conversely, for the VA MS PATs, the underestimation of experimental data in the order of 14% was assessed, as a consequence of their higher efficiencies at BEP (Fig. 4.51).

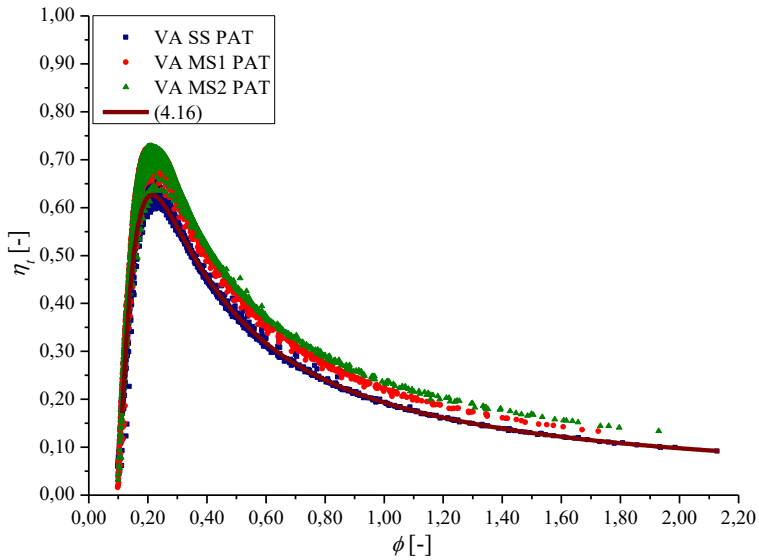


**Fig. 4.51 $\eta_t(\phi)$ experimental data and Eq. (4.16) – VA PATs**

The application of mono-dimensional models from the literature to predict the BEP in PAT mode, as a function of the BEP in pump operations, was performed, accordingly with how operated for the tested HA SS PAT. In Tab. 4.12 the experimental ratios are summarized at rotational speed $N$ = 2900 rpm; for the VA MS PATs a single string is inserted, having defined, for both the tested MS PATs, the same parameters at BEP.

| PAT | $Q_{tb}/Q_{pb}$ [-] | $H_{tb}/H_{pb}$ [-] | $P_{tb}/P_{pb}$ [-] | $\eta_{tb}/\eta_{pb}$ [-] | $Ns_{tb}/Ns_{pb}$ [-] |
|---|---|---|---|---|---|
| **VA SS PAT** | 1.26 | 1.46 | 0.91 | 0.86 | 0.84 |
| **VA MS PATs** | 1.26 | 1.36 | 0.93 | 0.94 | 0.89 |

**Tab. 4.12 Experimental ratios at BEP – VA PATs**

In Tab. 4.13 and Tab. 4.14 the theoretical flow rate $Q_{tb}/Q_{pb}$ and head $H_{tb}/H_{pb}$ ratios from the literature are reported and the relative errors are plotted in Fig. 4.52 and Fig. 4.53 for the VA SS PAT and the VA MS PATs, respectively.

| Model | $Q_{tb}/Q_{pb}$ [-] | $H_{tb}/H_{pb}$ [-] | $\Delta(Q_{tb}/Q_{pb})$ [%] | $\Delta(H_{tb}/H_{pb})$ [%] |
|---|---|---|---|---|
| Stepanoff (1957) | 1.14 | 1.31 | -8.90% | -10.69% |
| Childs (1962) | 1.31 | 1.31 | 4.15% | -10.69% |
| Hancock (1963) | 1.53 | 1.53 | 21.61% | 4.27% |
| Grover (1980) | 1.38 | 1.83 | 10.29% | 25.03% |
| Hergt (1982) | 1.25 | 1.13 | -0.32% | -23.00% |
| Sharma (1985) | 1.24 | 1.38 | -1.28% | -5.78% |
| Schmiedl (1988) | 1.89 | 1.57 | 50.59% | 7.34% |
| Alatorre-Frenk and Thomas (1990) | 1.68 | 1.65 | 33.77% | 12.42% |
| Amelio et al. (2000) | 3.35 | 1.39 | 167.05% | -4.96% |
| Joshi et al. (2005b) | 1.50 | 1.60 | 19.51% | 9.31% |
| Derakhshan and Nourbakhsh (2008a) | 1.29 | 1.44 | 2.91% | -1.91% |
| Nautiyal et al. (2011) | 0.98 | 1.02 | -21.57% | -30.35% |
| Yang et al. (2012a) | 1.39 | 1.61 | 10.79% | 10.08% |
| Tan and Engeda (2016) | 1.16 | 1.36 | -7.42% | -7.16% |

**Tab. 4.13 Flow rate and head ratios at BEP – VA SS PAT**

| Model | $Q_{tb}/Q_{pb}$ [-] | $H_{tb}/H_{pb}$ [-] | $\Delta(Q_{tb}/Q_{pb})$ [%] | $\Delta(H_{tb}/H_{pb})$ [%] |
|---|---|---|---|---|
| Stepanoff (1957) | 1.14 | 1.31 | -8.90% | -4.04% |
| Childs (1962) | 1.31 | 1.31 | 4.15% | -4.04% |
| Hancock (1963) | 1.39 | 1.39 | 10.48% | 1.80% |
| Grover (1980) | 1.33 | 1.78 | 5.89% | 30.84% |
| Hergt (1982) | 1.25 | 1.14 | -0.09% | -16.54% |
| Sharma (1985) | 1.24 | 1.38 | -1.28% | 1.25% |
| Schmiedl (1988) | 1.73 | 1.50 | 37.93% | 10.18% |
| Alatorre-Frenk and Thomas (1990) | 1.68 | 1.65 | 33.77% | 20.80% |
| Amelio et al. (2000) | 3.35 | 1.39 | 167.05% | 2.13% |
| Joshi et al. (2005b) | 1.50 | 1.60 | 19.51% | 17.46% |
| Derakhshan and Nourbakhsh (2008a) | 1.52 | 1.74 | 21.50% | 27.68% |
| Nautiyal et al. (2011) | 0.98 | 1.02 | -21.57% | -25.16% |
| Yang et al. (2012a) | 1.39 | 1.61 | 10.79% | 18.28% |
| Tan and Engeda (2016) | 1.16 | 1.36 | -7.42% | -0.23% |

**Tab. 4.14 Flow rate and head ratios at BEP – VA MS PATs**

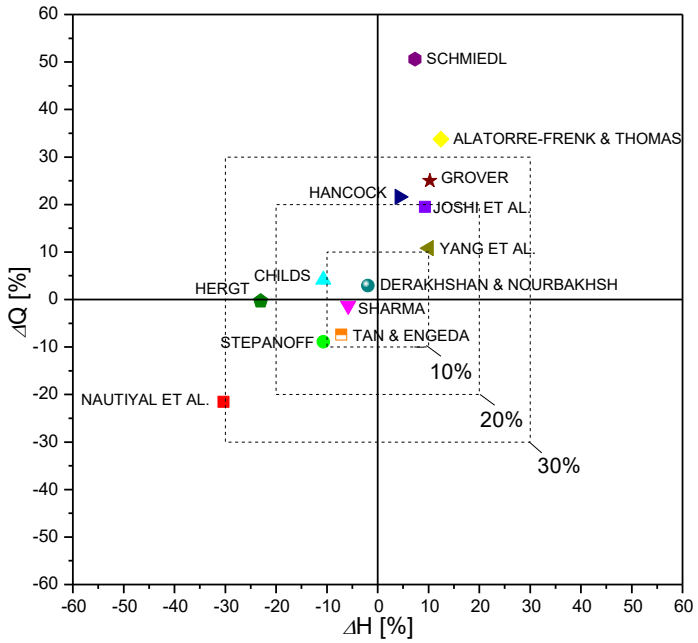


**Fig. 4.52 Flow rate and head ratios scatters at BEP – VA SS PAT**

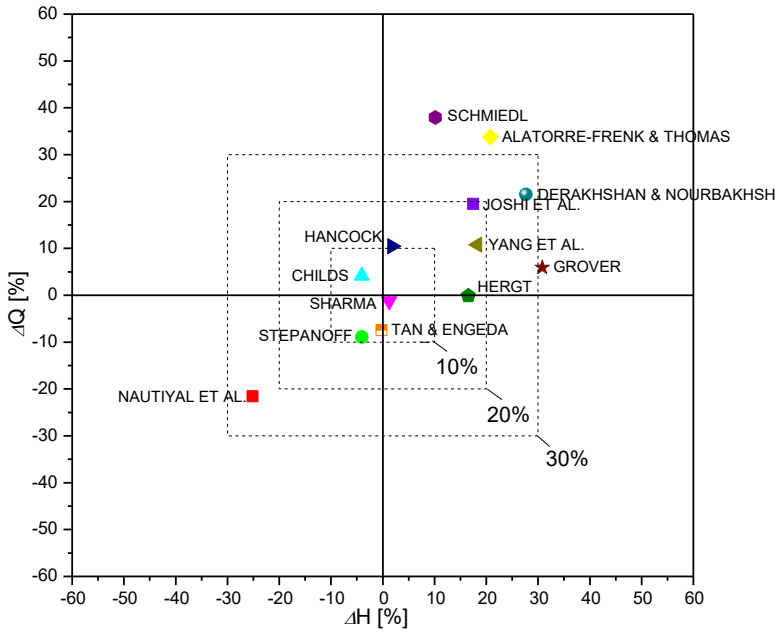


**Fig. 4.53 Flow rate and head ratios scatters at BEP – VA MS PATs**

For both VA SS PAT and VA MS PATs, Stepanoff (1957), Sharma (1985), Childs (1962) and Tan and Engeda (2016) formulations showed the best agreements with experiments, with relative errors in the range ±11%. With the Hancock (1963) model,

discrepancies in the order of 10% were assessed for the head drop ratio of both VA PAT models, whereas it overestimated the flow rate ratio of about 21% for the VA SS PAT. Derakhshan and Nourbakhsh (2008a) formulations significantly agreed with experiments for VA SS PAT, defining scatter of about +3% for flow rate ratio and -2% for head ratio. It overestimated the BEP for MS models of about 21.5% and 28%, instead.

Furthermore, Fernandez et al. (2004) Eq. (3.52) was applied to verify the head ratios for both the VA SS and the VA MS models, by estimating relative errors of about +18% and +27%, respectively.

The theoretical power ratios $P_{tb}/P_{pb}$ from Derakhshan and Nourbakhsh (2008a) and Tan and Engeda (2016) models overestimated the power ratio $P_{tb}/P_{pb}$, finding ratios greater than unity, whereas experiments gave ratios of 0.91 and 0.93 for VA SS and VA MS PATs, respectively. Specifically, Derakhshan and Nourbakhsh (2008a) formulations returned theoretical power ratios of 1.26 and 1.12, respectively, corresponding to relative errors of about +38% and +21%. Finally, the Tan and Engeda (2016) approach returned theoretical ratios of 1.26 and 1.16, respectively, equal to about +38% and +24% of the experimental values.

In terms of specific speed ratio $N_{st}/N_{sp}$, Amelio et al. (2000), Yang et al. (2012a) and Tan and Engeda (2016) approaches returned the same values, for both the VA SS and the VA MS PATs, being all the three methods depending on the specific speed in pump mode $N_{sp}$, assessed to 44.76 for all the three tested VA PATs. Amelio et al. (2000) and Yang et al. (2012a) formulas gave relative errors not greater than ±5% (Tab. 4.15), whereas the Tan and Engeda (2016) approach underestimated the specific speed ratio of about -10.5% and -15% for VA SS and VA MS PATs, respectively.

| **Model** | **VA SS PAT** | | **VA MS PATs** | |
|---|---|---|---|---|
| | **$Ns_{tb}/Ns_{pb}$ [-]** | **$\Delta(Ns_{tb}/Ns_{pb})$ [-]** | **$Ns_{tb}/Ns_{pb}$ [-]** | **$\Delta(Ns_{tb}/Ns_{pb})$ [-]** |
| Amelio et al. (2000) | 0.87 | 3.70% | 0.87 | -1.75% |
| Yang et al. (2012a) | 0.85 | 1.51% | 0.85 | -3.82% |
| Tan and Engeda (2016) | 0.75 | -10.44% | 0.75 | -15.14% |

**Tab. 4.15 Specific speed ratios at BEP – VA PATs**

From the performed analysis, the applicability of the above considered ratios to predict the BEP of pumps running as turbines was verified, also for Vertical Axis centrifugal models, determining rather restrained relative scatters. However, these approaches could be considered useful for the preliminary estimation of PAT characteristic curves. By combining them with more exhaustive tools, such as the Eq. (4.14), (4.15) and (4.16) proposed in the ambit of this Ph.D. work for Vertical Axis PATs, the estimation of PAT performances is more extensively performed.

## 4.8 Selecting Procedure of PAT Model in Water Distribution Networks

As a result of the performed experimental analysis, formulations to predict performances of centrifugal Horizontal Axis and Vertical Axis PATs are provided in Par. 4.5 and Par. 4.7, respectively.

Starting from these deductions, **an applicative procedure to select the centrifugal PAT model, able to maximize the producible energy in WDNs, is presented, aiming at representing a basic tool of a DSS for optimal PAT selection in WDNs**.

The proposed approach was developed under the hypothesis of performing the electrical regulation for PATs (Par. 3.2.2), thus supposing the variability of PAT rotational speed $N$ between a lower and an upper limit, in the range $[N_{min}...N_{max}]$.

The procedure was developed under the following hypotheses:

- the PAT location is established, knowing the flow modulation and the pressure level acting on the WDN;
- the daily pattern of users' demand and the related flow rate $Q_i$ and exceed pressure $H_{av,i}$ for each *i-th* time step are known;
- the characteristic curves in pump mode of a set of centrifugal pumps are available.

On these bases, the selecting procedure was developed as follows:

1. from manufacturers' datasheets, the operative parameters at BEP in pump mode of the *j-th* model are inferred; specifically, the impeller diameter $D_j$, the rotational speed $\overline{N}_j$, the flow rate $Q_{pb,j}$, the head $H_{pb,j}$ and the power $P_{pb,j}$ are deduced;
2. the flow rate ratio $Q_{tb,j}/Q_{pb,j}$, the head ratio $H_{tb,j}/H_{pb,j}$ and the power ratio $P_{tb,j}/P_{pb,j}$ at BEP are calculated by applying one of the mono-dimensional models in the

literature, in compliance with scatters defined in Tab. 4.5, Tab. 4.13 and Tab. 4.14 for Horizontal Axis PATs, Vertical Axis Single-Stage PATs and Vertical Axis Multi-Stage PATs, respectively;

3. the flow rate $Q_{tb,j}$, the head $H_{tb,j}$ and the power $P_{tb,j}$ at BEP in PAT mode are estimated, as a function of the rotational speed $\overline{N}_j$;
4. the dimensionless parameters at BEP $\phi_{b,j}$, $\psi_{b,j}$ and $\pi_{b,j}$ are calculated as a function of $\overline{N}_j$, resulting, according to the experimental results in Par. 4.4 and 4.6, to be constant at varying $N$;
5. the characteristic curves $\psi_{i,j}(\phi_j)$ and $\pi_{i,j}(\phi_j)$ are derived, by applying the Eqs. (3.62) and (4.8) for Horizontal Axis models and the Eqs. (4.14) and (4.15) for Vertical Axis models, in the form defined by the following Eqs. (4.17)-(4.18) and Eqs. (4.19)-(4.20), respectively:

   ***HORIZONTAL AXIS PATs***

$$\frac{\psi_{i,j}}{\psi_{b,j}} = 1.0283\left(\frac{\phi_{i,j}}{\phi_{b,j}}\right)^2 - 0.5468\left(\frac{\phi_{i,j}}{\phi_{b,j}}\right) + 0.5314 \tag{4.17}$$

$$\frac{\pi_{i,j}}{\pi_{b,j}} = 4.0\cdot 10^{-3}\left(\frac{\phi_{i,j}}{\phi_{b,j}}\right)^3 + 1.386\left(\frac{\phi_{i,j}}{\phi_{b,j}}\right)^2 - 0.390\left(\frac{\phi_{i,j}}{\phi_{b,j}}\right) \tag{4.18}$$

   ***VERTICAL AXIS PATs***

$$\frac{\psi_{i,j}}{\psi_{b,j}} = 1.358\left(\frac{\phi_{i,j}}{\phi_{b,j}}\right)^2 - 0.847\left(\frac{\phi_{i,j}}{\phi_{b,j}}\right) + 0.508 \tag{4.19}$$

$$\frac{\pi_{i,j}}{\pi_{b,j}} = 6.0\cdot 10^{-3}\left(\frac{\phi_{i,j}}{\phi_{b,j}}\right)^3 + 1.897\left(\frac{\phi_{i,j}}{\phi_{b,j}}\right)^2 - 0.934\left(\frac{\phi_{i,j}}{\phi_{b,j}}\right) + 0.003 \tag{4.20}$$

6. to initialize the procedure ($z=1$), knowing the flow rate $Q_i$, the maximum allowable rotational speed $N_{i,j}^{z=1} = N_{\max}$ is set to calculate the flow rate number $\phi_{i,j}^{z=1}$, being $z = 1\ldots S^*$ and $S^*$ the number of iterations required to reach the iterative convergence;
7. the head number $\psi_{i,j}^{z=1}$ is derived and the related head drop $H_{t,i,j}^{z=1}$ is estimated, from Eq. (4.17) or (4.19) for HA PATs and VA PATs, respectively;

8. if $H_{t,i,j}^{z=1} > H_{t,av,i}$, then the rotational speed $N_{i,j}^{z+1}$ is reduced to an allowable value; else if $H_{t,i,j}^{z=1} \leq H_{t,av,i}$, the power number $\pi_{i,j}^{k=1}$ is assessed from Eq. (4.18) or Eq. (4.20) and the power $P_{t,i,j}^{z=1}$ is estimated;

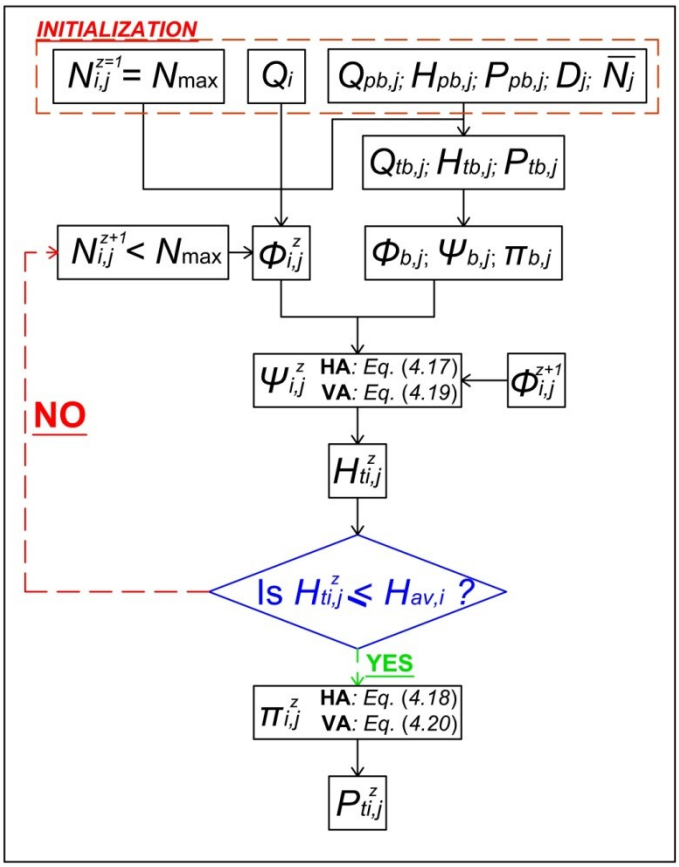


**Fig. 4.54 Flow chart of Steps 1-8 of PAT selection procedure in WDNs**

9. knowing the flow rate $Q_i$, the flow rate number $\phi_{i,j}$ is calculated at varying the rotational speed $N$ in the range $[N_{min}...N_{max}]$ and, for each $N$, the power number $\pi_{i,j}$ is assessed through the Eq. (4.18) and Eq. (4.20) for HA PATs and VA PATs, respectively. Thus, the power $P_{ti,j}$ is estimated for each $N$, in order to find out the maximum value $P_{tmax,i,j}$, reachable for the fixed $Q_i$ at varying $N$. The rotational speed $N^*_{i,j}$ related to $P_{tmax,i,j}$, is marked as the one able to maximize the produced power, in reference to the fixed flow rate $Q_i$ and the selected *j-th* pump model (Fig. 4.54);

10. if $P_{t,i,j}^{z=1} = P_{t\max,i,j}$, the fixed rotational speed $N_i^{z=1} = N_{\max}$ represents the $N^*_{i,j}$ able to maximize the produced power $P_{t,i,j}$; else, being $P_{t\max,i,j}(N)$ a monotonic increasing function (Eqs. 4.7, 4.11 and 4.13) and having initialized the procedure for $N_{i,j}^{z=1} = N_{\max}$, the $N_{i,j}^{z+1}$ is reduced at the next iteration;
11. if $N^*_{i,j} \geq N_{\max}$ or $N^*_{i,j} \leq N_{\min}$, then the $N_{\max}$ or $N_{\min}$ values are set, respectively, in order to maximize the power $P_{t,i,j}$ obtainable in the allowable range of rotational speeds $N$. Conversely, for $N_{\min} < N^*_{i,j} < N_{\max}$, the $\phi_i^{z+1}$ is calculated, as a function of $N^*_{i,j}$;
12. being valid the second condition at Step 11, the head number $\psi_{i,j}^{z+1}$ is derived and the related head drop $H_{t,i,j}^{z+1}$ estimated, by applying the Eq. (4.17) or the Eq. (4.19) for HA PATs and VA PATs, respectively;
13. being the $H_{ti,j}(N)$ not a monotonically increasing function for both HA and VA PATs (Fig. 4.21, Fig. 4.35 and Fig. 4.40), if $H_{t,i,j}^{z+1} > H_{t,av,i}$, the rotational speed $N_i^{z+2}$ is decreased again. Conversely, for $H_{t,i,j}^{z+1} \leq H_{t,av,i}$, the power number $\pi_{i,j}^{z+1}$ is assessed through the Eqs. (4.18) and (4.20) and the related $P_{t,i,j}^{z+1}$ estimated, by iterating the Steps 7-12 up to achieve the equivalence $P_{ti,j}^{z} = P_{t\max,i,j}^{z}$;
14. Once calculated the $N^*_{i,j}$ able to determine $P_{ti,j}^{z} = P_{t\max,i,j}^{z}$, the Eq. (4.1) is applied to estimate the overall PAT efficiency $\eta_{ti,j}$; if $\eta_{,i,j} \geq \overline{\eta_t}$ (fixed minimum threshold of allowable efficiency for PAT operations), the next *i+1-th* time step is considered, else the PAT model is rejected;
15. by iterating the abovementioned Steps 5-14 for each *i-th* time step, the maximum daily energy $E_{d,j}$, producible by the *j-th* pump model, is evaluated as:

$$E_{d,j} = \sum_{i=1}^{N^*} P_{t\max i,j} \cdot \Delta t_i \tag{4.21}$$

being $N^*$ the number of time steps and $\Delta t_i$ the time step duration;

16. by repeating the Steps 1-15 for each available *j-th* pump model, the selection is assessed in reference to the pump model able to maximize the Eq. (4.21).

In the following Fig. 4.55, the flow chart of the overall selection procedure is reported, in reference to a generic *j-th* pump model.

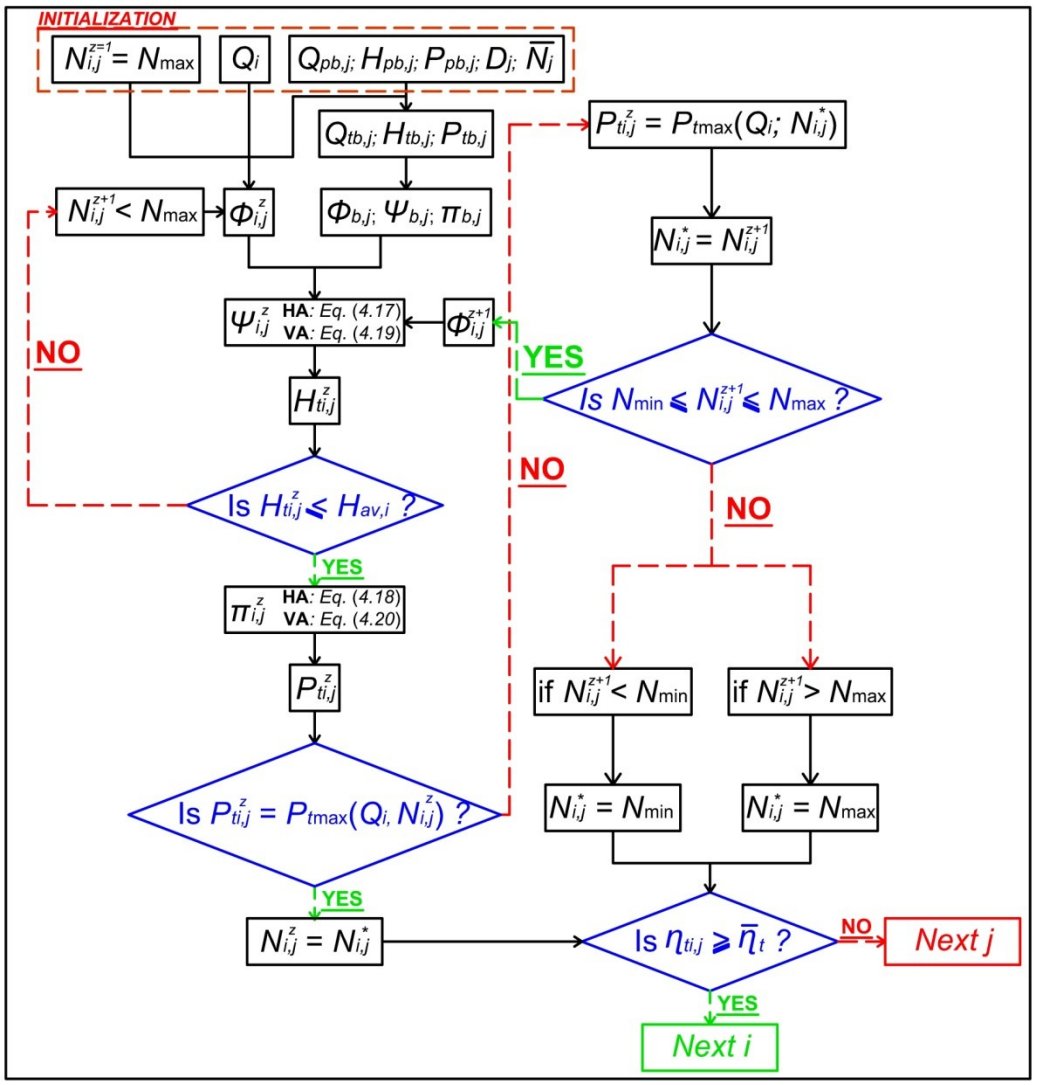


**Fig. 4.55 Flow chart of procedure for PAT selection in WDNs**

## References


- Abernethy R.B., Powell B.D., Colbert D.L., Sanders D.G., Thompson Jr. J.W. (1973). Handbook uncertainty in gas turbine measurements, USAF AEDC-TR, 73-75.
- Alatorre-Frenk C., Thomas T.H. (1990). The pumps as turbines approach to small hydropower. *World Congress on Renewable Energy* (reading).
- Amelio M., Barbarelli S., Scornaienchi N.M. (2000). Caratterizzazione al banco prova di pompe centrifughe utilizzate come turbine. *Proceedings of 55th National Congress ATI*, Bari and Potenza, Italy, 2000 (in Italian).
- Childs S.M. (1962). Convert pumps to turbine and recover HP. In: Hydrocarbon Processing and Petroleum Rejner, 41(10), 173-174.
- Dannier A., Del Pizzo A., Giugni M., Fontana N., Marini G., Proto D. (2015). Efficiency evaluation of a micro-generation system for energy recovery in water distribution networks. *Proceedings of the 5th International Conference on Clean Electrical Power. Renewable Energy Resources Impact ICCEP15*, 16th-18th June 2015, Taormina, Italy, http://dx.doi.org/10.1109/ICCEP.2015.7177566
- Derakhshan S., Nourbakhsh A. (2008a). Experimental study of characteristic curves of centrifugal pumps working as turbines in different specific speeds. *Experimental Thermal and Fluid Science*, 32, 800-807. http://dx.doi.org/10.1016/j.expthermflusci.2007.10.004
- Fernandez J., Blanco E., Parrondo J., Stickland M.T., Scanlon T.J. (2004). Performance of a centrifugal pump running in inverse mode. P*roceedings of the Institution of Mechanical Engineers, Part a: Journal of Power and Energy*, 218(4), 265-271. http://dx.doi.org/10.1243/095765004120063
- Fontana N., Giugni M., Glielmo L., Marini G. (2016). Real time control of a prototype for pressure regulation and energy production in water distribution networks. *Journal of Water Resources Planning and Management*, 142(7), 04016015, 1-9. http://dx.doi.org/10.1061/(ASCE)WR.1943-5452.0000651
- Grover K.M. (1980). Conversion of Pumps to Turbines. GSA Inter Corp, Katonah, New York, USA.
- Hancock J.W. (1963). Centrifugal pump or water turbine. *Pipe Line News*, 25-27.
- Hergt P. (1982). The influence of the volute casing on the position of the best efficiency point. *Proceedings of the 11th IAHR Symposium*, Amsterdam, Holland, 3, 69.
- International Electrotechnical Commission, IEC 60034, Int. Stand. 2008, 30.
- International Electrotechnical Commission, IEC 60034, Int. Stand. 2014, 30(1).
- Joshi S., Gordon A., Holloway L., Chang L. (2005b). Selecting a high specific speed pump for low head hydro-electric power generation. *Canadian Conference on Electrical and Computer Engineering*. http://dx.doi.org/10.1109/CCECE.2005.1557003
- Moffat R.J. (1982). Contributions to the theory of single-sample uncertainty analysis. *Journal of Fluid Engineering ASME*, 104, 250-260.
- Nautiyal H., Varun, Kumar A., Yadav S. (2011). Experimental investigation of centrifugal pump working as turbine for small hydropower systems. *Energy Science and Technology*, 1(1), 79-86.

- Pugliese F., De Paola F., Fontana N., Giugni M., Marini G. (2016). Experimental characterization of two Pumps As Turbines for hydropower generation. *Renewable Energy*, 99, 180-187. http://dx.doi.org/10.1016/j.renene.2016.06.051
- Schmiedl E. (1988). Serien-Kreiselpumpen im Turbinenbetrieb. *Pumpentagung Karlsruhe*, A6 (in German).
- Sharma K.R. (1985). Small Hydroelectric Project-use of Centrifugal Pumps as Turbines, Kirloskar Electric Co, Bangalore, India.
- Stepanoff A.J. (1957). Centrifugal and Axial Flow Pumps, 2nd ed., John Wiley & Sons, Inc, New York, USA, 276.
- Tan X., Engeda A. (2016). Performance of centrifugal pumps running in reverse as turbine: Part II – systematic specific speed and specific diameter based performance prediction. *Renewable Energy*, 99, 188-197. http://dx.doi.org/10.1016/j.renene.2016.06.052
- Yang S-S., Derakhshan S., Kong F-Y. (2012a). Theoretical, numerical and experimental prediction of pump as turbine performance. *Renewable Energy*, 48, 507-513. http://dx.doi.org/10.1016/j.renene.2012.06.002

# Chapter 5

# CFD Investigation of Centrifugal Pumps As Turbines

In this Chapter 5 the procedure to implement a Computational Fluid Dynamics model of a centrifugal PAT is introduced. In greater detail, the modelling application was developed during the experience, as visiting Ph.D. student, spent at the Department of Energy of the University of Oviedo (ES) in Gijón Campus. The analysis was focused on the numerical reproduction of the HA SS PAT (model LOWARA FH80-200) experimentally tested at the Hydraulic Laboratory of the University of Naples (IT) Federico II (Par. 4.4).

The modelling procedure provided, as first step, the acquisition of the geometric configuration of the tested turbo-machine, in order to accurately reproduce the internal pattern of the considered device (Silva et al., 2010).

The second step was focused on the extraction of the fluid domain related to the available geometry and its refinement for simulations. Hence, the mesh generation was developed, by analysing, through a sensitivity analysis, the most suitable resolution, intended as the right balance between the results reliability and the computational time-consuming. Following step was directed to the simulation setting, by properly choosing the turbulence model, the boundary conditions and the applied solution methods for simulations.

Thus, simulations were performed, aiming at reproducing the internal fluid dynamics field of the tested device, in order to analyse the computational results and to compare them with the performed experimental tests, discussed in Par. 4.4.

The attention was specifically drawn to the possibility of overcoming one of the most critical issue of many CFD models for PATs, available in the literature, based on approximate geometric configurations of the tested turbo-machines. During this Ph.D. work, the accurate definition of the internal asset of the tested PAT, combined with the analysis of wide operative conditions (in terms of both flow rates and rotational speeds), brought to implement a CFD model applicable to vast Horizontal Axis Single-Stage centrifugal PATs operating in similitude.

## 5.1 Modelling of the HA SS PAT

The first step of modelling regarded the geometric reproduction of the tested HA SS PAT. In this regard, in order to accurately reproduce the internal geometry, a 3D scanning procedure was performed on the tested turbo-machine; the final 3D geometric configuration was used, provided by the Department of Industrial Engineering of the University of Naples (IT) Federico II (Buono et al., 2015; Frosina et al., 2017).

In Tab. 5.1, the specific geometric characteristics of the HA SS PAT (model LOWARA FH80-200 IE2) are summarized and depicted in Fig. 5.1.

| **HA SS PAT** | | |
|---|---|---|
| Impeller Diameter $D$ | [m] | 0.189 |
| Suction Eye Diameter $D_s$ | [m] | 0.100 |
| Volute Outlet Diameter $D_o$ | [m] | 0.080 |
| Volute Height $H_v$ | [m] | 0.415 |
| Volute Width $W_v$ | [m] | 0.345 |
| Number of Blades | [-] | 6 |

**Tab. 5.1 Geometric properties of modelled HA SS PAT**

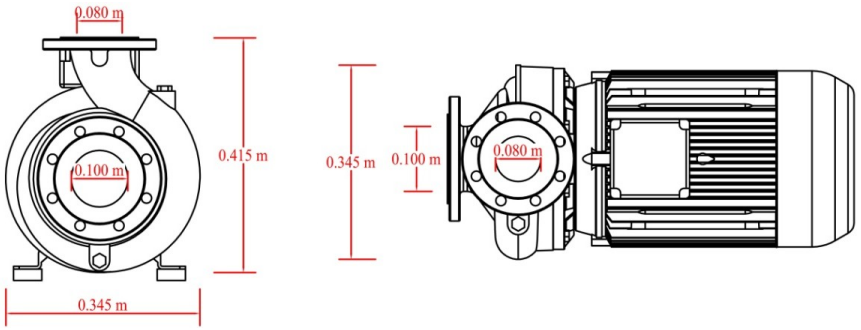


**Fig. 5.1 HA SS PAT geometric characteristics (www.xylemwatersolutions.com)**

## 5.2 3D Model and Meshing Generation of the HA SS PAT

The geometric model, generated by the 3D scanning procedure, was composed of the following main components: impeller, volute and shaft. In Fig. 5.2a-c and Fig. 5.3a-c the final impeller and volute geometric configurations are pictured, respectively.

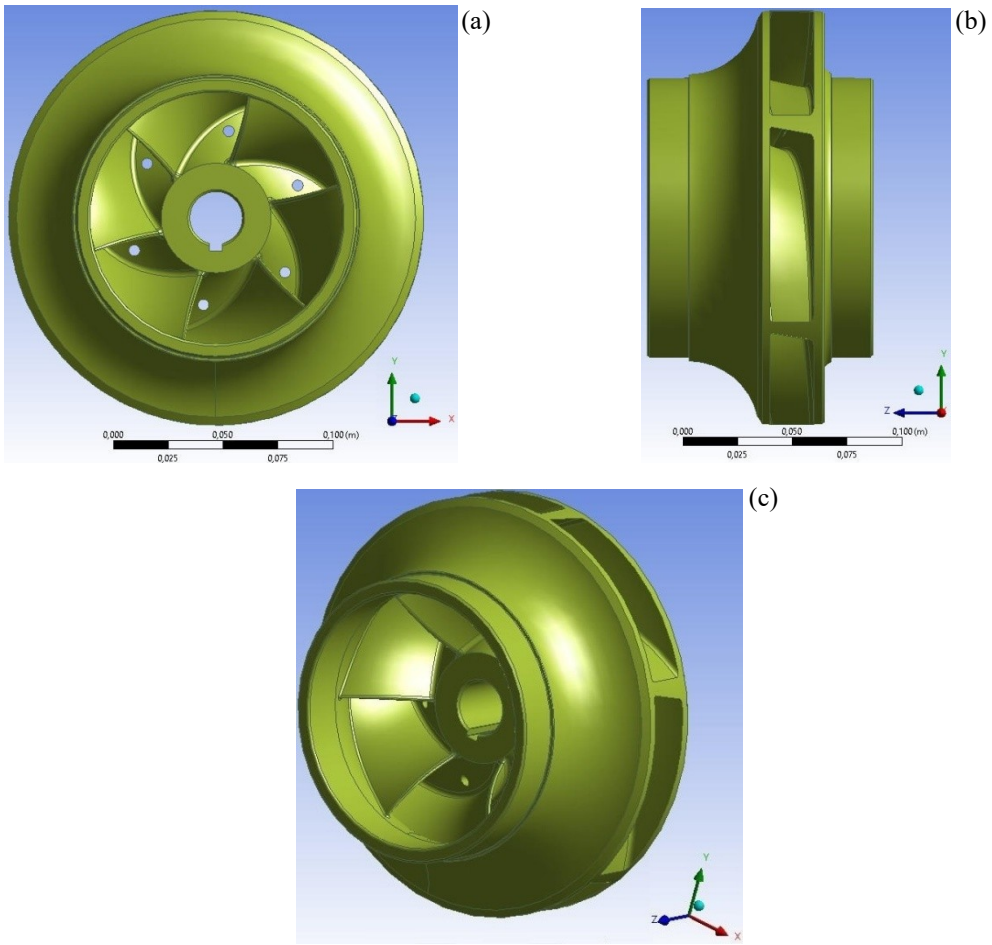


**Fig. 5.2 3D geometric reproduction of the HA SS PAT impeller: (a) front view, (b) side view and (c) isometric view**

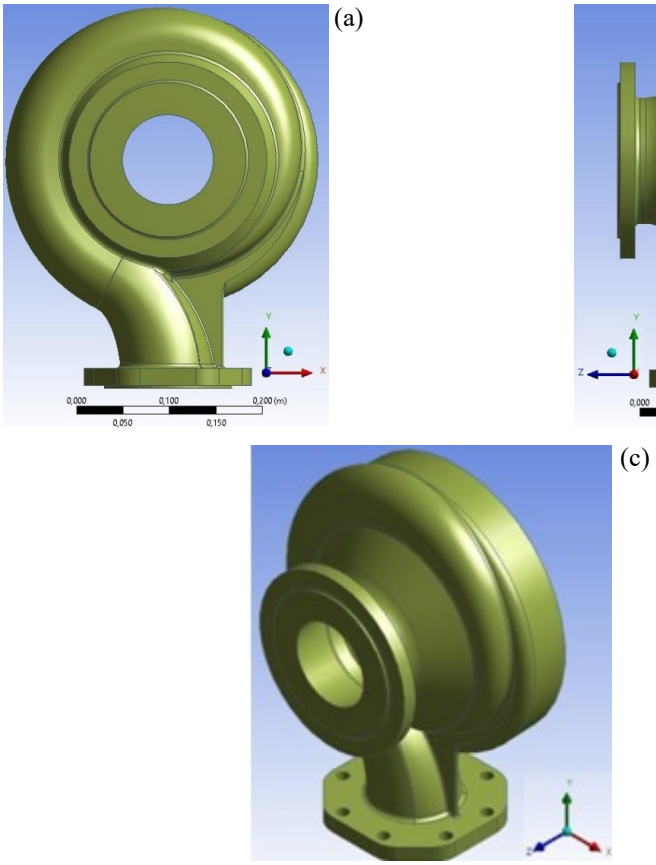


**Fig. 5.3 3D geometric reproduction of the HA SS PAT volute: (a) front view, (b) side view and (c) isometric view**

Thus, the assembled geometric configuration, considered for the extraction of the fluid domain, is depicted in Fig. 5.4a-b.

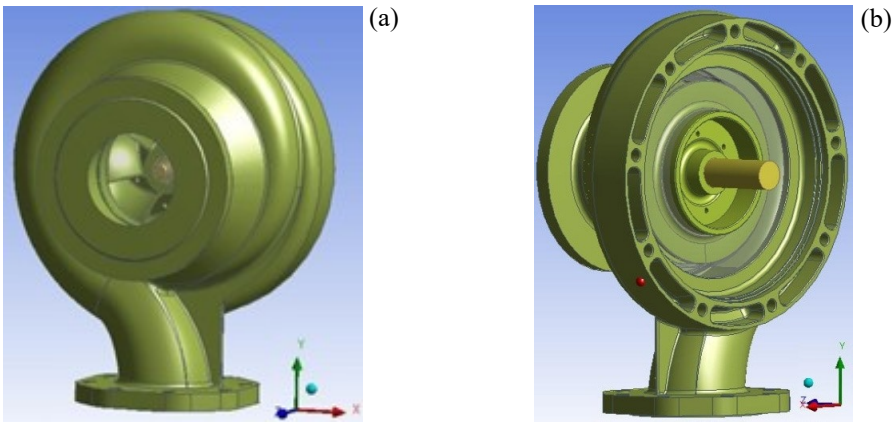


**Fig. 5.4 3D assembled geometric reproduction of the HA SS PAT: (a) front view, (b) back view**

Starting from the HA SS PAT geometric model, the fluid domain was extracted by using the ANSYS® DesignModeler™ tool. In compliance with Natanasabapathi and Kshirsagar (2004) and Fernandez et al. (2010) approaches, in order to improve the fluid motion on the contact zones between impeller and volute, two rings were merged into the impeller and the volute, respectively. These had same thickness, equal to half of the distance between volute and impeller, measured along the radial direction at the tongue vertex (equal to 0.01 m). Further secondary modifications to the fluid domain were also applied, by obtaining the final configuration of the impeller and volute fluid domains, as represented in the following Fig. 5.5a-d and Fig. 5.6a-d, respectively.

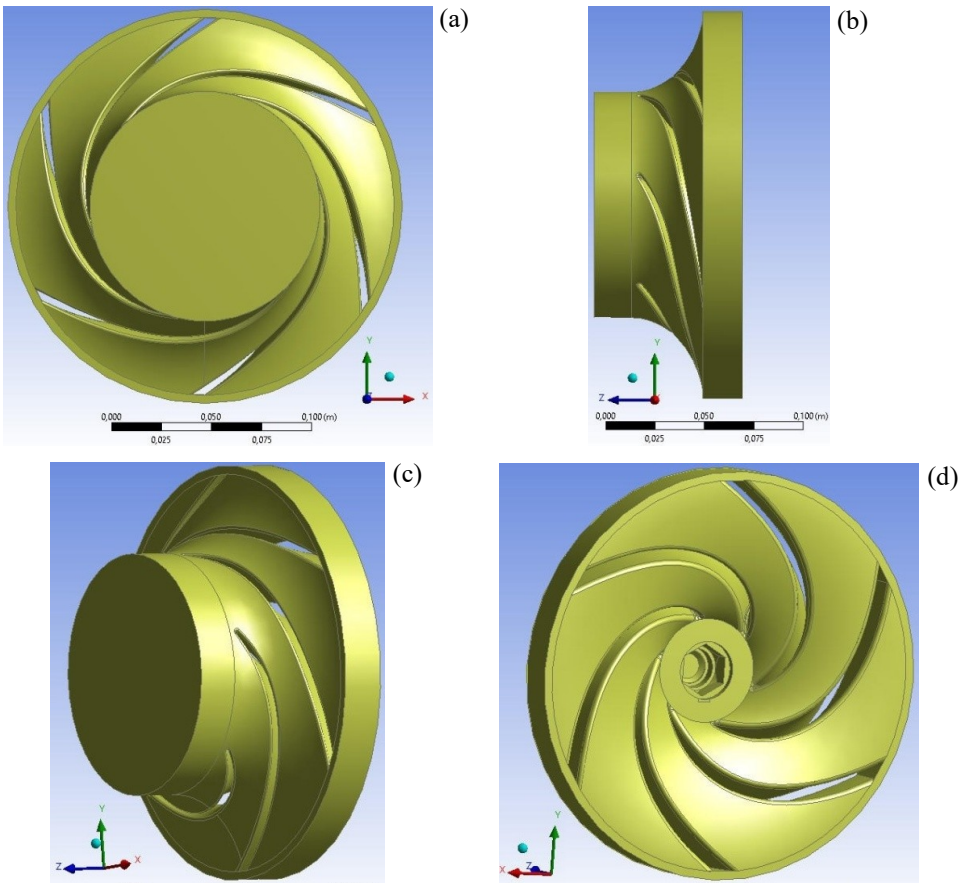


**Fig. 5.5 3D geometric reproduction of the HA SS PAT impeller fluid domain: (a) front view, (b) side view, (c) front rotate view and (d) back rotate view**

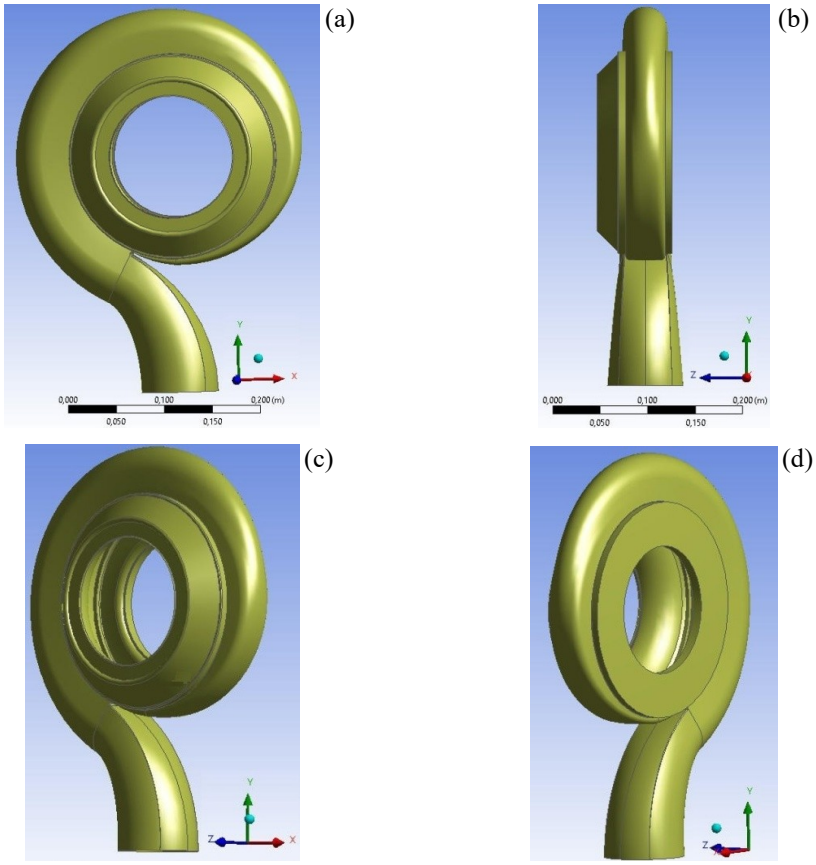


**Fig. 5.6 3D geometric reproduction of the HA SS PAT volute fluid domain: (a) front view, (b) side view, (c) front rotate view and (d) back rotate view**

In order to properly set the boundary conditions at inlet and outlet, two cylindrical pipes were added, having diameter equal to the suction eye $D_s$ and the volute outlet $D_o$, respectively. The height was set equal to four times the related diameter to reduce possible backflow, instead. In the following Fig. 5.7a-b the assembled geometric representation of the modelled fluid domain is depicted, including the abovementioned inlet and outlet pipes.

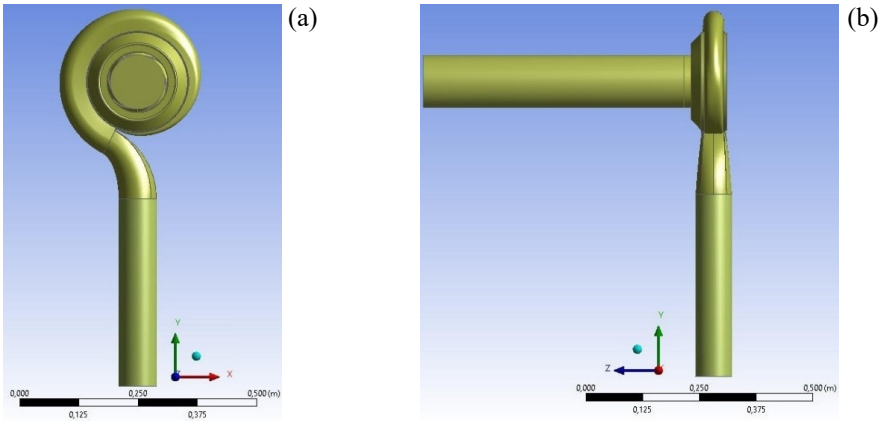


**Fig. 5.7 3D assembled geometric configuration of the HA SS PAT volute fluid domain: (a) front view and (b) side view**

The following step provided the mesh generation, performed by using the ANSYS® ICEM CFD™ tool. Specific mesh settings were set for each fluid domain component. Specifically, in reference to the inlet and outlet pipes, a structured hexahedral mesh was taken into account, whereas, as a consequence of their complex geometry, an unstructured tetrahedral mesh was accounted for the impeller and the volute meshing.

In compliance with both Fernandez et al. (2010) and Morros et al. (2011), a mesh refinement was also set for the volute region surrounding the tongue, with the aim of better reproducing the velocity and pressure fields in the fluid passage between the volute and the impeller. Thus, a spherical region having radius of 0.04 m was individuated to apply the mesh refinement, as depicted in Fig. 5.8a,b. Further refinements were also set on both the blade surfaces and the interfaces between the four elements which composed the assembled fluid domain, aiming at improving the mesh regularity and connection around the edges.

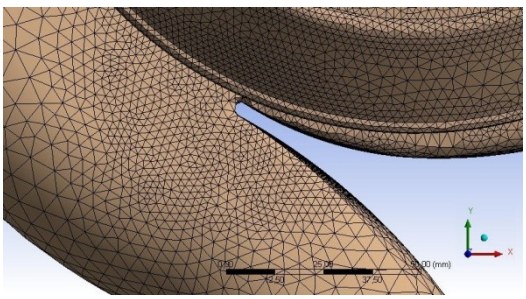

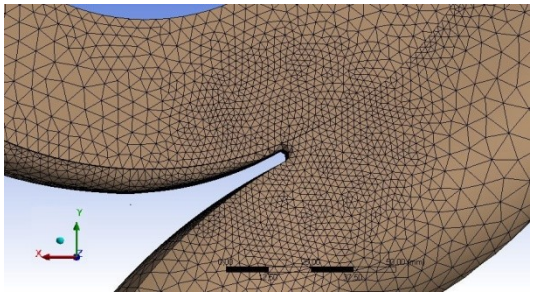
(b)

**Fig. 5.8 Mesh refinement of volute tongue: (a) front view and (b) side view**

A sensitivity analysis was performed, in order to establish the mesh resolution able to return allowable results in tolerable computational times. Simulations were performed by using an Intel i5-4200M CPU at 2.50GHz with 16 GB RAM. Three levels of mesh resolution were evaluated, by varying the number of elements for the impeller and volute domains. In greater detail, the sizing parameters were varied as summarized in Tab. 5.2.

| Resolution Level | Side Min Size [$\cdot 10^{-3}$ m] | Face Max Size [$\cdot 10^{-3}$ m] | Side Max Size [$\cdot 10^{-3}$ m] |
|---|---|---|---|
| Low | 4.0 | 30 | 100 |
| Medium | 2.0 | 15 | 50 |
| High | 1.5 | 10 | 25 |

**Tab. 5.2 Sizing settings for considered mesh resolution levels**

According to the above indicated settings, the number of elements for inlet and outlet pipes remained almost constant at varying the resolution level, whereas those for the impeller and volute fluid domains significantly increased, as summarized in the following Tab. 5.3.

| Resolution Level | Impeller [-] | Volute [-] | Inlet Pipe [-] | Outlet Pipe [-] | Total [-] |
|---|---|---|---|---|---|
| **Low** | 96023 | 488654 | 12654 | 12470 | **609801** |
| **Medium** | 240094 | 657973 | 12654 | 11426 | **922147** |
| **High** | 452911 | 1083355 | 10659 | 14094 | **1561019** |

**Tab. 5.3 Number of model elements for each mesh resolution level**

The sensitivity analysis brought to account for simulations the medium resolution level, because able to represent a right balance between the accuracy of results and the computational time-consuming. Indeed, high resolution level was able to define better correlations between experimental data and simulated ones, requiring, on the other

hand, computational times strongly longer than those spent by using the medium resolution level. In the following Tab. 5.4, the average relative scatters between experimental and numerical results (estimated in terms of static pressure at inlet section) and the average computational time efforts are reported, obtained for the BEP conditions at rotational speeds $N$ = 1200, 2100 and 2910 rpm, by performing the unsteady-state simulation mode (Par. 5.3).

| **Resolution Level** | **Experimental-Numerical Scatter [%]** | **Computational Time [hh:mm]** |
|---|---|---|
| Low | 23.1 | 10:36 |
| Medium | 9.2 | 28:24 |
| High | 5.7 | 96:47 |

**Tab. 5.4 Scatters and computational times for considered mesh resolution levels**

The definitive mesh from medium resolution level, applied for simulations, is depicted in the following figures, referring to the impeller (Fig. 5.9a,b), the volute (Fig. 5.10a,b), the inlet pipe (Fig. 5.11a), the outlet pipe (Fig. 5.11b) and the assembled fluid domain model (Fig. 5.12a,b).

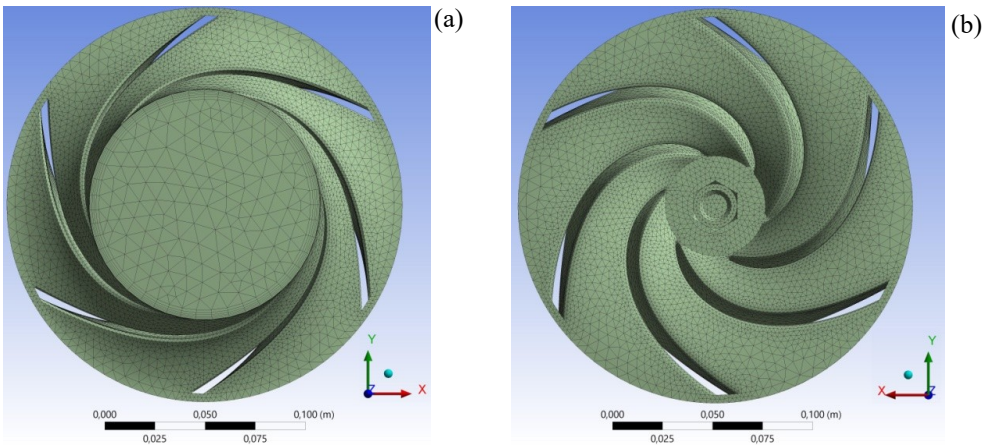


**Fig. 5.9 Mesh of the HA SS PAT impeller fluid domain: (a) front view and (b) back view**

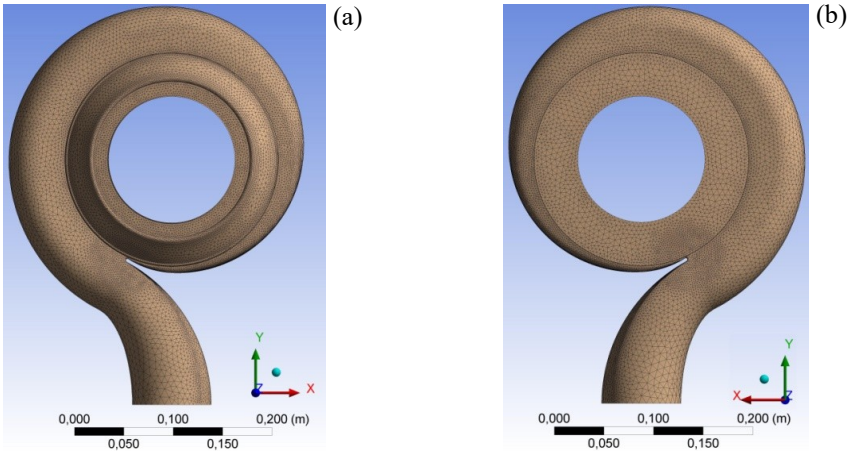


**Fig. 5.10 Mesh of the HA SS PAT volute fluid domain: (a) front view and (b) back view**

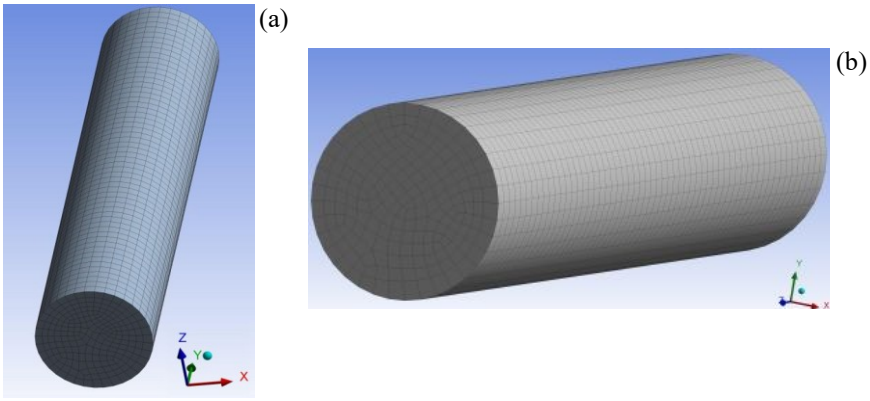


**Fig. 5.11 Mesh of the HA SS PAT fluid domain: (a) inlet and (b) outlet pipes**

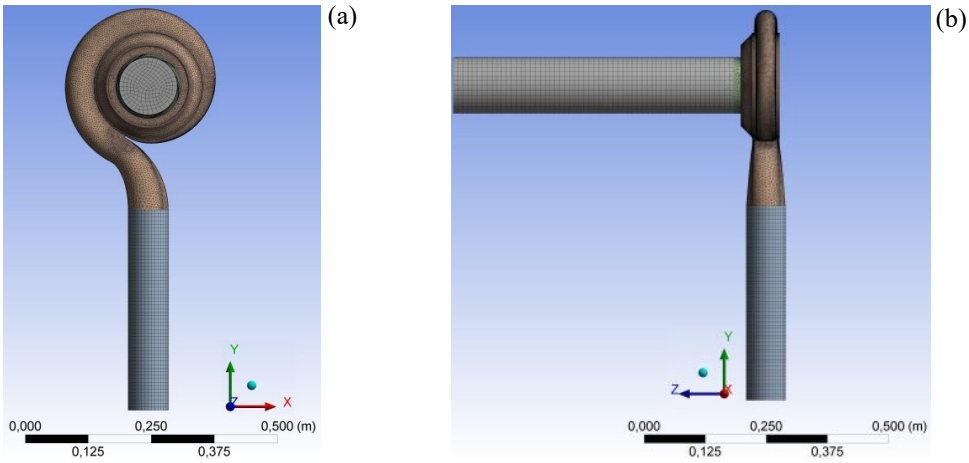


**Fig. 5.12 Mesh of the HA SS PAT fluid domain: (a) front view and (b) side view**

## 5.3 CFD Simulations of the HA SS PAT with ANSYS® Fluent™ Code

Simulations were performed by using the ANSYS® Fluent™ code (ANSYS, 2014). The Standard *k-ε* turbulence model (Par. 3.3.4) was selected among the settable turbulence models, and standard wall functions were applied for the near-wall treatment. The choice was due to the Standard *k-ε* model capability of providing comparable results with both the RNG *k-ε* and the Realizable *k-ε* models, guaranteeing shorter computational times.

Due to the significant complexity of the simulated model, a curvature correction was also introduced, useful to overcome the limitation of the *k-ε* turbulence model to be insensitive to the streamline curvature.

The Semi-Implicit Method for Pressure-Linked Equations (SIMPLE) algorithm was selected to characterize the linear dependence between velocity and pressure, established by the RANS equations (Par. 3.3.4). This model was based upon the application, for the iterative procedure to reach the convergence, of an approximation of the velocity field to solve the momentum equation. The pressure gradient term was computed as a function of the pressure distribution of the previous iteration, starting from which the pressure equation was explicated and solved to define the updated pressure distribution. The choice was addressed to the SIMPLE algorithm because able to overcome the limitations related to the use of the Semi-Implicit Method for Pressure-Linked Equations Consistent (SIMPLEC), due to the increased under-relaxation, which this last can potentially determine.

Moreover, second-order upwind spatial discretizations were used to solve the hyperbolic partial differential equations, coupled with high order terms relaxation, in order to reduce the probability of stalling and instability during the convergence procedure.

Being the model composed of four separated fluid solids (inlet, volute, impeller and outlet), three planar interfaces were inserted to generate the interaction between inlet-volute, volute-impeller and impeller-outlet, respectively.

For the definition of boundary conditions, the criterion followed during the experimental tests was considered, based upon the estimation of the head drop,

generated by the PAT, as a function of a set flow rate value. Thus, a uniform velocity distribution at inlet and a static pressure at outlet were respectively set, in compliance with Fernandez et al. (2010) approach. As stated in Par. 3.3.4, the consideration of the velocity and the pressure boundary condtions at inlet and outlet was also useful to facilitate the model convergence.

In greater detail, for each simulation, the velocity magnitude was set at inlet surface and a relative static pressure equal to 101325 Pa was set at outlet, in order to evaluate the head drop $H_t$ generated by the PAT as difference between the inlet and outlet pressure.

Simulations were performed according to two approaches working in series:

- *Steady-state calculations*, carried out by using the Moving Reference Frame (MRF) approach with a frozen-rotor interface, based upon the definition of the impeller-volute interaction for a given angular position of the impeller;
- *Unsteady-state calculations*, performed once the convergence of the steady-state approach was reached, by using results from the steady-state simulation, in terms of velocity and pressure fields, as initial conditions for the unsteady-state ones. In this case, the Sliding Mesh (SM) technique was applied to account for the relative motion between impeller and volute. The duration of a single time step was assessed, for each rotational speed $N$, so that a complete impeller revolution was performed in 150 time steps.

The generated power was evaluated through an integrative process of the instantaneous pressure and shear stress distribution on the blade walls, in order to estimate the generated torque $T$ acting on the impeller. The produced power $P_t^*$ (neglecting the volumetric and disc friction losses) was calculated by the product of the torque $T$ and the angular velocity $\omega$:

$$P_t^* = \omega T \tag{5.1}$$

Thus, the PAT hydraulic efficiency $\eta_{ht*}$ was estimated as:

$$\eta_{ht^*} = \frac{P_t^*}{\gamma_w Q_t H_t} \tag{5.2}$$

The power $P_t$, considered for experiments in Par. 4.4, being an output data from the frequency modulator (Par. 4.2), took implicitly into account the volumetric efficiency $\eta_{v*}$, the internal efficiency $\eta_{i*}$ and the motor efficiency $\eta_{m*}$ of the tested turbo-machine.

Hence, in order to compare the experimental results with the numerical ones, the numerical produced power $P_t$ was estimated as:

$$P_t = P_t^* \eta_{v*} \eta_{i*} \eta_{m*} \tag{5.3}$$

in which $\eta_{v*}$, $\eta_{i*}$ were evaluated, in compliance with Fernandez et al. (2009), according to the approximate Neumann (1991) model, whereas $\eta_{m*}$ was set equal to 0.98. Therefore, the overall efficiency $\eta_t$ was estimated by using the Eq. (4.1).

Results were analysed in reference to the unsteady-state conditions, by calculating, for each simulation, the mean value of flow variables corresponding to a single blade passage (equal to 25 time-steps), after running at least 5 complete impeller revolutions, necessary to achieve the periodicity of flow variables (Barrio et al., 2010).

As first set of simulations, the model was tested in directed operations, by simulating the turbo-machine behaviour in pump mode. Inlet and outlet pipes and related boundary conditions were inverted with respect to the simulations in PAT mode.

The second set of simulations was devoted to reproduce the reverse mode, instead. In both cases, the implemented numerical model resulted to be highly reliable to represent the internal behaviour of the considered turbo-machine, determining allowable flow fields and pressures with respect to both the simulated operations and the set boundary conditions. Specifically, in pump mode, the numerical consistence of the developed approach was verified by observing the pressure increase from the inlet to the oulet pipes, particularly defining a radial pressure increment across the impeller and the volute. Conversely, in PAT mode, the pressure decrease from the inverted inlet to the outlet was observed, individuating the generated pressure drop across the impeller and the volute. Specifically, particular attention was drawn to the passage between volute and impeller, around the tongue region, referring to which a greater regularity of the velocity field was observed when the pump was running in direct operations. Conversely, in PAT mode, the velocity vectors were strongly influenced by the tongue passage, by determing local head losses. However, this condition was

slightly negligible at BEP operations. For both simulation levels, the numerical consistency was also analysed by verifying the satisfaction of the relevant conservation principles, specifically checking the equality of flow rate at inlet and outlet. Consequently, the mean velocity magnitude at outlet was verified, as a function of the related flow rate.

As an example, in the following Fig. 5.13 the pressure field across both the impeller and the volute is depicted, in reference to the BEP operations at $N$ = 1200 and 1500 rpm, respectively.

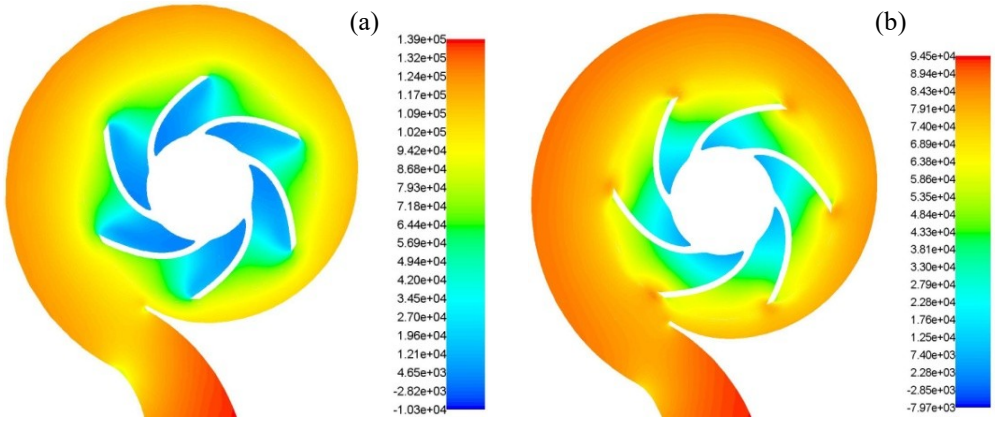


**Fig. 5.13 Pressure field at BEP for (a) $N$ = 1200 rpm and (b) 1500 rpm – PAT mode**

In Fig. 5.14 results, inferred to rotational speed $N$ = 2900 rpm in pump mode, are compared with those from manufacturer's datasheets plotted in Fig. 4.16.

Simulations in pump mode pointed out the good reliability of the developed model for flow rates $Q_p$ up to 50 ls$^{-1}$, by defining scatters not greater than -16%. Specifically, for $Q_p$ between 25 and 40 ls$^{-1}$, differences from +1.5% to -11.5% were observed. For $Q_p$ > 50 ls$^{-1}$, differences up to 35% were assessed, instead. Being the experimental tests, in PAT mode, performed at flow rates $Q_t$ not higher than 50 ls$^{-1}$, the analysis was carried on for PAT operations.

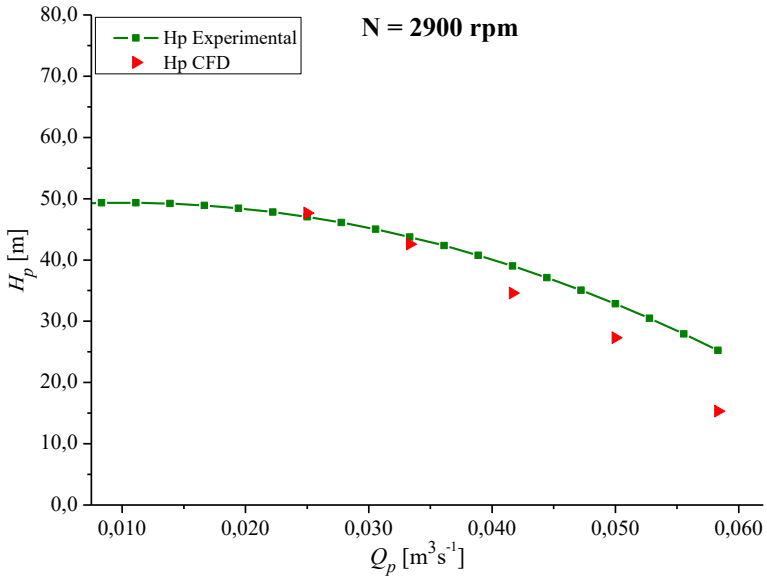


**Fig. 5.14 Experimental-numerical comparison of $H_p(Q_p)$ curve for $N$ = 2900 rpm – Pump mode**

In reference to the PAT mode, comparisons between experimental data and simulated ones are reported in the following Fig. 5.15, Fig. 5.16, Fig. 5.17, Fig. 5.18 and Fig. 5.19 for rotational speeds $N$ = 600, 1200, 1500, 2100 and 2910 rpm, respectively.

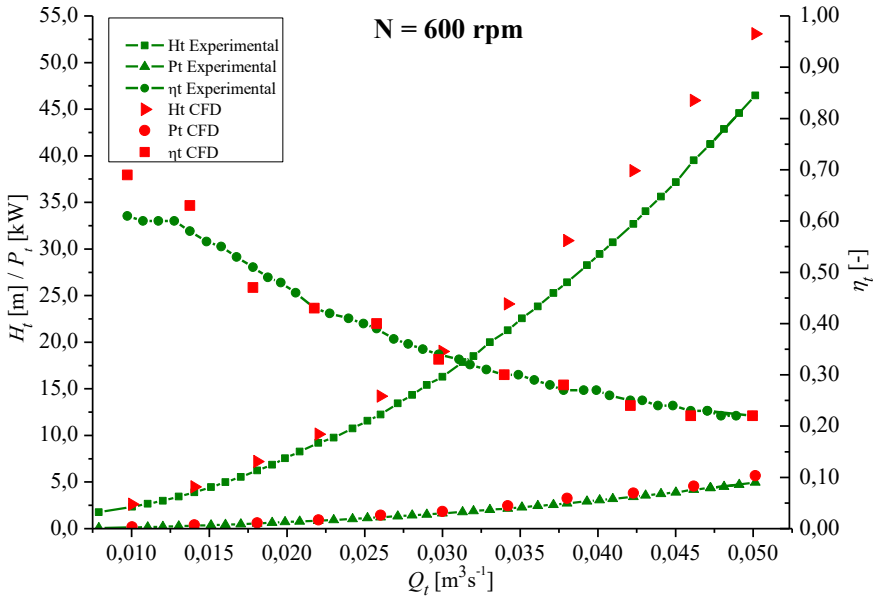


**Fig. 5.15 Experimental-numerical comparison for $H_t(Q_t)$, $P_t(Q_t)$ and $\eta_t(Q_t)$ curves – $N$ = 600 rpm**

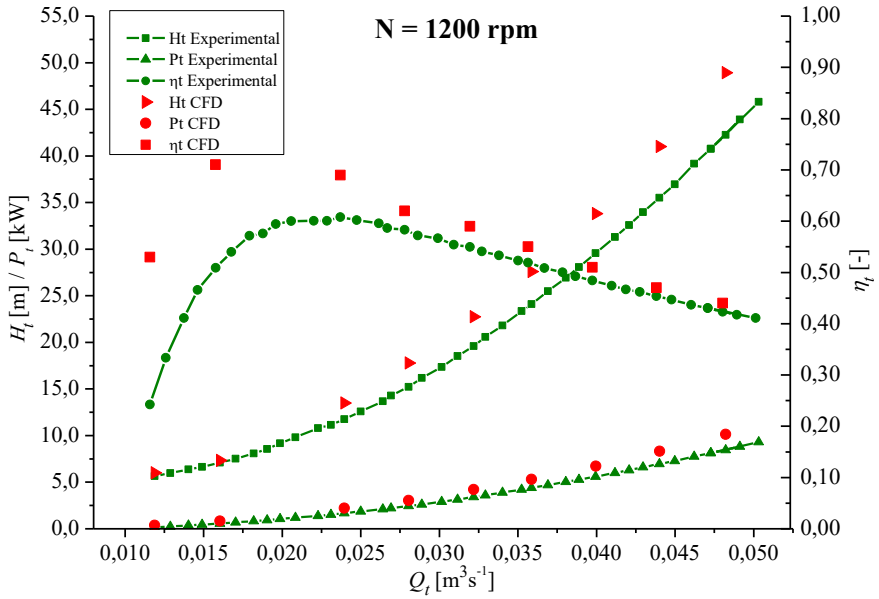


**Fig. 5.16 Experimental-numerical comparison for $H_t(Q_t)$, $P_t(Q_t)$ and $\eta_t(Q_t)$ curves – $N$ = 1200 rpm**

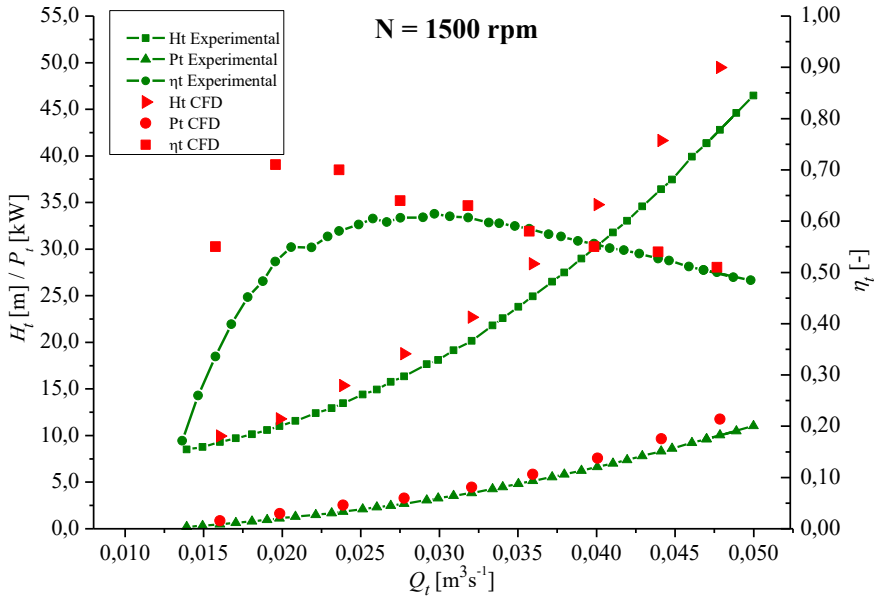


**Fig. 5.17 Experimental-numerical comparison for $H_t(Q_t)$, $P_t(Q_t)$ and $\eta_t(Q_t)$ curves – $N$ = 1500 rpm**

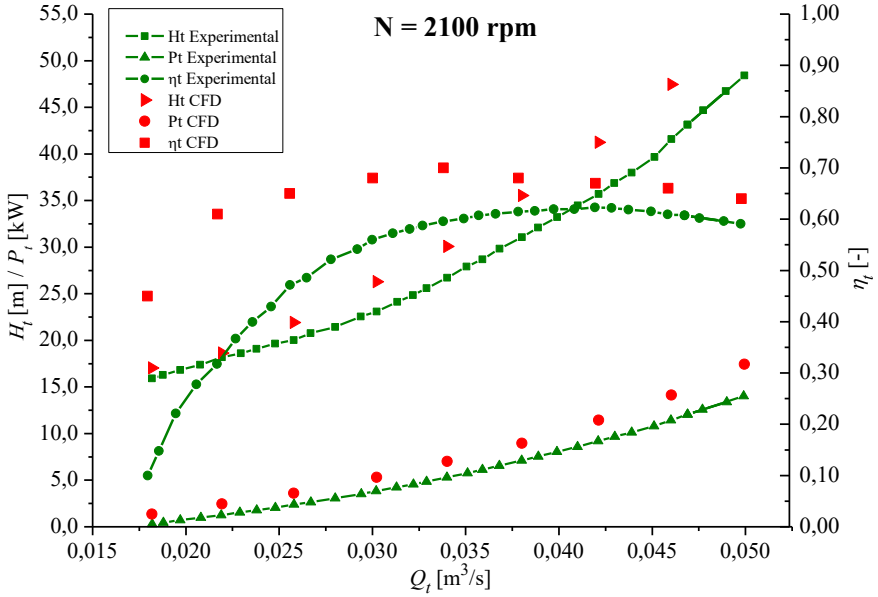


**Fig. 5.18 Experimental-numerical comparison for $H_t(Q_t)$, $P_t(Q_t)$ and $\eta_t(Q_t)$ curves – $N$ = 2100 rpm**

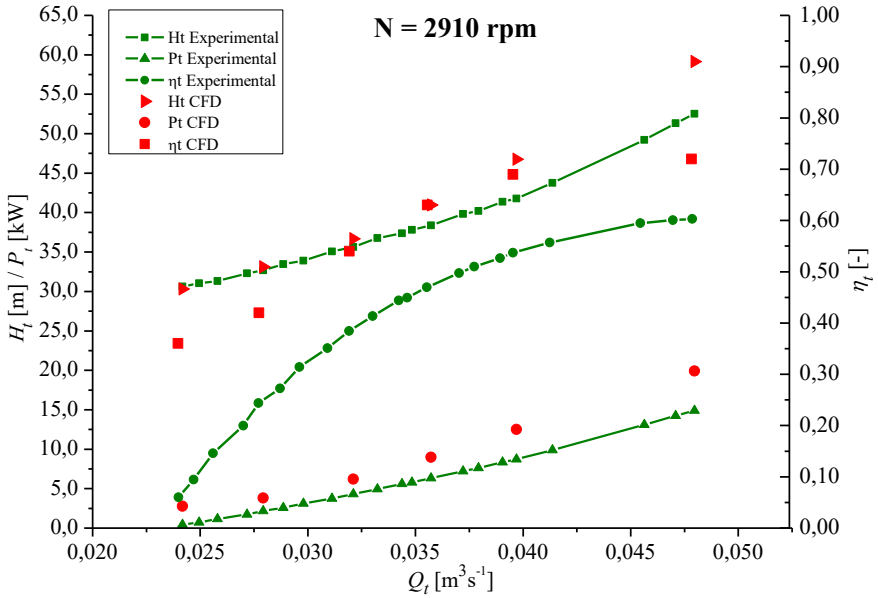


**Fig. 5.19 Experimental-numerical comparison for $H_t(Q_t)$, $P_t(Q_t)$ and $\eta_t(Q_t)$ curves – $N$ = 2910 rpm**

Comparison between experimental and numerical results for the flow rate-head drop $H_t(Q_t)$ correlations, pointed out the good reliability of the implemented CFD model to reproduce the experimental head drops, defining scatters not higher than 16% for the

whole set of considered rotational speed $N$. In greater detail, in reference to flow rates $Q_t \leq 25$ ls$^{-1}$ scatters up to 10% were estimated, whereas higher discrepancies were observed for $Q_t > 25$ ls$^{-1}$, defining slightly constant differences, in the order of 13÷16%. Simulated data always overestimated the experimental ones, thus defining greater head drops. This was symmetrically in accordance with results in pump operations, referring to which the numerical-experimental comparison for predicting the head curve, for flow rates $Q_p \leq 50$ ls$^{-1}$, was not greater than -16%.

Greater discrepancies were observed for the of $P_t(Q_t)$ function, instead. Specifically, for lower flow rates $Q_t$, significant differences were estimated, particularly in reference to experimental powers $P_t$ lower than 1 kW. Indeed, simulations significantly overestimated the shaft power for lower $Q_t$ and rotational speeds $N$, giving back power $P_t$ more than two times higher than the experimental ones. Conversely, for $Q_t > 25$ ls$^{-1}$, scatters of about 20% were assessed for low rotational speeds $N$, and in the order of 35% for higher $N$ values. The observed differences could be ascribed to the neglected frictional losses in the model which overestimated the effective shaft power. Furthermore, an overestimation of motor efficiency $\eta_{m*}$ in PAT mode might have committed.

In terms of efficiency curve $\eta_t(Q_t)$, due to the significant overestimation of $P_t$ values for lower $Q_t$, great differences were observed in reference to the increasing branch up to BEP, by determining a significant efficiency overestimation. Lower differences were defined for the decreasing branch, instead. Indeed, for lower rotational speeds $N$ (which corresponded to the decreasing efficiency branch for the investigated flow rate range) good correlations were achieved with differences in the order of 15% for the whole analysed flow rate range. The maximum efficiency $\eta_{tb}$ from simulations was equal to 76%, thus resulting to be significantly higher than the experimental value of 61.3%, of about 14.7%.

Experimental-numerical comparisons are plotted in dimensionless terms in the following Fig. 5.20, Fig. 5.21 and Fig. 5.22, in terms of $\psi(\phi)$, $\pi(\phi)$ and $\eta_t(\phi)$ equations, respectively. Eqs. (3.62), (3.63) and (3.64) from Derakhshan and Nourbakhsh (2008a) approach and Eqs. (4.8) and (4.9), proposed in the context of this Ph.D. work, are also

represented, with the aim of comparing the simulated results with the predictive performance equations for centrifugal HA PAT models.

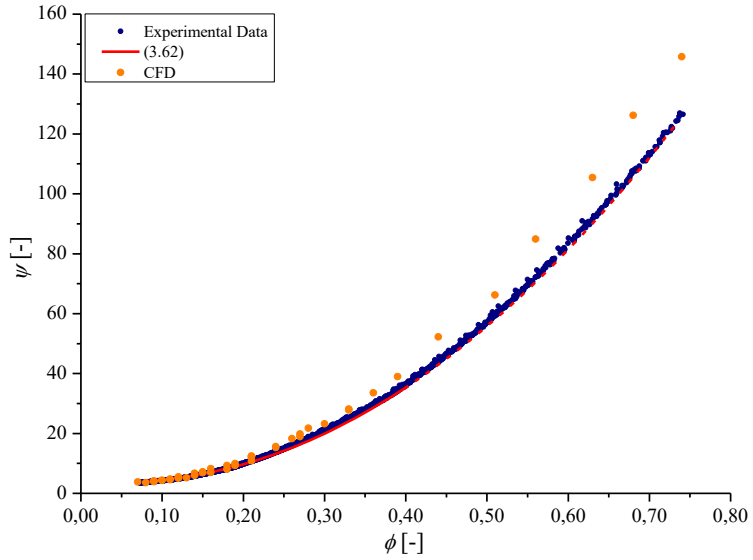


**Fig. 5.20 Experimental-numerical comparison for $\psi(\phi)$ – HA SS PAT**

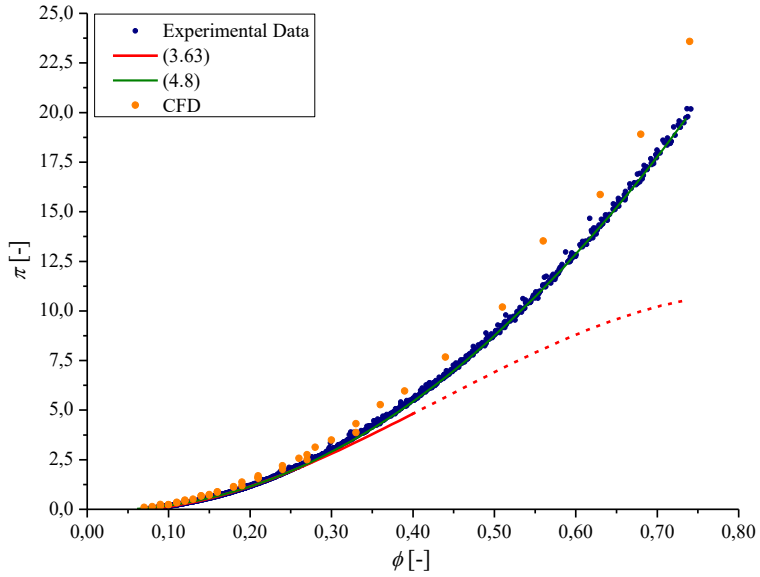


**Fig. 5.21 Experimental-numerical comparison for $\pi(\phi)$ – HA SS PAT**

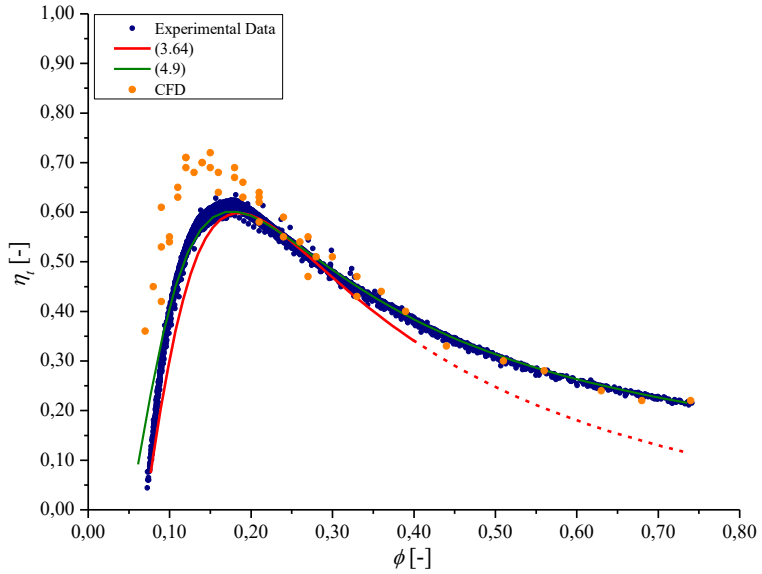


**Fig. 5.22 Experimental-numerical comparison for $\eta_t(\phi)$ – HA SS PAT**

Concerning the $\psi(\phi)$ function (Fig. 5.20), a good correlation of CFD results with the experimental data and the Derakhshan and Nourbakhsh (2008a) Eq. (3.62) was observed for $\phi \leq 0.30$, with scatters not higher than 5%, whereas increasing differences were determined for higher $\phi$. In greater detail, they were estimated in the order of at most 16%, with respect to the experimental data, and of at most 17% with respect to the Derakhshan and Nourbakhsh (2008a) approach.

In terms of $\pi(\phi)$ function (Fig. 5.21), similar considerations to those introduced in Par. 4.4 are applicable, individuating, by performing the CFD simulations, an increasing monotonic trend, in compliance with the proposed Eq. (4.8). The Derakhshan and Nourbakhsh (2008a) Eq. (3.63) was reliable up to the limit defined by the authors of $\phi \leq 0.40$. For higher $\phi$ values, the CFD returned head numbers, in any case, higher than both the experimental ones and those from Eq. (4.9), with relative errors in the order of 20%.

In terms of the efficiency curve $\eta_t(\phi)$ (Fig. 5.22), the overestimation at BEP of simulations was distinctly pointed out, highlighting its reaching for flow rate number $\phi$ = 0.15. It was slightly lower than the experimental determination of $\phi$ = 0.18. Conversely, a significant correlation was observed for high flow rate numbers $\phi$,

reached at low rotational speeds $N$ and thus correspondent to the decreasing branch of the efficiency curve $\eta_t(\phi)$.

The internal velocity fields at BEP, at varying the rotational speed $N$, are plotted in the following Fig. 5.23a-d, relative to the plane containing the impeller centre of gravity and normal to the outlet pipe axis direction.

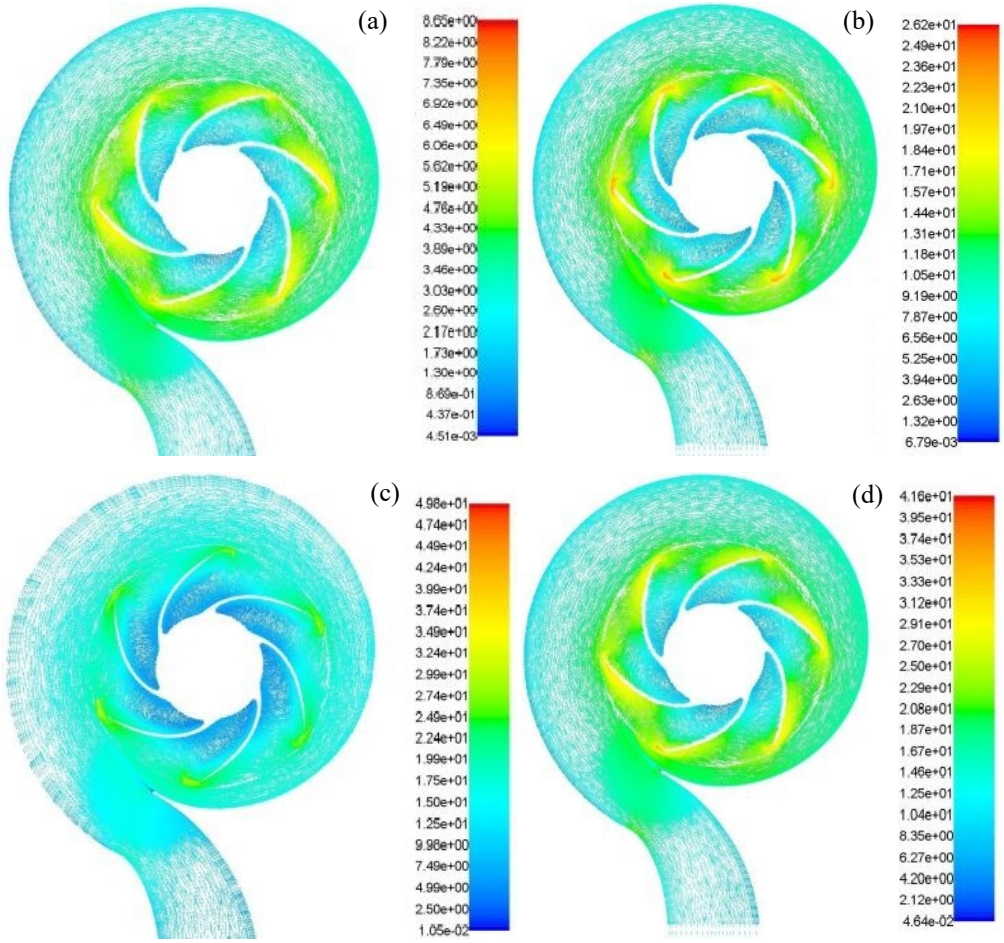


**Fig. 5.23 Velocity field at BEP for $N$ = (a) 600, (b) 1500, (c) 2100 and (d) 2910 rpm**

It was found the significant regularity of flow field across the impeller at BEP in the whole set of simulated $N$ values, showing the decrease of the velocity magnitude from the outer to inner region of the impeller. A greater irregularity of flow field was observed around the trailing edges of blades, resulting to be highly sharpened for lower rotational speeds. Even though, at BEP, it was quite limited, also around the blade near

the volute tongue, pointing out the relative interference in the flow passage from volute to impeller. As shown in Fig. 5.24a-d, the velocity field around the blade near the volute tongue, did not generate secondary flows, limiting the total pressure drop across the impeller, thus assuring higher efficiencies.

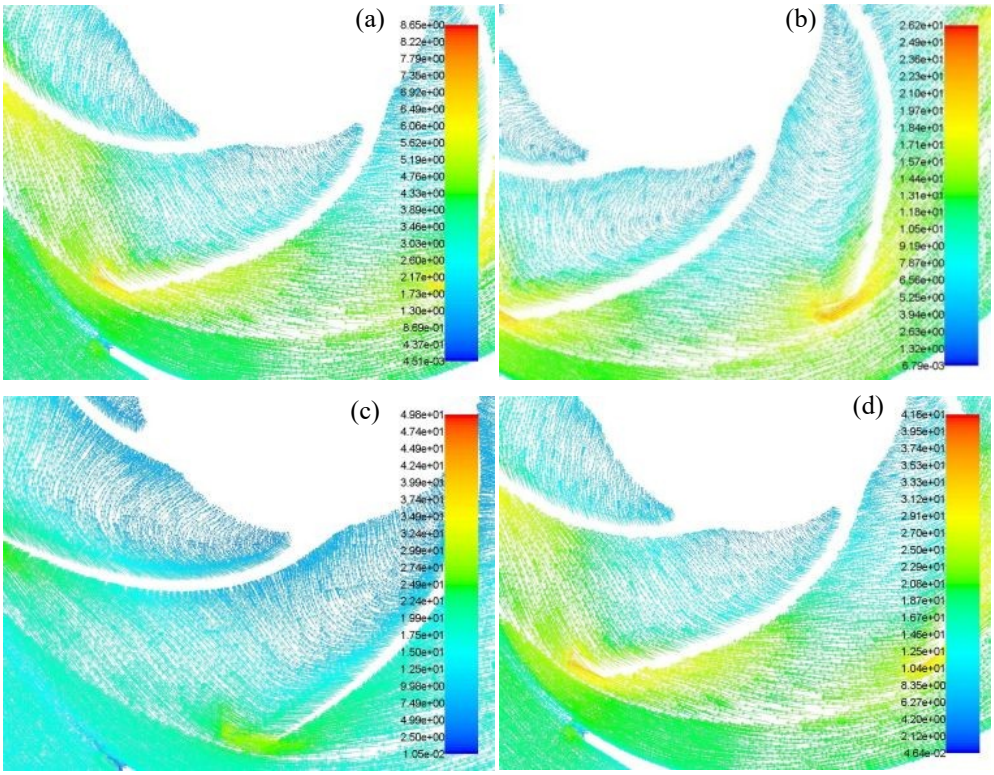


**Fig. 5.24 Velocity field around the blades at BEP for $N$ = (a) 600, (b) 1200, (c) 2100 and (d) 2910 rpm**

For operative conditions far from BEP, the formation of secondary flows was observed, instead, resulting to be highly emphasized for high flow rates $Q_t$ for medium-low rotational speeds $N$. As an example, in the following Fig. 5.25 the formation of secondary flows across the blades is represented, in reference to flow rates $Q_t$ = 38 ls$^{-1}$ and $N$ = 600 rpm and $Q_t$ = 48 ls$^{-1}$ and $N$ = 1500 rpm.

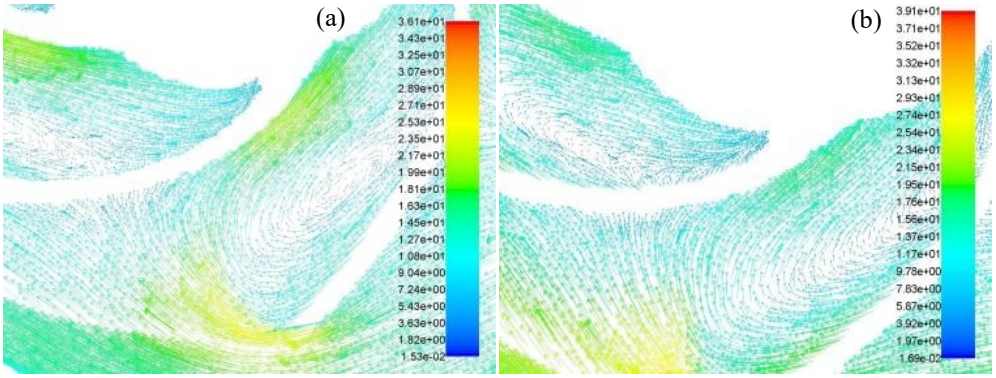


**Fig. 5.25 Velocity field around the blades for (a) $Q_t$ = 38 ls$^{-1}$ – $N$ = 600 rpm; (b) $Q_t$ = 48 ls$^{-1}$ – $N$ = 1500 rpm**

Thus, the performed simulations pointed out the realiability of the developed CFD model to provide effective information about the performances of centrifugl PATs. In greater detail, the consistency of the model was assured during simulations, being it able to effectively reproduce the flow and pressure fields across the turbo-machine, taking into account the interaction between its different physical parts. Low experimental-numerical differences were observed for the estimantion of the generated head drop in the whole set of the considered operative conditions. In adverse, to reproduce the generated power, greater discrepancies were defined, resulting greater at increasing the rotational speed $N$. Thus, this implied significant discrepancies in the definition of the efficiceny curve for high rotational speeds, which correspondend to the increasing branch of the efficiency curve, up to the BEP.

The reliability of the model could be improvable by refining the setting parameters, such as the mesh resolution and the frictional losses estimation. The effective motor efficiency at varying $N$ could also make the experimental-numerical correlation better.

The analysis of the internal fluid fields pointed out greater head losses generated during the PAT simulations than those observed in pump mode, specifically in the passage from the volute to the impeller. For operative conditions far from BEP, this aspect was emphasised across the impeller, as well. From these results, the developed analysis could be intended as a basic step to define the improvement reachable by modifying the geometric characteristics of a pump, with the aim of extending its operative range at high efficiencies when running in reverse mode.

## References


- ANSYS (2014). ANSYS Fluent User's Guide. http://148.204.81.206/Ansys/150/ANSYS%20Fluent%20Users%20Guide.pdf
- Barrio R., Fernandez J., Parrondo J., Blanco E. (2010). Performance prediction of a centrifugal pump working in direct and reverse mode using Computational Fluid Dynamics. *Proceedings of the International Conference on Renewable Energies and Power Quality ICREPQ '10*, 23rd-25th March 2010, Granada, Spain
- Buono D., Frosina E., Mazzone A., Cesaro U., Senatore A. (2015). Study of a Pump As Turbine for a hydraulic urban network using a tridimensional CFD modelling methodology. *Energy Procedia*, 82, 201-208. http://dx.doi.org/10.1016/j.egypro.2015.12.020
- Derakhshan S., Nourbakhsh A. (2008a). Experimental study of characteristic curves of centrifugal pumps working as turbines in different specific speeds. *Experimental Thermal and Fluid Science*, 32, 800-807. http://dx.doi.org/10.1016/j.expthermflusci.2007.10.004
- Fernandez J., Barrio R., Blanco E., Parrondo J., Marcos A. (2009). Experimental and numerical investigation of a centrifugal Pumps working as a Turbines. Proceedings of the *ASME Fluid Engineering Division Summer Conference*, 1(Part A), 471-479. http://dx.doi.org/10.1115/FEDSM2009-78524
- Fernandez J., Barrio R., Blanco E., Parrondo J., Marcos A. (2010). Numerical investigation of a centrifugal pump running in reverse mode. *Proceedings of the Institution of Mechanical Engineers, Part a: Journal of Power and Energy*, 224(3), 373-381. http://dx.doi.org/10.1243/09576509JPE757
- Frosina E., Buono D., Senatore A. (2017). A performance prediction method for Pumps As Turbines (PATs) using a Computational Fluid Dynamics (CFD) modelling approach. *Energies*, 10(103), 1-19. http://dx.doi.org/10.3390/en10010103
- Morros C.S., Fernandez Oro J.M., Arguelles Diaz K.M. (2011). Numerical modelling and flow analysis of a centrifugal pump running as a turbine: Unsteady flow structures and its effects on the global performance. *International Journal for Numerical Methods in Fluids*, 65, 542-562. http://dx.doi.org/10.1002/fld.2201
- Natanasabapathi S.R., Kshirsagar J.T. (2004). Pump As Turbine – An experience with CFX-5.6. Corporate Research and Eng. Division, Kiloskar Bros. Ltd.
- Neumann B. (1991). The interaction between geometry and performance of a centrifugal pump. John Wiley & Sons Inc. Ed., 336.
- Silva F.J., Pascoa J.C., Pinheiro J.S., Martins D.J. (2010). Turbulent flow structure computation inside a pump-PAT using an industrial benchmark test case. *Proceedings of the European Conference on Computational Fluid Dynamics ECCOMAS CFD 2010*, 14th-17th June 2010, Lisbon, Portugal.

# Chapter 6

# Synthesis and Conclusions

This thesis was addressed to the evaluation of PATs performances for hydropower generation in hydraulic systems, drawing specifically attention to their use in WDNs, with the aim of providing operative tools for the optimal PAT selection in WDNs.

As stated in the Chapter 1, this approach is extensively considered as an effective practice in water urban and rural systems for both pressure regulation and hydropower generation in urban areas. Thus, it is included into the field of Proactive Control of WDNs, because devoted to the active regulation of pressure levels acting on the water networks (Chapter 2).

The in-deep literature review in Chapter 3 was useful to individuate the existing lacking points for the performance evaluation of the wide set of centrifugal pump models, available in the commerce, and useful for running in reverse mode. Starting from these evaluations, it was found that, in spite of the availability of many models addressed to the preliminary estimation of the PAT characteristics at BEP, few instruments were able to characterize the PAT characteristic curves, for operative conditions far from BEP. Specifically, the analytic formulations from the literarature resulted to be not exhaustively applicable to wide flow rate ranges and to specific centrifugal PAT geometric configurations.

With the aim of overcoming this limitation, the experimental characterization of a classical centrifugal Single-Stage pump was considered in extensive ranges of both flow rate and rotational speed, aiming at verifying the reliability of the predictive

models available in the literature, to operative fields, typical for WDNs supplying small-medium sized urban and rural areas. Furthermore, the lack of information about the characteristics of further configurations, such as Vertical Axis Single-Stage and Multi-Stage models, brought to focus the interest on these categories, with the aim of testing the reliability of the available predictive approaches on models presenting variable geometric patterns and motor equipment. Hence, in Chapter 4 results of a wide experimental analysis performed at the Department of Civil, Architectural and Environmental Engineering of the University of Naples (IT) Federico II were analysed and discussed. Altogether, about 7400 tests were carried out in a wide set of flow rates (from 8 to 50 $ls^{-1}$) and rotational speeds (from 300 to 3000 rpm). Starting from the achieved results, analytic formulations were proposed, able to characterize the PAT performances for both Horizontal Axis and Vertical Axis centrifugal models. Moreover, an operative procedure for the optimal selection of PATs in WDNs was developed, which could be intended as a basic tool for the optimal PAT selection in urban and rural areas.

A CFD model was also enforced, with the aim of implementing a numerical model to both predict the PAT characteristics and evaluate the internal behaviour of the related flow variables (Chapter 5).

## 6.1 Research Novelty and Contributions

Concerning the developed approach, with respect to the models available in the literature, the experimental analysis was focused on the extension of the investigated fields, in terms of both flow rates and rotational speeds, aiming at characterizing the performance characteristics of several centrifugal PATs. Specifically, in reference to a classic Horizontal Axis Single-Stage PAT, the considered range of flow rate numbers, greater than that analysed in the literature, allowed to derive specific formulations to predict both the power and the efficiency curves, as a function of the operative conditions at BEP. Their applicability results to be greater than other analytic models from the literature.

Moreover, the experimental analysis of Vertical Axis Single-Stage and Multi-Stage PATs is significantly pristine, because very few considerations were performed in the literature on this turbo-machine category. Specifically, the evaluation of the performance dependency from the number of stages and the motor class equipment, was useful to analyse which were the effective advantages, connected to their application. The estimation of the performance benefits for PATs, reachable by using IE3 motor equipments, results to be a novel approach in the field of the PAT selection, defining the effectiveness, related to this motor class, used for pumps working in reverse mode.

Moreover, the proposed analytic formulations for predicting the performances of Vertical Axis PATs represent the unique instrument, specifically dedicated to this category of turbo-machine.

The proposed iterative procedure for the optimal PAT selection in WDNs, based upon the aforementioned results, provides a thorough tool for both technical applications and engineering studies.

Concerning the CFD model, the specific consideration of the PAT geometric characteristics and the model extendibility to wide flow rate and rotational speed ranges, permits to extend its application to a vast set of centrifugal PATs operating in similitude.

In greater detail, the achieved results are summarized as follows:

- in reference to the experimentally tested Single-Stage Horizontal Axis PAT, the reliability of the Affinity Laws to predict the characteristic curves at varying the rotational speed was observed in the whole set of considered operations. Conversely, the Derakhshan and Nourbakhsh model, available in the literature and usually applied to predict the characteristic curves of PATs, is partially applicable outer the range defined by the authors of flow rate numbers up to 0.40. Specifically, for the head drop prediction, it was valid for the whole set of tested operative conditions (flow rate numbers up to 1.50), whereas it failed to predict the generated power for flow rate numbers higher than 0.40. Thus, a new formulation was proposed, to estimate the power curve for centrifugal Horizontal Axis Single-Stage PATs, valid

for significantly wider flow rate operations. Furthermore, a formulation to predict the efficiency curve was derived, as a function of the operative conditions at BEP. From experiments, the efficiency ratio at BEP between PAT and pump operations was of about 75%, thus establishing a significant reduction of the BEP efficiency, with respect to the performances in direct operations. By comparing the experimental results with the theoretical models, available in the literature to predict the flow rate and the head drop ratios at BEP, differences generally not higher than 25÷30% were estimated, defining the overestimation of about 10% for both ratios with the Grover approach. Furthermore, for the power ratio prediction at BEP, the Derakhshan and Nourbakhsh approach resulted to be the most reliable, overestimating the experimental ratio of 7.5%;

- experiments on three Vertical Axis Single-Stage and Multi-Stage PATs showed, also for these models, the reliability of the Affinity Laws for the almost whole set of considered operations, defining remarkable scatters only for low flow rates and high rotational speeds. The Derakhshan and Nourbakhsh model resulted applicable only for flow rates up to 0.40, for both the head drop and the power curves. For higher flow rate numbers, an underestimation of about 25% was assessed for head curve, whereas it completely failed in terms of power estimation. Formulations, derived in the context of this Ph.D. work for Horizontal Axis PATs, showed better correlations in the whole set of investigated flow rates, however defining errors in the order of 20% for the head curve and 30% for the power curve for higher flow rate numbers. Thus, analytic formulations valid for Vertical Axis PATs were provided, able to determine satisfying reliability for both Vertical Axis Single-Stage and Multi-Stage PATs. From experiments, head drops generated by the VA SS model were slightly greater than those for VA MS models (being equal the number of stage). Conversely, the produced power was quite similar for both categories, thus determining lower efficiencies for the VA SS model. Specifically, at BEP, a lower efficiency of about 6% was estimated, presenting, in any case, few differences with respect to the pump operations. Indeed, efficiency ratios between direct and reverse operations were assessed in 0.86 and 0.94 for VA SS and VA MS models,

respectively. Moreover, for the two geometrically equivalent VA MS PATs, performance improvements, correlated to the IE3 Motor Efficiency Class equipment, were observed only at lower rotational speeds (thus for higher flow rate numbers), which resulted to be far from the BEP conditions. Models in the literature to estimate the discharge and head ratios at BEP provided scatters generally lower than 30% also for the Vertical Axis PATs, resulting the Stepanoff, Sharma, Childs and Tan and Engeda formulations the most accurate, with scatters in the range ±11%. Moreover, Derakhshan and Nourbakhsh criterion to predict the power ratio was in agreement with the experimental results only for the VA SS model, whereas differences higher than 20% were observed for the VA MS PATs;

- an original operative procedure was specifically introduced, to select the most suitable PAT in WDNs, under the hypothesis of applying an electrical regulation to modulate the PAT rotational speed. Being available the characteristics at BEP of a set of centrifugal pumps with Horizontal or Vertical Axis configurations, the model which maximizes the overall produced power in the WDN could be selected, in compliance with both allowable operative efficiencies and technical constraints;
- the development of a CFD model to reproduce the behaviour of the experimentally tested HA SS PAT pointed out its reliability to estimate the performances of PAT models, having at disposal specific knowledge about the internal geometric configuration. With respect to the further models available in the literature, specific considerations were paid to both the accurate reproduction of the internal geometric configuration of the tested PAT and the analysis of wide set of rotational speed,with the aim of implementing a model, applicable to the whole set of PATs, operating in similitude. In order to limit the computational time-consuming, a medium mesh resolution was accounted for simulations, defining an overestimation of the head drops generated by the PAT not higher than 16% of the experimental results. Conversely, a greater difference was observed to calculate the produced power, which was significantly higher for low flow rates and high rotational speeds. At flow rate increasing, a better reliability was observed for lower rotational speeds, with scatters in the order of 20%, instead. Furthermore, they were estimated up to 35%

for higher rotational speeds. These results were observable from the representation of the efficiency curve, as well, achieving a significant overestimation of the efficiency at BEP. Good correlations were assessed for operative conditions at higher flow rate numbers, corresponding to the lower rotational speeds, instead. Observed differences could be ascribed to both the mesh resolution and the estimation of the volumetric, internal and motor efficiencies. From the analysis of the velocity field, internal to the PAT, a significant flow regularity was observed at BEP for the whole set of simulated rotational speeds, whereas the definition of secondary flows around the blades were determined, for operative conditions far from BEP, especially for high flow rates and limited rotational speeds, by causing the increase of the internal energy losses and the related decrease of hydraulic efficiency.

## 6.2 Future Improvements of the Research

From results reached with this Ph.D. work, following improvements could be considered for the next developments of the research:

- concerning the experimental analysis, in order to validate the proposed predictive formulations to a wider set of centrifugal pump models, the extension of experiments on PATs with further internal configurations, could be accounted for. Specifically, their validation to models presenting a diversified impeller and volute geometries, with different number and geometric configurations of blades could generalize the applicability of the proposed formulations. In reference to the HA models, the analysis of Horizontal Axis Multi-Stage models could point out whether the proposed formulations are reliable for Multi-Stage configurations, as well. Verifying the efficiency improvements reachable with higher Motor Efficiency Classes to further Nominal Powers and geometric configurations could also improve the knowledge of motor equipment influence on the estimation of the overall PAT efficiency;
- in reference to the introduced procedure for PAT selection in WDNs, the implementation of optimization algorithms (such as meta-heuristic models) can be

contemplated as an applicative approach to calculate, being not available the characteristic curves of pumps, the BEP parameters of the pump model, able to maximize the overall produced power when running as turbine. Under these hypotheses, the model selection could be ascribed to the definition of the centrifugal pump model, available in the market, presenting, in direct operations, BEP parameters as close as possible to the estimated ones;

- concerning the numerical approach, the mesh resolution refinement could improve the correlation between experimental and numerical results. The investigation of the efficiency improvements, connected to modification of the impeller and/or the volute configurations, could be also intended as a starting point to implement innovate model prototypes of centrifugal pumps, able to operate at high performances for wider operative ranges in both direct and reverse operations. Moreover, the CFD modelling of Vertical Axis Multi-Stage PATs could be considered as a suitable intent to investigate the internal behaviour of this PAT category, not yet adequately taken into account from the engineering research.

## 6.3 Publications Related to This Thesis

- Pugliese F., De Paola F., Fontana N., Giugni M., Marini G. (2016). Experimental characterization of two Pumps As Turbines for hydropower generation. *Renewable Energy*, 99, 180-187. http://dx.doi.org/10.1016/j.renene.2016.06.051;
- Pugliese F., De Paola F., Fontana N., Giugni M., Marini G. (2016). Experimental analysis of Pumps As Turbines. *Proceedings of the 35$^{th}$ Convegno Nazionale di Idraulica e Costruzioni Idrauliche*, 14$^{th}$-16$^{th}$ September 2016, Bologna, Italy. http://dx.doi.org/10.6092/unibo/amsacta/5400;
- Pugliese F., De Paola F., Fontana N., Giugni M., Marini G. (2016). Performances of vertical axis Pumps running As Turbines. *Journal of Hydraulic Research* (under review).